Statistical mechanics approach to top eigenpairs of sparse symmetric random matrices

Susca, Vito

Awarding institution:
King's College London

Statistical Mechanics Approach to Top Eigenpairs of Sparse Symmetric Random Matrices

Vito Antonio Rocco Susca

Supervised by:

Pierpaolo Vivo

Reimer Kühn

A dissertation submitted for the degree of

Doctor of Philosophy

of

King's College London.

Department of Mathematics

King's College London

October 21, 2021

I, Vito Antonio Rocco Susca, confirm that the work presented in this thesis is my own. Where information has been derived from other sources, this has been indicated in the work.

I, Vito Antonio Rocco Susca, furthermore declare to have contributed to the following research outputs during the years of my doctorate studies.

- V. A. R. Susca, P. Vivo, and R. Kühn. Top eigenpair statistics for weighted sparse graphs. *Journal of Physics A: Mathematical and Theoretical*, 52(48):485002, 2019 [1].
- V. A. R. Susca, P. Vivo, and R. Kühn. Second largest eigenpair statistics for sparse graphs. *Journal of Physics A: Mathematical and Theoretical*, 54(1):015004, 2020 [2].
- V. A. R. Susca, P. Vivo, and R. Kühn. Cavity and replica methods for the spectral density of sparse symmetric random matrices. *SciPost Physics Lecture Notes*, 33, 2021 [3].

Abstract

The aim of this thesis is to characterise the statistics of the top eigenpairs of sparse symmetric random matrices, adopting the perspective and the tools of statistical physics of disordered systems.

Our first main result is the development of a statistical mechanics formalism to compute the statistics of the top eigenpair of sparse ensembles. Framing the problem in terms of optimisation of a quadratic form on the sphere and introducing a fictitious real temperature, we employ the cavity and the replica methods to determine the solution in terms of functional self-consistency equations, which are efficiently solved by a population dynamics algorithm. In our derivation, the structure of the density of the top eigenvector's components is understood in terms of the heterogeneous contributions coming from nodes of different degrees.

Then, introducing a "deflation" mechanism – that maps the largest eigenvalue of a matrix to zero while leaving its eigenvectors invariant – in conjunction with the statistical mechanics framework used for the top eigenpair, we study the statistics of the second largest eigenpair of sparse ensembles assuming that the top eigenpair statistics is known. This is the second main result of this thesis. The orthogonality condition between distinct eigenvectors naturally arises in the solution and is included in an appropriately modified version of the population dynamics algorithm. We also show that the population dynamics algorithm is not able to accurately capture the thermodynamic limit $N \to \infty$ when using a finite population size N_P. We find evidence of the existence of an optimal population size $N_P^\star$ for a given graph size N.

Our results are in perfect agreement with numerical diagonalisation of large sparse adjacency matrices, concentrating on the cases of random regular and Erdős-Rényi graphs and sparse Markov transition matrices for unbiased random walks.

Before deriving our main results, we provide an extensive presentation of the cavity and the replica methods, using the problem of the average spectral density as a case study.

Acknowledgements

I wish to thank Pierpaolo Vivo and Reimer Kühn for their guidance and mentoring during these years. They have been a source of scientific knowledge and enthusiasm, for which I am indebted. I also would like to acknowledge the precious support and funding by the CANES Centre for Doctoral Training. My sincere gratitude goes to all the friends in the Disordered Systems group at KCL for many stimulating discussions and enjoyable times outside the office.

Next, I want to thank my parents, my pole stars. Even from afar, they have helped me navigating through the PhD with their unconditional love, always providing encouragement and comfort when I felt lost. I am also deeply grateful for my family of friends. My deep gratitude is for those who welcomed a disoriented version of me more than four years ago at a tube station and, still now, stand by me. An equally deep gratitude is for those who joined me along the way, sharing their paths (and desks, chairs and dinners, at home and in the office) with me, and those who were geographically far away but never distant. They all made my journey better.

Contents

List of Figures

Chapter 1

Introduction

The primary goal of this thesis is to determine the statistics of the top eigenpairs of sparse symmetric random matrices, using methods borrowed from statistical physics of disordered systems.

Given a $N \times N$ *symmetric* matrix J (i.e. $J_{ij} = J_{ji}$ for any $i, j = 1, \ldots, N$) with real eigenvalues $\{\lambda_\alpha\}_{\alpha=1,\ldots,N}$ and corresponding eigenvectors $\{\boldsymbol{v}_\alpha\}_{\alpha=1,\ldots,N}$, an eigenpair is given by the pair $(\lambda_\alpha, \boldsymbol{v}_\alpha)$, for any $\alpha = 1, \ldots, N$. The N eigenvalues can be sorted in descending order, with $\lambda_1 \geq \lambda_2 \geq \ldots \geq \lambda_N$. Therefore, the pairs $(\lambda_1, \boldsymbol{v}_1)$ and $(\lambda_2, \boldsymbol{v}_2)$ represent respectively the top and the second largest eigenpair of J. When the matrix J is random, then so are its eigenvalues and eigenvectors. Thus, considering the *ensemble* of J identified by the joint distribution $P(\{J_{ij}\})$ of the matrix entries, one's aim is to characterise the average ensemble properties of eigenvalues and eigenvectors, namely the probability density function (pdf) of the eigenvalues (known as *average spectral density*), the typical average value of a specific eigenvalue λ_α and the pdf of the components of the associated eigenvector. We consider ensembles of *sparse* symmetric random matrices, where the word "sparse" indicates that most of the entries are zero. The pattern of the non-zero entries is random itself and encodes the structure of a random *graph*. Indeed, this kind of matrices can be regarded as weighted adjacency matrices of undirected graphs.

Focussing on such matrices, our goal is to set up a statistical mechanics framework to obtain the statistics of the top two eigenpairs. Namely, in Chapter 3 we focus on the typical average largest eigenvalue $\langle \lambda_1 \rangle_J$ and the density of the corresponding *top* eigenvector's components $\rho_J(u)$. In Chapter 4 we determine the average second largest eigenvalue $\langle \lambda_2 \rangle_J$ and the density of the associated *second* eigenvector's components $\rho_{J,2}(v)$.

Before tackling the extremal eigenpair problem for sparse symmetric random matrices,

in Chapter 2 we introduce and thoroughly explain the main methods employed in this thesis, namely the *cavity* and the *replica* method, using the spectral density problem for such matrices as an example. Indeed, the calculation of the average spectral density has traditionally been one of the pivotal questions in Random Matrix Theory (RMT), ever since the application of RMT to the statistics of energy levels of heavy nuclei [4]. Besides, another specific reason for which it is instructive to review the spectral problem as the first topic of this thesis is that in the pioneering work of Edwards and Jones [5], for the first time the determination of the spectral density was mapped into a statistical mechanics problem. Inspired by this framework, we will build the setup for the extremal eigenpairs analysis. Therefore, Chapter 2 will provide not only an introduction to the methods but also the statistical mechanics baseline that we will employ throughout the whole thesis.

1.1 A historical perspective on the spectral problem for sparse matrices

The spectral problem plays a central role in RMT and it has diverse applications in physics [6], computer science [7], finance [8–10] and statistics [11, 12]. The most celebrated results about the density of states such as the Wigner semicircle law [13] for Wigner matrices (including Gaussian ensembles) and the Marčenko-Pastur law [14] for covariance matrices refer to "dense" matrix ensembles, i.e. those for which most of the matrix entries are non-zero.

On the other hand, the spectral problem is very relevant also for sparse matrix models. Indeed, the spectral properties of adjacency matrices of sparse graphs encode the structural and topological features of many complex systems [15, 16]. For random walks on graphs, the eigenvalue spectrum is directly connected to the relaxation time spectrum [17, 18]. Moreover, from the condensed matter point of view, sparsely connected matrix models provide a test ground for physical systems described by a Hamiltonian with finite-range interactions (see for instance [19]).

The key result linking the spectral problem to statistical mechanics is the celebrated Edward-Jones formula [5]. Indeed, the formula recasts the determination of the average spectral density (2.1) into the problem of evaluating the average free energy $\langle \log Z(\lambda) \rangle_J$ of a disordered system with partition function $Z(\lambda)$. Edward and Jones were the first to use the *replica* method, extensively employed in spin-glass physics [20], to perform averages of this type in the context of random matrices.

Historically, the application of the Edwards-Jones recipe to sparse symmetric random matrices (in particular Erdős-Rényi [21, 22] adjacency matrices with the non-zero entries drawn from a Bernoulli distribution) was pioneered by Bray and Rodgers in [23] (and also for the analogous spectral problem of graph Laplacians in [24].). However, in their formulation the average spectral density $\rho(\lambda)$ depends on the solution of a very complicated integral equation, which, as of today is still unsolved – except in the limiting cases of Erdős-Rényi graphs with large mean degree, and for large values of the spectral parameter λ (see again [23] and also [25]). The same integral equation has been derived independently with a supersymmetric approach in [26] and later obtained in a rigorous manner in [27], thus confirming the exactness of the symmetry assumptions in [23]. The difficulties in dealing with such equation even from a numerical point of view stimulated the search for a variety of approximation schemes, such as the single defect approximation (SDA) [28] and the effective medium approximation (EMA) [29, 30]. Alongside approximation schemes, results from numerical diagonalisation such as in [31, 32] have been employed to investigate the spectral properties of sparse random matrices.

A different approach to the spectral problem of sparse symmetric random matrices was proposed in [33]. There, the order parameters of the replica calculation are represented as uncountably infinite superpositions of Gaussians with random variances, as suggested by earlier solutions of models for finitely coordinated harmonically coupled systems [34]. The intractable Bray-Rodgers integral equation is then replaced by another integral equation, which – although also highly non-linear – has the advantage that it can be solved efficiently by a stochastic population dynamics algorithm. In Chapter 2, we will review both approaches.

Almost in parallel to [33], the *cavity* method [35] was used by Rogers and collaborators in [36] to compute the spectrum of large single instances of sparse symmetric random matrices. The cavity method, also known as *belief propagation*, represents a much simpler alternative to replicas and its exactness for locally tree-like graphs with finite mean degree c was proved in [37]. The applicability of the cavity method is ensured by the tree-like structure of the underlying graphs. The ensemble average spectral density (2.1) is then obtained building on the single-instance results, circumventing the calculation of the average "free energy" $\langle \log Z(\lambda) \rangle_J$ altogether. Similarly to [33], the cavity treatment produces non-linear fixed-point integral equations that are completely equivalent to those obtained within the replica framework.

It has been shown in [38] that both the cavity and the replica method yield the same results

concerning the spectral density of Erdős-Rényi (ER) graphs and sparse covariance matrices. Both approaches in [33] and [36] recover known results such as the Kesten-McKay law for the spectra of random regular graphs [39,40], the Marčenko-Pastur law and the Wigner's semicircle law respectively for sparse covariance matrices and for ER adjacency matrices in the large mean degree limit. Moreover, both methods allow to characterise the spectral density of sparse Markov matrices [41,42] and graphs with modular [43] and small-world [44] structure and with topological constraints [45]. The localisation transitions in the spectra of sparse symmetric random matrices that were already observed in [33] were studied in greater detail in [46]. In a similar manner, both the cavity and the replica methods have also been employed to study the statistics of the top and second largest eigenpair of sparse symmetric random matrices [1, 2, 47]. The two methods have also been extended to the case of sparse non-Hermitian matrices [48–51]. A particular attention has been devoted to the spectral properties of the Hashimoto non-backtracking operator on random graphs [52, 53]. Both cavity and replica methods have been recently used to characterise the dense ($c \to \infty$) limit of the spectral density of adjacency matrices of undirected graphs within the configuration model, which reveals that the behaviour of the limiting spectral density is not universal but actually depends on degree fluctuations. Indeed the expected Wigner semicircle is recovered when the degree distribution tightly concentrates around the mean degree c for $c \to \infty$, whereas non trivial deviations from the semicircle are found when degree fluctuations are stronger [54]. Moreover, thanks to the extension of the replica method to the analysis of sparse loopy random graphs, the influence of loops on the spectra of sparse matrices has been lately investigated in [55, 56]. There is also a recent cavity analysis of the problem of loopy graphs by Newman and collaborators in [57].

1.2 Extremal eigenpairs

1.2.1 Importance of the top eigenpair

The largest eigenvalue and the associated *top* eigenvector of a matrix play a very important role in many applications, such as synchronisation problems on networks [58], percolation problems [59], linear stability of coupled ODEs [60], financial stability [61] and several other problems in physics and chemistry, connected to the applications of Perron-Frobenius's theorem [62]. Also in the realm of quantum mechanics, the search for the ground state of a complicated Hamiltonian essentially amounts to solving the top eigenpair problem for a differential operator [63]. The top eigenpair is also relevant in signal reconstruction problems employing algorithms based on the spectral method [64]. These extremal questions also arise in multivari-

ate data analysis. In Principal Component Analysis, the top eigenpair of a covariance matrix provides information about the most relevant correlations hidden in the dataset [65]. The role of the eigenvectors of the empirical covariance matrix for the estimation of the top eigenvector of the corresponding population covariance matrix has been discussed in [66].

In the context of graph theory, the eigenvectors of both adjacency and Laplacian matrices are employed to solve combinatorial optimisation problems, such as graph 3-colouring [67] and to develop clustering and cutting techniques [68–71]. In particular, the top eigenvector of graphs is intimately related to the "ranking" of the nodes of the network [72]. Indeed, beyond the natural notion of ranking of a node given by its degree, the relevance of a node can be estimated from how "important" its neighbours are. The vector expressing the importance of each node is exactly the top eigenvector of the network adjacency matrix. Google PageRank algorithm works in a similar way [73, 74]: the PageRanks vector is indeed the top eigenvector of a large Markov transition matrix between web pages.

1.2.2 Importance of the second largest eigenpair

The second largest eigenvalue and the associated *second* eigenvector of a matrix are of great significance as well. Plenty of applications can be found in many areas of science. In coding theory, the Hamming distance of a binary linear code can be expressed as a function of the second largest eigenvalue of the *coset* graph associated to the code [75]. In biology, it has been shown in [76] that the second largest eigenvalue of cancer metabolic networks describes the speed of cancer processes. In the context of clustering methods based on the adjacency matrix of a graph, the second eigenvector encodes inter-cluster connectivity, complementing the information about intra-cluster connectivity included in the top eigenvector [70, 77]. With regard to the power method algorithm, employed for the computation of the leading eigenpair of single matrix instances in many real-world applications, the ratio of the absolute value of the first two eigenvalues of a matrix determines the rate of convergence of the method [78]. Moreover, in Principal Component Analysis, the second eigenvector of the covariance matrix of standardised data represents the direction that accounts for the second largest source of variability within the dataset [65, 79] and complements the information coming from the first principal component.

The knowledge of the spectral gap, i.e. the distance between the largest and second largest eigenvalue, is essential for random walks on undirected graphs, which are substantially equivalent to finite time-reversible Markov chains, as pointed out by Lovasz in his survey [17].

Indeed, up to log-factors, the inverse spectral gap of the transition matrix represents the *mixing* rate of the Markov chain, i.e. how fast the state probability vector of a Markov chain approaches the limiting stationary distribution [80], given by the top right eigenvector of the transition matrix. The inverse of absolute value of second largest eigenvalue of the transition matrix denotes the largest relaxation time or *mixing* time, and the corresponding eigenvector describes the non-equilibrium mode with the slowest decay rate. The second largest eigenpair of Markov transition matrices also plays an important role in all processes that are described by means of random walks on graphs, such as out of equilibrium dynamics of glassy systems (see e.g. [81, 82]) and search algorithms such as Google PageRank [83].

1.3 Quantitative results on top eigenpairs of random graphs

1.3.1 Top eigenvalues

When the matrix J is random and symmetric with i.i.d. entries, analytical results on the statistics of the top eigenvalue date back to the classical work by Füredi and Komlós [84]: the largest eigenvalue of such matrices follows a Gaussian distribution with finite variance, provided that the moments of the distribution of the entries do not scale with the matrix size. This result directly relates to the largest eigenvalue of ER adjacency matrices in the case when the probability p for two nodes to be connected does not scale with the matrix size N. This result has been then extended by Janson [85] in the case when p is large. However, in our analysis we will be mostly dealing with the sparse case, i.e. when $p = c/N$, with c being the constant mean degree of nodes (or equivalently, the mean number of non-zero elements per row of the corresponding adjacency matrix). In this sparse regime, Krivelevich and Sudakov [86] proved a theorem stating that for any constant c the largest eigenvalue of ER graphs diverges slowly with N as $\sqrt{\log N/\log\log N}$. To ensure that the largest eigenvalue remains $\sim \mathcal{O}(1)$, the nodes with very large degree must be pruned (see [87]).

The second largest eigenvalue plays a pivotal role in the study of complex systems and graph theory, representing topological features of the graphs [88]. If the spectral gap is large, then the graph has good connectivity and expansion properties [72]. Therefore, many results have been derived about bounds for the second largest eigenvalue (see e.g. [89, 90]). In particular, bipartite regular graphs with very wide spectral gaps are called *expanders* (*magnifiers* if not bipartite) and have been widely studied since the seminal work of Alon [91]. To shed light on the expansion properties of regular graphs, specific bounds have been derived for their second largest eigenvalue (see e.g. [75] and [92]).

1.3.2 Eigenvectors

The characterisation of eigenvectors properties has proved to be much harder than the spectral problem and is generally a less explored area of RMT. Excluding the cases of i) invariant ensembles, where eigenvector components follow the celebrated Porter-Thomas distribution [93, 94], ii) dense non-Hermitian matrices (see for instance the seminal works of Chalker and Mehlig [95] along with results about correlations between eigenvectors [96, 97] and some more recent applications [98–101]) and iii) perturbed matrices [102–106], systematic results are scarcer for sparse Hermitian matrices, especially in the limit of high sparsity. Indeed, although Gaussian statistics and delocalisation of eigenvectors are known properties of adjacency matrices of ER and random regular graphs (RRGs) in the case where the mean degree $c = c(N)$ diverges with N [107–109], very few results are available in the case of high sparsity, i.e. with c being the constant mean degree of nodes, which we focus on.

In this limit, numerical studies have shown that most of the eigenvectors of a random regular graph follow a Gaussian distribution [110], as well as almost-eigenvectors[1] [111], whereas ER eigenvectors are localised especially for low values of c [31]. Localisation properties of eigenvectors of sparse directed random graphs have been recently investigated in [112].

The statistics of the top eigenvector's components for very sparse symmetric random matrices was first considered in the seminal works by Kabashima and collaborators [47, 113, 114]. The focus there is on specific classes of real sparse random matrices, i.e. when the matrix connectivity is either a random regular graph or a mixture of multiple degrees, and the nonzero elements are drawn from a Bernoulli distribution. More precisely, in [47] and [114] the cavity method was employed for the top eigenpair problem, while in [113] the replica formalism was instead adopted to study the same problem in the thermodynamic limit.

Inspired by the work of Kabashima and collaborators, in [1] we generalised and expanded the cavity and replica analyses that they pioneered, in order to build a versatile and flexible statistical mechanics framework to study the top eigenpair of weighted adjacency matrices of sparse random graphs. The configuration model is used to generate the pure $\{0,1\}$ adjacency matrices of uncorrelated random networks, whereas bonds weights are chosen independently. In [2], using a deflation technique and an improved version of the statistical mechanics setup that we proposed in [1], we were able to determine the statistics of the second largest eigenpair. Chapter 3 and Chapter 4 will be based on respectively [1] and [2].

[1] An almost-eigenvector of a matrix A with eigenvalue λ is a normalised vector $\boldsymbol{v}$ that satisfies the eigenvector equation $(A-\lambda I)\boldsymbol{v} = \mathbf{0}$ within some small tolerance ε, i.e. $||A\boldsymbol{v} - \lambda\boldsymbol{v}||_2 \leq \varepsilon$.

Chapter 2

Introduction to the cavity and replica methods for the spectral density of sparse symmetric random matrices

2.1 Introduction

Given a $N \times N$ symmetric random matrix J with eigenvalues $\{\lambda_i\}_{i=1,\dots,N}$, the avevage spectral density is defined as

$$\rho(\lambda) = \left\langle \frac{1}{N} \sum_{i=1}^{N} \delta(\lambda - \lambda_i) \right\rangle_J , \tag{2.1}$$

where the limit $N \to \infty$ is understood and $\langle \dots \rangle_J$ denotes the average over the matrix ensemble to which J belongs. The latter is also referred to as "disorder" average.

In this chapter, we will retrace the main milestones in the determination of the spectral density of sparse symmetric random matrices using a statistical mechanics approach. As examples, we will look at adjacency matrices of sparse random graph models (specifically the Erdős-Rényi and the random regular graph model). We will consider both the unweighted case, where the non-zero entries of the matrix J have a given value of 1, and the weighted case, where the non-zero entries of J are drawn from a Gaussian distribution. We will take advantage of this analysis also to explain in great detail the cavity and replica methods that will be the main calculation tools employed in this thesis.

We start with the analysis of the Edwards-Jones formula in Section 2.2, providing its proof in Section 2.2.1 and discussing how to deal with the average $\langle \log Z(\lambda) \rangle_J$ appearing in their formula in Section 2.2.2. For clarity and simplicity, we will first illustrate the cavity approach in Section 2.3. We outline the cavity setup in Section 2.3.1, then we deal with the spectrum

of large instances of sparse symmetric random matrices in Section 2.3.2. In Section 2.3.3 we show how the single-instance approach can be extended to the $N \to \infty$ limit to recover the ensemble average spectral density. Besides, in 2.3.4 we evaluate the large c limit of the average spectral density obtained within the cavity formalism, showing that it converges to the Wigner semicircle. We will then follow the historical development of the subject by documenting the Bray-Rodgers replica approach in Section 2.4. We will derive the Bray-Rodgers integral equation in Section 2.4.3, while in Section 2.4.4 we will obtain its large c asymptotic expansion, showing that its leading order gives rise to the Wigner semicircle, as expected. In Section 2.5 we will deal with the alternative replica solution proposed in [33], showing in Section 2.5.1 that the solution obtained with this approach coincides with that found by the cavity treatment in Section 2.3.3. In Section 2.6, we outline the stochastic population dynamics algorithm employed to solve the non-linear fixed-point integral equations that are found within both the cavity and replica frameworks respectively in Section 2.3.3 and Section 2.5.1.

2.2 Edwards-Jones formula

Edwards and Jones in [5] provide a formula to express the average spectral density of $N \times N$ random matrices (2.1) as

$$\rho(\lambda) = -\frac{2}{\pi N} \lim_{\varepsilon \to 0^+} \mathrm{Im} \frac{\partial}{\partial \lambda} \langle \log Z(\lambda) \rangle_J \ , \tag{2.2}$$

with

$$Z(\lambda) = \int_{\mathbb{R}^N} \mathrm{d}\boldsymbol{v} \exp\left[-\frac{\mathrm{i}}{2} \boldsymbol{v}^T \left(\lambda_\varepsilon \mathbb{1} - J \right) \boldsymbol{v} \right] \ , \tag{2.3}$$

where again the $\langle ... \rangle_J$ denotes the average over the matrix ensemble to which J belongs. In (2.2), which is valid for any N, Im indicates the imaginary part and log is the branch of the complex logarithm for which $\log \mathrm{e}^z = z$. In (2.3), the symbol $\mathbb{1}$ represents the $N \times N$ identity matrix, the symbol $\boldsymbol{v}$ describes a vector in $\mathbb{R}^N$ and the integral extends over $\mathbb{R}^N$. Moreover, $\lambda_\varepsilon = \lambda - \mathrm{i}\varepsilon$, where ε is a positive parameter ensuring that the integral (2.3) is convergent, since the absolute value of the integrand has the leading behaviour $\mathrm{e}^{-\frac{\varepsilon}{2} \sum_{i=1}^N v_i^2}$. The integral (2.3) can be interpreted as the canonical partition function of the Gibbs-Boltzmann distribution of N harmonically coupled particles with an imaginary (inverse) temperature, viz.

$$P_J(\boldsymbol{v}) = \frac{1}{Z(\lambda)} \exp\left[-\mathrm{i} H(\boldsymbol{v}) \right] \ , \tag{2.4}$$

with a complex "Hamiltonian"

$$H(\boldsymbol{v}) = \frac{1}{2}\boldsymbol{v}^T\,(\lambda_\varepsilon \mathbb{1} - J)\,\boldsymbol{v}\,. \tag{2.5}$$

In this framework, the computation of (2.1) requires to evaluate $\langle \log Z(\lambda)\rangle_J$, which is the canonical free energy of the associated N particles system, averaged over the random couplings.

2.2.1 Proof of the Edwards-Jones formula

The starting point is the definition (2.1). Looking for a representation of the Dirac delta, one considers the Sokhotski-Plemelj identity (see Appendix 2.A for a proof), viz.

$$\frac{1}{x \pm \mathrm{i}\varepsilon} \xrightarrow[\varepsilon\to 0^+]{} \mathrm{Pr}\left(\frac{1}{x}\right) \mp \mathrm{i}\pi\delta(x)\,, \tag{2.6}$$

where $x \in \mathbb{R}$ and Pr denotes the Cauchy principal value. The imaginary part of the identity, namely

$$\delta(x) = \frac{1}{\pi}\lim_{\varepsilon\to 0^+} \mathrm{Im}\frac{1}{x - \mathrm{i}\varepsilon}\,, \tag{2.7}$$

provides the desired representation. Therefore, inserting (2.6) into (2.1) results in

$$\begin{aligned}\rho(\lambda) &= \frac{1}{\pi N}\lim_{\varepsilon\to 0^+} \mathrm{Im}\left\langle \sum_{i=1}^{N} \frac{1}{\lambda - \lambda_i - \mathrm{i}\varepsilon}\right\rangle_J \\ &= -\frac{1}{\pi N}\lim_{\varepsilon\to 0^+} \mathrm{Im}\left\langle \sum_{i=1}^{N} \frac{1}{\lambda_i + \mathrm{i}\varepsilon - \lambda}\right\rangle_J\,,\end{aligned} \tag{2.8}$$

where the minus sign has been made explicit.

One would now express the ratio in the angle brackets as the derivative of the *principal branch* of the complex logarithm, denoted by Log. Unlike other properties, its derivative behaves exactly like that of the real logarithm, therefore

$$\sum_{i=1}^{N} \frac{1}{\lambda_i + \mathrm{i}\varepsilon - \lambda} = -\frac{\partial}{\partial\lambda}\sum_{i=1}^{N} \mathrm{Log}\,(\lambda_i + \mathrm{i}\varepsilon - \lambda)\,, \tag{2.9}$$

entailing for the average spectral density the formula

$$\rho(\lambda) = \frac{1}{\pi N}\lim_{\varepsilon\to 0^+} \mathrm{Im}\frac{\partial}{\partial\lambda}\left\langle \sum_{i=1}^{N} \mathrm{Log}\,(\lambda_i + \mathrm{i}\varepsilon - \lambda)\right\rangle_J\,. \tag{2.10}$$

The sum of logarithms in (2.10) can be related to the partition function $Z(\lambda)$ in (2.3) by ex-

ploiting the following identity [94, 115],

$$Z(\lambda) = \int_{\mathbb{R}^N} \mathrm{d}\boldsymbol{v} \exp\left[-\frac{\mathrm{i}}{2}\boldsymbol{v}^T(\lambda_\varepsilon \mathbb{1} - J)\boldsymbol{v}\right] = (2\pi)^{N/2} \exp\left[-\frac{1}{2}\sum_{i=1}^{N} \mathrm{Log}(\lambda_i + \mathrm{i}\varepsilon - \lambda) + \frac{\mathrm{i}\pi N}{4}\right] . \tag{2.11}$$

Caution is needed when taking the logarithm on both sides of (2.11), as in general $\mathrm{Log}(\mathrm{e}^z) \neq z$. Indeed, using the definition of the complex logarithm applied to the exponential function (see Eq. (2.B.8) in Appendix 2.B for more details) and taking the principal logarithm on both sides of (2.11), one would obtain

$$\sum_{i=1}^{N} \mathrm{Log}(\lambda_i + \mathrm{i}\varepsilon - \lambda) = -2\mathrm{Log}Z(\lambda) + N\mathrm{Log}(2\pi) + \frac{\mathrm{i}\pi N}{2} + 4\pi\mathrm{i}\left\lfloor \frac{1}{2} - \frac{g(\lambda)}{2\pi} \right\rfloor , \tag{2.12}$$

where

$$g(\lambda) = -\frac{1}{2}\sum_{i=1}^{N} \mathrm{Arg}(\lambda_i + \mathrm{i}\varepsilon - \lambda) + \frac{\pi N}{4} \tag{2.13}$$

is the imaginary part of the exponent in (2.11) and the symbol $\lfloor ... \rfloor$ denotes the floor operation, i.e. $\lfloor x \rfloor$ is the integer such that $x - 1 < \lfloor x \rfloor \leq x$ for $x \in \mathbb{R}$.

Note that this branch choice would make the r.h.s. not everywhere differentiable for $\lambda \in \mathbb{R}$. Therefore, it is convenient to pick the branch of the complex logarithm such that $\log \mathrm{e}^z = z$, i.e. for which the extra (non-differentiable) phase term in (2.12) is killed. This choice yields

$$\sum_{i=1}^{N} \mathrm{Log}(\lambda_i + \mathrm{i}\varepsilon - \lambda) = -2\log Z(\lambda) + N\log(2\pi) + \frac{\mathrm{i}\pi N}{2} , \tag{2.14}$$

where the constant terms on the r.h.s. depend on N, but not on λ. Taking the derivative, one eventually finds

$$\frac{\partial}{\partial\lambda}\sum_{i=1}^{N} \mathrm{Log}(\lambda_i + \mathrm{i}\varepsilon - \lambda) = -2\frac{\partial}{\partial\lambda}\log Z(\lambda) , \tag{2.15}$$

therefore the Edwards-Jones formula (2.2) is recovered.

2.2.2 Tackling the average in the Edwards-Jones formula

In order to obtain the spectral density, the average $\langle \log Z(\lambda) \rangle_J$ must be computed. It explicitly reads

$$\langle \log Z(\lambda) \rangle_J = \int \prod_{i<j} \mathrm{d}J_{ij} P(\{J_{ij}\}) \log \int_{\mathbb{R}^N} \mathrm{d}\boldsymbol{v} \exp\left[-\frac{\mathrm{i}}{2}\boldsymbol{v}^T(\lambda_\varepsilon \mathbb{1} - J)\boldsymbol{v}\right] , \tag{2.16}$$

where $P(\{J_{ij}\})$ is the joint distribution of the matrix entries. The presence of the logarithm in (2.16) prevents a factorisation of averages over edges (i, j) even for a factorised pdf of the J_{ij}.

The only available strategy seems to perform the inner N-fold integral over $\boldsymbol{v}$ first, compute the logarithm, and then average over the random matrix disorder. However, this sequence of operations would simply run the Edwards-Jones formula (2.2) backwards, leading to the useless identity $\rho(\lambda) = \rho(\lambda)$. The only chance to make some progress therefore relies on performing the disorder average *first*. However, the two integrations in (2.16) cannot be directly exchanged due to the presence of the logarithm in between.

Disorder averages such as (2.16) are called *quenched* averages. The technique to handle such averages is the *replica trick*. It is a well established method employed in the statistical mechanics of disordered systems that allows one to bypass the logarithm in (2.16) in favour of the computation of integers moments of $Z(\lambda)$ (see Section 2.4)[1].

The replica method for the calculation of the spectral density of dense random matrices was employed by Edwards and Jones in [5]. The same replica calculation for sparse ensembles was pioneered by Bray and Rodgers in [23]. However, we prefer to start with the cavity approach because it is technically much less involved and allows one to circumvent the direct computation of $\langle \log Z(\lambda) \rangle_J$. We will then follow the historical path traced in [23] in Section 2.4.

2.3 Cavity method for the spectral density

The cavity method as implemented in [36] makes it possible to derive the spectral density for a single instance of large sparse symmetric matrices. According to the physical interpretation of the Edwards-Jones formula, the calculation of the spectral density can be recast as a problem of interacting particles on a sparse graph. The basic idea behind the cavity method [35] is that observables related to a certain node of a network in which cycles are scarce (thereby called *tree-like*) can be determined from the same network where the node in question is removed. Due to the sparse structure, the removal of a node makes its neighbouring sites (as well as the signals coming from them) uncorrelated.

2.3.1 Definition of the sparse matrix ensemble

We consider a large $N \times N$ sparse symmetric random matrix J. It represents the weighted adjacency matrix of a graph $\mathscr{G}$, i.e. each entry can be expressed as $J_{ij} = c_{ij}K_{ij}$, where the c_{ij} represent the pure $\{0,1\}$ adjacency matrix and the K_{ij} encode the bond weights. In an undi-

[1] There exists also an alternative though only approximate strategy, known as *annealed* average, which does not rely on the replica method. It consists in "moving" the logarithm outside the disorder average. Although formally incorrect, the annealed protocol provides the correct spectral density of "dense" random matrices, such as Gaussian ones (see Section 15.4 in [94] for a thorough discussion).

rected graph, the degree k_i of the node i is defined as the number of nodes in its neighbourhood $\partial i = \{j : c_{ij} = 1\}$, viz.

$$k_i = \sum_{j \in \partial i} c_{ij} = |\partial i| \ . \tag{2.17}$$

We define $c = \frac{1}{N}\sum_{i=1}^{N} k_i$ as the mean degree. We consider locally tree-like sparse matrices, in which the probability of finding a cycle vanishes as $\ln N/N$ when $N \to \infty$. Alternatively, this property is implied by the requirement that the mean degree c does not increase with the matrix size N, hence $c/N \to 0$ as $N \to \infty$. In this very sparse regime, the cavity method predictions are approximate. However, they are exact on trees, and they become asymptotically exact on finitely connected networks as the thermodynamic limit is taken.

Following the statistical mechanics analogy, in the sparse case the N particles described by the variables v_i interact on the graph $\mathscr{G}$ where an edge is defined for any pair (i, j) of interacting particles. While the replica formalism analyses the partition function (2.3) in the limit $N \to \infty$, the cavity method focusses on the associated Gibbs-Boltzmann distribution (2.4) with imaginary inverse temperature i and complex Hamiltonian (2.5), as shown in the section below.

2.3.2 Cavity derivation for single-instances

The spectral density of J — i.e. the pdf of the eigenvalues of the matrix J — is obtained from the Edwards-Jones formula (2.2) for finite N as

$$\rho_J(\lambda) = -\frac{2}{\pi N} \lim_{\varepsilon \to 0^+} \mathrm{Im} \frac{\partial}{\partial \lambda} \log Z(\lambda) \ , \tag{2.18}$$

where $Z(\lambda)$ is defined in (2.3). The subscript indicates that $\rho_J(\lambda)$ refers to a single, specific instance J [2]. For the same reason, no averaging is needed. Performing explicitly the λ-derivative in (2.18) with $Z(\lambda)$ defined in (2.3), one obtains

$$\frac{\partial}{\partial \lambda} \log Z(\lambda) = -\frac{\mathrm{i}}{2} \sum_{i=1}^{N} \int \prod_{j=1}^{N} \mathrm{d}v_j \, P_J(\boldsymbol{v}) v_i^2 \ , \tag{2.19}$$

where

$$P_J(\boldsymbol{v}) = \frac{1}{Z(\lambda)} \exp\left[-\frac{\mathrm{i}}{2} \boldsymbol{v}^T (\lambda_\varepsilon \mathbb{1} - J) \boldsymbol{v} \right] \tag{2.20}$$

[2] We remark that $\rho_J(\lambda)$ is not the density of the top eigenvalue of J.

is the Gibbs-Boltzmann distribution defined in (2.4). For any given i, the average w.r.t. the joint pdf (2.20) in (2.19) reduces to the average w.r.t. the single-site marginal $P_i(v_i)$, viz.

$$\int \prod_{j=1}^{N} \mathrm{d}v_j \, P_J(\boldsymbol{v}) v_i^2 = \int \mathrm{d}v_i P_i(v_i) v_i^2 = \langle v_i^2 \rangle \ , \tag{2.21}$$

where the $\langle v_i^2 \rangle$ represent the single-site variances of each of the N marginal pdfs $P_i(v_i)$. Using (2.19) and (2.21), the spectral density in (2.18) can thus be written as

$$\rho(\lambda) = -\frac{2}{\pi N} \lim_{\varepsilon \to 0^+} \mathrm{Im} \left(-\frac{\mathrm{i}}{2} \sum_{i=1}^{N} \langle v_i^2 \rangle \right) = \frac{1}{\pi N} \lim_{\varepsilon \to 0^+} \sum_{i=1}^{N} \mathrm{Re} \langle v_i^2 \rangle \ . \tag{2.22}$$

Therefore, it is sufficient to determine the N single-site variances to calculate the spectral density using (2.22).

In order to find the $\langle v_i^2 \rangle$, one looks at each marginal pdf $P_i(v_i)$. Due to the sparse nature of J, the variable v_i is coupled (through J_{ij}) only to those v_j associated to nodes that are neighbours of i. Hence, the single-site marginal of the node i can be expressed as

$$P_i(v_i) = \int \prod_{j(\neq i)}^{N} \mathrm{d}v_j \, P_J(\boldsymbol{v}) = \frac{1}{Z_i} \mathrm{e}^{-\frac{\mathrm{i}}{2}\lambda_\varepsilon v_i^2} \int \mathrm{d}\boldsymbol{v}_{\partial i} \mathrm{e}^{\mathrm{i}\Sigma_{j\in\partial i} J_{ij} v_i v_j} P^{(i)}(\boldsymbol{v}_{\partial i}) \ . \tag{2.23}$$

In (2.23), the integration is over the "particles" interacting with particle i, i.e. those sitting on the neighbouring sites ∂i. The distribution $P^{(i)}(\boldsymbol{v}_{\partial i})$ collects the contributions coming from the interaction of each of the v_j $(j \in \partial i)$ with particles sitting on nodes that are not neighbours of i themselves (see Graph 1 on the l.h.s. of Fig. 2.1). The contributions to the integral defining $P_i(v_i)$ coming from nodes further away generate a constant term that is absorbed in the normalisation constant Z_i.

The distribution $P^{(i)}(\boldsymbol{v}_{\partial i})$ is called the *cavity* distribution, since it refers to a graph in which the node i has been removed. In a tree-like structure, the neighbouring sites of each node i are correlated mainly through the node i. Hence, when the node i is removed, its neighbours become uncorrelated (see Graph 2 on the r.h.s. of Fig. 2.1). Therefore, the joint cavity pdf $P^{(i)}(\boldsymbol{v}_{\partial i})$ factorises into the product of independent *cavity marginals* $P_j^{(i)}(v_j)$, i.e.

$$P^{(i)}(\boldsymbol{v}_{\partial i}) = \prod_{j\in\partial i} P_j^{(i)}(v_j) \ . \tag{2.24}$$

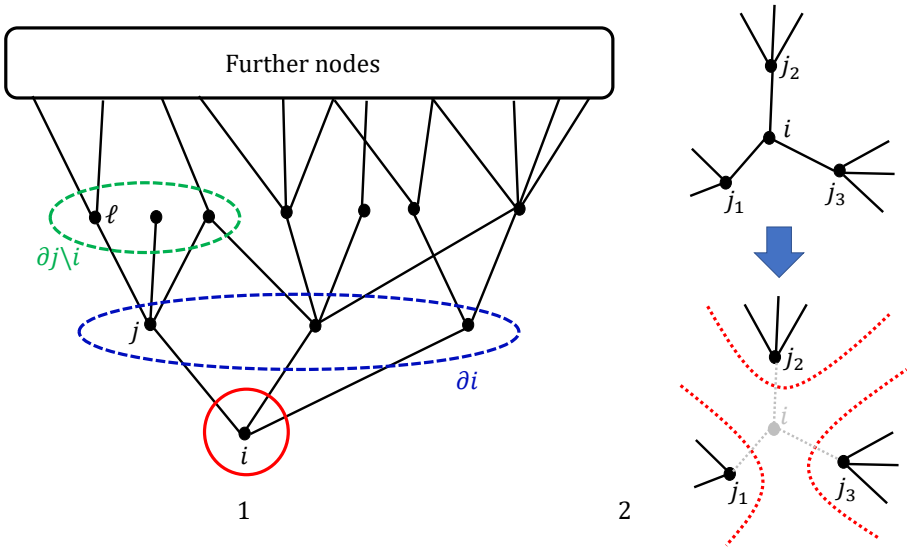

Figure 2.1: Graphs sketches. **Left graph 1**: a tree-like graph where the indices refer to the notation used in Section 2.3.1 to derive cavity single-instance equations. **Right graph 2**: example of the decorrelation occurring to the nodes j_1, j_2 and j_3, neighbours of the node i, after the removal of i.

Hence, the single-site marginal (2.23) can be expressed as

$$P_i(v_i) = \frac{1}{Z_i} e^{-\frac{i}{2}\lambda_\varepsilon v_i^2} \prod_{j\in\partial i} \int dv_j e^{iJ_{ij}v_i v_j} P_j^{(i)}(v_j) \, . \tag{2.25}$$

Eq. (2.25) shows that the marginal $P_i(v_i)$ is defined in terms of the cavity marginals $P_j^{(i)}(v_j)$. A self-consistent definition of each of the cavity marginal distributions $P_j^{(i)}(v_j)$ can be obtained by iterating the same reasoning as above. Indeed, one can now choose one of the nodes $j \in \partial i$ and define the marginal pdf associated to that node in the same way as in Eq. (2.25). However, the network one is considering at this stage is that where the node i has already been removed, therefore eventually obtaining the *cavity marginal* $P_j^{(i)}(v_j)$, namely

$$P_j^{(i)}(v_j) = \frac{1}{Z_j^{(i)}} e^{-\frac{i}{2}\lambda_\varepsilon v_j^2} \prod_{\ell\in\partial j\backslash i} \int dv_\ell e^{iJ_{j\ell}v_j v_\ell} P_\ell^{(j)}(v_\ell) \, , \tag{2.26}$$

where the symbol $\partial j\backslash i$ denotes the set of neighbours of node j excluding i (see again Graph 1 on the l.h.s. of Fig. 2.1). In turn, the cavity marginals $P_\ell^{(j)}(v_\ell)$ are defined on the graph where also the node $j \in \partial i$ has been removed.

Eq. (2.26) defines a set of recursion equations for any pair of interacting nodes (i, j). The set of recursion equations (2.26) is solved exactly by a zero-mean Gaussian ansatz for the

cavity marginals $P_j^{(i)}(v_j)$. Indeed, assuming that

$$P_j^{(i)}(v_j) = \sqrt{\frac{\omega_j^{(i)}}{2\pi}} \exp\left(-\frac{\omega_j^{(i)}}{2} v_j^2\right) , \tag{2.27}$$

and performing the Gaussian integrals on the r.h.s. of (2.26), one gets

$$P_j^{(i)}(v_j) = \frac{1}{Z_j^{(i)}} \exp\left[-\frac{1}{2}\left(\mathrm{i}\lambda_\varepsilon + \sum_{\ell \in \partial j \setminus i} \frac{J_{j\ell}^2}{\omega_\ell^{(j)}}\right) v_j^2\right] . \tag{2.28}$$

The comparison between the exponents of (2.27) and (2.28) entails

$$\omega_j^{(i)} = \mathrm{i}\lambda_\varepsilon + \sum_{\ell \in \partial j \setminus i} \frac{J_{j\ell}^2}{\omega_\ell^{(j)}} . \tag{2.29}$$

Therefore, the set of equations (2.26) translates into a set of self-consistency equations [3] for the set of cavity inverse variances $\omega_j^{(i)}$.

Similarly, the Gaussian ansatz (2.27) can be inserted in the single-site marginal expression (2.25), yielding a Gaussian structure for $P_i(v_i)$, viz.

$$P_i(v_i) = \frac{1}{Z_i} \exp\left(-\frac{1}{2} \omega_i v_i^2\right) , \tag{2.30}$$

with single-site inverse variances given by

$$\omega_i = \mathrm{i}\lambda_\varepsilon + \sum_{j \in \partial i} \frac{J_{ij}^2}{\omega_j^{(i)}} . \tag{2.31}$$

Once the cavity inverse variances are determined as the solution of (2.29), the single-site inverse variances $\langle v_i^2 \rangle = \frac{1}{\omega_i}$ are found from (2.31), and the spectral density is readily obtained from (2.22) as

$$\rho_J(\lambda) = \frac{1}{\pi N} \lim_{\varepsilon \to 0^+} \sum_{i=1}^{N} \mathrm{Re}\left[\frac{1}{\omega_i}\right] = \frac{1}{\pi N} \lim_{\varepsilon \to 0^+} \sum_{i=1}^{N} \frac{\mathrm{Re}[\omega_i]}{(\mathrm{Re}\,[\omega_i])^2 + (\mathrm{Im}[\,\omega_i])^2} . \tag{2.32}$$

As a concluding remark, it can be noticed that the set of self-consistency equations for the cavity inverse variances (2.29) only depends on the square of matrix entries, thus entailing that the spectrum of the matrix J is equal to that of the matrix $-J$ and therefore is perfectly

[3] The set of self-consistency equations (2.29) can be solved by a forward iteration algorithm.

symmetric around $\lambda = 0$. This property indeed holds exactly for trees, since every tree is a bipartite graph (see [72] or Appendix 2.G for a simple proof of this property). This check further corroborates that cavity equations are exact on trees, but only approximate on tree-like structures as long as cycles are negligible.

2.3.3 Thermodynamic limit within the cavity framework

In this section we depart from [36] and show that the ensemble average of the spectral density (2.1) can be recovered from the single-instance spectral density (2.32) as obtained through the cavity method. Indeed, by invoking the law of large number in (2.32), in the large N limit one gets

$$\rho_J(\lambda) = \frac{1}{\pi N} \lim_{\varepsilon \to 0^+} \sum_{i=1}^{N} \mathrm{Re}\left[\frac{1}{\omega_i}\right] \xrightarrow[N\to\infty]{} \rho(\lambda) = \frac{1}{\pi} \lim_{\varepsilon \to 0^+} \int \mathrm{d}\tilde{\omega}\tilde{\pi}(\tilde{\omega}) \mathrm{Re}\left[\frac{1}{\tilde{\omega}}\right] , \tag{2.33}$$

where $\tilde{\pi}(\tilde{\omega})$ is the pdf of the inverse variances ω_i taking values around $\tilde{\omega}$. In the r.h.s. of Eq. (2.33) the subscript J has been dropped, as the quantity $\rho(\lambda)$ characterises the ensemble of J, rather than a single matrix. Eq. (2.33) implicitly assumes that the spectral density enjoys the *self-averaging* property, meaning that a large single instance of the ensemble faithfully represents the average behaviour over many instances.

The task now is to find the pdf of the inverse variances $\tilde{\pi}(\tilde{\omega})$. Recalling the single-instance relation (2.31) between the single-site inverse variances ω_i and the cavity inverse variances $\omega_j^{(i)}$, the pdf $\tilde{\pi}(\tilde{\omega})$ will be determined in terms of the probability density $\pi(\omega)$ of $\omega_j^{(i)}$.

In order to find the pdf $\pi(\omega)$, two main observations are needed. First, it is worth remarking that we consider configuration model ensembles (such as the Erdős-Rényi ensemble), which are cases of random *uncorrelated* networks, i.e. where degree-degree correlations are absent. In general, in the presence of degree-degree correlations, the probability that a node of degree k is connected to a node of degree k' is conditional, namely $P(k'|k)$. However, for random uncorrelated networks, $P(k'|k)$ is independent of k and therefore $P(k'|k)$ reduces to the probability that an edge points to a node of degree k', which is simply given by $\frac{k'}{c}p(k')$. Indeed, it is defined as the ratio between the fraction of edges pointing to nodes of degree k' , $k'p(k')$, and the fraction of edges pointing to nodes of any degree, i.e. the sum $\sum_{k'} k'p(k') = c$.

Moreover, one also observes that the set of self-consistency equations for the cavity inverse variances (2.29) refers to the *links* of the underlying graph. In an infinitely large network, links can be distinguished from one another by the degree of the node they are pointing to.

Therefore, considering a link (i,j) pointing to a node j of degree k, the value ω of the cavity inverse variance $\omega_j^{(i)}$ living on this link is determined by the set $\{\omega_\ell\}_{k-1}$ of the $k-1$ values of the cavity inverse variances $\omega_\ell^{(j)}$ living on each of the edges connecting j with its neighbours $\ell \in \partial j \backslash i$. In an infinite system, these values can be regarded as $k-1$ independent realisations of the random variables of type $\omega_\ell^{(j)}$, each drawn from the same pdf $\pi(\omega)$. The entries of J appearing in (2.29) are replaced by a set $\{K_\ell\}_{k-1}$ of $k-1$ independent realisations of the random variables $K_{j\ell}$, each distributed according to the bond weights pdf $p_K(K)$. The distribution $\pi(\omega)$ is then obtained by averaging the contributions coming from every link w.r.t. the probability $\frac{k}{c}p(k)$ of having a link pointing to a node of degree k, as defined above. This reasoning leads to the self-consistency equation

$$\pi(\omega) = \sum_{k=1}^{\infty} p(k)\frac{k}{c}\int \{\mathrm{d}\pi\}_{k-1} \left\langle \delta\left(\omega - \left(\mathrm{i}\lambda_\varepsilon + \sum_{\ell=1}^{k-1}\frac{K_\ell^2}{\omega_\ell}\right)\right)\right\rangle_{\{K\}_{k-1}}, \tag{2.34}$$

where $\{\mathrm{d}\pi\}_{k-1} = \prod_{\ell=1}^{k-1}\mathrm{d}\omega_\ell \pi(\omega_\ell)$ and the angle brackets $\langle\cdot\rangle_{\{K\}_{k-1}}$ denote the average over $k-1$ independent realisations of the random variable K. Eq. (2.34) is generally solved via a population dynamics algorithm (see Section 2.6).

The same reasoning can be applied to find the pdf $\tilde{\pi}(\tilde{\omega})$ of inverse variances. Recalling (2.31), it can be noticed that the ω_i are variables related to *nodes*, rather than links. Since in the infinite size limit the nodes can be distinguished from one another by their degree, the pdf $\tilde{\pi}(\tilde{\omega})$ can be written in terms of (2.34) as

$$\tilde{\pi}(\tilde{\omega}) = \sum_{k=0}^{\infty} p(k)\int \{\mathrm{d}\pi\}_{k} \left\langle \delta\left(\tilde{\omega} - \left(\mathrm{i}\lambda_\varepsilon + \sum_{\ell=1}^{k}\frac{K_\ell^2}{\omega_\ell}\right)\right)\right\rangle_{\{K\}_{k}}, \tag{2.35}$$

where $p(k)$ is the degree distribution.

Inserting (2.35) into (2.33) gives (at the ensemble level)

$$\begin{aligned}\rho(\lambda) &= \frac{1}{\pi}\lim_{\varepsilon\to 0}\sum_{k=0}^{\infty} p(k)\mathrm{Re}\int\{\mathrm{d}\pi\}_k \left\langle \frac{1}{\mathrm{i}\lambda_\varepsilon + \sum_{\ell=1}^{k}\frac{K_\ell^2}{\omega_\ell}}\right\rangle_{\{K\}_k} \\ &= \frac{1}{\pi}\lim_{\varepsilon\to 0^+}\sum_{k=0}^{\infty} p(k)\int\{\mathrm{d}\pi\}_k \left\langle \frac{\mathrm{Re}\left[\sum_{\ell=1}^{k}\frac{K_\ell^2}{\omega_\ell}\right]+\varepsilon}{\left(\mathrm{Re}\left[\sum_{\ell=1}^{k}\frac{K_\ell^2}{\omega_\ell}\right]+\varepsilon\right)^2 + \left(\lambda + \mathrm{Im}\left[\sum_{\ell=1}^{k}\frac{K_\ell^2}{\omega_\ell}\right]\right)^2}\right\rangle_{\{K\}_k}.\end{aligned} \tag{2.36}$$

Eq. (2.36) is the ensemble generalisation of the single-instance formula (2.32) and provides the

ensemble average of the spectral density (2.1). The average spectral density as expressed in (2.36) can be interpreted as a weighted sum of local densities, each pertaining to sites of degree k. As shown by (2.36), the solution of the spectral problem is *completely determined* by the distribution π satisfying the self-consistency equation (2.34). Once π has been obtained, the average spectral density (2.36) is evaluated by *sampling* from a large population representing the distribution $\pi(\omega)$. Section 2.6 illustrates the algorithm that produces the solution of self-consistency equations of this type as well as the details of the sampling procedure.

2.3.4 The $c \to \infty$ limit in the cavity formalism

One can easily show that taking the $c \to \infty$ limit in Eq. (2.34), (2.35) and then eventually (2.33), the Wigner semicircle law is recovered. This has been first shown in [36]. According to [54], we consider graphs in the configuration model having a degree distribution with finite mean and variance such that $\frac{\sigma_k^2}{\langle k\rangle^2} = \frac{\langle k^2\rangle - \langle k\rangle^2}{\langle k\rangle^2} \to 0$ as $\langle k\rangle = c \to \infty$. Here, the symbol σ_k denotes the standard deviation of the degree distribution $p(k)$. For example, $\sigma_k = \sqrt{c}$ for Erdős-Rényi graphs.

A meaningful large-c limit is obtained for Eq. (2.34) or equivalently (2.35) by rescaling each instance of the bond random weights as $K_{ij} = \mathscr{K}_{ij}/\sqrt{c}$. Therefore, considering (2.34) one obtains

$$\pi(\omega) = \sum_{k=1}^{\infty} p(k)\frac{k}{c}\int \{\mathrm{d}\pi\}_{k-1}\left\langle \delta\left(\omega - \left(\mathrm{i}\lambda_\varepsilon + \frac{1}{c}\sum_{\ell=1}^{k-1}\frac{\mathscr{K}_\ell^2}{\omega_\ell}\right)\right)\right\rangle_{\{\mathscr{K}\}_{k-1}}, \tag{2.37}$$

where the $\mathscr{K}_\ell$ are independent realisations of the rescaled bond weights of type $\mathscr{K}_{ij}$, each drawn from the same pdf $p_{\mathscr{K}}(\mathscr{K})$. For large c, the sum over the degrees in Eq. (2.37) receives contributions only from $k = c \pm \mathscr{O}(\sigma_k)$. As $c \to \infty$, the degree distribution $p(k)$ becomes highly concentrated around $k = c$, thus the argument of the δ-function on the r.h.s of Eq. (2.37) can be evaluated using the Law of Large Number (LLN). Indeed, one finds that the r.h.s. of the condition

$$\omega = \mathrm{i}\lambda_\varepsilon + \frac{1}{c}\sum_{\ell=1}^{c-1}\frac{\mathscr{K}_\ell^2}{\omega_\ell} \tag{2.38}$$

does not fluctuate, hence ω itself is fixed and determined by the algebraic equation

$$\bar{\omega}_\varepsilon = \mathrm{i}\lambda_\varepsilon + \frac{\langle\mathscr{K}^2\rangle}{\bar{\omega}_\varepsilon} \Leftrightarrow \bar{\omega}_\varepsilon = \frac{\mathrm{i}\lambda_\varepsilon \pm \sqrt{4\langle\mathscr{K}^2\rangle - \lambda_\varepsilon^2}}{2}. \tag{2.39}$$

For large c, the quantity $\langle\mathscr{K}^2\rangle = \frac{1}{c}\sum_{\ell=1}^{c-1}\mathscr{K}_\ell^2 \simeq \frac{1}{c}\sum_{\ell=1}^{c}\mathscr{K}_\ell^2$ represents the second moment of

the pdf of the rescaled bond weights.

The very same reasoning can be applied to the argument of the δ function in (2.35), entailing that in the limit $c \to \infty$ the $\tilde{\omega}$ are non-fluctuating as well, and take the same constant values given by the solutions of Eq. (2.39), viz.

$$\tilde{\pi}(\tilde{\omega}) = \delta(\tilde{\omega} - \bar{\omega}_\varepsilon) \quad \text{as } c \to \infty \,. \tag{2.40}$$

Therefore, inserting Eq. (2.39) and (2.40) in Eq. (2.33), one finds that in the limit $c \to \infty$

$$\begin{aligned} \rho(\lambda) &= \frac{1}{\pi} \lim_{\varepsilon \to 0^+} \mathrm{Re} \left[\frac{1}{\bar{\omega}_\varepsilon} \right] \\ &= \frac{1}{\pi} \lim_{\varepsilon \to 0^+} \mathrm{Re} \left[\frac{2}{\mathrm{i}\lambda_\varepsilon \pm \sqrt{4\langle \mathscr{K}^2 \rangle - \lambda_\varepsilon^2}} \right] \\ &= \frac{1}{2\pi \langle \mathscr{K}^2 \rangle} \lim_{\varepsilon \to 0^+} \mathrm{Re} \left[\mathrm{i}\lambda_\varepsilon \mp \sqrt{4\langle \mathscr{K}^2 \rangle - \lambda_\varepsilon^2} \right] \,, \end{aligned} \tag{2.41}$$

which in the $\varepsilon \to 0^+$ limit eventually reduces to

$$\rho(\lambda) = \begin{cases} \frac{1}{2\pi \langle \mathscr{K}^2 \rangle} \sqrt{4\langle \mathscr{K}^2 \rangle - \lambda^2} & -2\sqrt{\langle \mathscr{K}^2 \rangle} < \lambda < 2\sqrt{\langle \mathscr{K}^2 \rangle} \\ 0 & \text{elsewhere} \end{cases} \,, \tag{2.42}$$

where the plus sign has been chosen to get a physical solution. The latter expression corresponds to the Wigner's semicircle.

2.4 Replica method: the Bray-Rodgers equation

In this section, we illustrate the replica calculation for the average spectral density, as originally proposed by Bray and Rodgers. Following [23], the goal is to evaluate the average spectral density (2.1) of an ensemble of $N \times N$ real symmetric sparse matrices. Leveraging on the notation of Section 2.3, given a matrix J, each matrix entry can be written as $J_{ij} = c_{ij} K_{ij}$, where the $c_{ij} = \{0, 1\}$ represent the pure adjacency matrix of the underlying graph and the K_{ij} encode the bond weights. In particular, the matrix model considered in [23] is the Erdős-Rényi (ER) model: the probability of having a non-zero entry is given by $p = c/N$, where c represents the mean degree of the nodes of the underlying graph. For more details on the ER model, see

Appendix 2.C. The joint distribution of the matrix entries is given by

$$P(\{J_{ij}\}) = \prod_{i<j} p_C(c_{ij})\delta_{c_{ij},c_{ji}} \prod_{i<j} p_K(K_{ij})\delta_{K_{ij},K_{ji}} \,, \tag{2.43}$$

where $p_C(c_{ij})$ represents the ER connectivity distribution, viz.

$$p_C(c_{ij}) = \frac{c}{N}\delta_{c_{ij},1} + \left(1 - \frac{c}{N}\right)\delta_{c_{ij},0} \,, \tag{2.44}$$

while $p_K(K_{ij})$ represents the bond weight pdf, which will be kept unspecified until the very end of the calculation.

2.4.1 Replica derivation

The Edwards-Jones formula (2.2) is used. As anticipated in Section 2.2, in order to deal with the *quenched* average (2.16) the replica identity will be employed, viz.

$$\langle \log Z(\lambda)\rangle_J = \lim_{n\to 0} \frac{1}{n} \log \langle Z(\lambda)^n\rangle_J \,, \tag{2.45}$$

where n is initially taken as an integer [4]. The replica identity is easily obtained considering that in the limit $n \to 0$

$$\log\langle Z(\lambda)^n\rangle_J = \log\left(1 + n\langle \log Z(\lambda)\rangle_J + \mathscr{O}(n^2)\right) \simeq n\langle \log Z(\lambda)\rangle_J \,. \tag{2.46}$$

The average replicated version of the partition function (2.3) reads

$$\langle Z(\lambda)^n\rangle_J = \int \prod_{a=1}^{n}\prod_{i=1}^{N} \mathrm{d}v_{ia} \exp\left(-\frac{\mathrm{i}}{2}\lambda_\varepsilon \sum_{i=1}^{N}\sum_{a=1}^{n} v_{ia}^2\right) \left\langle \exp\left(\frac{\mathrm{i}}{2}\sum_{i,j=1}^{N}\sum_{a=1}^{n} v_{ia}J_{ij}v_{ja}\right)\right\rangle_J \,. \tag{2.47}$$

The ensemble average $\langle ...\rangle_J$ splits into the connectivity average w.r.t. the c_{ij} and the disorder average w.r.t. the K_{ij}. The connectivity average can be performed explicitly exploiting the large N scaling, yielding

$$\left\langle \exp\left(\frac{\mathrm{i}}{2}\sum_{i,j=1}^{N}\sum_{a=1}^{n} v_{ia}J_{ij}v_{ja}\right)\right\rangle_J = \exp\left[\frac{c}{2N}\sum_{i,j=1}^{N}\left(\left\langle \mathrm{e}^{\mathrm{i}K\sum_a v_{ia}v_{ja}}\right\rangle_K - 1\right)\right] \,, \tag{2.48}$$

where $\langle ...\rangle_K$ denotes averaging over $p_K(K)$. The details of the calculation leading to (2.48) can

[4] It is implicitly expected that the average replicated partition function $\langle Z(\lambda)^n\rangle_J$ could be analytically continued in the vicinity of $n = 0$ in a safe manner, although in principle this is not guaranteed.

be found in Appendix 2.D.

In order to decouple sites, the following functional order parameter is introduced,

$$\varphi(\vec{v}) = \frac{1}{N}\sum_{i=1}^{N}\prod_{a=1}^{n}\delta\left(v_a - v_{ia}\right) \ , \tag{2.49}$$

via the path integral identity

$$1 = N\int \mathscr{D}\varphi\mathscr{D}\hat{\varphi}\exp\left[-\mathrm{i}\int \mathrm{d}\vec{v}\hat{\varphi}(\vec{v})\left(N\varphi(\vec{v}) - \sum_{i=1}^{N}\prod_{a=1}^{n}\delta(v_a - v_{ia})\right)\right] \ , \tag{2.50}$$

where $\vec{v}\in\mathbb{R}^n$ represents a n-dimensional vector in the replica space. Eq. (2.50) is the functional analogue of

$$1 = \int \mathrm{d}x\delta(x-\bar{x}) = \int \mathrm{d}x\int\frac{\mathrm{d}k}{2\pi}\mathrm{e}^{-\mathrm{i}k(x-\bar{x})} \ . \tag{2.51}$$

In terms of the order parameter (2.49), the average replicated partition function becomes

$$\begin{aligned}\langle Z(\lambda)^n\rangle_J = N\int \mathscr{D}\varphi\mathscr{D}\hat{\varphi}\exp\left(-\mathrm{i}N\int \mathrm{d}\vec{v}\hat{\varphi}(\vec{v})\varphi(\vec{v})\right)\\ \times\exp\left[\frac{Nc}{2}\int \mathrm{d}\vec{v}\mathrm{d}\vec{v'}\varphi(\vec{v})\varphi(\vec{v'})\left(\left\langle \mathrm{e}^{\mathrm{i}K\sum_a v_a v'_a}\right\rangle_K - 1\right)\right]\\ \times\int\prod_{a=1}^{n}\prod_{i=1}^{N}\mathrm{d}v_{ia}\exp\left[-\frac{\mathrm{i}}{2}\lambda_\varepsilon\sum_{i=1}^{N}\sum_{a=1}^{n}v_{ia}^2 + \mathrm{i}\sum_{i=1}^{N}\int \mathrm{d}\vec{v}\hat{\varphi}(\vec{v})\prod_{a=1}^{n}\delta(v_a - v_{ia})\right] \ .\end{aligned} \tag{2.52}$$

The multiple integral I in the last line of (2.52) factorises into N identical copies of the same n-dimensional integral over $\mathbb{R}^n$. Indeed, one finds

$$\begin{aligned}I &= \int\prod_{a=1}^{n}\prod_{i=1}^{N}\mathrm{d}v_{ia}\exp\left(-\frac{\mathrm{i}}{2}\lambda_\varepsilon\sum_{a=1}^{n}\sum_{i=1}^{N}v_{ia}^2 + \mathrm{i}\sum_{i=1}^{N}\hat{\varphi}(\vec{v}_i)\right)\\ &= \left[\int\prod_{a=1}^{n}\mathrm{d}v_a\exp\left(-\frac{\mathrm{i}}{2}\lambda_\varepsilon\sum_{a=1}^{n}v_a^2 + \mathrm{i}\hat{\varphi}(\vec{v})\right)\right]^N\\ &= \exp\left[N\mathrm{Log}\int \mathrm{d}\vec{v}\exp\left(-\frac{\mathrm{i}}{2}\lambda_\varepsilon\sum_{a=1}^{n}v_a^2 + \mathrm{i}\hat{\varphi}(\vec{v})\right)\right] \ ,\end{aligned} \tag{2.53}$$

where Log denotes again the principal branch of the complex logarithm.

The replicated partition function (2.52) can then be written in the form

$$\langle Z(\lambda)^n\rangle_J \propto \int \mathscr{D}\varphi\mathscr{D}\hat{\varphi}\exp\left(NS_n[\varphi,\hat{\varphi},\lambda]\right) \ , \tag{2.54}$$

where

$$S_n[\varphi,\hat{\varphi},\lambda] = S_1[\varphi,\hat{\varphi}] + S_2[\varphi] + S_3[\hat{\varphi},\lambda] \,, \tag{2.55}$$

with

$$S_1[\varphi,\hat{\varphi}] = -\mathrm{i}N \int \mathrm{d}\vec{v}\hat{\varphi}(\vec{v})\varphi(\vec{v}) \,, \tag{2.56}$$

$$S_2[\varphi] = \frac{c}{2}\int \mathrm{d}\vec{v}\mathrm{d}\vec{v'}\varphi(\vec{v})\varphi(\vec{v'})\left(\left\langle \mathrm{e}^{\mathrm{i}K\sum_a v_a v'_a}\right\rangle_K - 1\right) \,, \tag{2.57}$$

$$S_3[\hat{\varphi},\lambda] = \mathrm{Log}\int \mathrm{d}\vec{v}\exp\left(-\frac{\mathrm{i}}{2}\lambda_\varepsilon\sum_{a=1}^{n} v_a^2 + \mathrm{i}\hat{\varphi}(\vec{v})\right) \,. \tag{2.58}$$

Eq. (2.54) is amenable to a saddle-point evaluation for large N, yielding

$$\langle Z(\lambda)^n\rangle_J \approx \exp\left(NS_n[\varphi^\star,\hat{\varphi}^\star,\lambda]\right) \,, \tag{2.59}$$

where the star denotes the saddle-point value of the order parameter and its conjugate. The stationarity conditions of the action (2.55) w.r.t. the functional order parameter φ and its conjugate $\hat{\varphi}$ give

$$\left.\frac{\delta S_n}{\delta\varphi}\right|_{\varphi^\star,\hat{\varphi}^\star} = 0 \Rightarrow \mathrm{i}\hat{\varphi}^\star(\vec{v}) = \int \mathrm{d}\vec{v'}\varphi^\star(\vec{v'})\left[\left\langle \exp\left(\mathrm{i}K\sum_a v_a v'_a\right)\right\rangle_K - 1\right] \,, \tag{2.60}$$

$$\left.\frac{\delta S_n}{\delta\hat{\varphi}}\right|_{\varphi^\star,\hat{\varphi}^\star} = 0 \Rightarrow \varphi^\star(\vec{v}) = \frac{\exp\left[-\frac{\mathrm{i}}{2}\lambda_\varepsilon\sum_a v_a^2 + \mathrm{i}\hat{\varphi}^\star(\vec{v})\right]}{\int \mathrm{d}\vec{v'}\exp\left[-\frac{\mathrm{i}}{2}\lambda_\varepsilon\sum_a v_a'^2 + \mathrm{i}\hat{\varphi}^\star(\vec{v'})\right]} \,. \tag{2.61}$$

The two stationarity conditions (2.60) and (2.61) can be combined. Indeed, by calling $\mathrm{i}\hat{\varphi}^\star(\vec{v}) = cg(\vec{v})$ and inserting (2.61) in (2.60), one obtains

$$g(\vec{v}) = \frac{\int \mathrm{d}\vec{v'}f(\vec{v}\cdot\vec{v'})\exp\left[-\frac{\mathrm{i}}{2}\lambda_\varepsilon\sum_a v_a'^2 + cg(\vec{v'})\right]}{\int \mathrm{d}\vec{v'}\exp\left[-\frac{\mathrm{i}}{2}\lambda_\varepsilon\sum_a v_a'^2 + cg(\vec{v'})\right]} \,, \tag{2.62}$$

where $f(x) = \langle \mathrm{e}^{\mathrm{i}Kx}\rangle_K - 1$.

2.4.2 Average spectral density: replica symmetry assumption

The function $g(\vec{v})$ defined by (2.62) fully determines the average spectral density. Indeed, recalling (2.2) and using (2.59), one gets

$$\begin{aligned}\rho(\lambda) &= -\frac{2}{\pi N}\lim_{\varepsilon\to 0^+}\mathrm{Im}\frac{\partial}{\partial\lambda}\langle \log Z(\lambda)\rangle_J \\ &= -\frac{2}{\pi N}\lim_{\varepsilon\to 0^+}\mathrm{Im}\frac{\partial}{\partial\lambda}\lim_{n\to 0}\frac{1}{n}\log\langle Z^n(\lambda)\rangle_J \\ &\approx -\frac{2}{\pi N}\lim_{\varepsilon\to 0^+}\mathrm{Im}\frac{\partial}{\partial\lambda}\lim_{n\to 0}\frac{1}{n}\log\left[\exp\left(NS_n[\varphi^\star,\hat{\varphi}^\star,\lambda]\right)\right] \\ &= -\frac{2}{\pi}\lim_{\varepsilon\to 0^+}\mathrm{Im}\lim_{n\to 0}\frac{1}{n}\frac{\partial}{\partial\lambda}S_n[\varphi^\star,\hat{\varphi}^\star,\lambda]\,. \end{aligned} \tag{2.63}$$

The λ-derivative acts only on the terms of the action S_n explicitly depending on λ, due to the stationarity of S_n w.r.t. $\varphi^\star$ and $\hat{\varphi}^\star$. Indeed, one obtains

$$\frac{\partial}{\partial\lambda}S_n[\varphi^\star,\hat{\varphi}^\star,\lambda] = \frac{\partial\varphi}{\partial\lambda}\left.\frac{\delta S_n}{\delta\varphi}\right|_{\varphi=\varphi^\star,\hat{\varphi}=\hat{\varphi}^\star} + \frac{\partial\hat{\varphi}}{\partial\lambda}\left.\frac{\delta S_n}{\delta\hat{\varphi}}\right|_{\varphi=\varphi^\star,\hat{\varphi}=\hat{\varphi}^\star} + \left.\frac{\partial S_n}{\partial\lambda}\right|_{\varphi=\varphi^\star,\hat{\varphi}=\hat{\varphi}^\star} = \frac{\partial S_3[\hat{\varphi}^\star,\lambda]}{\partial\lambda}\,, \tag{2.64}$$

with $S_3[\hat{\varphi}^\star,\lambda]$ defined in (2.58) entailing the ratio

$$\frac{\partial}{\partial\lambda}S_n[\varphi^\star,\hat{\varphi}^\star,\lambda] = \frac{-\frac{\mathrm{i}}{2}\int \mathrm{d}\vec{v}\left(\sum_a v_a^2\right)\exp\left[-\frac{\mathrm{i}\lambda_\varepsilon}{2}\sum_a v_a^2 + cg(\vec{v})\right]}{\int \mathrm{d}\vec{v}\exp\left[-\frac{\mathrm{i}\lambda_\varepsilon}{2}\sum_a v_a^2 + cg(\vec{v})\right]}\,, \tag{2.65}$$

where $g(\vec{v})$ solves (2.62).

In order to perform the $n\to 0$ limit in (2.63), an assumption on the symmetries of the function $g(\vec{v})$, or equivalently of both $\varphi^\star(\vec{v})$ and $\hat{\varphi}^\star(\vec{v})$, under permutations of replica indices needs to be made. It is known that a replica-symmetric "high-temperature" solution, preserving both permutational and rotational symmetry in the replica space, is exact in the random matrix context [5]. Indeed, the "Hamiltonian" of the spectral problem describes a harmonic energy landscape, which only has a single minimum. Therefore, all the replicas will concentrate in this single minimum, excluding replica symmetry breaking. Hence, following [23], one can assume

$$g(\vec{v}) = g(v)\,, \tag{2.66}$$

where $v = |\vec{v}| = \sqrt{\sum_a v_a^2}$. Therefore, taking into account the ratio (2.65), the replica symmetric

[5] Rotational invariance in replica space is a stronger condition than the symmetry upon permutation of replicas. An example of an ansatz satisfying permutational symmetry, but not rotational invariance would be $g(\vec{v}) = g(\sum_{a=1}^n v_a)$.

ansatz (2.66) and that $\mathrm{Im}(\mathrm{i}x) = \mathrm{Re}(x)$ for any $x \in \mathbb{C}$, the average spectral density reads

$$\rho(\lambda) = \frac{1}{\pi} \lim_{\varepsilon \to 0^+} \mathrm{Re} \lim_{n \to 0} \frac{1}{n} \frac{\int \mathrm{d}\vec{v} v^2 \exp\left[-\frac{\mathrm{i}\lambda_\varepsilon}{2} v^2 + c g(v)\right]}{\int \mathrm{d}\vec{v} \exp\left[-\frac{\mathrm{i}\lambda_\varepsilon}{2} v^2 + c g(v)\right]} \,. \tag{2.67}$$

To further simplify the ratio of integrals in (2.67), n-dimensional spherical coordinates are introduced, with the symbol v representing the radial coordinate. The functions in both the numerator and the denominator of Eq. (2.67) have a radial dependency only, hence the factor arising in both in the numerator and denominator of (2.67) from the integration over the angular degrees of freedom cancels, yielding eventually

$$\rho(\lambda) = \frac{1}{\pi} \lim_{\varepsilon \to 0^+} \mathrm{Re} \lim_{n \to 0} \frac{1}{n} \frac{\int_0^\infty \mathrm{d}v v^{n+1} \exp\left[-\frac{\mathrm{i}\lambda_\varepsilon}{2} v^2 + c g(v)\right]}{\int_0^\infty \mathrm{d}v v^{n-1} \exp\left[-\frac{\mathrm{i}\lambda_\varepsilon}{2} v^2 + c g(v)\right]} \,. \tag{2.68}$$

The integral in the denominator can be further simplified integrating by parts, i.e.

$$\int_0^\infty \mathrm{d}v v^{n-1} \exp\left[-\frac{\mathrm{i}\lambda_\varepsilon}{2} v^2 + c g(v)\right] = \frac{1}{n} \int_0^\infty \mathrm{d}v v^n \exp\left[-\frac{\mathrm{i}\lambda_\varepsilon}{2} v^2 + c g(v)\right] \left(\mathrm{i}\lambda_\varepsilon v - c g'(v)\right) \,, \tag{2.69}$$

since the boundary contribution vanishes. Therefore, taking the $n \to 0$ limit, the average spectral density reads

$$\rho(\lambda) = \frac{1}{\pi} \lim_{\varepsilon \to 0^+} \mathrm{Re} \frac{\int_0^\infty \mathrm{d}v v \exp\left[-\frac{\mathrm{i}\lambda_\varepsilon}{2} v^2 + c g(v)\right]}{\int_0^\infty \mathrm{d}v \exp\left[-\frac{\mathrm{i}\lambda_\varepsilon}{2} v^2 + c g(v)\right] \left(\mathrm{i}\lambda_\varepsilon v - c g'(v)\right)} \,. \tag{2.70}$$

The expression (2.70) shows that the function $g(v)$ is the only ingredient needed to compute the average spectral density. The search for a (replica-symmetric) solution of (2.62) will be addressed in Section 2.4.3.

2.4.3 Replica symmetry assumption for the Bray-Rodgers integral equation

At this stage, in order to get a replica-symmetric version of (2.62), the replica-symmetric ansatz (2.66) is applied and spherical coordinates are again introduced. Assuming that $\phi_1 = \phi \in [0, \pi]$ is the angle between the vectors $\vec{v}$ and $\vec{v'}$ and $|\vec{v'}| = r$ one finds

$$g(v) = \frac{\int_0^\infty \mathrm{d}r r^{n-1} \exp\left[-\frac{\mathrm{i}}{2}\lambda_\varepsilon r^2 + c g(r)\right] \int_0^\pi \mathrm{d}\phi (\sin\phi)^{n-2} f(vr\cos\phi)}{\int_0^\infty \mathrm{d}r r^{n-1} \exp\left[-\frac{\mathrm{i}}{2}\lambda_\varepsilon r^2 + c g(r)\right] \int_0^\pi \mathrm{d}\phi (\sin\phi)^{n-2}} \,, \tag{2.71}$$

since all the remaining angular integrations cancel between numerator and denominator. We recall that $f(z) = \langle e^{iKz} \rangle_K - 1$. In order to proceed, a specific bond weight distribution must be introduced. The choice made by Rodgers and Bray in [23],

$$p_K(K) = \frac{1}{2}\delta_{K,1} + \frac{1}{2}\delta_{K,-1} \,, \tag{2.72}$$

entails that $f(z) = \cos z - 1$. This gives

$$g(v) = \frac{\int_0^\infty dr r^{n-1} \exp\left[-\frac{i}{2}\lambda_\varepsilon r^2 + cg(r)\right] \int_0^\pi d\phi (\sin\phi)^{n-2} [\cos(vr\cos\phi) - 1]}{\int_0^\infty dr r^{n-1} \exp\left[-\frac{i}{2}\lambda_\varepsilon r^2 + cg(r)\right] \int_0^\pi d\phi (\sin\phi)^{n-2}} \,. \tag{2.73}$$

The angular integral in the numerator in (2.73) yields (see formula 21 of Section 3.715 in [116])

$$\begin{aligned} I_{\text{num}}^{\text{ang}} &= \int_0^\pi d\phi (\sin\phi)^{n-2} [\cos(vr\cos\phi) - 1] \\ &= \frac{\sqrt{\pi}\Gamma\left(\frac{n-1}{2}\right)}{2} \left[\left(\frac{2}{vr}\right)^{\frac{n}{2}} \left(n J_{\frac{n}{2}}(vr) - vr J_{\frac{n}{2}+1}(vr) \right) - \frac{2}{\Gamma\left(\frac{n}{2}\right)} \right] \,, \end{aligned} \tag{2.74}$$

where $J_\alpha(x)$ indicates the Bessel function of the first kind, defined by the series

$$J_\alpha(x) = \sum_{m=0}^{\infty} \frac{(-1)^m}{m!\Gamma(m+\alpha+1)} \left(\frac{x}{2}\right)^{2m+\alpha} \,. \tag{2.75}$$

The angular integral in the denominator of (2.73) is independent of the radial one and gives

$$I_{\text{den}}^{\text{ang}} = \int_0^\pi d\phi (\sin\phi)^{n-2} = \frac{\sqrt{\pi}\Gamma\left(\frac{n-1}{2}\right)}{\Gamma\left(\frac{n}{2}\right)} \,, \tag{2.76}$$

thus canceling the divergent factor for $n < 1$ appearing in (2.74). The radial integral in the denominator in (2.73) can be simplified integrating by parts. By calling $G(r) = \exp\left[-\frac{i}{2}\lambda_\varepsilon r^2 + cg(r)\right]$, one obtains

$$I_{\text{den}}^{\text{rad}} = \int_0^\infty dr r^{n-1} G(r) = -\frac{1}{n} \int_0^\infty dr r^n G'(r) \,, \tag{2.77}$$

as the boundary contribution vanishes. Collecting the results, one finds

$$g(v) = -\frac{n\Gamma\left(\frac{n}{2}\right)}{2} \frac{\int_0^\infty dr r^{n-1} G(r) \left[\left(\frac{2}{vr}\right)^{\frac{n}{2}} \left(n J_{\frac{n}{2}}(vr) - vr J_{\frac{n}{2}+1}(vr) \right) - \frac{2}{\Gamma\left(\frac{n}{2}\right)} \right]}{\int_0^\infty dr r^n G'(r)} \,. \tag{2.78}$$

Lastly, the $n \to 0$ limit in (2.78) is taken. Recalling the definition of $G(r)$ and noticing

that

1.
$$\Gamma(n) \approx \frac{1}{n} \quad \text{as} \quad n \to 0 \Rightarrow \lim_{n\to 0} -n\Gamma\left(\frac{n}{2}\right) = -2 \,, \tag{2.79}$$

2.
$$\lim_{n\to 0} \int_0^\infty \mathrm{d}r\, r^n G'(r) = \int_0^\infty \mathrm{d}r\, G'(r) = G(\infty) - G(0) = -\mathrm{e}^{cg(0)} \,, \tag{2.80}$$

3.
$$\lim_{n\to 0} r^{n-1} G(r) \left[\left(\frac{2}{vr}\right)^{\frac{n}{2}} \left(n J_{\frac{n}{2}}(vr) - vr J_{\frac{n}{2}+1}(vr) \right) - \frac{2}{\Gamma\left(\frac{n}{2}\right)} \right] = -v J_1(vr) G(r) \,, \tag{2.81}$$

one obtains

$$g(v) = \frac{v \int_0^\infty \mathrm{d}r J_1(vr) \exp\left[-\frac{\mathrm{i}}{2}\lambda_\varepsilon r^2 + cg(r)\right]}{-\mathrm{e}^{cg(0)}} \,. \tag{2.82}$$

Given the structure of Eq. (2.82), it follows that $g(0) = 0$, therefore eventually

$$g(v) = -v \int_0^\infty \mathrm{d}r J_1(vr) \exp\left[-\frac{\mathrm{i}}{2}\lambda_\varepsilon r^2 + cg(r)\right] \,, \tag{2.83}$$

which is equivalent to Eq. (18) in [23]. This equation, also known as the Bray-Rodgers integral equation, fully defines the quantity $g(v)$. Despite numerous attempts, an exact analytical solution for (2.83) is currently not available. The numerical evaluation of Eq. (2.83) in the case of $c = 20$ has been carried out in [117], to obtain the average spectral density of Laplacians of ER graphs with bimodal weights. In this high connectivity regime, the quality of the numerical solution was comparable with the SDA approximation (see [28]). On the other hand, the authors in [19] describe a procedure for the solution of a similar integral equation employing a series expansion which is valid only for $c < 1/2$. Nonetheless, for values of c that are in between these two extremal cases, Eq. (2.83) has proved to be hard to tackle even numerically, due to the exponential non-linearity and the oscillatory Bessel term.

Taking into account Eq. (2.83), the average spectral density (2.70) can be further simplified as follows. Indeed, recalling that $G(v) = \exp\left[-\mathrm{i}\frac{\lambda_\varepsilon}{2}v^2 + cg(v)\right]$, the denominator in Eq. (2.70) can be expressed as

$$I_{\rho,\mathrm{den}} = -\int_0^\infty \mathrm{d}v\, G'(v) = G(0) - G(\infty) = \mathrm{e}^{cg(0)} = 1 \,, \tag{2.84}$$

therefore entailing that the average spectral density reduces to

$$\rho(\lambda) = \frac{1}{\pi} \lim_{\varepsilon \to 0^+} \mathrm{Re} \int_0^\infty \mathrm{d}v \, v \exp\left[-\frac{\mathrm{i}\lambda_\varepsilon}{2} v^2 + c g(v) \right] . \tag{2.85}$$

2.4.4 The average spectral density in the $c \to \infty$ limit

It can be shown that Eq. (2.83) can be solved perturbatively in powers of $1/c$ in the limit $c \to \infty$. In this framework, the average spectral density (2.85) is in turn expressed as a perturbative expansion, whose leading term is the Wigner semicircular law.

One possible way to extract the large c limit of the average spectral density in the replica formalism amounts to considering $K = \mathscr{K}/\sqrt{c}$ in Eq. (2.60), where the distribution of the rescaled weights being $p_{\mathscr{K}}(\mathscr{K}) = \frac{1}{2}\delta_{\mathscr{K},1} + \frac{1}{2}\delta_{\mathscr{K},-1}$, and expanding the exponential through its Taylor series. This choice would result in the conjugate order parameter being expressed as an expansion in powers of $\frac{1}{c}$, given that the odd powers of $\frac{1}{\sqrt{c}}$ are cancelled by the fact that the odd moments of $p_{\mathscr{K}}(\mathscr{K})$ are zero. Assuming that the order parameter (2.61) at the saddle point is expressed as a multivariate factorised zero-mean Gaussian, i.e.

$$\varphi^\star(\vec{v}) = \prod_{a=1}^{n} \frac{\mathrm{e}^{-\frac{v_a^2}{2\sigma^2}}}{\sqrt{2\pi\sigma^2}} , \tag{2.86}$$

the leading order of its conjugate results in a quadratic polynomial in the v_a, namely

$$\mathrm{i}\hat{\varphi}^\star(\vec{v}) = -\frac{\langle \mathscr{K}^2 \rangle_{\mathscr{K}}}{2} \sigma^2 \sum_{a=1}^{n} v_a^2 , \tag{2.87}$$

where σ^2 is determined by the condition

$$\frac{1}{\sigma^2} = \mathrm{i}\lambda_\varepsilon + \langle \mathscr{K}^2 \rangle_{\mathscr{K}} \sigma^2 \Rightarrow \sigma^2 = \frac{-\mathrm{i}\lambda_\varepsilon \pm \sqrt{-\lambda_\varepsilon^2 + 4\langle \mathscr{K}^2 \rangle_{\mathscr{K}}}}{2\langle \mathscr{K}^2 \rangle_{\mathscr{K}}} . \tag{2.88}$$

Using (2.87) and (2.88) in Eq. (2.63), one easily obtains the Wigner semicircle.

Another way to obtain the average spectral density as a perturbative series for large c is an expansion inspired to the one outlined in [23,25], which we detail below. At first, the following

changes of variables are introduced,

$$v^2 = -\frac{2\mathrm{i}s}{\lambda_\varepsilon}\,, \tag{2.89}$$

$$r^2 = -\frac{2\mathrm{i}u}{\lambda_\varepsilon}\,, \tag{2.90}$$

$$\lambda_\varepsilon^2 = cx_\delta^2\,, \tag{2.91}$$

where $x_\delta = x - \mathrm{i}\delta$, with $\delta > 0$. Moreover, it is assumed that $g(v) = \frac{1}{c}\gamma(s)$.

Eq. (2.91) implies rescaling the spectral density such that a meaningful $c \to \infty$ limit can be considered. This rescaling is equivalent to normalising the matrix entries by $\sqrt{c}$. After the change of variables, the spectral density will be expressed in terms of $x_\delta = x - \mathrm{i}\delta$, which does not scale with c. In this setting, the limit $\varepsilon \to 0^+$ is replaced by the limit $\delta \to 0^+$. Taking into account (2.91), for the l.h.s. of Eq. (2.85) before taking the $\varepsilon \to 0^+$ limit one finds

$$\rho(\lambda_\varepsilon) = \rho(x_\delta)\frac{\mathrm{d}x_\delta}{\mathrm{d}\lambda_\varepsilon} = \rho(x_\delta)\frac{1}{\sqrt{c}}\,, \tag{2.92}$$

entailing that

$$\rho(\lambda) = \lim_{\varepsilon\to 0^+}\rho(\lambda_\varepsilon) = \lim_{\delta\to 0^+}\rho(x_\delta)\frac{1}{\sqrt{c}} = \rho(x)\frac{1}{\sqrt{c}}\,. \tag{2.93}$$

One then rewrites Eq. (2.83) in terms of the new variables. The differential in (2.83) transforms as

$$\mathrm{d}r = -\frac{\mathrm{i}}{\lambda_\varepsilon}\sqrt{-\frac{\lambda_\varepsilon}{2\mathrm{i}u}}\mathrm{d}u = -\frac{\mathrm{i}}{\sqrt{c}x_\delta}\sqrt{-\frac{\sqrt{c}x_\delta}{2\mathrm{i}u}}\mathrm{d}u\,, \tag{2.94}$$

while the integration boundaries are unchanged. Indeed, from (2.90), one finds

$$u = \frac{\sqrt{c}r^2\delta}{2} + \mathrm{i}\frac{\sqrt{c}r^2x}{2} = \frac{\sqrt{c}r^2}{2}\sqrt{x^2+\delta^2}\,\mathrm{e}^{\mathrm{i}\arctan\left(\frac{x}{\delta}\right)} = \begin{cases} 0 & r = 0 \\ \infty & r \to \infty \end{cases}\,. \tag{2.95}$$

In terms of the new variables, after some algebra Eq. (2.83) converts to

$$\gamma(s) = \frac{s}{x_\delta^2}\int_0^\infty \mathrm{d}u \exp\left[-u + \gamma(u)\right] \sum_{m=0}^{\infty}\frac{1}{m!(m+1)!}\left(\frac{su}{cx_\delta^2}\right)^m\,, \tag{2.96}$$

corresponding to Eq. (23) in [23].

With these choices, it is natural to expand $\gamma(s)$ as a power series in s/c. High powers of s

are related to high powers of $1/c$. Therefore, one expects to find a solution of the form

$$\gamma(s) = c\sum_{r=1}^{\infty} b_r \left(\frac{s}{c}\right)^r , \tag{2.97}$$

where in turn the coefficients b_r are defined via the expansion

$$b_r = \sum_{\ell=0}^{\infty} \frac{b_r^{(\ell)}}{c^\ell} . \tag{2.98}$$

Eq. (2.97) and (2.98) allow one to obtain all possible combinations of powers of $\frac{s^r}{c^{r+\ell}}$. The target is to determine the coefficients $b_r^{(\ell)}$, by solving Eq. (2.96) order by order. This would permit a complete representation of $\gamma(s)$ as a power series. The following steps will be followed for the solution.

- Express γ via the expansions (2.97) and (2.98) in both the l.h.s. and the exponent of the r.h.s. of (2.96).
- Integrate w.r.t. u term by term in the r.h.s. of (2.96).
- Equate the coefficients of the powers $\frac{s^r}{c^{r+\ell}}$.

The expansion of $\gamma(s)$ will be stopped at $\mathscr{O}\left(\frac{1}{c}\right)$. Hence, the l.h.s. of (2.96) reads

$$\gamma(s) = b_1 s + b_2 \frac{s^2}{c} + \mathscr{O}\left(\frac{s^2}{c^2}\right) = b_1^{(0)} s + b_1^{(1)} \frac{s}{c} + b_2^{(0)} \frac{s^2}{c} + \mathscr{O}\left(\frac{s^2}{c^2}\right) . \tag{2.99}$$

Looking at the r.h.s., one notices that only the terms $m = 0$ and $m = 1$ of the sum in (2.96) are needed to match the powers $\frac{s^r}{c^{r+\ell}}$ in (2.99). Indeed, one finds

$$\gamma(s) = \frac{s}{x_\delta^2}\int_0^\infty \mathrm{d}u \exp\left[-u+\gamma(u)\right] + \frac{s^2}{2cx_\delta^4}\int_0^\infty \mathrm{d}u\, u \exp\left[-u+\gamma(u)\right] + \mathscr{O}\left(\frac{s^2}{c^2}\right) . \tag{2.100}$$

The first and second integral on the r.h.s. of (2.100) can be denoted respectively as I_A and I_B. Considering first the integral I_A, it has a pre-factor of order $\mathscr{O}(s)$, therefore it may yield contributions of any order in powers of $1/c$ depending on the order at which we stop the expansion of $\gamma(u)$ in the exponent. Expanding $\gamma(u)$ as in (2.99) is sufficient to obtain all the

$\mathscr{O}(1)$ and $\mathscr{O}\left(\frac{1}{c}\right)$ contributions. Indeed, we have

$$\begin{aligned} I_A &= \int_0^\infty \mathrm{d}u \exp\left[-u+\gamma(u)\right] \\ &\simeq \int_0^\infty \mathrm{d}u \exp\left[\frac{b_2^{(0)}}{c}u^2 + \left(b_1^{(0)} - 1 + \frac{b_1^{(1)}}{c}\right)u\right] \\ &= \frac{\sqrt{\pi}}{2\sqrt{-\frac{b_2^{(0)}}{c}}} \mathrm{e}^{y^2} \mathrm{erfc}(y) \,, \end{aligned} \tag{2.101}$$

where

$$y = -\frac{b_1^{(0)} - 1 + \frac{b_1^{(1)}}{c}}{2\sqrt{-\frac{b_2^{(0)}}{c}}} \,, \tag{2.102}$$

and $\mathrm{Re}\left(\frac{b_2^{(0)}}{c}\right) < 0$. The function denoted by $\mathrm{erfc}(z)$ is the complementary error function, defined for real z as

$$\mathrm{erfc}(z) = \frac{2}{\sqrt{\pi}} \int_z^\infty \mathrm{d}t \; \mathrm{e}^{-t^2} \,. \tag{2.103}$$

In order to express (2.101) as a power series, an asymptotic expansion of $\mathrm{erfc}(z)$ is employed. For large real z it is given by

$$\mathrm{erfc}(z) \simeq \frac{e^{-z^2}}{z\sqrt{\pi}} \left[1 + \sum_{n=1}^{\infty} (-1)^n \frac{(2n)!}{n!(2z)^{2n}}\right] \,. \tag{2.104}$$

The series is divergent for any finite z. However, few terms of it are sufficient to approximate $\mathrm{erfc}(z)$ well for any finite z. Using (2.104) in (2.101), one obtains

$$\begin{aligned} I_A &\approx -\frac{1}{b_1^{(0)} - 1 + \frac{b_1^{(1)}}{c}} \left[1 + \sum_{n=1}^{\infty} \frac{(2n)! \left(\frac{b_2^{(0)}}{c}\right)^n}{n! \left(b_1^{(0)} - 1 + \frac{b_1^{(1)}}{c}\right)^{2n}}\right] \\ &= -\frac{1}{b_1^{(0)} - 1 + \frac{b_1^{(1)}}{c}} - \sum_{n=1}^{\infty} \frac{(2n)!}{n!} \left(\frac{b_2^{(0)}}{c}\right)^n \frac{1}{\left(b_1^{(0)} - 1 + \frac{b_1^{(1)}}{c}\right)^{2n+1}} \,. \end{aligned} \tag{2.105}$$

Eq. (2.105) can be further simplified recalling that $(1+\beta x)^\alpha \approx 1 + \alpha\beta x$ for $x \ll 1$, entailing that the first term of (2.105) becomes

$$-\frac{1}{b_1^{(0)} - 1 + \frac{b_1^{(1)}}{c}} \approx \frac{1}{1 - b_1^{(0)}} + \frac{b_1^{(1)}}{\left(1 - b_1^{(0)}\right)^2} \frac{1}{c} \,. \tag{2.106}$$

Since the expansion is stopped at $\mathscr{O}\left(\frac{1}{c}\right)$, only the $n=1$ term in the sum in (2.105) needs to be considered, as the contributions for $n \geq 2$ are at least $\mathscr{O}\left(\frac{1}{c^2}\right)$. Moreover, since the $n=1$ term exhibits the $\mathscr{O}\left(\frac{1}{c}\right)$ scaling explicitly, only the $\mathscr{O}(1)$ contribution arising from the round brackets in the denominator of the general term of the sum in (2.105) must be taken into account. Indeed, using (2.106) the $n=1$ term in (2.105) becomes

$$\begin{aligned} 2\frac{b_2^{(0)}}{c}\left(-\frac{1}{b_1^{(0)}-1+\frac{b_1^{(1)}}{c}}\right)^3 &\approx 2\frac{b_2^{(0)}}{c}\left(\frac{1}{1-b_1^{(0)}}+\frac{b_1^{(1)}}{\left(1-b_1^{(0)}\right)^2}\frac{1}{c}\right)^3 \\ &= 2\frac{b_2^{(0)}}{\left(1-b_1^{(0)}\right)^3}\frac{1}{c}+\mathscr{O}\left(\frac{1}{c^2}\right) . \end{aligned} \tag{2.107}$$

Collecting all the leading contributions to the integral I_A one obtains

$$I_A=\int_0^\infty \mathrm{d}u \exp\left[-u+\gamma(u)\right]=\frac{1}{1-b_1^{(0)}}+\frac{1}{c}\left[\frac{b_1^{(1)}}{\left(1-b_1^{(0)}\right)^2}+\frac{2b_2^{(0)}}{\left(1-b_1^{(0)}\right)^3}\right]+\mathscr{O}\left(\frac{1}{c^2}\right) . \tag{2.108}$$

Considering now the second integral on the r.h.s. of (2.100), denoted by I_B, its pre-factor has already the $\mathscr{O}\left(\frac{1}{c}\right)$ scaling. Therefore, only the $\mathscr{O}(1)$ term arising from the $\frac{1}{c}$ expansion of I_B is needed. To this purpose, it is sufficient to consider the expansion of $\gamma(u)$ no further than $\mathscr{O}\left(\frac{u}{c}\right)$. Indeed, one finds

$$\begin{aligned} I_B &= \int_0^\infty \mathrm{d}u\, u \exp\left[-u+\gamma(u)\right] \\ &\approx \int_0^\infty \mathrm{d}u\, u \exp\left[-\left(1-b_1^{(0)}-\frac{b_1^{(1)}}{c}\right)u\right] \\ &\approx \frac{1}{\left(1-b_1^{(0)}\right)^2}+\mathscr{O}\left(\frac{1}{c}\right) , \end{aligned} \tag{2.109}$$

with $\mathrm{Re}\left(1-b_1^{(0)}-\frac{b_1^{(1)}}{c}\right)>0$.

In conclusion, using the expansions of I_A and I_B, respectively given by Eq. (2.108) and (2.109), Eq. (2.100) representing the r.h.s. of (2.96) becomes

$$\gamma(s)=\frac{1}{x_\delta^2\left(1-b_1^{(0)}\right)}s+\frac{1}{x_\delta^2}\left[\frac{b_1^{(1)}}{\left(1-b_1^{(0)}\right)^2}+2\frac{b_2^{(0)}}{\left(1-b_1^{(0)}\right)^3}\right]\frac{s}{c}+\frac{1}{2x_\delta^4}\frac{1}{\left(1-b_1^{(0)}\right)^2}\frac{s^2}{c}+\mathscr{O}\left(\frac{s^2}{c^2}\right) . \tag{2.110}$$

Equating term by term the expansion in Eq. (2.99) and (2.110), one gets a closed set of equations to determine the three coefficients $b_1^{(0)}$, $b_1^{(1)}$ and $b_2^{(0)}$, viz.

$$\mathscr{O}(s): \quad b_1^{(0)} = \frac{1}{x_\delta^2\left(1-b_1^{(0)}\right)}\,, \tag{2.111}$$

$$\mathscr{O}\left(\frac{s}{c}\right): \quad b_1^{(1)} = \frac{1}{x_\delta^2}\left[\frac{b_1^{(1)}}{\left(1-b_1^{(0)}\right)^2}+\frac{2b_2^{(0)}}{\left(1-b_1^{(0)}\right)^3}\right]\,, \tag{2.112}$$

$$\mathscr{O}\left(\frac{s^2}{c}\right): \quad b_2^{(0)} = \frac{1}{2x_\delta^4\left(1-b_1^{(0)}\right)^2}\,, \tag{2.113}$$

corresponding to Eq. (25), (26) and (27) in [23]. The latter system of equations can be easily solved, yielding

$$b_1^{(0)} = \frac{1}{2}\left[1\pm A^{\frac{1}{2}}\right]\,, \tag{2.114}$$

$$b_1^{(1)} = \mp\frac{{x_\delta}^2}{16}\frac{\left[1\pm A^{\frac{1}{2}}\right]^4}{A^{\frac{1}{2}}}\,, \tag{2.115}$$

$$b_2^{(0)} = \frac{1}{2}\left(b_1^{(0)}\right)^2\,, \tag{2.116}$$

where $A = 1-\frac{4}{x_\delta^2}$.

Finally, the average spectral density (2.85) can be evaluated perturbatively. Indeed, taking into account Eq. (2.93) and applying the change of variables (2.89), (2.91) and $g(v)=\frac{1}{c}\gamma(s)$ to the r.h.s. of Eq. (2.85), one finds

$$\begin{aligned}\rho(x)\frac{1}{\sqrt{c}} &= \frac{1}{\pi}\lim_{\delta\to 0^+}\mathrm{Re}\left[\left(-\frac{\mathrm{i}}{\sqrt{c}x_\delta}\right)\int_0^\infty \mathrm{d}s\exp\left[-s+\gamma(s)\right]\right]\Rightarrow\\ \rho(x) &= \frac{1}{\pi}\lim_{\delta\to 0^+}\mathrm{Im}\left[\frac{1}{x-\mathrm{i}\delta}\int_0^\infty \mathrm{d}s\exp\left[-s+\gamma(s)\right]\right]\,,\end{aligned} \tag{2.117}$$

where the dependence on c is only through the power series (2.97) expressing $\gamma(s)$.

The goal is to obtain the $\mathscr{O}(1)$ leading term dominating in Eq. (2.117) for large c, along with its $\mathscr{O}(1/c)$ correction. It is worth noticing that the integral appearing on the r.h.s. of Eq. (2.117) has been already evaluated up to $\mathscr{O}(\frac{1}{c})$. Indeed, it corresponds to the integral I_A of Eq. (2.108). Therefore, using (2.108) in (2.117) one gets

$$\rho(x) = \rho_0(x)+\frac{1}{c}\rho_1(x)+\mathscr{O}\left(\frac{1}{c^2}\right)\,, \tag{2.118}$$

where

$$\rho_0(x) = \frac{1}{\pi} \lim_{\delta \to 0^+} \mathrm{Im} \left[\frac{1}{x - \mathrm{i}\delta} \frac{1}{1 - b_1^{(0)}} \right] , \tag{2.119}$$

$$\rho_1(x) = \frac{1}{\pi} \lim_{\delta \to 0^+} \mathrm{Im} \left[\frac{1}{x - \mathrm{i}\delta} \left(\frac{b_1^{(1)}}{\left(1 - b_1^{(0)}\right)^2} + \frac{2 b_2^{(0)}}{\left(1 - b_1^{(0)}\right)^3} \right) \right] , \tag{2.120}$$

and the coefficients $b_1^{(0)}$, $b_1^{(1)}$ and $b_2^{(0)}$ have been defined respectively in (2.114), (2.115) and (2.116).

The $\mathscr{O}(1)$ leading term $\rho_0(x)$ in Eq. (2.119) is simply obtained by observing that

$$\mathrm{Im} \left[\frac{1}{x - \mathrm{i}\delta} \frac{1}{1 - b_1^{(0)}} \right] = \frac{1}{2} \mathrm{Im} \left[x - \mathrm{i}\delta \pm \sqrt{(x - \mathrm{i}\delta)^2 - 4} \right] . \tag{2.121}$$

Using (2.121), considering the imaginary part and taking the $\delta \to 0^+$ limit, the $\mathscr{O}(1)$ leading term in Eq. (2.118) becomes

$$\rho_0(x) = \begin{cases} \frac{1}{2\pi} \sqrt{4 - x^2} & -2 < x < 2 \\ 0 & \text{elsewhere} \end{cases} , \tag{2.122}$$

where we have used that

$$\mathrm{Im} \left[\sqrt{y} \right] = \begin{cases} \sqrt{-y} & y < 0 \\ 0 & y > 0 \end{cases} , \tag{2.123}$$

and the plus sign in front of the square root has been chosen in order to get a physical (non-negative) solution. This sign choice amounts to selecting the top alternative for the signs appearing in the expansion coefficients (2.114), (2.115) and (2.116). Eq. (2.122) corresponds to the Wigner's semicircle as expected.

Similarly, using the definitions (2.114), (2.115) and (2.116), taking the $\delta \to 0^+$ limit and employing the property (2.123), after some algebra the $\mathscr{O}\left(\frac{1}{c}\right)$ correction (2.120) is obtained as

$$\rho_1(x) = \begin{cases} \frac{x^4 - 4x^2 + 2}{2\pi\sqrt{4 - x^2}} & -2 < x < 2 \\ 0 & \text{elsewhere} \end{cases} , \tag{2.124}$$

where the sign is determined by the same sign convention for the coefficients of the expansion

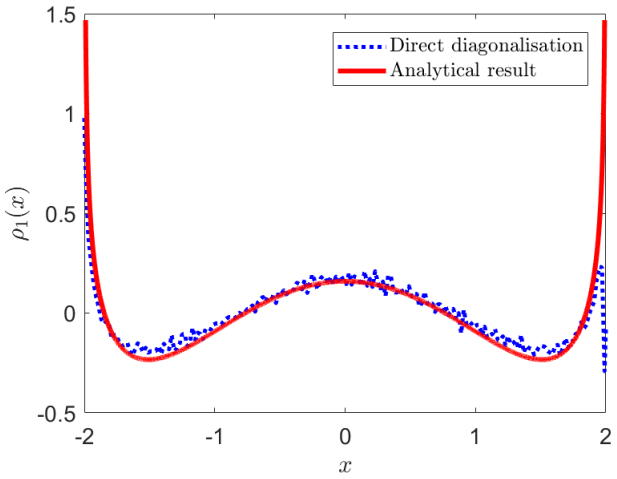

Figure 2.2: The $\mathscr{O}(1/c)$ correction $\rho_1(x)$ found in Eq. (2.124) to the average spectral density of ER matrices with bimodal weights distribution in the large c limit (red line), compared to the histogram of 9.99×10^6 eigenvalues of matrices from the ER ensemble with $c=50$ and bond weight distribution $p_K(K)=\frac{1}{2}\delta_{K,1/\sqrt{c}}+\frac{1}{2}\delta_{K,-1/\sqrt{c}}$ (blue dotted line). The $\mathscr{O}(1)$ contribution $\rho_0(x)$ in Eq. (2.122) has been removed from the histogram.

adopted for the evaluation of $\rho_0(x)$. The correction (2.124) is non-zero only in the interval $-2<x<2$ and diverges at the edges. Moreover, one can notice that the total average spectral density (2.118) is correctly normalised up to order $\mathscr{O}\left(\frac{1}{c}\right)$, given that the integral of the correction (2.124) over its domain $-2<x<2$ is zero.

In Fig. 2.2, we compare the analytical expression for $\rho_1(x)$ against the data from direct diagonalisation of sparse ER matrices, with bond weights distribution $p_K(K)=\frac{1}{2}\delta_{K,1/\sqrt{c}}+\frac{1}{2}\delta_{K,-1/\sqrt{c}}$, in the case of $c=50$. We obtained the eigenvalues of 10000 matrices of size $N=1000$ and discarded the isolated contribution due to the top eigenvalue of such matrices, which lies outside the spectrum. We then organised the remaining 9.99×10^6 eigenvalues in a normalised histogram and removed from the data the semicircular contribution $\rho_0(x)$ evaluated at the middle-point of each histogram bin. We found a very good agreement between the analytical curve representing $\rho_1(x)$ (red line) and the numerical diagonalisation data (blue dotted line).

2.5 Alternative Replica solution: uncountably infinite superposition of Gaussians

Kühn in [33] suggested a different approach for the average spectral density problem, which completely bypasses (2.83). At the outset, the treatment in [33] is the same as in [23], but departs from the Bray-Rodgers original derivation at the level of the stationarity conditions (2.60) and (2.61). The order parameter $\varphi(\vec{v})$ and its conjugate $\mathrm{i}\hat{\varphi}(\vec{v})$ are represented as an

uncountably infinite superposition of complex Gaussians, i.e.

$$\varphi(\vec{v}) = \int \mathrm{d}\omega\pi(\omega) \prod_{a=1}^{n} \frac{\mathrm{e}^{-\frac{\omega}{2}v_a^2}}{Z(\omega)} , \tag{2.125}$$

$$\mathrm{i}\hat{\varphi}(\vec{v}) = \hat{c} \int \mathrm{d}\hat{\omega}\hat{\pi}(\hat{\omega}) \prod_{a=1}^{n} \frac{\mathrm{e}^{-\frac{\hat{\omega}}{2}v_a^2}}{Z(\hat{\omega})} , \tag{2.126}$$

where $Z(x) = \sqrt{\frac{2\pi}{x}}$ and $\pi(\omega)$ and $\hat{\pi}(\hat{\omega})$ are normalised pdfs of the inverse variances ω and $\hat{\omega}$[6] with $\mathrm{Re}(\omega), \mathrm{Re}(\hat{\omega}) \geq 0$. The constant $\hat{c}$ is chosen to enforce the normalisation of $\hat{\pi}(\hat{\omega})$.

Eq. (2.125) and (2.126) are expansions of φ and $\hat{\varphi}$ in an over-complete function system. One can also notice that $\pi(\omega)$ is the inverse Laplace transform of φ, if one consider φ as a function of the v_a^2. The structure of this ansatz derives from the study of models for amorphous systems. In that context, it was noticed that harmonically coupled systems — such as the model defined by our "Hamiltonian" (2.5) — admit a solution in terms of superposition of Gaussian [34, 118]. This ansatz exhibits permutation symmetry among replicas as well as rotational symmetry in replica space, therefore sharing the same symmetries assumed in [23] (see Eq. (2.66)). The advantage of the ansätze (2.125) and (2.126) is that they allow us to extract the leading contribution to the saddle-point of (2.54) in the limits $N \to \infty$ and $n \to 0$.

The path integral over the φ and $\hat{\varphi}$ is thus replaced by a path integral over π and $\hat{\pi}$. Therefore, Eq. (2.54) becomes

$$\langle Z(\lambda)^n \rangle_J \propto \int \mathscr{D}\pi \mathscr{D}\hat{\pi} \exp\left(N S_n[\pi, \hat{\pi}, \lambda]\right) , \tag{2.127}$$

where

$$S_n[\pi, \hat{\pi}, \lambda] = S_1[\pi, \hat{\pi}] + S_2[\pi] + S_3[\hat{\pi}, \lambda] , \tag{2.128}$$

and

$$S_1[\pi, \hat{\pi}] = -\hat{c} - n\hat{c} \int \mathrm{d}\pi(\omega)\mathrm{d}\hat{\pi}(\hat{\omega}) \log \frac{Z(\omega + \hat{\omega})}{Z(\omega)Z(\hat{\omega})} , \tag{2.129}$$

$$S_2[\pi] = n\frac{c}{2} \int \mathrm{d}\pi(\omega)\mathrm{d}\pi(\omega') \left\langle \log \frac{Z_2(\omega, \omega', K)}{Z(\omega)Z(\omega')} \right\rangle_K , \tag{2.130}$$

$$S_3[\hat{\pi}, \lambda] = \hat{c} + n \sum_{k=0}^{\infty} p_{\hat{c}}(k) \int \{\mathrm{d}\hat{\pi}\}_k \log \frac{Z(\mathrm{i}\lambda_\varepsilon + \{\hat{\omega}\}_k)}{\prod_{\ell=1}^{k} Z(\hat{\omega}_\ell)} . \tag{2.131}$$

In the latter expressions, the shorthands $\mathrm{d}\pi = \mathrm{d}\omega\pi(\omega)$, $\{\mathrm{d}\hat{\pi}\}_k = \prod_{\ell=1}^{k} \mathrm{d}\hat{\omega}_\ell\hat{\pi}(\hat{\omega}_\ell)$ and $\{\hat{\omega}\}_k =$

[6] We employ the same labels used in the cavity treatment, as the two objects will eventually coincide.

$\sum_{\ell=1}^{k}\hat{\omega}_\ell$ have been used. Moreover, $Z_2(\omega,\omega',K)=Z(\omega)Z(\omega'+\frac{K^2}{\omega})$. The function $p_{\hat{c}}(k)$ is the Poisson degree distribution $p_{\hat{c}}(k)=\frac{\mathrm{e}^{-\hat{c}}\hat{c}^k}{k!}$, which naturally crops up in the calculation when representing $\mathrm{e}^{\mathrm{i}\hat{\varphi}^\star(\vec{v})}$ appearing in (2.61) as a power series. The derivation of (2.129), (2.130) and (2.131) is detailed in Appendix 2.E. We notice that the $\mathscr{O}(1)$ contributions in (2.129) and (2.131) cancel each other, making the action (2.128) of $\mathscr{O}(n)$.

The stationarity conditions (2.60) and (2.61) are replaced by the stationarity conditions w.r.t. π and $\hat{\pi}$. They are

$$\begin{aligned}&\frac{\delta S_n}{\delta\pi}=0\Rightarrow\\&\frac{\hat{c}}{c}\int \mathrm{d}\hat{\pi}\log\frac{Z(\omega+\hat{\omega})}{Z(\omega)Z(\hat{\omega})}=\int\mathrm{d}\pi'\left\langle\log\frac{Z_2(\omega,\omega',K)}{Z(\omega)Z(\omega')}\right\rangle_K+\frac{\gamma}{c}\,,\end{aligned}\tag{2.132}$$

and

$$\begin{aligned}&\frac{\delta S_n}{\delta\hat{\pi}}=0\Rightarrow\\&\int\mathrm{d}\pi\log\frac{Z(\omega+\hat{\omega})}{Z(\omega)Z(\hat{\omega})}=\sum_{k=1}^{\infty}p_{\hat{c}}(k)\frac{k}{\hat{c}}\int\{\mathrm{d}\hat{\pi}\}_{k-1}\log\frac{Z(\mathrm{i}\lambda_\varepsilon+\{\hat{\omega}\}_{k-1}+\hat{\omega})}{Z(\hat{\omega})\prod_{\ell=1}^{k-1}Z(\hat{\omega}_\ell)}+\frac{\hat{\gamma}}{\hat{c}}\,,\end{aligned}\tag{2.133}$$

where γ and $\hat{\gamma}$ are two Lagrange multipliers to enforce the normalisation condition of π and $\hat{\pi}$. The equality (2.132) is realised by making sure that γ satisfies the equality

$$-\frac{\hat{c}}{c}\int\mathrm{d}\hat{\pi}(\hat{\omega})\log Z(\hat{\omega})=\frac{\gamma}{c}\,,\tag{2.134}$$

while the remaining part (which is a function of ω) should satisfy

$$\frac{\hat{c}}{c}\int\mathrm{d}\hat{\pi}(\hat{\omega})\log\frac{Z(\omega+\hat{\omega})}{Z(\omega)}=\int\mathrm{d}\pi(\omega')\left\langle\log\frac{Z\left(\omega+\frac{K^2}{\omega'}\right)}{Z(\omega)}\right\rangle_K\,,\tag{2.135}$$

where $Z_2(\omega,\omega',K)=Z(\omega')Z(\omega+\frac{K^2}{\omega'})$ has been used. Since eq. (2.135) must hold for any value of ω in order for (2.132) to be satisfied, one notices that the following definition

$$\hat{\pi}(\hat{\omega})=\frac{\hat{c}}{c}\int\mathrm{d}\pi(\omega)\left\langle\delta\left(\hat{\omega}-\frac{K^2}{\omega}\right)\right\rangle_K\,,\tag{2.136}$$

once inserted in the l.h.s. of (2.136), indeed produces the r.h.s. Likewise, also in (2.133) a

constant part can be isolated,

$$-\int \mathrm{d}\pi(\omega)\log Z(\omega) = -\sum_{k=1}^{\infty} p_{\hat{c}}(k)\frac{k}{\hat{c}}\int \{\mathrm{d}\hat{\pi}\}_{k-1}\log\prod_{\ell=1}^{k-1} Z(\hat{\omega}_\ell) + \frac{\hat{\gamma}}{\hat{c}}\,, \tag{2.137}$$

and a part that is a function of $\hat{\omega}$, viz.

$$\int \mathrm{d}\pi(\omega)\log\frac{Z(\omega+\hat{\omega})}{Z(\hat{\omega})} = \sum_{k=1}^{\infty} p_{\hat{c}}(k)\frac{k}{\hat{c}}\int \{\mathrm{d}\hat{\pi}\}_{k-1}\log\frac{Z(\mathrm{i}\lambda_\varepsilon + \{\hat{\omega}\}_{k-1}+\hat{\omega})}{Z(\hat{\omega})}\,. \tag{2.138}$$

As before, since (2.138) must hold for any $\hat{\omega}$, it follows that

$$\pi(\omega) = \sum_{k=1}^{\infty} p_{\hat{c}}(k)\frac{k}{\hat{c}}\int \{\mathrm{d}\hat{\pi}\}_{k-1}\,\delta\left(\omega - (\mathrm{i}\lambda_\varepsilon + \{\hat{\omega}\}_{k-1})\right)\,. \tag{2.139}$$

In order for both $\hat{\pi}$ and π to be normalised to 1, the condition $\hat{c} = c$ must be imposed.

2.5.1 Average spectral density unfolded

The solutions of the two coupled functional equations

$$\hat{\pi}(\hat{\omega}) = \int \mathrm{d}\pi(\omega)\left\langle \delta\left(\hat{\omega} - \frac{K^2}{\omega}\right)\right\rangle_K\,, \tag{2.140}$$

$$\pi(\omega) = \sum_{k=1}^{\infty} p_c(k)\frac{k}{c}\int \{\mathrm{d}\hat{\pi}\}_{k-1}\,\delta\left(\omega - \left(\mathrm{i}\lambda_\varepsilon + \sum_{\ell=1}^{k-1}\hat{\omega}_\ell\right)\right)\,, \tag{2.141}$$

represent the saddle-point evaluation of (2.127). The symbol $p_c(k)$ represents the Poisson degree distribution, which is expected for ER sparse graphs. However, it has been shown in [1, 34, 44] that the above equations hold *unmodified* also for *any* non-Poissonian degree distributions $p(k)$ within the configuration model framework, as long as the mean degree $\langle k\rangle = c$ is a finite constant, i.e. does not scale with N, and the variance is finite. Unlike (2.83), the equations (2.140) and (2.141) can be very efficiently solved numerically by a population dynamics algorithm (see Section 2.6). Some remarks are in order.

- Inserting (2.140) into (2.141) yields a unique self-consistency equation for π that is exactly identical to (2.34), obtained using the cavity method in the thermodynamic limit. This fact demonstrates once more the equivalence between the replica and cavity methods.

- Alternatively, one could insert (2.141) into (2.140), obtaining a single self-consistency

equation for $\hat{\pi}$ that reads

$$\hat{\pi}(\hat{\omega}) = \sum_{k=1}^{\infty} p_c(k) \frac{k}{c} \int \{\mathrm{d}\hat{\pi}\}_{k-1} \left\langle \delta\left(\hat{\omega} - \frac{K^2}{\mathrm{i}\lambda_\varepsilon + \sum_{\ell=1}^{k-1} \hat{\omega}_\ell}\right)\right\rangle_K . \tag{2.142}$$

The solution of the latter equation via a population dynamics algorithm will be described below in Section 2.6. While the two approaches are equivalent, here we choose to work with the $\{\hat{\omega}\}$ since the final equation for the spectral density is more naturally expressed in terms of those, as shown in the following.

The pdf $\hat{\pi}(\hat{\omega})$ defined in (2.142) *fully determines* the average spectral density. Indeed, recalling (2.2) one gets

$$\begin{aligned}
\rho(\lambda) &= -\frac{2}{\pi N} \lim_{\varepsilon\to 0^+} \mathrm{Im} \frac{\partial}{\partial \lambda} \langle \log Z(\lambda)\rangle_J \\
&\simeq -\frac{2}{\pi} \lim_{\varepsilon\to 0^+} \mathrm{Im} \lim_{n\to 0} \frac{1}{n} \frac{\partial}{\partial \lambda} S_3[\hat{\pi}, \lambda] \\
&= \frac{1}{\pi} \lim_{\varepsilon\to 0^+} \sum_{k=0}^{\infty} p_c(k) \mathrm{Re} \int \{\mathrm{d}\hat{\pi}\}_k \frac{1}{\mathrm{i}\lambda_\varepsilon + \{\hat{\omega}\}_k} \\
&= \frac{1}{\pi} \lim_{\varepsilon\to 0^+} \sum_{k=0}^{\infty} p_c(k) \int \{\mathrm{d}\hat{\pi}\}_k \frac{\mathrm{Re}\left[\{\hat{\omega}\}_k\right] + \varepsilon}{\left(\mathrm{Re}\left[\{\hat{\omega}\}_k\right] + \varepsilon\right)^2 + \left(\lambda + \mathrm{Im}\left[\{\hat{\omega}\}_k\right]\right)^2} ,
\end{aligned} \tag{2.143}$$

where the latter expression corresponds to Eq. (33) in [33]. We notice that (2.143) is completely equivalent to (2.36) if $\hat{\pi}(\hat{\omega})$ is expressed in terms of $\pi(\omega)$ according to (2.140). All the observations made about (2.36) hold here as well. The average spectral density as expressed in (2.143) is evaluated by sampling from a large population distributed according to $\hat{\pi}(\hat{\omega})$: this procedure will also be illustrated in Section 2.6.

2.5.2 Singular contributions, the presence of localised states and the role of ε

The average spectral density (2.143) can be rewritten in order to isolate singular pure-point contributions from the continuous spectrum. Indeed, defining

$$P(a,b) = \sum_{k=0}^{\infty} p_c(k) \int \{\mathrm{d}\hat{\pi}\}_k \delta\left(a - \mathrm{Re}[\{\hat{\omega}\}_k]\right) \delta\left(b - \mathrm{Im}[\{\hat{\omega}\}_k]\right) , \tag{2.144}$$

one finds the identity

$$\rho(\lambda) = \frac{1}{\pi} \lim_{\varepsilon\to 0^+} \int \mathrm{d}a\mathrm{d}b P(a,b) \frac{a+\varepsilon}{(a+\varepsilon)^2 + (\lambda + b)^2} . \tag{2.145}$$

The integrand in (2.145) becomes singular as $\varepsilon \to 0$ for $a = 0$. These singular contributions can be isolated representing $P(a,b)$ as

$$P(a,b) = P_0(b)\delta(a) + \tilde{P}(a,b) \,, \tag{2.146}$$

yielding for the spectral density

$$\rho(\lambda) = \frac{1}{\pi} \lim_{\varepsilon\to 0^+} \int \mathrm{d}b P_0(b) \mathscr{L}_\varepsilon(\lambda+b) + \frac{1}{\pi} \lim_{\varepsilon\to 0^+} \int_{a>0} \mathrm{d}a\mathrm{d}b \tilde{P}(a,b) \frac{a+\varepsilon}{(a+\varepsilon)^2 + (\lambda+b)^2} \,. \tag{2.147}$$

Here, $\mathscr{L}_\varepsilon(\lambda+b)$ is a Cauchy distribution with scale (half-width at half-maximum) parameter ε, viz.

$$\mathscr{L}_\varepsilon(\lambda+b) = \frac{1}{\pi} \frac{\varepsilon}{\varepsilon^2 + (\lambda+b)^2} \xrightarrow[\varepsilon\to 0^+]{} \delta(\lambda+b) \,, \tag{2.148}$$

that reduces to a delta-peak in $b = -\lambda$ for any value of λ as $\varepsilon \to 0^+$. The spectral density $\rho(\lambda)$ can then be easily evaluated by sampling (see Section 2.6) from the population of the a and b (i.e. the $\hat{\omega}$). Relying on the law of large numbers and calling $\mathscr{M}$ the number of samples $\{(a_i, b_i)\}$, the two integrals in (2.147) can indeed be rewritten as

$$\begin{aligned} \rho(\lambda) &\simeq \rho_S(\lambda) + \rho_C(\lambda) \\ &\simeq \frac{1}{\mathscr{M}} \sum_{i=0 \wedge a_i = 0}^{\mathscr{M}} \mathscr{L}_\varepsilon(\lambda + b_i) + \frac{1}{\pi\mathscr{M}} \sum_{i=0 \wedge a_i > 0}^{\mathscr{M}} \frac{a_i + \varepsilon}{(a_i+\varepsilon)^2 + (\lambda+b_i)^2} \,, \end{aligned} \tag{2.149}$$

where $\rho_S(\lambda)$ and $\rho_C(\lambda)$ indicate respectively the singular and the continuous part of the average spectral density. Eq. (2.149) corresponds to Eq. (40) in [33].

We are now going to present some evidence that the singular contribution $\rho_S(\lambda)$ to the average spectral density is related to localisation properties.

Figure 2.3 shows the spectral density obtained for ER matrices with mean degree $c = 2$ and Gaussian weights with zero mean and variance $1/c$. It has been numerically shown [32,33] that the tails of the distribution and the central peak in $\lambda = 0$ are dominated by localised states, i.e. the eigenvectors corresponding to those values of λ have most of their components equal to zero. Given that there is a one-to-one matching between the eigenvectors of graphs and their nodes, a localised state can be also described as an eigenvector that is concentrated on few sites of the graph. Quantitatively, the presence and location of localised states in the spectrum is confirmed by the numerical analysis of the *Inverse Participation Ratio* (IPR) of the

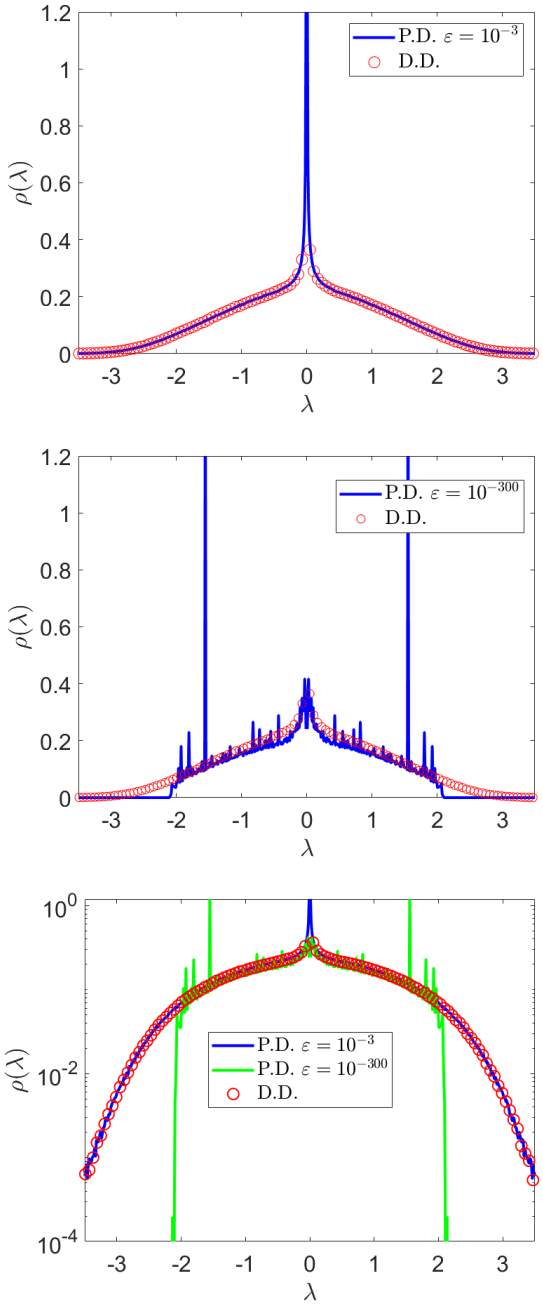

Figure 2.3: Spectral density of ER matrices with mean degree $c = 2$ and Gaussian bond weights with zero mean and variance $1/c$. In all panels, direct diagonalisation results (red circles) are obtained from a sample of 10000 matrices of size $N = 1000$. **Top**: population dynamics result obtained with a regulariser $\varepsilon = 10^{-3}$ (solid blue line) vs. the direct diagonalisation results. **Medium**: population dynamics result obtained with a regulariser $\varepsilon = 10^{-300}$ (solid blue line) vs. the direct diagonalisation results. **Bottom**: comparison between population dynamics result obtained with a regulariser $\varepsilon = 10^{-3}$ (solid blue line), population dynamics result obtained with a regulariser $\varepsilon = 10^{-300}$ (solid green line) and direct diagonalisation on a logarithmic scale. An extremely small value of ε is not able to capture the tails of the spectral density related to localised states, where the singular contributions prevail.

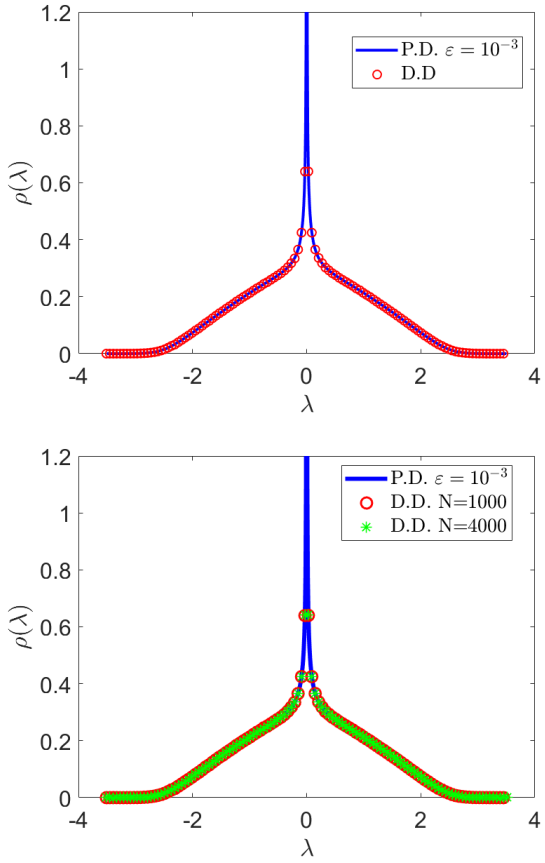

Figure 2.4: Spectral density of ER matrices with mean degree $c = 4$ and Gaussian bond weights with zero mean and variance $1/c$. **Top**: population dynamics result (solid blue line) obtained with a regulariser $\varepsilon = 10^{-3}$ vs. direct diagonalisation results (red circles) are obtained from a sample of 10000 matrices of size $N = 1000$. **Bottom**: comparison between population dynamics result with $\varepsilon = 10^{-3}$ (solid blue line), direct diagonalisation results obtained from a sample of 10000 matrices of size $N = 1000$ (red circles) and direct diagonalisation results obtained from a sample of 2500 matrices of size $N = 4000$ (green stars).

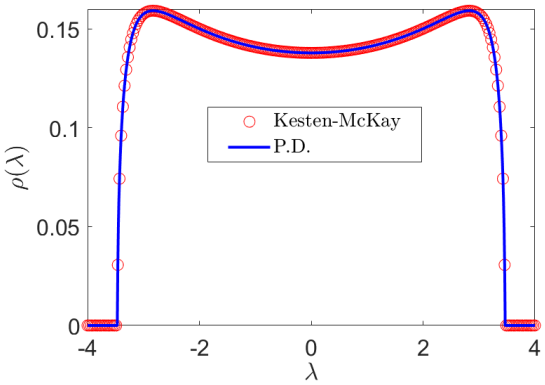

Figure 2.5: Spectral density of adjacency matrices of random regular graphs with coordination $c = 4$. The population dynamics result (solid blue line) is compared to the analytical expression of the spectral density, found in [39, 40], known as Kesten-McKay pdf (red circles).

eigenvectors in [33]. Given an eigenvector $\boldsymbol{v}$ of a $N \times N$ matrix, its IPR is defined as

$$\mathrm{IPR}(\boldsymbol{v}) = \frac{\sum_{i=1}^{N} v_i^4}{\left(\sum_{i=1}^{N} v_i^2\right)^2} \,. \tag{2.150}$$

The above definition is independent of the eigenvector's normalisation. The IPR of localised states is $\mathscr{O}(1)$, as opposed to the $\mathscr{O}(N^{-1})$ scaling for delocalised states. Indeed, the aforementioned numerical studies in [32, 33] show that the $\mathscr{O}(1)$ scaling for IPR is found in correspondence of the tails and around the peak in $\lambda = 0$. Moreover, the IPR analysis makes it possible to relate localised states with the singular contributions to the overall spectrum $\rho(\lambda)$. Indeed, the regions of the spectrum where the IPR is $\mathscr{O}(1)$ are also those where the singular contribution $\rho_S(\lambda)$ dominates over $\rho_C(\lambda)$.

Moreover, when comparing numerical direct diagonalisation and population dynamics results two fundamental aspects must be taken into account.

- On the one hand, the eigenvalues obtained by direct diagonalisation must be suitably binned in order to produce the numerical spectral density profile. The binning procedure can smoothen peaks originating from singular contributions, making them harder to detect. Ideally, the bin size Δ should be small enough to resolve the local variability of the spectral density, but also large enough to include enough eigenvalues. Quantitatively, if N_S is the total number of eigenvalues from direct diagonalisation, then a suitable Δ is the smallest value ensuring that the average number of eigenvalues per bin is $N_S \rho(\lambda)\Delta \gg 1$. Here, we used $N_S = 10^7$ and $\Delta = 10^{-2}$, allowing us to faithfully represent cases where $\rho(\lambda)$ is as small as $\mathscr{O}(10^{-5})$.

- On the other hand, the parameter ε plays an essential role in highlighting the singular contributions to the spectrum. In the evaluation of (2.149) only the samples such that $b_i \in [-\lambda - \mathscr{O}(\varepsilon), -\lambda + \mathscr{O}(\varepsilon)]$ for any given value of λ contribute to $\rho_S(\lambda)$. Therefore, in order to have enough data for a reliable evaluation of the singular contribution $\rho_S(\lambda)$, one must refrain from using a very small $\varepsilon > 0$ (such as $\varepsilon = \mathscr{O}(10^{-300})$), but rather use a relatively large value $\varepsilon > 0$ (such as $\varepsilon = \mathscr{O}(10^{-3})$), to ensure that $\mathscr{M}\varepsilon\rho_S(\lambda) \gg 1$. Here $\mathscr{M}$ indicates the number of samples used to evaluate the sums in (2.149).

The effects of the choice of the regulariser ε are evident in the case $c = 2$ (see Fig. 2.3), since for such low c localised states prevail in the spectrum. Indeed, this is due to the structure of the graph itself, which is made of a giant cluster component and a collection of isolated finite

connected clusters of nodes of any size (see Appendix 2.C). An excellent agreement between direct diagonalisation and population dynamics results is achieved for $\varepsilon = 10^{-3}$ (top panel). Indeed, in the $\varepsilon = 10^{-3}$ case, the Cauchy peaks related to the singular contributions to the spectral density are broadened into "wider" Cauchy pdfs. On the other hand, when using a smaller regulariser such as $\varepsilon = 10^{-300}$ (medium panel), the spectral density exhibits large fluctuations mainly due to errors that occur when sampling isolated states, as the condition $\mathscr{M}\varepsilon\rho_S(\lambda) \gg 1$ cannot be satisfied. The peaks are superimposed on the continuous curve representing $\rho_C(\lambda)$.

However, the curve $\rho_C(\lambda)$ is unable to capture the tails of the spectral density: this effect is highlighted on a logarithmic scale (bottom panel). This is the typical signature of a *localisation transition*: the tails of the spectral density are dominated by localised states, hence they cannot be represented by the continuous part of the spectrum. At the same time, using too small values for ε makes it impossible to observe the localised state contributions in the tails. If a larger regulariser (hence better local statistics) were employed (bottom panel), then the tails could be revealed. For an extensive discussion of these phenomena, see [33].

These effects are much less evident in the $c = 4$ case, shown in Fig. 2.4, as localised states are much less relevant as the mean degree c increases. Indeed it has been shown in [119, 120] that the weight of the delta-peaks related to localised states is an exponentially decreasing function of c, hence the peaks tend to disappear and merge into the continuous part of the spectrum as c grows. Moreover, the proportion of isolated nodes and isolated tree-like clusters of nodes in the graph is strongly reduced (see again Appendix 2.C). Therefore, the choice of the regulariser is of lesser importance, and population dynamics simulations run with different values of ε yield very similar results. Here, the peak at $\lambda = 0$ due to isolated nodes can still be noticed. The case of the spectral density of ER matrices with Gaussian couplings with $c = 4$ is used to show that finite size effects are barely present in the spectral problem (bottom panel of Fig. 2.4). In fact, numerical diagonalisation of matrices of different size (in particular $N = 1000$ and $N = 4000$) are barely distinguishable if compared to the same population dynamics simulation. Indeed, the Kolmogorov-Smirnoff test for the two samples returns a p-value of 32%, in favour of the hypothesis that they come from the same distribution.

Finally, as an illustration of the fact that the formalism presented here can be used to obtain the spectral density for other ensembles in the configuration model class having a degree distribution with finite mean and variance, we show in Fig. 2.5 the spectral density of the ensemble of adjacency matrices of random regular graphs (RRG), having degree distribution

$p(k) = \delta_{k,c}$. In Fig. 2.5 we consider the case $c = 4$. For RRGs adjacency matrices, there are no localised states for any $c > 2$. Conversely, there are mainly localised states for $c = 2$ (see again [33] for a detailed discussion). The population dynamics algorithm perfectly reproduces the Kesten-McKay distribution [39, 40], given by the analytical formula

$$\rho(\lambda) = \frac{c\sqrt{4(c-1)-\lambda^2}}{2\pi(c^2-\lambda^2)} \quad \text{for } |\lambda| \leq 2\sqrt{(c-1)}\,. \tag{2.151}$$

We remark that (2.151) can be derived analytically within the formalism of Section 2.5.1 employing a "peaked" ansatz for the distribution of inverse variances as $\hat{\pi}(\hat{\omega}) = \delta(\hat{\omega} - \bar{\omega})$. This is shown in Appendix 2.F.

2.6 Population dynamics algorithm

In this section, we sketch the stochastic population dynamics algorithm that allows us to solve the self-consistency equation (2.142) and the sampling procedure to evaluate (2.143). This kind of algorithm is widely used in the study of spin glasses [121, 122]. This procedure is general and allows to solve every equation having the same structure as (2.142) (including for instance (2.34)).

In order to solve (2.142), one represents the pdf $\hat{\pi}(\hat{\omega})$ in terms of a population of N_P complex values $\{(\hat{\omega}_i)\}_{1\leq i\leq N_P}$, which are assumed to be sampled from that pdf. Given that the true pdf is initially unknown, a starting population is randomly initialised with $\mathrm{Re}[\hat{\omega}_i] > 0$. Then, a stochastic algorithm for which the solution of Eq. (2.142) is the unique stationary solution is constructed.

To start, we fix $\varepsilon = 10^{-300}$. Indeed, when solving (2.142), we may choose ε to be as small as possible in order not to bias the values of the $\hat{\omega}$ [7]. Moreover, we define a set I of equally spaced real positive numbers, starting at zero. The parameter λ will take values in I. The distance between two consecutive values in I, denoted by $\Delta\lambda$, represents the λ-*scan*. For the plots shown in this chapter, we have employed $\Delta\lambda = \mathcal{O}(10^{-3})$. However, the mesh precision can be tuned depending on the desired resolution of the spectrum. Since the average spectral density as expressed by Eq. (2.145) (or equivalently Eq. (2.149)) is an even function of λ, it can be evaluated in the interval I and then simply mirrored w.r.t. 0 to obtain the full spectral density shape. As a last remark, it is convenient to normalise the bond weights drawn from $p_K(K)$ by $\sqrt{c}$, where c is the mean degree.

[7] This morally corresponds to considering the $\varepsilon \to 0^+$ limit in eq. (2.142).

Given these initial remarks, the stochastic algorithm consists of iterating the following step until a statistically stationary population is obtained, for any given $\lambda \in I$.

1. Generate a random k according to the distribution $\frac{k}{c}p(k)$, where $p(k)$ is the degree distribution of interest and $c = \langle k \rangle$.

2. Generate K from the bond weights pdf $p_K(K)$.

3. Select $k-1$ elements $\hat{\omega}_\ell$ from the population at random, then compute

$$\hat{\omega}^{(new)} = \frac{K^2}{i\lambda_\varepsilon + \sum_{\ell=1}^{k-1} \hat{\omega}_\ell} , \tag{2.152}$$

   which is the equality enforced by the delta function in (2.142) . Replace a randomly selected population member $\hat{\omega}_j$ (where $j = 1,...,N_P$) with $\hat{\omega}^{(new)}$.

4. Return to (i).

A *sweep* is completed when every member of the population $\hat{\omega}_j$ with $j = 1,...,N_P$ has been updated once according to the previous steps. We denote the i-th sweep for a given λ as $S_i(\lambda)$. A sufficient number N_{eq} of sweeps is needed to equilibrate the population. Stationarity can be assessed by looking at the sample estimate of the first moments of the $\hat{\omega}$ variables. The convergence is granted by the fact that recursive distributional equations such as Eq. (2.142) admit a unique probability distribution as a solution, as it has been shown in [37].

The population dynamics algorithm can also be employed for the sampling procedure that allows one to numerically evaluate (2.143) (and in a similar fashion (2.36)). Once (for a given value of λ) the population $\{(\hat{\omega}_i)\}_{1\leq i\leq N_P}$ has been brought to convergence after N_{eq} equilibration sweeps, a number N_{meas} of so-called *measurement sweeps* $M(\lambda)$ is performed. Here, N_{meas} is the number of the measurement sweeps.

Each measurement sweep $M_j(\lambda)$ ($j = 1,...,N_{\text{meas}}$) can be divided into two parts. In the first part, the population in equilibrium is updated via a sweep $S_j(\lambda)$, as described before. The second part is the actual measurement part $m_j(\lambda)$, involving the following steps. Two (real) empty arrays $\{a_i\}_{\{1\leq i\leq N_{\text{sam}}\}}$ and $\{b_i\}_{\{1\leq i\leq N_{\text{sam}}\}}$ of size N_{sam} are initialised. Here, N_{sam} is the number of samples per measurement sweep. Each of the a_i and the b_i will eventually play the role of the real and the imaginary parts of sums of the $\hat{\omega}_\ell$, respectively. Then, for $i = 1,...,N_{\text{sam}}$:

1. Generate a random k according to the degree distribution $p_c(k)$ (or in general $p(k)$)

2. Select k numbers $\hat{\omega}_\ell$ from the population $\{\omega_i\}_{1\leq i\leq N_P}$ at random and compute

$$x_i = \sum_{\ell=1}^{k} \hat{\omega}_\ell \ . \tag{2.153}$$

3. Compute

$$a_i = \mathrm{Re}[x_i] \ , \tag{2.154}$$

$$b_i = \mathrm{Im}[x_i] \ . \tag{2.155}$$

When all N_{meas} measurement sweeps $M_j(\lambda)$ have been completed (typically, $N_{\mathrm{meas}} \approx 10^4$), the resulting N_{meas} arrays of the type $\{a_i\}_{\{1\leq i\leq N_{\mathrm{sam}}\}}$ (respectively $\{b_i\}_{\{1\leq i\leq N_{\mathrm{sam}}\}}$) are merged together, yielding a unique large array $\{A_j\}_{\{1\leq j\leq \mathscr{M}\}}$ (respectively $\{B_j\}_{\{1\leq j\leq \mathscr{M}\}}$) of size $\mathscr{M} = N_{\mathrm{sam}} \times N_{\mathrm{meas}}$, which is the total number of samples (typically, we choose N_{sam} such that $\mathscr{M}$ is $\mathscr{O}(10^7)$ for the chosen value of N_{meas}). Therefore we can eventually compute

$$\rho(\lambda) = \frac{1}{\pi \mathscr{M}} \sum_{j=1}^{\mathscr{M}} \frac{A_j + \varepsilon}{(A_j+\varepsilon)^2 + (B_j+\lambda)^2} \ , \tag{2.156}$$

which represents the contribution to the average spectral density for a given value of λ. Eq. (2.156) corresponds to Eq. (2.149). The evaluation of the sample average (2.156) requires a careful choice of ε, since the value of ε in (2.156) will determine the width of the Cauchy distributions approximating the delta-peaks in the spectrum (see the discussion in Section 2.5.2). In general, the value of ε employed in (2.156) can be larger (up to $\varepsilon = \mathscr{O}(10^{-3})$) than the value $\varepsilon = 10^{-300}$ chosen for the equilibration sweeps in (2.152), in order to have sufficient statistics to faithfully represent the singular part of the spectrum. Eq. (2.156), corresponding to eq. (40) in [33], is a discretised version of (2.145). This step concludes the sampling algorithm for a given value of λ. The full sampling algorithm can be summarised as follows.

Algorithm 1 Population dynamics sampling algorithm

1: **for** $\lambda \in I$ **do**
2: **for** $e = 1, ..., N_{\text{eq}}$ **do**
3: $S_e(\lambda)$ ▷ Equilibration sweeps.
4: **end for**
5: **for** $j = 1, ..., N_{\text{meas}}$ **do**
6: $S_j(\lambda)$
7: $m_j(\lambda)$ ▷ $S_j(\lambda)$ and $m_j(\lambda)$ jointly form the measurement sweep $M_j(\lambda)$.
8: **end for**
9: Compute (2.156) for given λ using results from steps 5 to 8.
10: **end for** .

2.7 Summary

We have provided a comprehensive overview of the computation of the average spectral density of sparse symmetric random matrices using a statistical mechanics setup. We started with the celebrated Edwards-Jones formula (2.2) and outlined its proof. The formula allows to recast the determination of the density of states of a $N \times N$ matrix into the calculation of the average free energy of a system of N interacting particles at equilibrium, described by a Gibbs-Boltzmann distribution at imaginary inverse temperature. Therefore, techniques from the statistical physics of disordered systems, such as the replica method, can be employed to correctly deal with the calculation of the average free energy (see Eq. (2.16)) that features in the Edwards-Jones formula. The replica method was indeed the strategy used in the seminal work of Bray and Rodgers, which represents the first attempt to obtain the spectral density for matrices with ER connectivity. We have reproduced their calculations in detail, showing how to derive the integral equation (2.83) whose solution still represents a challenging open problem. We also described how to obtain the Wigner semicircle as the leading order of the large mean degree expansion of Eq. (2.83).

Considering sparse tree-like graphs within the Edwards-Jones framework, we have described how to apply the cavity method to the spectral problem for single instances. The cavity method circumvents the averaging of the free energy by making the associated Gibbs-Boltzmann distribution the target of its analysis. We have demonstrated that in this context the only ingredients needed to compute the spectral density are the inverse variances of each of the N marginal pdfs of the Gibbs-Boltzmann distribution (see Eq. (2.22)). These inverse variances are easily obtained in terms of a set of self-consistency equations (2.29) for the cavity inverse variances. We have also discussed an algorithm to perform the single-instance cavity analy-

sis. Moreover, we have explained how in the thermodynamic limit the cavity single-instance recursions give rise to a self-consistency integral equation (2.34) for the pdf of the inverse cavity variances, in terms of which the average spectral density (2.36) is fully determined at the ensemble level.

We have also illustrated an alternative replica derivation, where the high-temperature replica symmetry ansatz employed by Bray and Rodgers is realised by assuming that the order parameter and its conjugate are expressed through an infinite superposition of zero-mean complex Gaussians, with random inverse variances (see Eq. (2.125) and (2.126)). We showed that the two coupled integral equations (2.140) and (2.141) that define the pdfs of the aforementioned inverse variances reduce to a unique self-consistency equation (2.142), which is equivalent to Eq. (2.34) found within the cavity treatment in the thermodynamic limit. In the replica framework, too, the average spectral density (2.143) depends only on this single pdf defined in (2.142). Therefore, once again the equivalence between the cavity and replica approaches is confirmed. Indeed, both methods permit to express the average spectral density as a weighted sum of local contributions coming from nodes of different degree k. On the practical side, the average spectral density is obtained by sampling from a large population of complex numbers distributed according to the pdf of the inverse variances (2.142) (or equivalently (2.34)). We remark that both approaches are not restricted to ER graphs, but can handle any degree distribution with finite mean and variance.

The essential tool for solving self-consistency equations of the kind of Eq. (2.142) and performing the sampling procedure to evaluate the spectral density (2.143) is a stochastic population dynamics algorithm which we outlined in detail. Results obtained with the population dynamics algorithm are in excellent agreement with the numerical diagonalisation of large weighted adjacency matrices of tree-like graphs, provided that the correct choice of the value of the regulariser ε used in the algorithm is made. Indeed, we thoroughly describe the important role of ε in unveiling the contribution of the localised states to the spectral density, also in connection with the graph's mean degree and structure. We are also able to show that the spectral density does not significantly suffer from finite size effects, away from any localisation transition. In the immediate vicinity of localisation transitions, it is expected that finite size effects will affect results as in other continuous phase transitions. However, this phenomenology has not been fully investigated.

Appendices

2.A Sokhotski-Plemelj formula

The Sokhotski-Plemelj identity is

$$\lim_{\varepsilon\to 0^+}\frac{1}{x\pm \mathrm{i}\varepsilon}=\mathrm{Pr}\left(\frac{1}{x}\right)\mp \mathrm{i}\pi\delta(x)\ . \tag{2.A.1}$$

It is employed for the solution of some improper integrals. A quick proof for a real test function $g(x)$ follows. We have

$$\lim_{\varepsilon\to 0^+}\int_{-\infty}^{\infty}\mathrm{d}x\,\frac{g(x)}{x\pm \mathrm{i}\varepsilon}=\lim_{\varepsilon\to 0^+}\int_{-\infty}^{\infty}\mathrm{d}x\,x\frac{g(x)}{x^2+\varepsilon^2}\mp \mathrm{i}\pi\lim_{\varepsilon\to 0^+}\int_{-\infty}^{\infty}\mathrm{d}x\,g(x)\frac{1}{\pi}\frac{\varepsilon}{x^2+\varepsilon^2}\ , \tag{2.A.2}$$

where the real and imaginary part of the integrand have been separated. The first integral on the r.h.s. of (2.A.2) can be written as a Cauchy principal value, viz.

$$\lim_{\varepsilon\to 0^+}\int_{-\infty}^{\infty}\mathrm{d}x\,x\frac{g(x)}{x^2+\varepsilon^2}=\lim_{\varepsilon\to 0^+}\int_{-\infty}^{\infty}\mathrm{d}x\,\frac{g(x)}{x}\frac{x^2}{x^2+\varepsilon^2} \tag{2.A.3}$$

$$=\lim_{\varepsilon\to 0^+}\left(\int_{-\infty}^{-\varepsilon}\mathrm{d}x\,\frac{g(x)}{x}+\int_{\varepsilon}^{\infty}\mathrm{d}x\,\frac{g(x)}{x}\right)=\left[\mathrm{Pr}\left(\frac{1}{x}\right)\right](g)\ . \tag{2.A.4}$$

The second integral on the r.h.s of (2.A.2) reduces to

$$\lim_{\varepsilon\to 0^+}\int_{-\infty}^{\infty}\mathrm{d}x\,g(x)\frac{1}{\pi}\frac{\varepsilon}{x^2+\varepsilon^2}=\int_{-\infty}^{\infty}\mathrm{d}x\,g(x)\delta(x)=g(0)\ , \tag{2.A.5}$$

where $\lim_{\varepsilon\to 0^+}\frac{1}{\pi}\frac{\varepsilon}{x^2+\varepsilon^2}=\delta(x)$ has been employed.

2.B The principal branch of the complex logarithm

The logarithm in the complex plane is in general a multi-valued function. Whenever a well defined, single-valued function is needed, the *principal branch* of the complex logarithm can

be considered. It is denoted by "Log" and defined such that for any $z \in \mathbb{C}$ with $r = |z|$,

$$\mathrm{Log}(z) = \ln(r) + \mathrm{i}\mathrm{Arg}(z) \;\text{ with } \mathrm{Arg}(z) \in]-\pi, \pi] \ . \tag{2.B.6}$$

The function $\mathrm{Arg}(z)$ denotes the *principal value* of the argument of the complex number z. In particular, given $z = re^{\mathrm{i}\theta} \in \mathbb{C}$, the argument of z is given by $\arg(z) = \theta$ and is in general a multi-valued function. The single-valued principal argument $\mathrm{Arg}(z)$ is related to $\arg(z)$ via the following relation,

$$\mathrm{Arg}(z) = \arg(z) + 2\pi \left\lfloor \frac{1}{2} - \frac{\arg(z)}{2\pi} \right\rfloor \ , \tag{2.B.7}$$

where the symbol $\lfloor ... \rfloor$ denotes the floor operation, i.e. $\lfloor x \rfloor$ is the integer number such that $x - 1 < \lfloor x \rfloor \leq x$ for $x \in \mathbb{R}$.

In general $\mathrm{Log}\, e^z \neq z$ for $z \in \mathbb{C}$. Indeed, for any $z = x + \mathrm{i}y \in \mathbb{C}$ the following property holds:

$$\begin{aligned}
\mathrm{Log}(e^z) &= \mathrm{Log}|e^z| + \mathrm{i}\mathrm{Arg}(e^z) = \mathrm{Log}(e^x) + \mathrm{i}\mathrm{Arg}(e^{\mathrm{i}y}) \\
&= x + \mathrm{i}\left\{ \arg(e^{\mathrm{i}y}) + 2\pi \left\lfloor \frac{1}{2} - \frac{\arg(e^{\mathrm{i}y})}{2\pi} \right\rfloor \right\} \\
&= x + \mathrm{i}y + 2\pi\mathrm{i} \left\lfloor \frac{1}{2} - \frac{y}{2\pi} \right\rfloor \\
&= z + 2\pi\mathrm{i} \left\lfloor \frac{1}{2} - \frac{\mathrm{Im}[z]}{2\pi} \right\rfloor \ ,
\end{aligned} \tag{2.B.8}$$

where $\mathrm{Log}(x) = \ln(x)$ for $x \in \mathbb{R}$ and the definition (2.B.7) has been used for the principal value of the argument $\mathrm{Arg}(z)$.

2.C Erdős-Rényi graphs

The Erdős-Rényi (ER) graph is the prototypical example of a random graph, introduced by Erdős and Rényi in [21,22]. It is the simplest and most studied uncorrelated undirected random network. It can be denoted by $G(N, p)$, where N is the number of nodes and $p \in [0, 1]$ is the probability that any two nodes (there are $N(N-1)/2$ possible pairs, hence possible links) are connected. In other words, p is the probability that a link exists *independently* from the others. In formulae, the probability that a link exists between nodes i and j is

$$p_C(c_{ij}) = p\delta_{c_{ij},1} + (1-p)\,\delta_{c_{ij},0} \ . \tag{2.C.9}$$

All properties of the ER model depend on the two parameters N and p. Its degree distribution is binomial, viz.

$$\Pr[\text{a random node has degree } k] = p(k) = \binom{N-1}{k} p^k (1-p)^{N-1-k} . \tag{2.C.10}$$

Indeed, a node has degree k if it is connected to k nodes (the probability of this event being p^k) and at the same it is not connected to all the remaining $N-1-k$ nodes (the probability of this event being $(1-p)^{N-1-k}$). The binomial coefficient accounts for the fact that the specific subset of k nodes we choose out of the remaining $N-1$ does not matter. The mean degree is then $c = p(N-1)$. In the limit $N \to \infty$ where $N-1 \simeq N$ and keeping $c = Np$ constant, the binomial distribution in (2.C.10) converges to the Poisson distribution,

$$p_c(k) = \frac{c^k \mathrm{e}^{-c}}{k!} . \tag{2.C.11}$$

The condition for this limit to hold is exactly verified in the sparse ER ensemble that we consider in our analysis. Indeed, we explicitly ask that the mean degree c be a finite constant, hence ensuring that $p = \frac{c}{N} \to 0$ as $N \to \infty$. The Poisson distribution in (2.C.11) is decaying exponentially for large degree k.

The structure of an ER graph and in particular the existence of a giant component depend on the value of p [22]. The giant component of a graph is the largest connected component (i.e. cluster of nodes) in the graph, containing a finite fraction of the total N nodes. In a connected component, every two nodes are connected by a path, whereas there are no connections between two nodes belonging to two different components. We have the following properties [123, 124].

- For $p < \frac{1}{N}$ (i.e. $c < 1$), the probability of having a giant component is zero. Indeed, almost every $G(N,p)$ graph has no connected components with size larger than $\mathcal{O}(\ln(N))$, and can be described as a disjoint union of trees and unicycle components, i.e. trees with an extra link forming a cycle.

- For $p > \frac{1}{N}$ (i.e. $c > 1$), the probability of having a giant component is 1. Almost every $G(N,p)$ graph will have a unique giant component whose size is $\mathcal{O}(N)$ containing cycles of any length, while the remaining smaller components (typically trees and unicycles) have at most size $\mathcal{O}(\ln(N))$.

- $p = \frac{1}{N} = p_c$ represents the *percolation threshold* as it separates the two regimes: indeed at $p = p_c$ (i.e. $c = 1$) most of the isolated components for $c < 1$ merge together, giving rise to a giant component of size $\mathcal{O}(N^{2/3})$. As the (constant) mean degree $c > 1$ increases, the smaller components join the giant component, which then becomes $\mathcal{O}(N)$ in size. The smaller the size of the isolated components, the longer they will survive the merging process.

- For $p \leq \frac{\ln(N)}{N}$, almost every $G(N,p)$ graph contains isolated nodes, hence it is disconnected. As soon as $p > \frac{\ln(N)}{N}$, almost every $G(N,p)$ graph becomes connected, as the isolated nodes attach to the giant component entailing that every pair of nodes in the graph is connected by a path. The value $p = \frac{\ln(N)}{N}$ is then a threshold for the *connectivity* of the graph.

The structural properties of the graph are reflected in the spectrum. Indeed, the variety of peaks in the spectrum related to singular contributions are due to isolated nodes and isolated finite clusters of nodes that are still present for finite constant $c > 1$, alongside with the giant component.

The ER graph can also be seen as a model of link percolation [125]. Indeed, ER graphs can be generated also starting from a fully connected graph and removing links at random with constant probability $1 - p$.

An algorithm for the generation of the adjacency matrix of any generic random graphs within the configuration model is described in Section 8.1 and detailed in Appendix J.5 (Algorithm 27) of [126].

2.D How to perform the average (2.48)

The goal is to perform the average

$$\left\langle \exp\left(\frac{\mathrm{i}}{2} \sum_{i,j=1}^{N} \sum_{a=1}^{n} v_{ia} J_{ij} v_{ja} \right) \right\rangle_J \tag{2.D.12}$$

w.r.t. the joint distribution of the matrix entries

$$P(\{J_{ij}\}) = \prod_{i<j} p_C(c_{ij}) \delta_{c_{ij},c_{ji}} \prod_{i<j} p_K(K_{ij}) \delta_{K_{ij},K_{ji}} \,, \tag{2.D.13}$$

where

$$p_C(c_{ij}) = \frac{c}{N}\delta_{c_{ij},1} + \left(1 - \frac{c}{N}\right)\delta_{c_{ij},0} \tag{2.D.14}$$

represents the ER connectivity distribution, and $p_K(K_{ij})$ is the bond weight pdf. The average is computed for large N as follows,

$$\begin{aligned}
&\left\langle \exp\left(\frac{\mathrm{i}}{2}\sum_{i,j=1}^{N}\sum_{a=1}^{n} v_{ia}J_{ij}v_{ja}\right)\right\rangle_J = \left\langle \prod_{i<j}\exp\left(\mathrm{i}\sum_{a=1}^{n} v_{ia}c_{ij}K_{ij}v_{ja}\right)\right\rangle_{\{c\},\{K\}} \\
&= \prod_{i<j}\left\langle \exp\left(\mathrm{i}\sum_{a=1}^{n} v_{ia}c_{ij}K_{ij}v_{ja}\right)\right\rangle_{c,K} \\
&= \prod_{i<j}\left[1 + \frac{c}{N}\left(\langle \mathrm{e}^{\mathrm{i}K\sum_a v_{ia}v_{ja}}\rangle_K - 1\right)\right] \\
&\simeq \exp\left[\frac{c}{2N}\sum_{i,j=1}^{N}\left(\langle \mathrm{e}^{\mathrm{i}K\sum_a v_{ia}v_{ja}}\rangle_K - 1\right)\right],
\end{aligned} \tag{2.D.15}$$

where the subscripts $\{c\}$ and $\{K\}$ respectively denote averaging w.r.t. the joint pdfs of the $\{c_{ij}\}$ and the bond weights $\{K_{ij}\}$, whereas the non-bracketed subscripts c and K refers to the average over a single random variable drawn from $p_C(c)$ and $p_K(K)$, respectively. Moreover, in the second line we have used independence of the random variables and in the last line we have re-exponentiated the product and the factor $1/2$ prevents from over-counting symmetric terms in the double sum.

2.E The action S_n in terms of π and $\hat{\pi}$

The following action is derived in Section 2.5,

$$S_n[\pi,\hat{\pi},\lambda] = S_1[\pi,\hat{\pi}] + S_2[\pi] + S_3[\hat{\pi},\lambda]\,. \tag{2.E.16}$$

The contributions (2.129), (2.130) and (2.131) are obtained from (2.56), (2.57) and (2.58) respectively, using the saddle-point expressions (2.125) and (2.126) for the order parameter $\varphi^\star(\vec{v})$ and its conjugate $\mathrm{i}\hat{\varphi}^\star(\vec{v})$. Defining the shorthands $\mathrm{d}\pi(\omega) = \mathrm{d}\omega\pi(\omega)$, $\{\mathrm{d}\hat{\pi}\}_k = \prod_{\ell=1}^{k}\mathrm{d}\hat{\omega}_\ell\hat{\pi}(\hat{\omega}_\ell)$,

$\{\hat{\omega}\}_k = \sum_{\ell=1}^k \hat{\omega}_\ell$ and $Z(x) = \int \mathrm{d}v\, \mathrm{e}^{-\frac{x}{2}v^2} = \sqrt{\frac{2\pi}{x}}$, one finds

$$\begin{aligned} S_1[\pi,\hat{\pi}] &= -\hat{c}\int \mathrm{d}\pi(\omega)\mathrm{d}\hat{\pi}(\hat{\omega})\int \mathrm{d}\vec{v}\prod_{a=1}^n \frac{\mathrm{e}^{-\left(\frac{\omega+\hat{\omega}}{2}\right)v_a^2}}{Z(\omega)Z(\hat{\omega})} \\ &= -\hat{c}\int \mathrm{d}\pi(\omega)\mathrm{d}\hat{\pi}(\hat{\omega})\left(\frac{Z(\omega+\hat{\omega})}{Z(\omega)Z(\hat{\omega})}\right)^n \\ &\simeq -\hat{c} - n\hat{c}\int \mathrm{d}\pi(\omega)\mathrm{d}\hat{\pi}(\hat{\omega})\log\left(\frac{Z(\omega+\hat{\omega})}{Z(\omega)Z(\hat{\omega})}\right), \end{aligned} \tag{2.E.17}$$

where we have used a small n expansion in the last line. Concerning S_2, one has

$$\begin{aligned} S_2[\pi] &= \frac{c}{2}\int \mathrm{d}\vec{v}\mathrm{d}\vec{v'}\int \mathrm{d}\pi(\omega)\mathrm{d}\pi(\omega')\prod_{a=1}^n \frac{\mathrm{e}^{-\frac{\omega}{2}v_a^2}}{Z(\omega)}\frac{\mathrm{e}^{-\frac{\omega'}{2}{v'_a}^2}}{Z(\omega')}\left(\langle \mathrm{e}^{\mathrm{i}K\sum_a v_a v'_a}\rangle_K - 1\right) \\ &= \frac{c}{2}\int \mathrm{d}\pi(\omega)\mathrm{d}\pi(\omega')\left[\left\langle\left(\frac{Z_2(\omega,\omega',K)}{Z(\omega)Z(\omega')}\right)^n\right\rangle_K - 1\right] \\ &\simeq n\frac{c}{2}\int \mathrm{d}\pi(\omega)\mathrm{d}\pi(\omega')\left\langle \log\frac{Z_2(\omega,\omega',K)}{Z(\omega)Z(\omega')}\right\rangle_K, \end{aligned} \tag{2.E.18}$$

where we have used $Z_2(\omega,\omega',K) = \int \mathrm{d}v\mathrm{d}v' \mathrm{e}^{-\frac{\omega}{2}v^2 - \frac{\omega'}{2}v'^2 + \mathrm{i}Kvv'}$ and again a small n expansion. Concerning S_3, one gets

$$\begin{aligned} S_3[\hat{\pi},\lambda] &= \mathrm{Log}\int \mathrm{d}\vec{v}\,\mathrm{e}^{-\mathrm{i}\frac{\lambda}{2}\sum_a v_a^2 + \mathrm{i}\hat{\varphi}(\vec{v})} \\ &= \mathrm{Log}\int \mathrm{d}\vec{v}\,\mathrm{e}^{-\mathrm{i}\frac{\lambda}{2}\sum_a v_a^2}\sum_{k=0}^\infty \frac{(\mathrm{i}\hat{\varphi}(\vec{v}))^k}{k!} \\ &= \mathrm{Log}\sum_{k=0}^\infty \frac{\hat{c}^k}{k!}\int \mathrm{d}\vec{v}\,\mathrm{e}^{-\mathrm{i}\frac{\lambda}{2}\sum_a v_a^2}\int \{\mathrm{d}\hat{\pi}\}_k \prod_{\ell=1}^k\prod_{a=1}^n \frac{\mathrm{e}^{-\frac{\hat{\omega}_\ell}{2}v_a^2}}{Z(\hat{\omega}_\ell)} \\ &= \mathrm{Log}\sum_{k=0}^\infty \frac{\hat{c}^k}{k!}\int \{\mathrm{d}\hat{\pi}\}_k \left[\frac{Z(\mathrm{i}\lambda_\varepsilon + \{\hat{\omega}\}_k)}{\prod_{\ell=1}^k Z(\hat{\omega}_\ell)}\right]^n \\ &\simeq \mathrm{Log}\sum_{k=0}^\infty \frac{\hat{c}^k}{k!}\int \{\mathrm{d}\hat{\pi}\}_k \left(1 + n\log\frac{Z(\mathrm{i}\lambda_\varepsilon + \{\hat{\omega}\}_k)}{\prod_{\ell=1}^k Z(\hat{\omega}_\ell)}\right) \\ &= \mathrm{Log}\,\mathrm{e}^{\hat{c}}\left[1 + n\sum_{k=0}^\infty \frac{\hat{c}^k}{k!}\mathrm{e}^{-\hat{c}}\int \{\mathrm{d}\hat{\pi}\}_k \log\frac{Z(\mathrm{i}\lambda_\varepsilon + \{\hat{\omega}\}_k)}{\prod_{\ell=1}^k Z(\hat{\omega}_\ell)}\right] \\ &\simeq \hat{c} + n\sum_{k=0}^\infty p_{\hat{c}}(k)\int \{\mathrm{d}\hat{\pi}\}_k \log\frac{Z(\mathrm{i}\lambda_\varepsilon + \{\hat{\omega}\}_k)}{\prod_{\ell=1}^k Z(\hat{\omega}_\ell)}, \end{aligned} \tag{2.E.19}$$

where $p_{\hat{c}}(k) = \frac{\hat{c}^k}{k!}\mathrm{e}^{-\hat{c}}$ is a Poisson distribution with parameter $\hat{c}$. We remark that in the second line we have expressed $\exp(\mathrm{i}\hat{\varphi}(\vec{v}))$ through its power series and a small n expansion has been used across the entire calculation.

2.F The Kesten-McKay distribution from a peaked $\hat{\pi}$

We analytically derive the spectral density of the ensemble of adjacency matrices of random regular graphs (RRGs), using the formalism of Section 2.5. We employ eq. (2.142) and (2.143), specialised to the RRG case where $p(k) = \delta_{k,c}$ and $p_K(K) = \delta(K-1)$. Therefore, we obtain for the self-consistency equation for $\hat{\pi}$

$$\hat{\pi}(\hat{\omega}) = \int \{\mathrm{d}\hat{\pi}\}_{c-1} \delta\left(\hat{\omega} - \frac{1}{\mathrm{i}\lambda_\varepsilon + \sum_{\ell=1}^{c-1}\hat{\omega}_\ell}\right) , \tag{2.F.20}$$

whereas for the spectral density we get

$$\rho(\lambda) = \frac{1}{\pi}\lim_{\varepsilon\to 0^+}\mathrm{Re}\int\{\mathrm{d}\hat{\pi}\}_c\left[\frac{1}{\mathrm{i}\lambda_\varepsilon + \sum_{\ell=1}^{c}\hat{\omega}_\ell}\right] . \tag{2.F.21}$$

Eq. (2.F.20) can be solved by a degenerate pdf of the form

$$\hat{\pi}(\hat{\omega}) = \delta(\hat{\omega} - \bar{\omega}_\varepsilon) , \tag{2.F.22}$$

provided that $\bar{\omega}_\varepsilon$ solves

$$\bar{\omega}_\varepsilon = \frac{1}{\mathrm{i}\lambda_\varepsilon + (c-1)\bar{\omega}_\varepsilon} \Leftrightarrow \bar{\omega}_\varepsilon = \frac{-\mathrm{i}\lambda_\varepsilon \pm \sqrt{(\mathrm{i}\lambda_\varepsilon)^2 + 4(c-1)}}{2(c-1)} . \tag{2.F.23}$$

Therefore, the spectral density reads

$$\begin{aligned}\rho(\lambda) &= \frac{1}{\pi}\lim_{\varepsilon\to 0^+}\mathrm{Re}\left[\frac{1}{\mathrm{i}\lambda_\varepsilon + c\bar{\omega}_\varepsilon}\right] \\ &= \frac{1}{2\pi}\lim_{\varepsilon\to 0^+}\mathrm{Re}\left[\frac{(c-2)(\mathrm{i}\lambda_\varepsilon) \mp c\sqrt{4(c-1)-\lambda_\varepsilon^2}}{\lambda_\varepsilon^2 - c^2}\right] .\end{aligned} \tag{2.F.24}$$

Taking the real part and thereafter the $\varepsilon \to 0^+$ limit in (2.F.24), one obtains

$$\rho(\lambda) = \frac{c\sqrt{4(c-1)-\lambda^2}}{2\pi(c^2-\lambda^2)} \quad \text{for } |\lambda| \le 2\sqrt{(c-1)} , \tag{2.F.25}$$

where the minus sign has been chosen in order to have a physical solution. The latter expression is the Kesten-McKay pdf in Eq. (2.151).

2.G Trees have a symmetric spectrum

A tree is a connected acyclic undirected graph. Acyclic means that it contains no cycles. In a tree, any two nodes are connected via a unique path [127]. In particular, trees are examples of *bipartite* graphs, in which nodes can be divided into two disjoint subgraphs S_1 and S_2, such that every node in subgraph S_1 only has neighbours in the complementary subgraph S_2 and vice versa.

Here, we show that the $N \times N$ adjacency matrix A (whether it is weighted or not) of a tree with N nodes has a spectrum that is symmetric around $\lambda = 0$. In other words, for any eigenvalue λ of A, then $-\lambda$ is also an eigenvalue of A. This result is encoded in the fact that in the set of recursion equations for the cavity inverse variances (2.29) and single-site inverse variances (2.31), the matrix entries appear only through their square.

Let $\boldsymbol{x}$ be the eigenvector of A corresponding to the eigenvalue λ . Given $\boldsymbol{x}$ and λ, we will be able to construct a vector $\boldsymbol{y}$ that is an eigenvector of A corresponding to the eigenvalue $-\lambda$. Indeed, considering the eigenvalue equation for the component x_i,

$$\lambda x_i = \sum_{j \in \partial i} A_{ij} x_j \ , \tag{2.G.26}$$

the node i contributing to the l.h.s. of (2.G.26) and the nodes $\{j : j \in \partial i\}$ contributing to the r.h.s. of (2.G.26) always belong to different subgraphs. Therefore, the signs of all the components x_j with $j \in \partial i$ all belonging to one of the two subgraphs (S_1 or S_2) can be changed, giving rise to

$$-\lambda x_i = \sum_{j \in \partial i} (A_{ij})(-x_j) \Leftrightarrow -\lambda y_i = \sum_{j \in \partial i} (A_{ij})(y_j) \ . \tag{2.G.27}$$

This reasoning can be iterated for any $i = 1, \ldots, N$. Therefore, given the eigenvector $\boldsymbol{x}$ corresponding to λ, one can construct a vector $\boldsymbol{y}$ such that

$$y_i = \begin{cases} x_i & i \in S_1 \\ -x_i & i \in S_2 \end{cases} \ . \tag{2.G.28}$$

Of course, the choice of inverting the sign of the components of $\boldsymbol{x}$ on the set S_2 is arbitrary. The same result is achieved by changing the sign of the components living on nodes in S_1 while leaving the components defined on nodes in S_2 unchanged. The vector $\boldsymbol{y}$ is thus an eigenvector

of the matrix A corresponding to $-\lambda$.

Chapter 3

Top Eigenpair Statistics for Weighted Sparse Graphs

3.1 Introduction

Building on the statistical mechanics framework that has been presented in Chapter 2, we present a cavity and replica formulation of the top eigenpair problem which is close in spirit to the Edwards-Jones setup for the spectral problem. Indeed, the top eigenpair problem is framed as the search for the ground state of a system of particles interacting on a sparse graph, described by a Gibbs-Boltzmann distribution with *real* inverse temperature β. Our cavity derivation differs from the one in [47] in that it targets directly the Gibbs-Boltzmann distribution of the associated physical systems, in analogy to the treatment for the spectral density in Chapter 2. Moreover, the method we propose is able to accommodate hard constraints, thereby providing a flexible setup that can be easily expanded to deal with more structured problems.

The plan of the chapter is as follows. In Section 3.2, we will formulate the search of the top eigenpair in terms of its statistical mechanics analogy. In Section 3.3, we will describe the cavity approach to the problem for the single instance case (in 3.3.1), deriving the single-instance recursion equations already found in [47]. In addition, we provide in Appendix 3.A a detailed analysis of these recursion equations, showing that their convergence is strictly related to the spectral properties of a modified non-backtracking operator associated with the single-instance matrix. We extend the cavity derivation to the thermodynamic limit (i.e. at the ensemble level) in 3.3.2. In Section 3.3.3, we also show how to derive the Porter-Thomas distribution [93,94] from the ensemble equations in the large c limit. In Section 3.4, we formulate the replica approach to the same problem, first focussing on the largest eigenvalue problem (in 3.4.1) and then on the density of top eigenvector's components (in 3.4.2). Our replica deriva-

tion is valid for any degree distribution $p(k)$ with finite mean and variance characterising sparse graphs within the configuration model. Thanks to the replica analysis, we show the equivalence of the cavity and replica methods at the ensemble level. Moreover, we are able to better understand the behaviour of the stochastic integral recursions that provide the solution of the top eigenpair problem in the thermodynamic limit. In Section 3.5, we test our formalism in the case of Markov transition matrices on a random graph structure. In Section 3.6, we provide the details of the population dynamics algorithm employed to solve these recursions. This algorithm allows us to characterise the distributions of the cavity fields in the thermodynamic limit and identify the individual contributions of nodes of different degrees k to the top eigenvector's entries. Finally, in Section 3.7 we offer a summary.

3.2 Formulation of the problem

We consider a sparse random $N \times N$ symmetric matrix $J = (J_{ij})$, with real i.i.d. entries. The matrix entries are defined as

$$J_{ij} = c_{ij} K_{ij} \,, \tag{3.1}$$

where the $c_{ij} \in \{0,1\}$ constitute the connectivity matrix, i.e. the adjacency matrix of the underlying graph, and the K_{ij} encode bond weights.

Similarly to Chapter 2, we consider locally tree-like sparse matrices, characterised by the fact that their degree distribution $p(k)$ has a finite constant mean $\langle k \rangle = c$ (hence $c/N \to 0$ as $N \to \infty$), and finite variance. We will consider *bounded* degree distributions, i.e. with a finite maximum degree $k_{\max}$ not scaling with N. For instance, a suitable candidate can be a bounded Poisson distribution

$$P(k_i = k) = p_c(k) = \mathscr{N}^{-1} \mathrm{e}^{-\bar{c}} \bar{c}^k / k! \,, \qquad k = 0, \ldots, k_{\max} \,, \tag{3.2}$$

with the mean degree a finite constant $c \equiv \langle k \rangle$ and $\mathscr{N} = \sum_{k=0}^{k_{\max}} \mathrm{e}^{-\bar{c}} \bar{c}^k / k!$ to ensure normalisation. The bond weights K_{ij} will be i.i.d. random variables drawn from a parent pdf $p_K(K)$ with bounded support. This setting is sufficient to ensure that the largest eigenvalue λ_1 of J will remain of $\mathscr{O}(1)$ for $N \to \infty$.

The spectral theorem ensures that J can be diagonalised via an orthonormal basis of eigenvectors $\boldsymbol{v}_\alpha$ with corresponding real eigenvalues λ_α ($\alpha = 1, \ldots, N$),

$$J \boldsymbol{v}_\alpha = \lambda_\alpha \boldsymbol{v}_\alpha \,, \tag{3.3}$$

for each eigenpair $\alpha = 1,\dots,N$. The N eigenvalues can be sorted in descending order, $\lambda_1 \geq \lambda_2 \geq \dots \geq \lambda_N$. In particular, for unweighted adjacency matrices and adjacency matrices with positive weights the Perron-Frobenius theorem ensures that the top eigenvalue is not degenerate, entailing that $\lambda_1 > \lambda_2$.

The goal of this chapter is to set up a formalism based on the statistical mechanics of disordered systems to find:

- the average (or typical value) $\langle \lambda_1 \rangle_J$ of the largest eigenvalue λ_1;
- the density $\rho_J(u) = \left\langle \frac{1}{N}\sum_{i=1}^{N} \delta(u - v_1^{(i)}) \right\rangle_J$ of the top eigenvector's components, $\boldsymbol{v}_1 = (v_1^{(1)},\dots,v_1^{(N)})$,

where the average $\langle\cdot\rangle_J$ is taken over the distribution of the matrix J.

The problem can be formulated as the optimisation problem of a quadratic function $\hat{H}(\boldsymbol{v})$, according to which $\boldsymbol{v}_1$ is the vector normalized to N that realises the condition

$$N\lambda_1 = \min_{|\boldsymbol{v}|^2=N} \left[\hat{H}(\boldsymbol{v})\right] = \min_{|\boldsymbol{v}|^2=N} \left[-\frac{1}{2}(\boldsymbol{v}, J\boldsymbol{v})\right] , \tag{3.4}$$

as dictated by the Courant-Fischer definition of eigenvectors. The round brackets $(\cdot,\cdot)$ indicate the dot product between vectors in $\mathbb{R}^N$. It is easy to show that $\hat{H}(\boldsymbol{v})$ is bounded

$$-\frac{1}{2}\lambda_1 N \leq \hat{H}(\boldsymbol{v}) \leq -\frac{1}{2}\lambda_N N , \tag{3.5}$$

and attains its minimum when computed on the top eigenvector. The function $\hat{H}(\boldsymbol{v})$ can be thought of as the "Hamiltonian" of a system of N particles interacting pairwise along the edges of the graph defined by the adjacency matrix $C = (c_{ij})$.

For a fixed matrix J, the minimum in (3.5) can be computed by introducing a fictitious canonical ensemble of N-dimensional vectors $\boldsymbol{v}$ at inverse temperature β, whose Gibbs-Boltzmann distribution reads

$$P_{\beta,J}(\boldsymbol{v}) = \frac{1}{Z_N} \exp\left[\frac{\beta}{2}(\boldsymbol{v}, J\boldsymbol{v})\right] \delta(|\boldsymbol{v}|^2 - N) , \tag{3.6}$$

where the delta function enforces normalisation. Clearly, in the low temperature limit $\beta \to \infty$, only one 'state' remains populated, which corresponds to $\boldsymbol{v} = \boldsymbol{v}_1$, the top eigenvector of the matrix J. Moreover, in view of (3.5) the intensive free energy per particle $\frac{F}{N}$ in the zero

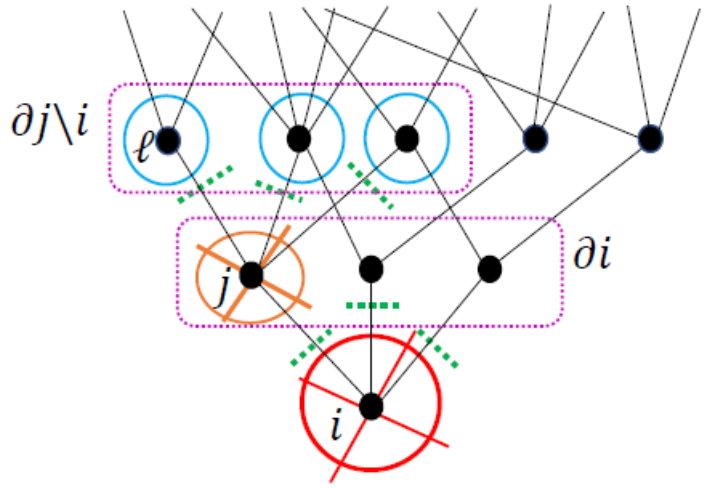

Figure 3.1: Tree-like structure of a graph. The indexing refers to the labels used in the cavity method treatment in subsection 3.3.1.

temperature limit reduces to λ_1, up to a factor $-1/2$, viz.

$$\left.\frac{F}{N}\right|_{\beta\to\infty} = -\frac{\lambda_1}{2} \,. \tag{3.7}$$

On the other hand, the free energy can be expressed through the partition function Z_N at any β as

$$\frac{F}{N} = -\frac{1}{\beta N}\ln Z_N \,, \tag{3.8}$$

therefore entailing that

$$\lambda_1 = \lim_{\beta\to\infty}\frac{2}{\beta N}\ln Z_N \,. \tag{3.9}$$

We will employ the latter definition to obtain the top eigenvalue of J in both the cavity and the replica framework.

3.3 Cavity analysis

In what follows, we will use a cavity method [35] formulation for the top eigenpair problem which is deeply rooted in the statistical mechanics approach to disordered systems. Our formulation provides equations for the statistics of the top eigenpair that are fully equivalent to those found earlier by Kabashima et al. in [47]. Our treatment, however, brings more neatly to the surface a few subtleties related to the solution of self-consistency equations and their range of applicability, this way providing a more transparent derivation.

3.3.1 Cavity derivation for a single instance

Consider for the time being a single instance of the random matrix J. As shown at the end of the previous section, its top eigenvalue can be defined as

$$\lambda_1 = \lim_{\beta\to\infty} \frac{2}{\beta N} \ln Z_N \,, \tag{3.10}$$

where the partition function Z_N reads

$$Z_N = \int \mathrm{d}\boldsymbol{v}\, \exp\left[\frac{\beta}{2}(\boldsymbol{v}, J\boldsymbol{v})\right] \delta(|\boldsymbol{v}|^2 - N) \,. \tag{3.11}$$

Employing a Fourier representation for the Dirac delta in (3.11), one finds

$$Z_N = \left(\frac{\beta}{4\pi}\right) \int \mathrm{d}\lambda \exp\left[\beta N S_N(\lambda)\right] \,, \tag{3.12}$$

where the action $S_N(\lambda)$ reads

$$S_N(\lambda) = \frac{\mathrm{i}\lambda}{2} + \frac{1}{\beta N} \mathrm{Log}\tilde{Z}_N(\lambda) \,, \tag{3.13}$$

with

$$\tilde{Z}_N(\lambda) = \int \mathrm{d}\boldsymbol{v}\, \exp\left[-\frac{\beta}{2}(\boldsymbol{v}, A\boldsymbol{v})\right] = \sqrt{\frac{(2\pi)^N}{\beta^N \det A}} \,, \tag{3.14}$$

and we have considered the matrix $A = \mathrm{i}\lambda \mathbb{1}_N - J$. Evaluating the integral (3.12) with a saddle point approximation for large β, one notices that the contribution to the integral (3.12) coming from (3.14) can be neglected. Therefore, the partition function reduces to

$$Z_N \approx \exp\left[\frac{\beta N}{2} \mathrm{i}\lambda^\star\right] \,, \tag{3.15}$$

where the symbol $\lambda^\star$ denotes the saddle-point value of the variable λ. Using (3.10), Eq. (3.15) entails that

$$\lambda_1 = \mathrm{i}\lambda^\star \,. \tag{3.16}$$

In order to determine the value $\mathrm{i}\lambda^\star$, we consider Eq. (3.12) without calculating explicitly the integral (3.14) defining $\tilde{Z}_N$. The stationarity condition of the action S_N w.r.t. to λ requires

$$1 = \frac{1}{N} \sum_{i=1}^{N} \langle v_i^2 \rangle \,, \tag{3.17}$$

where the angle brackets indicate the average w.r.t. the distribution

$$P_\beta(\boldsymbol{v}|\mathrm{i}\lambda^\star) = \frac{1}{\tilde{Z}_N}\exp\left[\frac{\beta}{2}(\boldsymbol{v},J\boldsymbol{v}) - \frac{\beta\mathrm{i}\lambda^\star}{2}(\boldsymbol{v},\boldsymbol{v})\right] . \tag{3.18}$$

The pdf in (3.18) is the *grand canonical* version of the canonical Gibbs-Boltzmann distribution (3.6). For large N, the two pdfs are expected to provide the same physical results, entailing that in the limit $\beta \to \infty$ the top eigenvector of J can be found by studying the ground state of (3.18) instead of that of (3.6).

The saddle-point value $\mathrm{i}\lambda^\star$ is defined as the only value such that Eq. (3.17) is satisfied in the $\beta \to \infty$ limit . Actually, Eq. (3.17) expresses the *normalisation* condition for the components of the top eigenvector. Indeed, the variables v_i appearing in (3.17) represent the components of the top eigenvector of J when the low temperature limit is considered.

In view of Eq. (3.16), we set $\mathrm{i}\lambda^\star = \lambda \in \mathbb{R}$, since it must be real because of the symmetry of the matrix J. The distribution (3.18) then reads

$$P_\beta(\boldsymbol{v}|\lambda) = \frac{1}{\tilde{Z}_N(\lambda)}\exp\left[\frac{\beta}{2}(\boldsymbol{v},J\boldsymbol{v}) - \frac{\beta\lambda}{2}(\boldsymbol{v},\boldsymbol{v})\right] \tag{3.19}$$

and represents the starting point of the cavity analysis. Considering its partition function

$$\tilde{Z}_N(\lambda) = \int \mathrm{d}\boldsymbol{v}\exp\left\{\beta\left[\frac{1}{2}(\boldsymbol{v},J\boldsymbol{v}) - \frac{\lambda}{2}(\boldsymbol{v},\boldsymbol{v})\right]\right\} , \tag{3.20}$$

one notices that the condition $\lambda > \lambda_1$ is necessary to ensure convergence for all β.

Our goal is to obtain a factorisation of the pdf (3.19) in order to easily perform the $\beta \to \infty$ limit. We then start looking at the structure of its marginals, using the cavity method as in Section 2.3.2. For a given component v_i its marginal distribution $P_i(v_i)$ is obtained by integrating out all other components in (3.19) using the sparsity condition $J_{ij} = 0$ if $j \notin \partial i$ (where ∂i denotes the immediate neighbourhood of i). Thus, it reads

$$P_i(v_i) = \frac{1}{Z_i}\exp\left(-\beta\frac{\lambda}{2}v_i^2\right)\int \mathrm{d}\boldsymbol{v}_{\partial i}\exp\left(\beta\sum_{j\in\partial i}J_{ij}v_iv_j\right)P^{(i)}(\boldsymbol{v}_{\partial i}) , \tag{3.21}$$

where $P^{(i)}(\boldsymbol{v}_{\partial i})$ is the joint distribution of the components pertaining to the immediate neighbourhood of i, ∂i, when the node i has been removed. Indeed, all the components outside ∂i can be integrated out without difficulty, and the resulting constant term can be just reabsorbed

in the normalisation constant. $P^{(i)}(\boldsymbol{v}_{\partial i})$ is also known as *cavity probability distribution*.

Adopting now a tree-like approximation, which is accurate for very sparse graphs, all nodes j in ∂i are connected with each other only through i (see Fig. 3.1), therefore they get disconnected when the node i is removed from the network: this implies that the integral appearing in (3.21) factorises as

$$P_i(v_i) = \frac{1}{Z_i} \exp\left(-\beta \frac{\lambda}{2} v_i^2\right) \prod_{j \in \partial i} \int \mathrm{d}v_j \exp\left(\beta J_{ij} v_i v_j\right) P_j^{(i)}(v_j) \,. \tag{3.22}$$

In the same way, a similar expression can be derived for the marginal cavity distribution $P_j^{(i)}(v_j)$ now appearing in (3.22). Iterating the reasoning as before, and further removing the node $j \in \partial i$ in the network in which the node i had already been removed, one can write

$$P_j^{(i)}(v_j) = \frac{1}{Z_j^{(i)}} \exp\left(-\beta \frac{\lambda}{2} v_j^2\right) \prod_{\ell \in \partial j \setminus i} \int \mathrm{d}v_\ell \exp\left(\beta J_{j\ell} v_j v_\ell\right) P_\ell^{(j)}(v_\ell) \,, \tag{3.23}$$

where the symbol $\partial j \setminus i$ denotes the neighbourhood of j excluding i.

Equation (3.23) has now become a self-consistent equation for the cavity probability distributions, which can be solved by a Gaussian ansatz for $P_j^{(i)}(v_j)$, namely

$$P_j^{(i)}(v_j) = \sqrt{\frac{\beta \omega_j^{(i)}}{2\pi}} \exp\left(-\frac{\beta h_j^{(i)\,2}}{2\omega_j^{(i)}}\right) \exp\left(-\frac{\beta}{2} \omega_j^{(i)} v_j^2 + \beta h_j^{(i)} v_j\right) \,, \tag{3.24}$$

where the parameters $\omega_i^{(i)}$ and $h_j^{(i)}$ are called *cavity fields*. The $\omega_i^{(i)}$ play the role of *cavity inverse variances*, whereas the $h_j^{(i)}$ can be considered as *cavity biases*. Unlike the spectral problem, here we employ a non-zero mean Gaussian ansatz. It is chosen to obtain a solution $\boldsymbol{v}$ whose components are not peaked at zero in the $\beta \to \infty$ limit. Inserting the Gaussian ansatz (3.24) in (3.23) and performing the resulting Gaussian integrals, one obtains

$$P_j^{(i)}(v_j) = \frac{1}{Z_j^{(i)}} \exp\left(-\frac{\beta}{2} \lambda v_j^2\right) \prod_{\ell \in \partial j \setminus i} \exp\left[\frac{\beta}{2} \frac{\left(J_{j\ell} v_j + h_\ell^{(j)}\right)^2}{\omega_\ell^{(j)}}\right] \,. \tag{3.25}$$

Comparing the coefficients of the same powers of v_j between (3.24) and (3.25), one obtains the

following two self-consistent relations which define the cavity fields $\omega_i^{(i)}$ and $h_j^{(i)}$, viz.

$$\omega_j^{(i)} = \lambda - \sum_{\ell \in \partial j \setminus i} \frac{J_{j\ell}^2}{\omega_\ell^{(j)}} \,, \tag{3.26}$$

$$h_j^{(i)} = \sum_{\ell \in \partial j \setminus i} \frac{J_{j\ell}}{\omega_\ell^{(j)}} h_\ell^{(j)} \,. \tag{3.27}$$

These equations have been obtained before in [47].

The Gaussian ansatz (3.24) can then be inserted in (3.22), resulting in a Gaussian distribution for the single-site marginals

$$P_i(v_i) = \frac{1}{Z_i} \exp\left(-\frac{\beta}{2} \omega_i v_i^2 + \beta h_i v_i \right) \,, \tag{3.28}$$

where the N coefficients ω_i and h_i are given by

$$\omega_i = \lambda - \sum_{j \in \partial i} \frac{J_{ij}^2}{\omega_j^{(i)}} \,, \tag{3.29}$$

$$h_i = \sum_{j \in \partial i} \frac{J_{ij}}{\omega_j^{(i)}} h_j^{(i)} \,. \tag{3.30}$$

Here, $\omega_j^{(i)}$ and $h_j^{(i)}$ are the fixed-point solutions of (3.26) and (3.27). Therefore, using (3.28) to express (3.19), one finds

$$P_\beta(\boldsymbol{v}|\lambda) = \prod_{i=1}^N \frac{1}{Z_i} \exp\left(-\frac{\beta}{2} \omega_i v_i^2 + \beta h_i v_i \right) \,. \tag{3.31}$$

In the limit $\beta \to \infty$, Eq. (3.31) converges to

$$P(\boldsymbol{v}|\lambda) = \prod_{i=1}^N \delta\left(v_i - \frac{h_i}{\omega_i} \right) \,, \tag{3.32}$$

from which one concludes that the components of the top eigenvector of the fixed matrix J (a single instance of the ensemble) must be given by $v_1^{(i)} = h_i/\omega_i$, where h_i and ω_i are the values obtained from (3.29) and (3.30), after the fixed-points of the recursions (3.26) and (3.27) have been obtained. The normalisation condition (3.17) then becomes

$$1 = \frac{1}{N} \sum_{i=1}^N \left(\frac{h_i}{\omega_i} \right)^2 \,. \tag{3.33}$$

A detailed analysis of the recursions (3.26) and (3.27) is deferred to Appendix 3.A. There we show that their convergence and the possibility for the condition (3.33) to be satisfied are strongly interlaced and determined by the value of λ. Indeed, convergence is achieved only for $\lambda = \lambda_1$, as it should according to Eq. (3.16).

We conclude this section by noticing that although the single-instance derivation only relies on the tree-like approximation for the local connectivity and is arguably very easy and intuitive, it is not particularly useful as it stands. Indeed, we show in Appendix 3.A that the cavity algorithm essentially transforms the original top eigenpair problem for the $N \times N$ matrix J into the top eigenpair problem for the related larger $Nc \times Nc$ non-symmetric matrix B, i.e. the *non-backtracking* operator of J. It is, however, a conceptually necessary ingredient to discuss infinite-size matrices, as we do in the next subsection below.

3.3.2 Thermodynamic limit

In an infinitely large network, it is no longer possible to keep track of an infinite number of cavity fields. We then consider first the *joint probability density* that the cavity fields of type $\omega_j^{(i)}$ and $h_j^{(i)}$ take up values around ω and h

$$\begin{aligned}\pi(\omega,h) &= \text{Prob}\left(\omega_j^{(i)} = \omega, h_j^{(i)} = h\right) \\ &= \left(\sum_{i=1}^{N} k_i\right)^{-1} \sum_{i=1}^{N} \sum_{j\in\partial i} \delta\left(\omega - \omega_j^{(i)}\right) \delta\left(h - h_j^{(i)}\right) ,\end{aligned} \tag{3.34}$$

where N is now large but finite. This is a properly normalised pdf: indeed, we can associate two cavity fields $\omega_j^{(i)}$ and $h_j^{(i)}$ to any link (i,j) of the network. Since every node i is the source of k_i links, their total number is given by $\sum_{i=1}^{N} k_i$.

As is done in Section 2.3.3, one may appeal to the single-instance update rules given by (3.26) and (3.27) to characterise the above distribution self-consistently, with the only differences that in this case the cavity fields pdf $\pi(\omega,h)$ is bivariate and the ω and h are real valued. Following the exact same reasoning of Section 2.3.3, the joint pdf $\pi(\omega,h)$ is given by the self-consistency equation

$$\pi(\omega,h) = \sum_{k=1}^{k_{\max}} r(k) \int \left[\prod_{\ell=1}^{k-1} \mathrm{d}\pi(\omega_\ell,h_\ell)\right] \left\langle \delta\left(\omega - \lambda + \sum_{\ell=1}^{k-1} \frac{K_\ell^2}{\omega_\ell}\right) \delta\left(h - \sum_{\ell=1}^{k-1} \frac{h_\ell K_\ell}{\omega_\ell}\right) \right\rangle_{\{K\}_{k-1}} , \tag{3.35}$$

where $\mathrm{d}\pi(\omega_\ell,h_\ell) \equiv \mathrm{d}\omega_\ell \mathrm{d}h_\ell \pi(\omega_\ell,h_\ell)$, the average $\langle\cdot\rangle_{\{K\}_{k-1}}$ is taken over $k-1$ independent realisations of the random variable K and $r(k) = \frac{k}{c} p(k)$ denotes the probability mass function

of having a random link pointing to a node of degree k. The sum in (3.35) starts from $k = 1$ since we should not be concerned with isolated nodes. Eq. (3.35) is generally solved via a population dynamics algorithm (see Section 3.6 for details). In some exceptional cases, such as for adjacency matrices of random regular graphs, it can be solved analytically (see discussion in sections 3.4.1.2 and 3.4.2.2 below).

Similarly, the joint pdf of the coefficients ω_i and h_i can be expressed as

$$\tilde{\pi}\left(\tilde{\omega},\tilde{h}\right) = \frac{1}{N}\sum_{i=1}^{N}\delta\left(\tilde{\omega}-\omega_i\right)\delta\left(\tilde{h}-h_i\right) \ . \tag{3.36}$$

In this case, there is a pair of marginal coefficients ω_i and h_i living on each *node*. Categorising nodes by their degree and following the same line of reasoning that led to (3.35), in the infinite size limit the joint pdf of the random variables of the type ω_i and h_i can be written as

$$\tilde{\pi}\left(\tilde{\omega},\tilde{h}\right) = \sum_{k=0}^{k_{\max}} p\left(k\right)\int\left[\prod_{\ell=1}^{k}\mathrm{d}\pi\left(\omega_\ell,h_\ell\right)\right]\left\langle\delta\left(\tilde{\omega}-\lambda+\sum_{\ell=1}^{k}\frac{K_\ell^2}{\omega_\ell}\right)\delta\left(\tilde{h}-\sum_{\ell=1}^{k}\frac{h_\ell K_\ell}{\omega_\ell}\right)\right\rangle_{\{K\}_k} , \tag{3.37}$$

where $p(k)$ is the degree distribution. Here, $\pi\left(\omega_\ell,h_\ell\right)$ is the fixed-point distribution of cavity fields, i.e. the solution of the self-consistency equation (3.35), which should therefore be solved beforehand.

The distribution of the top eigenvector's components in the thermodynamic limit is then obtained in terms of the pdf $\tilde{\pi}\left(\tilde{\omega},\tilde{h}\right)$ in (3.37), exploiting the analogy with the single-instance case in (3.32), and reads

$$\begin{aligned}\rho_J(u) &= \int \mathrm{d}\tilde{\omega}\mathrm{d}\tilde{h}\ \tilde{\pi}\left(\tilde{\omega},\tilde{h}\right)\delta\left(u-\frac{\tilde{h}}{\tilde{\omega}}\right)\\ &= \sum_{k=0}^{k_{\max}} p\left(k\right)\int\left[\prod_{\ell=1}^{k}\mathrm{d}\pi\left(\omega_\ell,h_\ell\right)\right]\left\langle\delta\left(u-\frac{\sum_{\ell=1}^{k}\frac{h_\ell K_\ell}{\omega_\ell}}{\lambda-\sum_{\ell=1}^{k}\frac{K_\ell^2}{\omega_\ell}}\right)\right\rangle_{\{K\}_k} .\end{aligned} \tag{3.38}$$

Moreover, Eq. (3.16) generalises at the ensemble level as

$$\langle\lambda_1\rangle_J = \lambda \ , \tag{3.39}$$

where the value of λ must be fixed taking into account the normalisation condition (3.33) of

the top eigenvector, that in the thermodynamic limit becomes

$$1 = \int \mathrm{d}\tilde{\omega}\mathrm{d}\tilde{h}\, \tilde{\pi}\left(\tilde{\omega},\tilde{h}\right)\left(\frac{\tilde{h}}{\tilde{\omega}}\right)^2$$
$$= \sum_{k=0}^{k_{\max}} p(k) \int \left[\prod_{\ell=1}^{k} \mathrm{d}\pi\left(\omega_\ell, h_\ell\right)\right] \left\langle \left(\frac{\sum_{\ell=1}^{k} \frac{h_\ell K_\ell}{\omega_\ell}}{\lambda - \sum_{\ell=1}^{k} \frac{K_\ell^2}{\omega_\ell}}\right)^2 \right\rangle_{\{K\}_k} . \tag{3.40}$$

Eq. (3.39) is crucially confirmed by the behaviour of the stochastic integral equation (3.35). Indeed, for every $\lambda > \langle\lambda_1\rangle_J$, the distribution of the h's shrinks to a delta peak located at zero, whereas for $\lambda < \langle\lambda_1\rangle_J$, negative values of the ω's start to appear while the h's grow without bounds in the self-consistency solution of (3.35). This is not surprising, since $\lambda < \langle\lambda_1\rangle_J$ is precisely the range of values for λ that makes the Gibbs-Boltzmann distribution (3.19) not normalisable. Therefore, the only value of λ such that the normalisation condition (3.40) can be satisfied is exactly $\langle\lambda_1\rangle_J$.

In summary, Eq. (3.35), (3.38), (3.39) and (3.40) provide the solution to the top eigenpair problem within the cavity formalism. We anticipate that they will match respectively (3.106), (3.145), (3.117) and (3.107) obtained with the replica method in Section 3.4 below.

3.3.3 Large-c limit for weighted adjacency matrices

Here we study the large c behaviour of the equations (3.35), (3.38), (3.39) and (3.40) representing the solution to the top eigenpair problem of sparse ensembles. As done in the case of the average spectral density in Section 2.3.4, we consider a configuration model graph, whose degree distribution $p(k)$ – with finite mean, finite variance and a bounded maximum degree – satisfies the condition $\frac{\sigma_k^2}{\langle k\rangle^2} = \frac{\langle k^2\rangle - \langle k\rangle^2}{\langle k\rangle^2} \to 0$ as $\langle k\rangle = c \to \infty$. A meaningful large-$c$ limit is obtained for Eq. (3.35) by rescaling each instance of the bond random weights as $K_{ij} = \mathscr{J}_{ij}/\sqrt{c}$, leading to

$$\pi(\omega,h) = \sum_{k\geq 1} \frac{k}{c} p(k) \int \{\mathrm{d}\pi\}_{k-1} \left\langle \delta\left(\omega - \lambda + \frac{1}{c}\sum_{\ell=1}^{k-1} \frac{\mathscr{J}_\ell^2}{\omega_\ell}\right) \delta\left(h - \frac{1}{\sqrt{c}}\sum_{\ell=1}^{k-1} \frac{h_\ell \mathscr{J}_\ell}{\omega_\ell}\right)\right\rangle_{\{\mathscr{J}\}_{k-1}} . \tag{3.41}$$

In the $c \gg 1$ limit, the k-sum in Eq. (3.41) is restricted to $k = c \pm \mathscr{O}(\sigma_k)$, so that the argument appearing in the first δ-function on the r.h.s of this equation can be evaluated by appeal to the Law of Large Number (LLN). This entails that

$$\omega = \lambda - \frac{1}{c}\sum_{\ell=1}^{k-1} \frac{\mathscr{J}_\ell^2}{\omega_\ell} \tag{3.42}$$

is *non-fluctuating*, hence the self-consistency equation demands that

$$\pi(\omega,h) = \delta(\omega-\bar{\omega}) \times P(h) \,, \tag{3.43}$$

with (by the LLN)

$$\bar{\omega} = \lambda - \frac{1}{c}\sum_{\ell=1}^{k-1} \frac{\mathscr{J}_\ell^2}{\bar{\omega}} = \lambda - \frac{\langle \mathscr{J}^2 \rangle_{\mathscr{J}}}{\bar{\omega}} \,. \tag{3.44}$$

Specializing to $\langle \mathscr{J}^2 \rangle_{\mathscr{J}} = 1$, we see that

$$\bar{\omega}_{1,2} = \frac{1}{2}\left(\lambda \pm \sqrt{\lambda^2-4}\right) \,, \tag{3.45}$$

which requires $\lambda \geq 2$ to have real positive $\bar{\omega}$.

Similarly, the argument of the second δ-function on the r.h.s of (3.41) exhibits a scaling that allows one to conclude (for $\langle \mathscr{J}_\ell \rangle_{\mathscr{J}} = 0$) that

$$h = \frac{1}{\sqrt{c}}\sum_{\ell=1}^{k-1} \frac{h_\ell \mathscr{J}_\ell}{\omega_\ell} = \frac{1}{\sqrt{c}}\sum_{\ell=1}^{k-1} \frac{h_\ell \mathscr{J}_\ell}{\bar{\omega}} \sim \mathscr{N}(0,\sigma_h^2)$$

which follows from the Central Limit Theorem. The variance follows using independence of the $\{h_\ell\}$ and $\{\mathscr{J}_\ell\}$

$$\sigma_h^2 = \langle h^2 \rangle = \frac{1}{c\bar{\omega}^2}\sum_{\ell=1}^{k-1} \langle h_\ell^2 \rangle \langle \mathscr{J}_\ell^2 \rangle_{\mathscr{J}} = \frac{\sigma_h^2}{\bar{\omega}^2} \,. \tag{3.46}$$

This equation allows a finite variance if and only if $\bar{\omega}^2 = 1$, which requires $\lambda = \pm 2$, i.e. that λ – the most probable location of the largest eigenvalue – is at the edge of the Wigner semi-circle (and we require the positive solution).

To obtain the distribution $\rho_J(u)$ of eigenvector components, we consider Eq. (3.37), (3.38) and (3.40). After the rescaling $K_\ell = \mathscr{J}_\ell/\sqrt{c}$ and in the large c-limit, it is easy to see from (3.37) that $\tilde{\omega} = \bar{\omega}$ and that $\tilde{h}$ is a sum of Gaussians, and thus itself Gaussian, of variance $\sigma_h^2/\bar{\omega}^2 \equiv \sigma_h^2$ by (3.46). It then follows from the normalisation condition (3.40) that $\sigma_h^2 = 1$, so eventually

$$\rho_J(u) = \frac{1}{\sqrt{2\pi}} \mathrm{e}^{-u^2/2} \,. \tag{3.47}$$

Looking now at the variable $\eta = u^2$, and noting that positive and negative u give rise to the

same η, one obtains by the simple transformation of pdf's

$$\rho(\eta) = \frac{1}{\sqrt{2\pi\eta}} \mathrm{e}^{-\eta/2} \,, \tag{3.48}$$

which is the standard form of the Porter-Thomas distribution for real-valued (invariant) random matrices (see [94], Eq. (9.10)).

3.4 Replica derivation

The cavity approach has the advantage of leading rather quickly to the result. It is, however, instructive to reconsider the problem from the point of view of the replica approach, which provides a lengthier but rather systematic procedure. Similarly to what has been shown in Chapter 2 regarding the spectral problem, we make a quite transparent and convincing case for the equivalence between the cavity and replica methods for the top eigenpair problem.

In this section, we evaluate the average location of the largest eigenvalue and the density of top eigenvectors' components within the replica framework. For the sake of clarity, we will keep the two pathways (typical largest eigenvalue vs. density of top eigenvector's components) clearly separate until the point where we realise that the same self-consistency equation governs the statistics of both quantities. Our derivation provides a general and robust methodology that can be applied to any graph within the configuration model, whose degree distribution has finite mean, finite variance and bounded maximal degree. As we did for the cavity approach, we thoroughly discuss bounds on the values of parameters that guarantee a converging solution. Across the whole section, we will first provide the formulation for a generic degree distribution $p(k)$ with the aforementioned characteristics. Then we will give numerical results for the Erdős-Rényi (ER) case and derive an analytical solution for adjacency matrices of random regular graphs (RRGs).

3.4.1 Typical largest eigenvalue

Consider again a $N \times N$ symmetric matrix $J_{ij} = c_{ij}K_{ij}$. The joint distribution of the matrix entries is

$$P\left(\{J_{ij}\}\middle|\{k_i\}\right) = P\left(\{c_{ij}\}\middle|\{k_i\}\right) \prod_{i<j} \delta_{K_{ij},K_{ji}} p_K\left(K_{ij}\right) \,, \tag{3.49}$$

where, in the framework of the configuration model [44], the distribution $P\left(\{c_{ij}\}\middle|\{k_i\}\right)$ of connectivities $\{c_{ij}\}$ compatible with a given degree sequence $\{k_i\}$ is given by

$$P\left(\{c_{ij}\}\middle|\{k_i\}\right)=\frac{1}{\mathscr{M}}\prod_{i<j}\delta_{c_{ij},c_{ji}}\left(\frac{c}{N}\delta_{c_{ij},1}+\left(1-\frac{c}{N}\right)\delta_{c_{ij},0}\right)\prod_{i=1}^{N}\delta_{\sum_j c_{ij},k_i}\,, \tag{3.50}$$

and the pdf $p_K(K_{ij})$ of bond weights (with compact support and upper edge ζ) can be kept unspecified until the very end. The average of the largest eigenvalue can be computed as the formal limit

$$\langle\lambda_1\rangle_J=\lim_{\beta\to\infty}\frac{2}{\beta N}\langle\ln Z\rangle_J\,,\qquad Z=\int \mathrm{d}\boldsymbol{v}\exp\left[\frac{\beta}{2}(\boldsymbol{v},J\boldsymbol{v})\right]\delta\left(|\boldsymbol{v}|^2-N\right)\,, \tag{3.51}$$

in terms of the quenched free energy of the model defined in (3.6). The average over J is computed using the replica trick as follows

$$\langle\lambda_1\rangle_J=\lim_{\beta\to\infty}\frac{2}{\beta N}\lim_{n\to 0}\frac{1}{n}\ln\langle Z^n\rangle_J\,, \tag{3.52}$$

where n is initially taken as an integer, and then analytically continued to real values in the vicinity of $n=0$. The replicated partition function is

$$\langle Z^n\rangle_J=\int\left(\prod_{a=1}^{n}\mathrm{d}\boldsymbol{v}_a\right)\left\langle\exp\left(\frac{\beta}{2}\sum_{a=1}^{n}\sum_{i,j}^{N}v_{ia}J_{ij}v_{ja}\right)\right\rangle_J\prod_{a=1}^{n}\delta\left(|\boldsymbol{v}_a|^2-N\right)\,. \tag{3.53}$$

Taking the average w.r.t. the joint distribution (3.50) of matrix entries yields [44]

$$\begin{aligned}\left\langle\exp\left(\frac{\beta}{2}\sum_{a=1}^{n}\sum_{i,j}^{N}v_{ia}J_{ij}v_{ja}\right)\right\rangle_J=\frac{1}{\mathscr{M}}\int_{-\pi}^{\pi}\left(\prod_{i=1}^{N}\frac{\mathrm{d}\phi_i}{2\pi}\right)\exp\left(-\mathrm{i}\sum_i\phi_i k_i\right)\\ \times\exp\left[\frac{c}{2N}\sum_{i,j}\left(\left\langle\mathrm{e}^{\beta K\sum_a v_{ia}v_{ja}+\mathrm{i}(\phi_i+\phi_j)}\right\rangle_K-1\right)\right]\,,\end{aligned} \tag{3.54}$$

where $\langle\cdot\rangle_K$ denotes averaging over the single-variable pdf $p_K(K)$ characterising the i.i.d. bond weights K_{ij}. A Fourier representation of the Kronecker deltas expressing the degree constraints in (3.50) has been employed. We also employ a Fourier representation of the Dirac delta enforcing the normalisation constraints,

$$\prod_{a=1}^{n}\delta\left(|\boldsymbol{v}_a|^2-N\right)=\int_{-\infty}^{\infty}\left(\prod_{a=1}^{n}\frac{\beta}{2}\frac{\mathrm{d}\lambda_a}{2\pi}\right)\prod_{a=1}^{n}\exp\left[-\mathrm{i}\frac{\beta}{2}\lambda_a\left(\sum_{i=1}^{N}v_{ia}^2-N\right)\right]\,. \tag{3.55}$$

The replicated partition function thus becomes

$$\langle Z^n \rangle_J = \frac{1}{\mathscr{M}} \left(\frac{\beta}{4\pi} \right)^n \int \left(\prod_{a=1}^{n} \mathrm{d}\boldsymbol{v}_a \mathrm{d}\lambda_a \right) \exp\left(\mathrm{i} \frac{\beta}{2} N \sum_a \lambda_a \right) \exp\left(-\mathrm{i} \frac{\beta}{2} \sum_a \sum_i \lambda_a v_{ia}^2 \right) \\ \times \int_{-\pi}^{\pi} \left(\prod_{i=1}^{N} \frac{\mathrm{d}\phi_i}{2\pi} \right) \exp\left(-\mathrm{i} \sum_i \phi_i k_i \right) \exp\left[\frac{c}{2N} \sum_{i,j} \left(\left\langle \mathrm{e}^{\beta K \sum_a v_{ia} v_{ja} + \mathrm{i}(\phi_i + \phi_j)} \right\rangle_K - 1 \right) \right] . \tag{3.56}$$

In order to decouple sites, we introduce the functional order parameter

$$\varphi(\vec{v}, \phi) = \frac{1}{N} \sum_{i=1}^{N} \delta(\phi - \phi_i) \prod_{a=1}^{n} \delta(v_a - v_{ia}) , \tag{3.57}$$

where the symbol $\vec{v}$ denotes a n-dimensional vector in replica space. We then consider its integrated version [44]

$$\varphi(\vec{v}) = \int \mathrm{d}\phi \ \mathrm{e}^{\mathrm{i}\phi} \varphi(\vec{v}, \phi) = \frac{1}{N} \sum_{i=1}^{N} \mathrm{e}^{\mathrm{i}\phi_i} \prod_{a=1}^{n} \delta(v_a - v_{ia}) , \tag{3.58}$$

and enforce the latter definition using the integral identity

$$1 = \int N \mathscr{D}\varphi \mathscr{D}\hat{\varphi} \exp\left\{ -\mathrm{i} \int \mathrm{d}\vec{v} \ \hat{\varphi}(\vec{v}) \left[N\varphi(\vec{v}) - \sum_i \mathrm{e}^{\mathrm{i}\phi_i} \prod_{a=1}^{n} \delta(v_a - v_{ia}) \right] \right\} . \tag{3.59}$$

In terms of the integrated order parameter (3.58) and its conjugate, the replicated partition function can be written as

$$\langle Z^n \rangle_J = \frac{1}{\mathscr{M}} \left(\frac{\beta}{4\pi} \right)^n N \int \mathscr{D}\varphi \mathscr{D}\hat{\varphi} \mathrm{d}\vec{\lambda} \exp\left(-\mathrm{i} N \int \mathrm{d}\vec{v} \hat{\varphi}(\vec{v}) \varphi(\vec{v}) \right) \\ \times \exp\left[\frac{Nc}{2} \left(\int \mathrm{d}\vec{v} \mathrm{d}\vec{v'} \varphi(\vec{v}) \varphi(\vec{v'}) \left\langle \mathrm{e}^{\beta K \sum_a v_a v'_a} \right\rangle_K - 1 \right) \right] \exp\left(\mathrm{i} \frac{\beta}{2} N \sum_a \lambda_a \right) \\ \times \int_{-\pi}^{\pi} \left(\prod_{i=1}^{N} \frac{\mathrm{d}\phi_i}{2\pi} \right) \mathrm{e}^{-\mathrm{i} \sum_i \phi_i k_i} \int \prod_{a=1}^{n} \mathrm{d}\boldsymbol{v}_a \exp\left[-\mathrm{i} \frac{\beta}{2} \sum_a \sum_i \lambda_a v_{ia}^2 + \mathrm{i} \sum_i \mathrm{e}^{\mathrm{i}\phi_i} \hat{\varphi}(\vec{v}_i) \right] . \tag{3.60}$$

The multiple integral in the last line above is the product of N n-dimensional integrals, each related to a degree k_i. It can be written as

$$\begin{aligned} I &= \prod_{i=1}^{N} \int_{-\pi}^{\pi} \frac{\mathrm{d}\phi_i}{2\pi} \int \mathrm{d}\vec{v}_i \exp\left(-\mathrm{i}\phi_i k_i - \mathrm{i}\frac{\beta}{2} \sum_a \lambda_a v_{ia}^2 + \mathrm{i}\hat{\varphi}(\vec{v}_i) \mathrm{e}^{\mathrm{i}\phi_i} \right) \\ &= \exp\left[\sum_{i=1}^{N} \mathrm{Log} \int \mathrm{d}\vec{v}_i \exp\left(-\mathrm{i}\frac{\beta}{2} \sum_a \lambda_a v_{ia}^2 \right) I[k_i, \vec{v}_i] \right] , \end{aligned} \tag{3.61}$$

where Log denotes the principal branch of the complex logarithm, and

$$I[k_i, \vec{v}_i] = \int_{-\pi}^{\pi} \frac{\mathrm{d}\phi_i}{2\pi} \exp\left(-\mathrm{i}\phi_i k_i + \mathrm{i}\hat{\varphi}(\vec{v}_i) \mathrm{e}^{\mathrm{i}\phi_i} \right) . \tag{3.62}$$

Each of the ϕ_i integrals can be performed by rewriting the last exponential factor as a power series, viz.

$$I[k_i, \vec{v}_i] = \int_{-\pi}^{\pi} \frac{\mathrm{d}\phi_i}{2\pi} \mathrm{e}^{-\mathrm{i}\phi_i k_i} \sum_{s=0}^{\infty} \frac{(\mathrm{i}\hat{\varphi}(\vec{v}_i))^s}{s!} \mathrm{e}^{\mathrm{i}s\phi_i} = \sum_{s=0}^{\infty} \frac{(\mathrm{i}\hat{\varphi}(\vec{v}_i))^s}{s!} \delta_{s,k_i} = \frac{(\mathrm{i}\hat{\varphi}(\vec{v}_i))^{k_i}}{k_i!} , \tag{3.63}$$

for any k_i with $i = 1, \ldots, N$. Thus, by invoking the Law of Large Numbers, the single-site integral I in (3.61) can be expressed as

$$\begin{aligned} I &= \exp\left[\sum_{i=1}^{N} \mathrm{Log} \int \mathrm{d}\vec{v}_i \exp\left(-\mathrm{i}\frac{\beta}{2} \sum_a \lambda_a v_{ia}^2 \right) \frac{\left(\mathrm{i}\hat{\varphi}(\vec{v}_i)^{k_i}\right)}{k_i!} \right] \\ &= \exp\left[N \sum_{k=k_{\min}}^{k_{\max}} p(k) \left[\mathrm{Log} \int \mathrm{d}\vec{v} \exp\left(-\mathrm{i}\frac{\beta}{2} \sum_a \lambda_a v_a^2 \right) (\mathrm{i}\hat{\varphi}(\vec{v}))^k - \mathrm{Log}(k!) \right] \right], \end{aligned} \tag{3.64}$$

where we have used

$$\frac{1}{N} \sum_{i=1}^{N} \mathrm{Log} f(k_i) \simeq \sum_{k=k_{\min}}^{k_{\max}} p(k) \mathrm{Log} f(k) , \tag{3.65}$$

and $p(k)$ is the actual degree distribution of the graph. Henceforth, we will consider $k_{\min} = 0$.

The replicated partition function thus takes a form amenable to a saddle point evaluation for large N (where we assume we can safely exchange the limits $n \to 0$ and $N \to \infty$)

$$\langle Z^n \rangle_J \propto \frac{1}{\mathscr{M}} \int \mathscr{D}\varphi \mathscr{D}\hat{\varphi} \mathrm{d}\vec{\lambda} \exp\left(N S_n[\varphi, \hat{\varphi}, \vec{\lambda}] \right) , \tag{3.66}$$

where

$$S_n[\varphi, \hat{\varphi}, \vec{\lambda}] = S_1[\varphi, \hat{\varphi}] + S_2[\varphi] + S_3(\vec{\lambda}) + S_4[\hat{\varphi}, \vec{\lambda}] , \tag{3.67}$$

and

$$S_1[\varphi,\hat{\varphi}] = -\mathrm{i}\int \mathrm{d}\vec{v}\,\hat{\varphi}(\vec{v})\varphi(\vec{v})\ , \tag{3.68}$$

$$S_2[\varphi] = \frac{c}{2}\left(\int \mathrm{d}\vec{v}\mathrm{d}\vec{v'}\,\varphi(\vec{v})\varphi(\vec{v'})\left\langle \mathrm{e}^{\beta K\sum_a v_a v'_a}\right\rangle_K - 1\right)\ , \tag{3.69}$$

$$S_3(\vec{\lambda}) = \mathrm{i}\frac{\beta}{2}\sum_a \lambda_a\ , \tag{3.70}$$

$$S_4[\hat{\varphi},\vec{\lambda}] = \sum_{k=0}^{k_{\max}} p(k)\left[\mathrm{Log}\int \mathrm{d}\vec{v}\exp\left(-\mathrm{i}\frac{\beta}{2}\sum_a \lambda_a v_a^2\right)\left(\mathrm{i}\hat{\varphi}(\vec{v})\right)^k - \mathrm{Log}(k!)\right]\ . \tag{3.71}$$

The stationarity of the action S_n w.r.t. variations of φ and $\hat{\varphi}$ requires that the order parameter at the saddle point $\varphi^\star$ and its conjugate $\hat{\varphi}^\star$ satisfy the following coupled equations

$$\mathrm{i}\hat{\varphi}^\star(\vec{v}) = c\int \mathrm{d}\vec{v'}\varphi^\star(\vec{v'})\left\langle \exp\left(\beta K\sum_a v_a v'_a\right)\right\rangle_K\ , \tag{3.72}$$

$$\varphi^\star(\vec{v}) = \sum_{k=1}^{k_{\max}} p(k)k\frac{\exp\left(-\mathrm{i}\frac{\beta}{2}\sum_a \lambda_a v_a^2\right)\left(\mathrm{i}\hat{\varphi}(\vec{v})\right)^{k-1}}{\int \mathrm{d}\vec{v'}\exp\left(-\mathrm{i}\frac{\beta}{2}\sum_a \lambda_a {v'_a}^2\right)\left(\mathrm{i}\hat{\varphi}(\vec{v'})\right)^k}\ , \tag{3.73}$$

which have to be solved together with the stationarity conditions w.r.t. each component $\lambda_{\bar{a}}$ of $\vec{\lambda}$

$$1 = \sum_{k=0}^{k_{\max}} p(k)\frac{\int \mathrm{d}\vec{v}\exp\left(-\mathrm{i}\frac{\beta}{2}\sum_a \lambda_a {v_a}^2\right)\left(\mathrm{i}\hat{\varphi}(\vec{v})\right)^k v_{\bar{a}}^2}{\int \mathrm{d}\vec{v'}\exp\left(-\mathrm{i}\frac{\beta}{2}\sum_a \lambda_a {v'_a}^2\right)\left(\mathrm{i}\hat{\varphi}(\vec{v'})\right)^k} \qquad \forall \bar{a} = 1,\dots,n\ . \tag{3.74}$$

The equations (3.72) and (3.73) show some resemblance with the saddle-point equations leading to the spectral density of Erdős-Rényi random graphs (see for instance Eq. (2.60) and (2.61) in Chapter 2 and also [23] where they have first been derived). The most noticeable difference is that the "Hamiltonian" of our problem is real-valued and includes the inverse temperature β.

Following [33] as in Section 2.5 of Chapter 2, we will now search for a replica-symmetric solution, expressing the order parameter $\varphi(\vec{v})$ and its conjugate $\hat{\varphi}(\vec{v})$ in the form of a superposition of uncountably infinite Gaussians. However, at odds with the choice in [33], we choose these Gaussians with a *non-zero* mean. This ansatz will be preserving permutational symmetry between replicas, but not the rotational invariance in the space of replicas. Indeed, a rotationally invariant ansatz would not produce a physically meaningful result for this problem, as the "ground state" solution we look for would collapse onto the trivial zero-vector solution. The

ansätze read

$$\lambda_{\bar{a}} = \lambda \qquad \forall \bar{a} = 1, \ldots, n \,, \tag{3.75}$$

$$\varphi(\vec{v}) = \varphi_0 \int \mathrm{d}\omega \mathrm{d}h \; \pi(\omega, h) \prod_{a=1}^{n} \frac{1}{Z_\beta(\omega, h)} \exp\left[-\frac{\beta}{2} \omega v_a^2 + \beta h v_a \right] \,, \tag{3.76}$$

$$\hat{\varphi}(\vec{v}) = \hat{\varphi}_0 \int \mathrm{d}\hat{\omega} \mathrm{d}\hat{h} \; \hat{\pi}(\hat{\omega}, \hat{h}) \prod_{a=1}^{n} \exp\left[\frac{\beta}{2} \hat{\omega} v_a^2 + \beta \hat{h} v_a \right] \,, \tag{3.77}$$

where

$$Z_\beta(x, y) = \sqrt{\frac{2\pi}{\beta x}} \exp\left(\frac{\beta y^2}{2x} \right) \,. \tag{3.78}$$

The justification for this kind of ansatz given for the spectral case in Section 2.5 of Chapter 2 holds here as well. Indeed we are still dealing with an harmonically coupled system, despite a real-valued Hamiltonian. Hence, our derivation is not that far from the spectral problem of sparse random matrices for which the assumption of replica symmetry has been established rigorously in [27]. In (3.76) and (3.77), π and $\hat{\pi}$ are normalised joint pdfs of the parameters appearing in the Gaussian distributions. We employ the name π for the auxiliary distribution appearing in (3.76) since it will eventually coincide with what found in Section 3.3.2. The φ_0 and $\hat{\varphi}_0$ are determined such that the distributions $\pi(\omega, h)$ and $\hat{\pi}(\hat{\omega}, \hat{h})$ are normalised. A few remarks are in order.

- The constant φ_0 in (3.76) is needed since $\varphi(\vec{v})$ is the saddle-point expression of the integrated order parameter, therby it needs not be normalised.
- The different signs in front of ω and $\hat{\omega}$ in (3.76) and (3.77) are picked with an eye towards performing the subsequent $\vec{v}$-integrals: since $\hat{\varphi}(\vec{v})$ is not a pdf, $\hat{\omega}$ being positive is not problematic.

Once inserted into the action (3.67), the replica-symmetric assumptions (3.75), (3.76) and (3.77) allow one to perform explicitly the $\vec{v}$-integrals and extract the leading $\mathscr{O}(n)$ contribution to S_n in the limit $n \to 0$. In this setting, the action (3.67) becomes a functional of π, $\hat{\pi}$ and λ and the path integral over φ and $\hat{\varphi}$ in (3.66) is thus replaced by a path integral over π and $\hat{\pi}$, viz.

$$\langle Z^n \rangle_J \propto \frac{1}{\mathscr{M}} \int \mathscr{D}\pi \mathscr{D}\hat{\pi} \mathrm{d}\lambda \exp\left(N S_n[\pi, \hat{\pi}, \lambda] \right) \,, \tag{3.79}$$

where

$$S_n[\pi, \hat{\pi}, \lambda] = S_1[\pi, \hat{\pi}] + S_2[\pi] + S_3(\lambda) + S_4[\hat{\pi}, \lambda] \,, \tag{3.80}$$

Extracting the leading $n \to 0$ contribution yields

$$S_1[\pi,\hat{\pi}] = -\mathrm{i}\varphi_0\hat{\varphi}_0 - \mathrm{i}\varphi_0\hat{\varphi}_0 n \int \mathrm{d}\pi(\omega,h)\mathrm{d}\hat{\pi}(\hat{\omega},\hat{h}) \ln \frac{Z_\beta(\omega-\hat{\omega},h+\hat{h})}{Z_\beta(\omega,h)} \,, \tag{3.81}$$

$$S_2[\pi] = \frac{c}{2}\left(\varphi_0^2 - 1\right) + n\frac{c}{2}\varphi_0^2 \int \mathrm{d}\pi(\omega,h)\mathrm{d}\pi(\omega',h') \left\langle \ln \frac{Z_\beta^{(2)}(\omega,\omega',h,h',K)}{Z_\beta(\omega,h)Z_\beta(\omega',h')} \right\rangle_K \,, \tag{3.82}$$

$$S_3(\lambda) = \mathrm{i}\frac{\beta}{2} n\lambda \,, \tag{3.83}$$

$$S_4[\hat{\pi},\lambda] = c\mathrm{Log}(\mathrm{i}\hat{\varphi}_0) - \sum_{k=0}^{k_{\max}} p(k)\mathrm{Log}(k!) + n\sum_{k=0}^{k_{\max}} p(k) \int \{\mathrm{d}\hat{\pi}\}_k \, \mathrm{Log}\, Z_\beta\left(\mathrm{i}\lambda - \{\hat{\omega}\}_k, \{\hat{h}\}_k\right) \,, \tag{3.84}$$

where we have introduced the shorthands

$$Z_\beta^{(2)}(\omega,\omega',h,h',K) = Z_\beta(\omega',h')Z_\beta\left(\omega - \frac{K^2}{\omega'}, h + \frac{h'K}{\omega'}\right) \tag{3.85}$$

and $\{\mathrm{d}\hat{\pi}\}_s = \prod_{\ell=1}^s \mathrm{d}\hat{\omega}_\ell \mathrm{d}\hat{h}_\ell \hat{\pi}(\hat{\omega}_\ell,\hat{h}_\ell)$, along with $\{\hat{\omega}\}_s = \sum_{\ell=1}^s \hat{\omega}_\ell$ and $\{\hat{h}\}_s = \sum_{\ell=1}^s \hat{h}_\ell$.

We note that the action contains $\mathscr{O}(1)$ and $\mathscr{O}(n)$ terms as $n \to 0$: the $\mathscr{O}(1)$ terms are cancelled by the $\mathscr{O}(1)$ terms arising from the evaluation of the normalisation constant $\mathscr{M}$ at the saddle-point. Indeed, by following a very similar reasoning as in (3.54), we find that

$$\mathscr{M} = \int_{-\pi}^{\pi} \left(\prod_{i=1}^N \frac{\mathrm{d}\phi_i}{2\pi}\right) \mathrm{e}^{-\mathrm{i}\sum_i \phi_i k_i} \exp\left[\frac{c}{2N}\sum_{i,j}\left(\mathrm{e}^{\mathrm{i}(\phi_i+\phi_j)} - 1\right)\right] \,. \tag{3.86}$$

We then introduce in (3.86) the scalar order parameter

$$\varphi_0 = \frac{1}{N}\sum_{i=1}^N \mathrm{e}^{\mathrm{i}\phi_i} \tag{3.87}$$

via the integral representation

$$1 = \int N\frac{\mathrm{d}\varphi_0 \mathrm{d}\hat{\varphi}_0}{2\pi} \exp\left[-\mathrm{i}\hat{\varphi}_0\left(N\varphi_0 - \sum_i \mathrm{e}^{\mathrm{i}\phi_i}\right)\right] \,. \tag{3.88}$$

By using the same argument as in (3.64), the normalisation constant $\mathscr{M}$ can be written in a

form amenable to a saddle-point evaluation,

$$\begin{aligned}\mathscr{M} &= \int N\frac{\mathrm{d}\varphi_0\mathrm{d}\hat{\varphi}_0}{2\pi}\exp\left[N\left(-\mathrm{i}\varphi_0\hat{\varphi}_0+\frac{c}{2}(\varphi_0^2-1)+c\mathrm{Log}(\mathrm{i}\hat{\varphi}_0)-\sum_{k=0}^{k_{\max}}p(k)\mathrm{Log}(k!)\right)\right]\\ &= \int N\frac{\mathrm{d}\varphi_0\mathrm{d}\hat{\varphi}_0}{2\pi}\exp\left[NS_{\mathscr{M}}(\varphi_0,\hat{\varphi}_0)\right]\ . \end{aligned} \tag{3.89}$$

The stationarity conditions[1] for $S_{\mathscr{M}}$ are

$$\frac{\partial S_{\mathscr{M}}}{\partial\varphi_0}=0\Rightarrow\mathrm{i}\hat{\varphi}_0=c\varphi_0\ , \tag{3.90}$$

and

$$\frac{\partial S_{\mathscr{M}}}{\partial\hat{\varphi}_0}=0\Rightarrow\mathrm{i}\varphi_0=\frac{c}{\hat{\varphi}_0}\ . \tag{3.91}$$

entailing that

$$\mathrm{i}\varphi_0\hat{\varphi}_0=c\ , \tag{3.92}$$

$$\varphi_0^2=1\ . \tag{3.93}$$

The two conditions above exhibit a gauge invariance [44]. Once the same gauge has been chosen for the saddle-point solution of $\mathscr{M}$ and the $\mathscr{O}(1)$ terms of the action (3.80) in the numerator, they cancel out so that the action (3.80) is $\mathscr{O}(n)$ as expected. Thus, taking into account the cancellation coming from (3.92) and (3.93), the action terms in (3.80) read

$$S_1[\pi,\hat{\pi}]=-nc\int\mathrm{d}\pi(\omega,h)\mathrm{d}\hat{\pi}(\hat{\omega},\hat{h})\ln\frac{Z_\beta(\omega-\hat{\omega},h+\hat{h})}{Z_\beta(\omega,h)}\ , \tag{3.94}$$

$$S_2[\pi]=n\frac{c}{2}\int\mathrm{d}\pi(\omega,h)\mathrm{d}\pi(\omega',h')\left\langle\ln\frac{Z_\beta^{(2)}(\omega,\omega',h,h',K)}{Z_\beta(\omega,h)Z_\beta(\omega',h')}\right\rangle_K\ , \tag{3.95}$$

$$S_3(\lambda)=\mathrm{i}\frac{\beta}{2}n\lambda\ , \tag{3.96}$$

$$S_4[\hat{\pi},\lambda]=n\sum_{k=0}^{k_{\max}}p(k)\int\{\mathrm{d}\hat{\pi}\}_k\ \mathrm{Log}\ Z_\beta\left(\mathrm{i}\lambda-\{\hat{\omega}\}_k,\{\hat{h}\}_k\right)\ , \tag{3.97}$$

We can finally consider the stationarity conditions of the action (3.80) w.r.t. λ, π and $\hat{\pi}$.

[1] In what follows, we indicate the saddle-point values of φ and $\hat{\varphi}$ without labelling them with a star.

The stationarity condition w.r.t. λ entails the condition

$$\frac{\partial S}{\partial \lambda}\Big|_{\lambda=\lambda^\star} = 0 \Rightarrow 1 = \sum_{s=0}^{\infty} p_{\hat{c}}(s) \int \{\mathrm{d}\hat{\pi}\}_s \langle v^2 \rangle_{\bar{P}} \,, \tag{3.98}$$

where the average $\langle \cdot \rangle_{\bar{P}}$ is taken with respect to the Gaussian measure

$$\bar{P}_\beta(v) = \sqrt{\frac{\beta\,(\mathrm{i}\lambda^\star - \{\hat{\omega}\}_s)}{2\pi}} \exp\left[-\frac{\beta}{2}\,(\mathrm{i}\lambda^\star - \{\hat{\omega}\}_s) \left(v - \frac{\{\hat{h}\}_s}{\mathrm{i}\lambda^\star - \{\hat{\omega}\}_s} \right)^2 \right] . \tag{3.99}$$

Eq. (3.98) more explicitely reads

$$1 = \sum_{k=0}^{\infty} p(k) \int \{\mathrm{d}\hat{\pi}\}_k \left[\frac{1}{\beta(\mathrm{i}\lambda^\star - \{\hat{\omega}\}_k)} + \left(\frac{\{\hat{h}\}_k}{\mathrm{i}\lambda^\star - \{\hat{\omega}\}_k} \right)^2 \right] , \tag{3.100}$$

where we note that the β-dependent term vanishes as $\beta \to \infty$. The stationarity condition w.r.t. variations of π, $\frac{\delta S}{\delta \pi} = 0$, entails the condition

$$\int \mathrm{d}\hat{\pi}(\hat{\omega},\hat{h}) \ln \frac{Z_\beta(\omega - \hat{\omega}, h + \hat{h})}{Z_\beta(\omega,h)} = \int \mathrm{d}\pi(\omega',h') \left\langle \ln \frac{Z_\beta^{(2)}(\omega,\omega',h,h',K)}{Z_\beta(\omega,h)} \right\rangle_K + \frac{\gamma}{c} \,, \tag{3.101}$$

where γ is a Lagrange multiplier introduced to enforce the normalisation of π. Given the definition of $Z_\beta^{(2)}$, Eq. (3.101) is equivalent to

$$\int \mathrm{d}\hat{\pi}(\hat{\omega},\hat{h}) \ln Z_\beta(\omega - \hat{\omega}, h + \hat{h}) = \int \mathrm{d}\pi(\omega',h') \left\langle \ln Z_\beta \left(\omega - \frac{K^2}{\omega'}, h + \frac{h'K}{\omega'} \right) \right\rangle_K + \frac{\gamma}{c} \,. \tag{3.102}$$

Since Eq. (3.102) must hold for all ω and h, it follows that

$$\hat{\pi}(\hat{\omega},\hat{h}) = \int \mathrm{d}\omega \mathrm{d}h\, \pi(\omega,h) \left\langle \delta\left(\hat{\omega} - \frac{K^2}{\omega} \right) \delta\left(\hat{h} - \frac{hK}{\omega} \right) \right\rangle_K \,, \tag{3.103}$$

Similarly, the stationarity condition w.r.t. variations of $\hat{\pi}$, $\frac{\delta S}{\delta \hat{\pi}} = 0$, produces the condition

$$\begin{aligned} &\int \mathrm{d}\pi(\omega,h) \ln Z_\beta\left(\omega - \hat{\omega}, h + \hat{h}\right) = \\ &= \sum_{k=1}^{k_{\max}} \frac{k}{c} p(k) \int \{\mathrm{d}\hat{\pi}\}_{k-1} \mathrm{Log}\, Z_\beta(\mathrm{i}\lambda^\star - \{\hat{\omega}\}_{k-1} - \hat{\omega}, \{\hat{h}\}_{k-1} + \hat{h}) + \frac{\hat{\gamma}}{c} \,, \end{aligned} \tag{3.104}$$

where $\hat{\gamma}$ is the Lagrange multiplier enforcing the normalisation of $\hat{\pi}$. We can then conclude

that the saddle-point pdf π must satisfy

$$\pi(\omega,h) = \sum_{k=1}^{k_{\max}} \frac{k}{c} p(k) \int \{\mathrm{d}\hat{\pi}\}_{k-1} \delta\left(\omega - (\mathrm{i}\lambda^\star - \{\hat{\omega}\}_{k-1})\right) \delta(h - \{\hat{h}\}_{k-1}) \,. \tag{3.105}$$

Inserting (3.103) into (3.105) yields

$$\pi(\omega,h) = \sum_{k=1}^{k_{\max}} \frac{k}{c} p(k) \int \{\mathrm{d}\pi\}_{k-1} \left\langle \delta\left(\omega - \left(\lambda - \sum_{\ell=1}^{k-1} \frac{K_\ell^2}{\omega_\ell}\right)\right) \delta\left(h - \sum_{\ell=1}^{k-1} \frac{h_\ell K_\ell}{\omega_\ell}\right) \right\rangle_{\{K\}_{k-1}} , \tag{3.106}$$

where we have also defined $\lambda \equiv \mathrm{i}\lambda^\star$ since it will turn out to be real-valued. The constant λ needs to be tuned so as to enforce (3.100) for $\beta \to \infty$, which reads (trading $\hat{\pi}$ for π)

$$1 = \sum_{k=0}^{k_{\max}} p(k) \int \{\mathrm{d}\pi\}_k \left\langle \left(\frac{\sum_{\ell=1}^k \frac{h_\ell K_\ell}{\omega_\ell}}{\lambda - \sum_{\ell=1}^k \frac{K_\ell^2}{\omega_\ell}} \right)^2 \right\rangle_{\{K\}_k} , \tag{3.107}$$

Note that Eq. (3.106) is identical to the self-consistent equation (3.35) found for the cavity fields pdf. Surprisingly, even though the cavity and replica methods depart from completely different assumptions, they converge towards the same result: this has been already shown in [38] for the spectral problem in the Erdős-Rényi case.

A few remarks are in order:

- For the action to converge, we need the conditions $\omega > \zeta$, $\omega > \hat{\omega}$ and $\lambda \equiv \mathrm{i}\lambda^\star > \{\hat{\omega}\}_k$, where ζ is the upper bound of the support of the bond weights $p_K(K)$.

- In Eq. (3.106), the contribution corresponding to $k = 1$ in the sum gives rise to the term $\delta(\omega - \lambda)$ on the right hand side. Therefore, we expect to see a pronounced peak at the location of $\lambda = \langle \lambda_1 \rangle_J$ in the plot of the marginal pdf $\pi(\omega) = \int \mathrm{d}h \; \pi(\omega,h)$, once the contributions coming from nodes of different degrees are "unpacked". This is confirmed in Fig. 3.4 below.

- Both the cavity and replica approaches can be applied to any degree distributions $p(k)$, as long as the mean connectivity c and its variance remain finite as $N \to \infty$, thus considerably enlarging the class of models for which the equivalence between cavity and replicas holds true.

- The value of $\lambda \equiv \mathrm{i}\lambda^\star$ is real, given the symmetry of the matrix, and corresponds to the typical value of the largest eigenvalue $\langle \lambda_1 \rangle_J$, as it will be shown in subsections 3.4.1.1

and 3.4.1.2. This is again compatible with the cavity results.

3.4.1.1 *General case: weighted adjacency matrix.*

We proceed here with the calculation of the average top eigenvalue of weighted adjacency matrices of sparse graphs in configuration model ensembles, characterised by the degree distribution $p(k)$, with finite mean degree $\langle k\rangle = c$, finite variance and bounded maximal degree $k_{\max}$. The bond weights are drawn from the pdf $p_K(K)$. The pure $\{0,1\}$-adjacency matrix case is recovered considering $p_K(K) = \delta(K-1)$. Given the distributions (3.106) and (3.103) at stationarity and recalling Eq. (3.78), the $\mathscr{O}(n)$ terms of the action S_n in (3.80) - keeping only the leading $\beta \to \infty$ term - are expressed as:

$$S_1[\pi,\hat{\pi}] \simeq -nc\frac{\beta}{2}\int \mathrm{d}\pi(\omega,h)\mathrm{d}\pi(\omega',h')\left\langle \frac{\left(h+\frac{h'K}{\omega'}\right)^2}{\omega-\frac{K^2}{\omega'}} - \frac{h^2}{\omega}\right\rangle_K = -nc\frac{\beta}{2}I_1 \,, \tag{3.108}$$

$$S_2[\pi] \simeq nc\frac{\beta}{4}\int \mathrm{d}\pi(\omega,h)\mathrm{d}\pi(\omega',h')\left\langle \frac{\left(h+\frac{h'K}{\omega'}\right)^2}{\omega-\frac{K^2}{\omega'}} - \frac{h^2}{\omega}\right\rangle_K = nc\frac{\beta}{4}I_1 \,, \tag{3.109}$$

$$S_3(\lambda) = n\frac{\beta}{2}\lambda \,, \tag{3.110}$$

$$S_4[\hat{\pi},\lambda] \simeq n\frac{\beta}{2}\sum_{k=0}^{k_{\max}} p(k)\int \{\mathrm{d}\hat{\pi}\}_k \left(\frac{\left(\sum_{\ell=1}^k \hat{h}_\ell\right)^2}{\lambda-\sum_{\ell=1}^k \hat{\omega}_\ell}\right) \,. \tag{3.111}$$

Multiplying and dividing the integrand of (3.111) by $\lambda - \sum_{\ell=1}^k \hat{\omega}_\ell$, and using (3.107), we get

$$S_4[\hat{\pi},\lambda] = n\frac{\beta}{2}\lambda - n\frac{\beta}{2}\sum_{k=1}^{\infty} p(k)k\int \mathrm{d}\hat{\pi}(\hat{\omega},\hat{h})\{\mathrm{d}\hat{\pi}\}_{k-1}\left(\frac{\sum_{\ell=1}^{k-1}\hat{h}_\ell+\hat{h}}{\lambda-\sum_{\ell=1}^{k-1}\hat{\omega}_\ell-\hat{\omega}}\right)^2\hat{\omega} \,. \tag{3.112}$$

Multiplying the second term by $1 = \int \mathrm{d}\omega\mathrm{d}h\,\delta\left(\omega-(\lambda-\{\hat{\omega}\}_{k-1})\right)\delta(h-\{\hat{h}\}_{k-1})$, and using (3.105) and (3.103), we obtain

$$S_4[\pi,\lambda] = n\frac{\beta}{2}\lambda - nc\frac{\beta}{2}\int \mathrm{d}\pi(\omega,h)\mathrm{d}\pi(\omega',h')\left\langle \frac{K^2}{\omega'}\left(\frac{h+h'K/\omega'}{\omega-K^2/\omega'}\right)^2\right\rangle_K = n\frac{\beta}{2}\lambda - nc\frac{\beta}{2}I_2 \,. \tag{3.113}$$

Summing up all terms, the action at the saddle point reads

$$S_n = \frac{n\beta}{2}\left(-\frac{c}{2}I_1 - cI_2 + 2\lambda\right) \,, \tag{3.114}$$

which would imply from (3.52) for the average of the largest eigenvalue the formula

$$\langle \lambda_1 \rangle_J = -\frac{c}{2} I_1 - c I_2 + 2\lambda \ . \tag{3.115}$$

However, we were able to numerically show (see Section 3.6) that at the saddle point

$$\lambda = c\left(I_2 + \frac{1}{2} I_1 \right) \ , \tag{3.116}$$

implying that

$$\langle \lambda_1 \rangle_J = \lambda \ , \tag{3.117}$$

as expected from the corresponding cavity calculation. The identity (3.116) can be more easily checked numerically once expressed in the alternative way

$$\langle \lambda_1 \rangle_J = \lambda = c \int \mathrm{d}\pi(\omega,h)\mathrm{d}\pi(\omega',h') \left\langle \left(\frac{h + \frac{h'K}{\omega'}}{\omega - \frac{K^2}{\omega'}} \right) \left(\frac{h' + \frac{hK}{\omega}}{\omega' - \frac{K^2}{\omega}} \right) K \right\rangle_K \ , \tag{3.118}$$

which has the additional advantage of showing explicitly that $\lambda \equiv \mathrm{i}\lambda^\star$ is indeed a real-valued quantity.

We apply this formalism to the case of Erdős-Rényi adjacency matrices, for which the degree distribution $p(k)$ is the bounded Poisson degree distribution $p_c(k)$ given in Eq. (3.2). Fig. 3.2 refers to the ensemble of pure ER $\{0,1\}$-adjacency matrix, with mean connectivity is $c = 4$ and $k_{\max} = 16$. The resulting typical top eigenvalue is $\langle \lambda_1 \rangle_J \approx 5.254$,within a 0.001% error w.r.t. the reference value $\lambda_{1,\infty} = 5.2541$ obtained by extrapolation from the direct diagonalisation data. The panels in Fig. 3.2 show the marginal distributions $\pi(\omega) = \int \mathrm{d}h \ \pi(\omega,h)$ and $\pi(h) = \int \mathrm{d}\omega \ \pi(\omega,h)$ referring to this case. Every single peak of $\pi(\omega)$ is due to the contribution of a specific degree k. In Fig. 3.3, we plot the behaviour of the typical largest eigenvalue of ER unweighted adjacency matrices as the maximum degree $k_{\max}$ is varied. In this case we consider the mean connectivity parameter $\bar{c}$ appearing in (3.2) is set to 4. Clearly, the mean degree c tends to $\bar{c} = 4$ as $k_{\max}$ increases. As expected, $\langle \lambda_1 \rangle$ grows as $k_{\max}$ increases, but the growth becomes slower as the probability of finding a node of higher and higher degree becomes negligible even in the thermodynamic limit. Figure 3.4 instead shows the marginal distributions $\pi(\omega)$ and $\pi(h)$ for the ensemble of ER weighted adjacency matrices, with a uniform bond pdf $p_K(K) = 1/2$ for $K \in (1,3)$. Here again the mean connectivity is $c = 4$ and $k_{\max} = 16$. The resulting typical top eigenvalue is $\langle \lambda_1 \rangle_J \approx 10.8407$, within a 0.12% error w.r.t. the reference

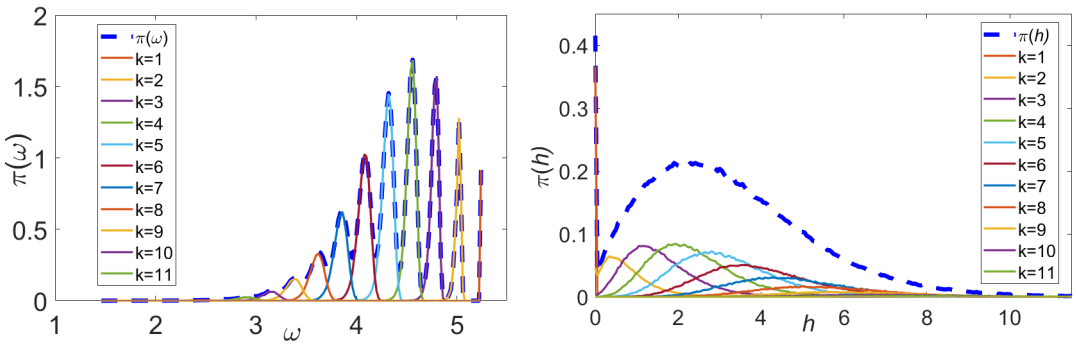

Figure 3.2: The panels refer to the unweighted Erdős-Rényi (ER) adjacency matrix. The plots are obtained via the population dynamics algorithm described in Section 3.6. For both panels, the population size is $N_P = 10^6$. **Left panel**: marginal distribution of the inverse single site variances ω. The thick dashed line represents the full pdf, the thinner curves underneath stand for the single degree contributions, from $k = 1$ to $k = 16$. The rightmost peak at $\omega = \lambda$ corresponds to $k = 1$: the peaks are centred at lower ω as the degree k increases. Also in this case, only the degree contributions up to $k = 11$ are highlighted. **Right panel**: marginal pdf of the single-site bias fields h. Again, the thick dashed line represents the full distribution, the thinner curves stand for the degree contributions from $k = 1$ to $k = 16$. The leftmost peak at $h = 0$ corresponds to $k = 1$: as h grows, the pdf $\pi(h)$ receives contributions from higher degrees. Also in this case, only the degree contributions up to $k = 11$ are highlighted.

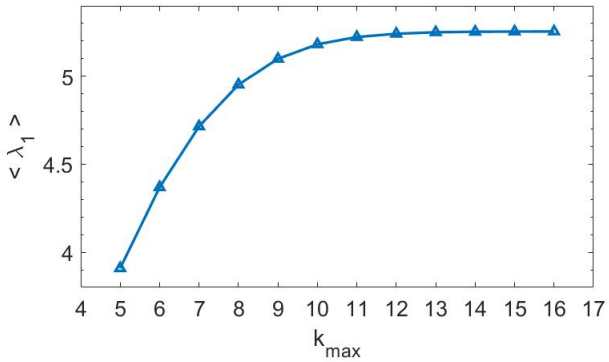

Figure 3.3: The behaviour of the typical largest eigenvalue in the Erdős-Rényi adjacency matrix case as the maximum degree $k_{\max}$ is varied. The value of $\langle \lambda_1 \rangle$ is found via population dynamics for any fixed value of $k_{\max}$. Each value has been then checked against direct diagonalisation extrapolation at $N \to \infty$. The population size is $N_P = 10^6$ for any data point.

value $\lambda_{1,\infty} = 10.8536$ obtained by extrapolation from the direct diagonalisation data. The peculiar structure of the distribution $\pi(\omega)$ in the case of the pure adjacency matrix (see Fig. 3.2) where every single degree contribution corresponds to a specific peak in $\pi(\omega)$ is lost here, due to the presence of non-trivial bond weights.

3.4.1.2 *Random regular graph: adjacency matrix.*

We now consider the simpler and analytically tractable case of the random regular graph (RRG). A RRG with connectivity c is characterized by the property that every node has exactly c neighbours, or equivalently every row of its $\{0,1\}$-adjacency matrix has exactly c nonzero entries. This implies that the largest eigenvalue of such matrix is $\langle \lambda_1 \rangle_J = \lambda = c$ (deterministi-

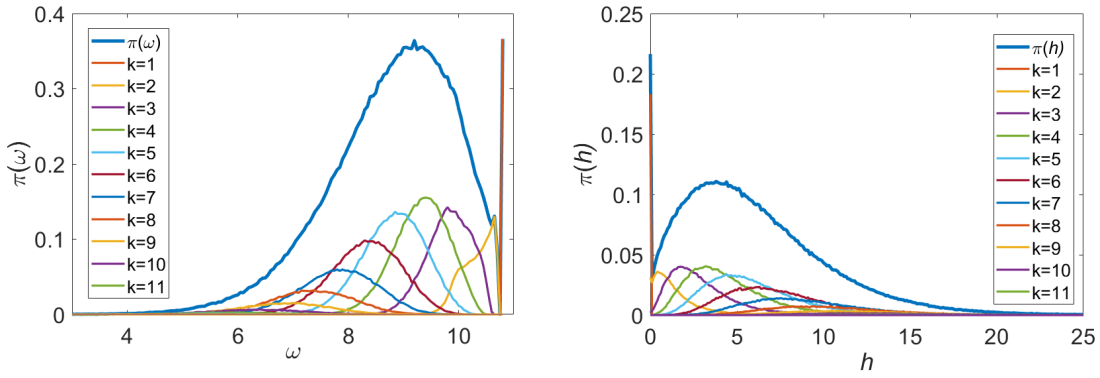

Figure 3.4: Marginal distributions $\pi(\omega)$ and $\pi(h)$ for the ensemble of ER weighted adjacency matrices. The graphs are obtained via the population dynamics algorithm, using a population of size $N_P = 10^6$. **Left panel**: marginal distribution of the ω-variables; the thick blue line represents the full distribution, the thinner curves underneath correspond to the various degree contributions from $k = 1$ up to $k = 16$ (labelled and shown up to $k = 11$). The contribution of nodes with degree $k = 1$ corresponds to the peak located at $\omega = \langle \lambda_1 \rangle_J \approx 10.8407$, as expected from Eq. (3.106). **Right panel**: marginal distribution of the bias fields h; again, the thick blue line represents the full distribution, while the thinner curves underneath correspond to the different degree contributions. Again, only the degree contributions up to $k = 11$ are labelled.

cally), and its corresponding eigenvector has all identical components $\boldsymbol{v}_1 = (1, 1, ..., 1)^T$.

In this case, the degree distribution $p(k)$ featuring in (3.106) is simply $\delta_{k,c}$. Furthermore, if we consider the pure adjacency matrix case (i.e. with $p_K(K) = \delta(K-1)$), Eq. (3.106) and (3.107) become

$$\pi(\omega, h) = \int \{d\pi\}_{c-1} \delta\left(\omega - \left(\lambda - \sum_{\ell=1}^{c-1} \frac{1}{\omega_\ell}\right)\right) \delta\left(h - \sum_{\ell=1}^{c-1} \frac{h_\ell}{\omega_\ell}\right) , \tag{3.119}$$

$$1 = \int \{d\pi\}_c \left(\frac{\sum_{\ell=1}^{c} \frac{h_\ell}{\omega_\ell}}{\lambda - \sum_{\ell=1}^{c} \frac{1}{\omega_\ell}}\right)^2 , \tag{3.120}$$

which can be exactly solved by the ansatz

$$\pi(\omega, h) = \delta(\omega - \bar{\omega}) \delta(h - \bar{h}) , \tag{3.121}$$

leading to the following equations for the parameters $\bar{\omega}, \bar{h}$ and λ

$$\bar{\omega} = \lambda - \frac{c-1}{\bar{\omega}} , \tag{3.122}$$

$$\bar{h} = (c-1)\frac{\bar{h}}{\bar{\omega}} , \tag{3.123}$$

$$1 = \left(\frac{c\bar{h}/\bar{\omega}}{\lambda - c/\bar{\omega}}\right)^2 . \tag{3.124}$$

Eq. (3.123) entails that $\bar{\omega} = c - 1$. Then, inserting this value in (3.122), we find $\lambda = c$. The

value of $\bar{h}$ can then be found exploiting the normalisation condition (3.124), yielding $\bar{h} = c - 2$. The action at the saddle-point reads then

$$S_n = n\frac{\beta}{2}\frac{\bar{h}^2}{\bar{\omega}}\left[-\frac{\bar{\omega}+1}{\bar{\omega}-1} + \frac{2}{\bar{\omega}-1} + 1\right] + n\frac{\beta}{2}c = n\frac{\beta}{2}c\,, \tag{3.125}$$

and therefore entailing for the typical largest eigenvalue

$$\langle \lambda_1 \rangle_J = \lim_{\beta\to\infty} \frac{2}{\beta N} \lim_{n\to 0} \frac{1}{n} N S_n = c\,, \tag{3.126}$$

equal to λ as expected.

3.4.2 Density of the top eigenvector's components

In this statistical mechanics framework, the quantity

$$\tilde{\rho}_\beta(u) = \left\langle \frac{1}{N}\sum_{i=1}^{N} \delta(u - v_i) \right\rangle \tag{3.127}$$

is defined such that in the limit $\beta \to \infty$ it gives the density of the top eigenvector components for a given $N \times N$ sparse symmetric random matrix J. The simple angle brackets $\langle \ldots \rangle$ stands for thermal averaging, i.e. with respect to the Gibbs-Boltzmann distribution (3.6) of the system, here reported again

$$P_{\beta,J}(\boldsymbol{v}) = \frac{\exp\left(\frac{\beta}{2}(\boldsymbol{v}, J\boldsymbol{v})\right)\delta\left(|\boldsymbol{v}|^2 - N\right)}{\int \mathrm{d}\boldsymbol{v}' \exp\left(\frac{\beta}{2}(\boldsymbol{v}', J\boldsymbol{v}')\right)\delta\left(|\boldsymbol{v}'|^2 - N\right)}\,. \tag{3.128}$$

Defining an auxiliary partition function as

$$Z_\varepsilon^{(\beta)}(t, J; u) = \int \mathrm{d}\boldsymbol{v} \exp\left[\frac{\beta}{2}(\boldsymbol{v}, J\boldsymbol{v}) + \beta t \sum_i \delta_\varepsilon(u - v_i)\right]\delta\left(|\boldsymbol{v}|^2 - N\right)\,, \tag{3.129}$$

where δ_ε is a smooth regulariser of the delta function, the quantity (3.127) can be formally expressed as

$$\tilde{\rho}_\beta(u) = \lim_{\varepsilon\to 0^+} \frac{1}{\beta N}\frac{\partial}{\partial t} \ln Z_\varepsilon^{(\beta)}(t, J; u)\Big|_{t=0}\,. \tag{3.130}$$

Averaging now over the matrix ensemble

$$\rho_{\beta,J}(u) = \left\langle \tilde{\rho}_\beta(u) \right\rangle_J \tag{3.131}$$

and sending $\beta \to \infty$ at the very end, the density of the top eigenvector's components is eventually given by the formula

$$\rho_J(u) = \lim_{\beta\to\infty} \lim_{\varepsilon\to 0^+} \frac{1}{\beta N} \frac{\partial}{\partial t} \left\langle \ln Z_\varepsilon^{(\beta)}(t,J;u) \right\rangle_J \Big|_{t=0} . \tag{3.132}$$

To compute the average of the logarithm of the auxiliary partition function $Z_\varepsilon^{(\beta)}(t,J;u)$, we will employ the replica trick once again

$$\left\langle \ln Z_\varepsilon^{(\beta)}(t,J;u) \right\rangle_J = \lim_{n\to 0} \frac{1}{n} \ln \left\langle [Z_\varepsilon^{(\beta)}(t,J;u)]^n \right\rangle_J . \tag{3.133}$$

We find that the replicated partition function will take the form

$$\left\langle [Z_\varepsilon^{(\beta)}(t,J;u)]^n \right\rangle_J \propto \int \mathscr{D}\varphi \mathscr{D}\hat{\varphi} \mathrm{d}\vec{\lambda} \exp\left[N S_n^{(\beta)} \left[\varphi, \hat{\varphi}, \vec{\lambda}; t, \varepsilon; u \right] \right] , \tag{3.134}$$

where φ and $\hat{\varphi}$ are functional order parameters. The integral (3.134) can be evaluated using a saddle point approximation for large N. As in Section 3.4.1, in order to extract the explicit n-dependence of the action $S_n^{(\beta)}$ in the limit $n \to 0$, we consider a replica-symmetric setting where we represent φ and $\hat{\varphi}$ as an infinite superposition of Gaussians whose parameters fluctuate according to the pdfs π and $\hat{\pi}$. Thus, the path integral in (3.134) is rewritten in terms of π, $\hat{\pi}$ and λ, entailing

$$\left\langle [Z_\varepsilon^{(\beta)}(t,J;u)]^n \right\rangle_J \approx \exp\left[N S_n^{(\beta)} \left[\pi, \hat{\pi}, \lambda^\star; t, \varepsilon; u \right] \right] . \tag{3.135}$$

The stationarity conditions defining π, $\hat{\pi}$ and $\lambda^\star$ at the saddle point for $t = 0$ are just identical to those already found in Section 3.4.1 for the replica calculation for the largest eigenvalue. The parameter t can be safely set to zero in the stationarity conditions since the partial derivative $\frac{\partial}{\partial t}$ in (3.132) only acts on terms containing any *explicit* dependence on t, and not through any other indirect functional dependence. Inserting (3.135) into (3.133), and assuming that

$$S_n^{(\beta)} \left[\pi, \hat{\pi}, \lambda^\star; t, \varepsilon; u \right] \sim n s_\beta \left(t, \varepsilon; u \right) + o(n) \tag{3.136}$$

as $n \to 0$, the final expression for the average density of top eigenvector's components for $N \to \infty$ reduces to

$$\rho_J(u) = \lim_{\beta\to\infty} \frac{1}{\beta} s'_\beta \left(0, 0; u \right) , \tag{3.137}$$

where $(\cdot)'$ stands for differentiation with respect to t.

In the next subsections, we outline this formalism for the general case of sparse weighted matrices within the configuration model with degree distribution $p(k)$ with finite mean and variance and bounded largest degree. We will give numerical results for the case of weighted ER ensemble. Then we will provide an analytical solution for the case of adjancency matrices of RRGs.

3.4.2.1 *General case: weighted adjacency matrix.*

Considering (3.129), the average replicated partition function becomes

$$\begin{aligned}\left\langle [Z_\varepsilon^{(\beta)}(t,J;u)]^n \right\rangle_J &= \frac{1}{\mathscr{M}} \left(\frac{\beta}{4\pi}\right)^n \int \left(\prod_{a=1}^{n} \mathrm{d}\boldsymbol{v}_a \mathrm{d}\lambda_a\right) \exp\left(\mathrm{i}\frac{\beta}{2} N \sum_a \lambda_a\right) \\ &\times \exp\left(-\mathrm{i}\frac{\beta}{2}\sum_a\sum_i \lambda_a v_{ia}^2 + \beta t \sum_a \sum_i \delta_\varepsilon(u - v_{ia})\right) \\ &\times \int_{-\pi}^{\pi} \left(\prod_{i=1}^{N} \frac{\mathrm{d}\phi_i}{2\pi}\right) \exp\left(-\mathrm{i}\sum_i \phi_i k_i\right) \exp\left[\frac{c}{2N}\sum_{i,j}\left(\left\langle \mathrm{e}^{\beta K \sum_a v_{ia} v_{ja} + \mathrm{i}(\phi_i+\phi_j)}\right\rangle_K - 1\right)\right] . \end{aligned} \tag{3.138}$$

The only difference between Eq. (3.138) and Eq. (3.56) is the presence of the t-dependent term. The replica derivation thus matches step by step the one presented in Section 3.4.1.

By introducing the functional order parameter (3.58), the replicated partition function can be once again cast in a form that allows for a saddle point approximation,

$$\left\langle [Z_\varepsilon^{(\beta)}(t,J;u)]^n \right\rangle_J \propto \int \mathscr{D}\varphi \mathscr{D}\hat{\varphi} \mathrm{d}\vec{\lambda} \exp\left[N S_n^{(\beta)}\left[\varphi, \hat{\varphi}, \vec{\lambda}; t, \varepsilon; u\right]\right] , \tag{3.139}$$

where the action $S_n^{(\beta)}\left[\varphi, \hat{\varphi}, \vec{\lambda}; t, \varepsilon; u\right]$ is the sum of four terms

$$S_n^{(\beta)}\left[\varphi, \hat{\varphi}, \vec{\lambda}; t, \varepsilon; u\right] = S_1[\varphi, \hat{\varphi}] + S_2[\varphi] + S_3(\vec{\lambda}) + S_4[\hat{\varphi}, \vec{\lambda}; t, \varepsilon; u] . \tag{3.140}$$

The first three contributions are identical to those appearing in the largest eigenvalue calculation (see (3.68), (3.69) and (3.70)). The explicit t and u dependence is confined to the fourth contribution,

$$\begin{aligned} S_4[\hat{\varphi}, \vec{\lambda}; t, \varepsilon; u] = \sum_{k=0}^{k_{\max}} p(k) \Bigg[\mathrm{Log} \int \mathrm{d}\vec{v} \exp\Bigg(-\mathrm{i}\frac{\beta}{2}\sum_a \lambda_a v_a^2 \\ + \beta t \sum_a \delta_\varepsilon(u - v_a) \Bigg) (\mathrm{i}\hat{\varphi}(\vec{v}))^k - \mathrm{Log}(k!) \Bigg] . \end{aligned} \tag{3.141}$$

We now assume replica symmetry and represent φ and $\hat{\varphi}$ as uncountably infinite superposition

of Gaussians, whose parameters fluctuate according to joint pdfs π and $\hat{\pi}$, as in (3.75), (3.76) and (3.77). Such joint pdfs satisfy the very same set of coupled saddle-point equations as in (3.105) and (3.103) and for these reasons we can use the same labels as before. The only difference with respect to the previous case is in the extra t-derivative that we have to take from the contribution $S_4[\hat{\pi},\lambda^\star;t,\varepsilon;u]$. Inserting the ansatz (3.77) into Eq. (3.141), we obtain (in the limit $n\to 0$)

$$S_4[\hat{\pi},\lambda^\star;t,\varepsilon;u] = n\sum_{k=0}^{k_{\max}} p(k)\int\{\mathrm{d}\hat{\pi}\}_k\,\mathrm{Log}\int \mathrm{d}v\exp\Big[-\frac{\beta}{2}\left(\mathrm{i}\lambda^\star-\{\hat{\omega}\}_k\right)v^2 + \beta t\delta_\varepsilon(u-v)+\beta\{\hat{h}\}_k v\Big]\,. \tag{3.142}$$

Therefore, we can isolate the function $s_\beta(t,\varepsilon;u)$ in (3.136) as

$$s_\beta(t,\varepsilon;u) = \sum_{k=0}^{k_{\max}} p(k)\int\{\mathrm{d}\hat{\pi}\}_k\,\mathrm{Log}\int \mathrm{d}v\exp\Big[-\frac{\beta}{2}\left(\mathrm{i}\lambda^\star-\{\hat{\omega}\}_k\right)v^2 + \beta t\delta_\varepsilon(u-v)+\beta\{\hat{h}\}_k v\Big]\,, \tag{3.143}$$

in view of the identification $\mathrm{i}\lambda^\star\equiv\lambda$ as before. Taking the t-derivative and setting t and ε to zero, we get

$$s'_\beta(0,0;u) = \beta\sum_{k=0}^{k_{\max}} p(k)\int\{\mathrm{d}\hat{\pi}\}_k\frac{\exp\left[-\frac{\beta}{2}(\lambda-\{\hat{\omega}\}_k)u^2+\beta\{\hat{h}\}_k u\right]}{\int\mathrm{d}v\exp\left[-\frac{\beta}{2}(\lambda-\{\hat{\omega}\}_k)v^2+\beta\{\hat{h}\}_k v\right]}\,.$$

Taking the $\beta\to\infty$ limit as in (3.137), we eventually find

$$\rho_J(u) = \sum_{k=0}^{k_{\max}} p(k)\int\{\mathrm{d}\hat{\pi}\}_k\,\delta\left(u-\frac{\{\hat{h}\}_k}{\lambda-\{\hat{\omega}\}_k}\right)\,. \tag{3.144}$$

Expressing Eq. (3.144) in terms of the π-distribution, we eventually obtain

$$\rho_J(u) = \sum_{k=0}^{k_{\max}} p(k)\int\{\mathrm{d}\pi\}_k\left\langle\delta\left(u-\frac{\sum_{\ell=1}^k\frac{h_\ell K_\ell}{\omega_\ell}}{\lambda-\sum_{\ell=1}^k\frac{K_\ell^2}{\omega_\ell}}\right)\right\rangle_{\{K\}_k}\,, \tag{3.145}$$

where $\pi(\omega,h)$ satisfies the self-consistency equation (3.106), supplemented with the normalisation condition (3.107). Once again, the brackets $\langle\cdot\rangle_{\{K\}_k}$ denote averaging w.r.t. to a collection of k i.i.d. random variables K_ℓ, each drawn from the bond weight pdf $p_K(K)$.

Eq. (3.145) essentially recovers Eq. (3.38) found with the cavity method. As a general remark, it is worth noticing that the β-dependent distribution $\rho_\beta(u)$ in Eq. (3.131) is related to the distribution in (3.99) that had already arisen naturally in the eigenvalue calculation when evaluating the stationarity conditions with respect to λ. Indeed, Eq. (3.131) is obtained by averaging the pdf (3.99) over $\{\hat{\pi}\}_k$ and $p(k)$. Moreover, in the cavity formalism, $\rho_\beta(u)$ is also closely related to the single-site marginal of a single instance (3.28).

We remark once again that – in analogy with the typical largest eigenvalue calculation – the validity of Eq. (3.145) for the weighted adjacency matrix of *any* configuration model with a degree distribution with finite mean, finite variance and bounded maximal degree as a weighted superposition of delta functions, one for each degree of the graph. It is then natural to identify the quantity $\frac{\sum_{\ell=1}^{k} \frac{h_\ell K_\ell}{\omega_\ell}}{\lambda - \sum_{\ell=1}^{k} \frac{K_\ell^2}{\omega_\ell}}$ as the contribution to the density coming from nodes of degree k. The $k=0$ contribution from isolated nodes indeed gives rise to the sharp peak at $u=0$.

The $\rho_J(u)$ of a Erdős-Rényi $\{0,1\}$-adjacency matrix is shown in the panels of the top row of Fig. 3.5: in the left top panel we compare results for the density of top eigenvector's components obtained via population dynamics with results from the direct diagonalisation of 2000 matrices of size $N=5000$. In the right top panel we show the contributions from nodes of various degree k to the full top eigenvector's components pdf. We clearly observe the aforementioned peak at $u=0$. The bottom row plots of Fig. 3.5 show instead the same kind of plots for the pdf of top eigenvector's components of the ensemble of Erdős-Rényi weighted adjacency matrices, with $c=4$, $k_{\max}=16$ and uniform bond weight distribution, namely $p(K)=1/2$ for all $K \in [1,3]$. Also in the weighted case, the peak at $u=0$ corresponds to the contribution of isolated nodes ($k=0$) whereas larger degree nodes contribute to the tail of the distribution. The comparison between population dynamics and direct diagonalisation results shows perfect agreement.

3.4.2.2 *Random regular graph: adjacency matrix*

In this case, building on subsection 3.4.1.2 and recalling that $p(k)=\delta_{k,c}$ and $p_K(K)=\delta(K-1)$, the ratio in (3.145) simply becomes $c(c-2)/[c(c-1)-c]=1$, entailing

$$\rho_J(u) = \delta(u-1), \tag{3.146}$$

as expected.

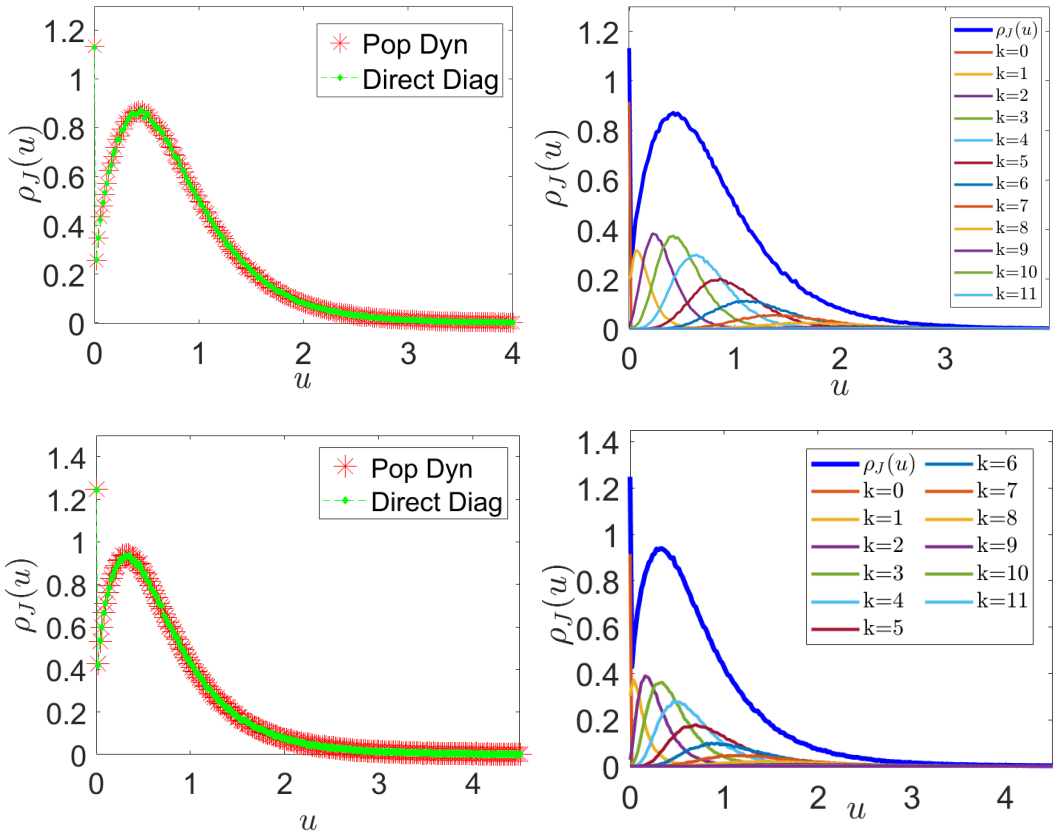

Figure 3.5: Density of the top eigenvector components (3.145) for ER adjacency matrices. All the plots are obtained via the population dynamics algorithm, using a population size $N_P = 10^6$. The top row refers to the unweighted case, whereas the bottom row refers to the weighted case. **Top left panel**: pdf of the components of the top eigenvector in the case of ER unweighted adjacency matrices, obtained by population dynamics (red stars) and by direct diagonalisation of 2000 matrices of size N = 5000 (green diamonds) exhibiting excellent agreement. **Top right panel**: pdf of the top eigenvector's components in the ER unweighted case (thick blue line) where the contributions from nodes of various degree from $k = 0$ to $k = 16$ have been disentangled (thinner coloured curves). Only the degree contributions up to $k = 11$ are labelled: all the other (larger) degree contributions are barely distinguishable as they fall on top of each other in the tail of the distribution. **Bottom left panel**: comparison between results for the density of top eigenvector's components obtained with population dynamics (red stars) and direct diagonalisation (green diamonds) in the case of ER weighted adjacency matrices. **Bottom right panel**: the full pdf $\rho_J(u)$ of the top eigenvector's components of weighted ER adjacency matrices (thick blue line) with the thinner curves underneath indicating the various degree contributions k (labelled up to $k = 11$).

3.5 Application: sparse random Markov transition matrices

In this section, we cross-check the formalism with an ensemble of transition matrices W for discrete Markov chains in an N-dimensional state space. The evolution equation for the probability vector $\boldsymbol{p}(t)$ is given by

$$\boldsymbol{p}(t+1) = W\,\boldsymbol{p}(t)\ . \tag{3.147}$$

The transition matrix W is such that $W_{ij} \geq 0\ \forall (i,j)$ and $\sum_i W_{ij} = 1\ \forall j$. For an irreducible chain, the top right eigenvector of the matrix W corresponding to the Perron-Frobenius eigenvalue $\lambda_1 = 1$ represents the unique equilibrium distribution, i.e. $\boldsymbol{v}_1 = \boldsymbol{p}^{\rm eq}$. The matrix W is in gen-

eral not symmetric: however, if the Markov process satisfies a detailed balance condition, i.e. $W_{ij}p_j^{\rm eq} = W_{ji}p_i^{\rm eq}$, it can be symmetrised via a similarity transformation, yielding

$$W_{ij}^S = (p_i^{\rm eq})^{-1/2} W_{ij} (p_j^{\rm eq})^{1/2} \, . \tag{3.148}$$

The symmetrised matrix W^S will be the target of our analysis: even though it is not itself a Markov matrix since the columns normalisation constraint is lost, in view of the detailed balance condition W^S has the same (real) spectrum of W, and its top eigenvector $\boldsymbol{v}_1$ is given in terms of the top right eigenvector of W, $\boldsymbol{p}_{\rm eq}$, as

$$v_1^{(i)} = (N p_i^{\rm eq})^{1/2} \, . \tag{3.149}$$

We will consider the case of an unbiased random walk: the matrix W is then defined as

$$W_{ij} = \begin{cases} \frac{c_{ij}}{k_j}, & i \neq j \\ 1, & i = j \text{ and } k_j = 0 \end{cases} , \tag{3.150}$$

where c_{ij} represents the connectivity matrix and $k_j = \sum_i c_{ij}$ is the degree of the node j. In this case, the top right eigenvector of W is proportional to the vector expressing the degree sequence, i.e. $p_i^{\rm eq} = k_i/(N\langle k \rangle)$. The symmetrised matrix W^S is expressed as

$$W_{ij}^S = \begin{cases} \frac{c_{ij}}{\sqrt{k_i k_j}}, & i \neq j \\ 1, & i = j \text{ and } k_j = 0 \end{cases} , \tag{3.151}$$

with its top eigenvector being $v_1^{(i)} = \sqrt{k_i/\langle k \rangle}$. Therefore, we expect that

$$\rho_{W^S}(u) = \sum_{k \geq k_{\rm min}} p(k) \delta \left(u - \sqrt{\frac{k}{\langle k \rangle}} \right) \, , \tag{3.152}$$

where $p(k)$ is the degree distribution of the connectivity matrix $\{c_{ij}\}$. In order to avoid isolated nodes and isolated clusters of nodes, we consider a shifted Poissonian degree distribution with $k_{\rm min} = 2$, i.e.

$$p(k) = \frac{{\rm e}^{-c} c^{k-2}}{(k-2)!} \mathbb{1}_{k \geq 2} \, , \tag{3.153}$$

with mean degree $\langle k \rangle = c + 2$.

The single-instance cavity treatment starts from the grand-canonical Gibbs-Boltzmann distribution

$$P_{\beta,W^S}(\boldsymbol{v}|\lambda) = \frac{1}{Z}\exp\left[\beta\left(\frac{1}{2}\sum_{ij}^{N} v_i \frac{c_{ij}}{\sqrt{k_i k_j}} v_j - \frac{\lambda}{2}\sum_{i}^{N} v_i^2\right)\right] , \tag{3.154}$$

which, after the change of variable $\tilde{v}_i = v_i/\sqrt{k_i}$, becomes

$$P_{\beta,W^S}(\tilde{\boldsymbol{v}}|\lambda) = \frac{1}{\tilde{Z}}\exp\left[\beta\left(\frac{1}{2}\sum_{ij}^{N} \tilde{v}_i c_{ij} \tilde{v}_j - \frac{\lambda}{2}\sum_{i}^{N} k_i \tilde{v}_i{}^2\right)\right] . \tag{3.155}$$

It is convenient to frame and solve the problem in terms of the vector $\tilde{\boldsymbol{v}}$, since in this case the matrix involved in the analysis is just the standard $\{0,1\}$-adjacency matrix of the underlying graph, as in [41, 42]. The cavity single-instance equations for this problem read

$$\omega_j^{(i)} = \lambda k_j - \sum_{\ell\in\partial j\setminus i} \frac{1}{\omega_\ell^{(j)}} , \tag{3.156}$$

$$h_j^{(i)} = \sum_{\ell\in\partial j\setminus i} \frac{h_\ell^{(j)}}{\omega_\ell^{(j)}} , \tag{3.157}$$

whereas the equations for the single-site marginal coefficients read

$$\omega_i = \lambda k_i - \sum_{j\in\partial i} \frac{1}{\omega_j^{(i)}} , \tag{3.158}$$

$$h_i = \sum_{j\in\partial i} \frac{h_j^{(i)}}{\omega_j^{(i)}} . \tag{3.159}$$

Therefore, in analogy to Eq. (3.31), Eq. (3.155) can be written as

$$P_{\beta,W^S}(\tilde{\boldsymbol{v}}|\lambda) = \prod_{i=1}^{N} \frac{1}{\tilde{Z}_i}\exp\left(-\frac{\beta}{2}\omega_i \tilde{v}_i^2 + \beta h_i \tilde{v}_i\right) . \tag{3.160}$$

Reversing the aforementioned change of variable and taking the $\beta\to\infty$ limit in Eq. (3.160), the components of the top eigenvector of a single instance of W^S are given by

$$P_{W^S}(\boldsymbol{v}|\lambda) = \prod_{i=1}^{N} \delta\left(v_i - \frac{h_i}{\omega_i}\sqrt{k_i}\right) . \tag{3.161}$$

In the thermodynamic limit $N\to\infty$, in complete analogy to Eq. (3.35), Eq. (3.156) and (3.157)

allow one to define the pdf of the cavity fields as

$$\pi(\omega,h)=\sum_{k=2}^{\infty}\frac{k}{\langle k\rangle}p(k)\int\left[\prod_{\ell=1}^{k-1}\mathrm{d}\pi(\omega_\ell,h_\ell)\right]\delta\left(\omega-\lambda k+\sum_{\ell=1}^{k-1}\frac{1}{\omega_\ell}\right)\delta\left(h-\sum_{\ell=1}^{k-1}\frac{h_\ell}{\omega_\ell}\right)\ . \quad (3.162)$$

Similarly, taking into account Eq. (3.158), (3.159) and (3.161), the density of the top eigenvector's components is given by

$$\rho_{W^S}(u)=\sum_{k=2}^{\infty}p(k)\int\left[\prod_{\ell=1}^{k}\mathrm{d}\pi(\omega_\ell,h_\ell)\right]\delta\left(u-\frac{\sum_{\ell=1}^{k}\frac{h_\ell}{\omega_\ell}}{\lambda k-\sum_{\ell=1}^{k}\frac{1}{\omega_\ell}}\sqrt{k}\right)\ , \quad (3.163)$$

in analogy with Eq. (3.38). Eq. (3.162) and (3.163) must be then complemented by the normalisation condition

$$1=\sum_{k=2}^{\infty}p(k)k\int\left[\prod_{\ell=1}^{k}\mathrm{d}\pi(\omega_\ell,h_\ell)\right]\left(\frac{\sum_{\ell=1}^{k}\frac{h_\ell}{\omega_\ell}}{\lambda k-\sum_{\ell=1}^{k}\frac{1}{\omega_\ell}}\right)^2\ . \quad (3.164)$$

As before, Eq. (3.162) is efficiently solved via a population dynamics algorithm. As expected, the convergence is attained for $\lambda=1$, i.e. in correspondence of the largest eigenvalue of W^S, which is also the only value such that the normalisation condition (3.164) can be satisfied. Comparing Eq. (3.152) with Eq. (3.163), one expects that the ratios $\frac{\sum_{\ell=1}^{k}\frac{h_\ell}{\omega_\ell}}{\lambda k-\sum_{\ell=1}^{k}\frac{1}{\omega_\ell}}$ appearing in Eq. (3.163) should all be equal and constant for any k. Indeed, by looking at the distribution of these ratios, we exactly find that it converges to a delta peak centred at a finite real positive value which corresponds to $1/\sqrt{\langle k\rangle}$ once the normalisation is fixed according to (3.164). In Fig. 3.6, we compare the population dynamics results with the theoretical predictions for the density (3.163) of the top eigenvector's components for sparse Markov matrices (representing the transition matrices of unbiased random walks) characterised by a shifted Poissonian degree distribution with minimum degree $k_{\min}=2$ and average degree $\langle k\rangle=6$ ($c=4$).

3.6 Population dynamics

The population dynamics algorithm employed to solve (3.35) (or equivalently (3.106)) is deeply rooted in the statistical mechanics of spin glasses [121, 122]. It has already been presented in Section 2.6. The main difference that can be found in this context is that Eq. (3.35) only converges for a specific value of the parameter λ. Moreover, here the cavity fields are real variables and a regulariser is not needed. The algorithm can be summarised as follows.

A population with N_P pairs of variables $\{(\omega_i,h_i)\}_{1\leq i\leq N_P}$ are randomly initialised, taking

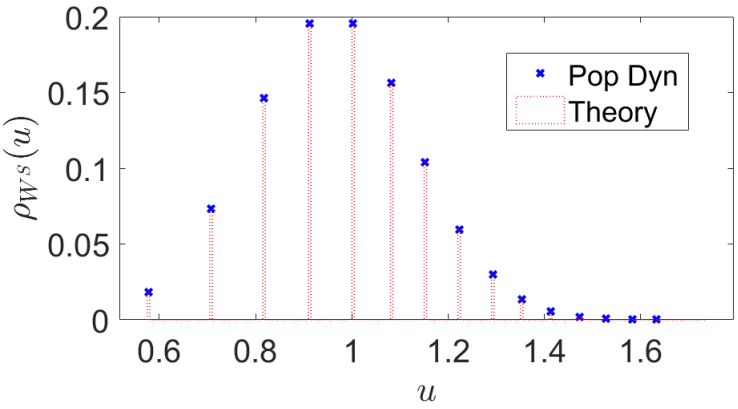

Figure 3.6: Density of the top eigenvector's components for symmetrised sparse Markov matrices representing the transition matrices of unbiased random walks in the thermodynamic limit $N \to \infty$. The histogram has been produced by population dynamics with a population of size $N_P = 10^6$.The simulation results (blue crosses) match the theoretical predictions (red dashed bars).

into account that $\omega_i > \zeta$, where ζ is the upper edge of the support of the pdf $p_K(K)$.

For any suitable value of $i\lambda^* \equiv \lambda \in \mathbb{R}$, the following steps are iterated until stable populations are obtained:

1. Generate a random $k \sim \frac{k}{c} p(k)$, where $p(k)$ is the degree distribution of interest, with $c = \langle k \rangle$.

2. Generate $k-1$ i.i.d. random variables K_ℓ from the bond weights pdf $p_K(K)$.

3. Select $k-1$ pairs (ω_ℓ, h_ℓ) from the population at random, then compute

$$\omega^{(new)} = \lambda - \sum_{\ell=1}^{k-1} \frac{K_\ell^2}{\omega_\ell} \,, \tag{3.165}$$

$$h^{(new)} = \sum_{\ell=1}^{k-1} \frac{h_\ell K_\ell}{\omega_\ell} \,, \tag{3.166}$$

   and replace a randomly selected pair (ω_j, h_j) where $j = 1, \ldots, N_P$ with the pair $\left(\omega^{(new)}, h^{(new)}\right)$.

4. Return to (1).

A *sweep* is completed when all the N_P pairs (ω_j, h_j) of the population have been updated at least once according to the steps above. At the end of a sweep, the first and second sample moment of both the ω_i and the h_i are computed. Convergence is achieved when both moments of both type of variables become stable, i.e. when their relative variation w.r.t. their values found at the previous sweep falls below a certain threshold ε, which we choose to be $\mathscr{O}(10^{-15})$.

The procedure to evaluate (3.37) (or alternatively (3.38)) is almost identical, except for the details concerning the k-sampling. Starting from two coupled populations with N_P members $\{(\tilde{\omega}_i, \tilde{h}_i)\}_{1\leq i\leq N_P}$, the following steps are iterated:

1. Generate a random $k \sim p(k)$, where $c = \langle k \rangle$.

2. Generate k i.i.d. random variables K_ℓ from the bond weights pdf $p_K(K)$.

3. Select k pairs (ω_ℓ, h_ℓ) from the population $\{(\omega_i, h_i)\}_{1\leq i\leq N_P}$ at random, then compute

$$\tilde{\omega}^{(new)} = \lambda - \sum_{\ell=1}^{k} \frac{K_\ell^2}{\omega_\ell} \,, \tag{3.167}$$

$$\tilde{h}^{(new)} = \sum_{\ell=1}^{k} \frac{h_\ell K_\ell}{\omega_\ell} \,. \tag{3.168}$$

4. Replace a randomly selected pair $\left(\tilde{\omega}_j, \tilde{h}_j\right)$ where $j = 1, \ldots, N_P$ with the pair $\left(\tilde{\omega}^{(new)}, \tilde{h}^{(new)}\right)$, which is then a new sample from $\tilde{\pi}(\tilde{\omega}, \tilde{h})$. It can be used via Eq. (3.38) to create $u^{(new)} = \tilde{h}^{(new)} / \tilde{\omega}^{(new)}$ as a new sample from $\rho_J(u)$.

5. Return to (1).

The value of the parameter λ controls the convergence of the algorithm: indeed, the convergence to a non-trivial distribution is achieved only when λ is equal to the typical largest eigenvalue $\langle \lambda_1 \rangle_J$, as prescribed by the theory: for any $\lambda > \langle \lambda_1 \rangle_J$, the variables of type h will shrink to zero, whereas for $\lambda < \langle \lambda_1 \rangle_J$ they will blow up in norm. Hence, the value $\lambda = \langle \lambda_1 \rangle_J$ is the only value for which the normalisation condition (3.107) (or equivalently (3.40)) can be satisfied.

In view of the expected behaviour described above, we will initially start from a large value of λ, which is then progressively decreased until convergence is achieved. A suitable starting value is given by the largest degree appearing in the connectivity distribution multiplied by the average bond weight, i.e. $k_{\max} \cdot \langle K \rangle_K$. The value of $k_{\max}$ is fixed in such a way that $p(k_{\max}) N_P \geq 1$: only if this condition is met, the value $k_{\max}$ appears at least once in the degree array that is created to sample from $p(k)$. Because of this choice, the largest degree depends on the limits of the machine that is used to run the population dynamics algorithm. For instance, by using a population size $N_P = 10^6$ and a parameter $\bar{c} = 4$ in (3.2), we are able to reach $k_{\max} = 16$. Thus, the normalisation constant $\mathcal{N}$ in (3.2) is not very different from 1 and $\bar{c} \simeq c = \langle k \rangle$, making the truncation of the Poisson distribution - for all practical purposes - ineffective.

Once λ has been set to the only value ($=\langle\lambda_1\rangle_J$) for which a non-trivial finite normalisation can be found, the value of such normalisation can be adjusted by properly rescaling the h's. Such rescaling is always allowed due to the linear nature of the recursion that governs their update. This recursion will be discussed in detail in Appendix 3.A.

The population dynamics algorithm can also be employed to evaluate numerically the integral in (3.118). The integral has the following structure:

$$I = \int \mathrm{d}\pi(\omega,h)\mathrm{d}\pi(\omega',h')\left\langle f\left(\omega,h,\omega',h',K\right)\right\rangle_K , \tag{3.169}$$

where f is a generic function of the cavity fields and K. Once the correct value of $\lambda = \langle\lambda_1\rangle_J$ has been found, a number N_{eq} of equilibration sweeps is performed, following the protocol illustrated above.

After equilibration, a variable $F = 0$ is initialised. Then for $j = 1,\dots,N_{\mathrm{meas}}$:

1. Perform a sweep
2. Pick (ω,h) and (ω',h') at random, generate $K \sim p_K(K)$ and compute $f(\omega,h,\omega',h',K)$.
3. Update F: $F = F + f(\omega,h,\omega',h',K)$.

The value of the integral (3.169) is approximated by invoking the law of large numbers, as

$$I \simeq \frac{F}{N_{\mathrm{meas}}} , \tag{3.170}$$

where the typical fluctuation is of the order of $1/\sqrt{N_P N_{\mathrm{meas}}}$.

3.7 Summary

We have developed a formalism to compute the statistics of the largest eigenvalue and of the corresponding top eigenvector for some ensembles of sparse symmetric matrices, i.e. (weighted) adjacency matrices of graphs whose degree distribution is characterised by finite mean c, finite variance and bounded maximum degree. The top eigenpair problem can be recast as the optimisation of a quadratic Hamiltonian on the sphere: introducing the associated Gibbs-Boltzmann distribution and a fictitious inverse temperature β, the top eigenvector represents the ground state of the system, which is attained in the limit $\beta \to \infty$. In order to extract this limit, we have employed two methods, cavity and replicas, both borrowed from the statistical mechanics approach to disordered systems. We first analysed the case of a single-instance ma-

trix within a "grand canonical" cavity framework. The single-instance cavity method quickly leads to a set of recursion equations for the cavity fields. However, the method essentially turns the original top eigenpair problem for the $N \times N$ single matrix J into the top eigenpair problem for the associated $Nc \times Nc$ non-backtracking operator B, as detailed in Appendix 3.A. Therefore it does not substantially simplify the search for the solution of the top eigenpair problem on a single instance.

Nonetheless, the cavity single-instance recursions constitute an essential ingredient to arrive at the equations (3.35), (3.38) and (3.40) for the associated joint probability densities of the auxiliary fields of type ω and h that characterise both the typical largest eigenvalue and the statistic of the top eigenvector in the thermodynamic limit $N \to \infty$. Moreover, the exact same equations (see (3.106), (3.145) and (3.107)) are found via the completely alternative replica derivation, entailing that the two methods are equivalent in the thermodynamic limit. Within the population dynamics algorithm employed to solve the stochastic recursion (3.35) (or equivalently (3.106)), we are able to identify the typical largest eigenvalue as the parameter controlling the convergence of the algorithm, and unpack the contributions coming from nodes of different degrees to the average density of the top eigenvector's components. The simulations show excellent agreement of the theory with the direct diagonalisation of large matrices. As a further cross-check of the formalism, we computed the average density of the top eigenvector's components of sparse Markov matrices representing unbiased random walks on a sparse network under the detailed balance condition, thus retrieving the expected relation between such components and the node degrees of the underlying network.

Our results on the statistics of the top eigenpair can be connected to the analysis of localisation properties of the top eigenvector. In principle, the cavity single instance results for a sample of large $N \times N$ sparse symmetric matrices drawn from a certain ensemble can be used to compute the *IPR* of the top eigenvector, using the formula (2.150). However, in this work we did not look at matrix ensembles with a localised top eigenvector. Indeed, we derive our results with a setup that requires a *finite* largest degree $k_{\max}$. On the other hand, the localisation of the top eigenvector of uncorrelated random networks is driven by the presence of a largest degree $k_{\max}$ which *diverges* with the size of the network N [128, 129]. Therefore, our framework prevents us from observing cases in which the top eigenvector is localised. It has been

noticed [129, 130] that if the top eigenvalue λ_1 of an uncorrelated random network is such that

$$\lambda_1 \simeq \sqrt{k_{\max}} > \frac{\langle k^2 \rangle}{\langle k \rangle} , \tag{3.171}$$

then the corresponding top eigenvector is localised. Precisely, the dense subgraph associated with the *hub* (i.e. the node with the largest degree $k_{\max}$) and its neighbours represents the set of nodes where the top eigenvector is localised. In none of the examples that we study was the condition (3.171) met. Conversely, a case in which the top eigenvector is localised can be represented by the ensemble of random networks with a power-law degree distribution decaying for large k as $p(k) \sim k^{-\gamma}$ with $\gamma > 5/2$. Moreover, the localisation of the top eigenvector characterises many real-world networks [131].

Appendices

3.A The single instance self-consistency equations and the non-backtracking operator.

The set of self-consistency equations (3.26) and (3.27) for the cavity fields, supplemented with Eq. (3.29) and (3.30) for the coefficients of the marginal distributions, constitutes the full solution of the top eigenpair problem for a single instance of a sparse matrix. The convergence of the update equations (3.26) and (3.27) is dictated by the value of the parameter λ, which is related to the possibility to normalise the resulting top eigenvector.

Indeed, Eq. (3.27) is a linear recursion driven by the operator B, whose elements can be defined as

$$B_{(i,j),(k,\ell)} = \begin{cases} \frac{J_{j\ell}}{\omega_\ell^{(j)}} & i \neq \ell \wedge j = k \\ 0 & \text{otherwise} \end{cases} . \tag{3.A.1}$$

The matrix B is an example of *non-backtracking* operator, first introduced by Hashimoto in [132]. For a given graph, the Hashimoto non-backtracking operator $\tilde{B}$ in its original form counts the number of paths from a node i to a node ℓ passing through a third node j, for every choice of these three different nodes. It is defined as

$$\tilde{B}_{(i,j),(k,\ell)} = \begin{cases} 1 & i \neq \ell \wedge j = k \\ 0 & \text{otherwise} \end{cases} . \tag{3.A.2}$$

In our case, if the absolute value of the largest eigenvalue of the modified non-backtracking operator B is greater than 1, the absolute values of the cavity fields $h_j^{(i)}$'s will blow up, whereas if it smaller than 1, they will shrink to zero. Therefore, λ must be tuned appropriately in Eq. (3.26) to prevent the linear recursion (3.27) from landing on a trivial solution. Indeed, when λ is "too large", the $\omega_j^{(i)}$'s will be large too, resulting in a largest eigenvalue of B with magnitude

smaller than 1. This would suggest to progressively decrease λ from a large value down to its lower bound λ_1, necessary to ensure that the optimisation problem is well-defined. In other words, the largest eigenvalue of the operator B must be exactly 1 for the $h_j^{(i)}$'s to have a finite norm. This will happen only when $\lambda = \lambda_1$.

Collecting the $h_j^{(i)}$'s in a $2M = \sum_{i=1}^{N} k_i$ dimensional vector, Eq. (3.27) can be rewritten as a linear vector iteration driven by B as

$$h_j^{(i)} = \sum_{(k,\ell)} B_{(i,j),(k,\ell)} h_\ell^{(k)} \,, \tag{3.A.3}$$

where the entries $B_{(i,j),(k,\ell)}$ are defined in (3.A.1). Relabelling with a new, single index a any pair of connected indices (i,j), Eq. (3.A.3) reads

$$h_a = \sum_{b=1}^{2M} B_{ab} h_b \,, \tag{3.A.4}$$

which can interpreted as a vector linear iteration,

$$\underline{h}_t = B \underline{h}_{t-1} \,, \tag{3.A.5}$$

with the index t labelling each iteration.

Starting from a certain initial condition $\underline{h}_0$, the solution of (3.27) is obtained after successive iterations according (3.A.5) until $\underline{h}_t$ stabilises. The stability can be assessed by looking at the norm of the vector $\underline{h}_t$. After a suitable number of iterations t, expanding the initial condition vector in the basis $\{\boldsymbol{b}_i\}$ formed by the right eigenvectors of B, the leading contribution is expressed in terms of its top eigenpair

$$\underline{h}_t = B^t \underline{h}_0 = B^t \left(\sum_{i=1}^{2M} c_i(0) \boldsymbol{b}_i \right) \approx c_1(0) \gamma_1^t \boldsymbol{b}_1 \,, \tag{3.A.6}$$

where the contributions coming from the other eigenpairs $\{\boldsymbol{b}_i, \gamma_i\}_{i \geq 2}$ are exponentially suppressed, all the other eigenvalues of B being smaller than γ_1.

The ratio η_t of the norms of two successive iterations approaches a constant value $\eta^\star$ as $t \to \infty$, corresponding to the absolute value of largest eigenvalue of B,

$$\eta_t = \frac{\|\underline{h}_t\|}{\|\underline{h}_{t-1}\|} = \frac{\|B\underline{h}_{t-1}\|}{\|\underline{h}_{t-1}\|} \to \eta^\star = |\gamma_1| \,. \tag{3.A.7}$$

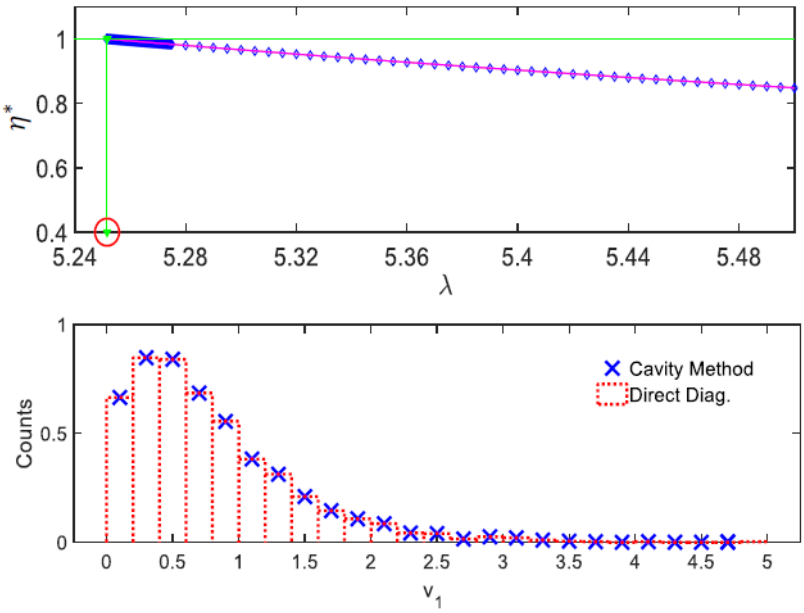

Figure 3.A.1: Cavity single instance. **Top panel**: the plot of the ratio $\eta^\star$ (see (3.A.7)) as a function of the parameter λ: λ is lowered (blue diamonds) until $\eta^\star = 1$. In correspondence of this value, $\lambda = \lambda_1$ (red circle). **Bottom panel**: the histogram of top eigenvector components of the same matrix as predicted by (3.32) shows perfect agreement with the components obtained by direct diagonalisation.

Thus, the convergence of (3.27) is attained when the value of $\eta^\star = |\gamma_1|$ reaches 1 as λ approaches λ_1 from above. We again recall that $\lambda = \lambda_1$ is the smallest possible value such that the cavity partition function (3.20) is well defined, and so the actual value λ_1 can be found by asymptotic extrapolation. Figure 3.A.1 shows an example of this procedure for the case of a single Erdős-Rényi adjacency matrix of size $N = 2000$ and mean degree $c = 4$. The cavity method predicts the value $\lambda = \lambda_1 = 5.251599$, to be compared with the value $\lambda_1^{\text{diag}} = 5.251575$ obtained by direct diagonalisation, resulting in a relative error of 0.001%. We also plot the corresponding top eigenvector's components histogram.

We remark that the procedure above holds *only* if the largest eigenvalue of B is real: if it is complex, there will be a pair of complex conjugate first eigenvalues, i.e. those with the largest norm, which dictate the asymptotic behavior of (3.A.5). In this case, the bi-orthonormal basis of left and right eigenvectors must be taken into account

$$\underline{h}_t \approx c_1(0)\gamma_1^t \boldsymbol{b}_1 + c_2(0)(\gamma_1^\star)^t \boldsymbol{b}_1^\star \,, \tag{3.A.8}$$

where the coefficients $c_1(0)$ and $c_2(0)$ are in general complex. Therefore, the quantity η_t does not approach a steady limit for large t in this case, and oscillations arise. In fact, it can be

shown that

$$\frac{\|\underline{h}_t\|^2}{\left\|\underline{h}_{t-1}\right\|^2} = \eta^2 \frac{\left[|c_1|^2+|c_2|^2+2a\cos\left(2\phi t+\psi\right)\right]}{\left[|c_1|^2+|c_2|^2+2a\cos\left(2\phi\left(t-1\right)+\psi\right)\right]} , \tag{3.A.9}$$

where

$$a = \alpha|c_1||c_2| , \tag{3.A.10}$$

$$\psi = \phi_1 - \phi_2 + \theta . \tag{3.A.11}$$

Here, $(|c_1|,|c_2|)$ and (ϕ_1,ϕ_2) are the moduli and phases of the complex coefficients $c_1(0)$ and $c_2(0)$, η is the ratio of the radial part of the vectors $\underline{h}_t$ and $\underline{h}_{t-1}$, α and θ are respectively the modulus and the phase of the dot product between the right (and left) eigenvector $\boldsymbol{b}_1$ (respectively $\boldsymbol{b}_1^\star$) with itself, and ρ and ϕ are the modulus and phase of the pair of the complex eigenvalues with the largest norm.

In this case, the recursion (3.A.5) does not converge to a single limit, and the cavity formalism does not lead to an acceptable solution. Therefore, the strongest limitation of the single instance cavity method is that the largest eigenvalue γ_1 of the non-backtracking operator B associated to the matrix J must be real. This restriction unfortunately rules out a variety of interesting sparse matrix ensembles.

Chapter 4

Second largest Eigenpair Statistics for Sparse Graphs

4.1 Introduction

In this chapter we look at the second largest eigenpair problem for a sparse matrix J as the top eigenpair problem for a *deflated* version $\tilde{J}$ of the original sparse matrix J. Indeed, the *deflation* mechanism consists in "neutralising" the top eigenvector of J by subtracting from the original matrix the projector onto its first eigenspace. For a suitable amount of deflation, quantified by the deflation parameter x, the top eigenpair of the deflated matrix $\tilde{J}$ corresponds to the second largest eigenpair of the original matrix J. Therefore, in order to characterise the statistics of the second largest eigenpair of J one can study the top eigenpair problem of the deflated matrix $\tilde{J}$. To this purpose, we will employ the same statistical mechanics setting developed in Chapter 3.

As in Chapter 3, we will show that even for the second eigenpair problem the solution at the ensemble level is given in terms of functional self-consistency equations. The crucial difference between the present chapter and Chapter 3 is the presence of the orthogonality condition between the top and second eigenvectors in the set of final equations. The population dynamics algorithm employed to solve these recursions is thus complemented by a wise implementation of the orthogonality constraint, which is essential for the convergence of the aforementioned self-consistency equations.

The plan of the chapter is as follows. In Section 4.2, we describe the mechanism of the *deflation*, outlining the role of the deflation parameter x. We then formalise the top eigenpair problem of the deflated matrix by adopting the same statistical mechanics setting of Chapter 3. In Section 4.3, we provide a cavity analysis of the problem. Specifically, in Section 4.3.1, we describe the single-instance scenario for a generic value of x. We then apply the cavity

approach to fully deflated matrices, first focussing on the single instance case in Section 4.3.2, and then at the ensemble level in Section 4.3.3. We highlight the role of the orthogonality constraint in 4.3.4. To complement the cavity results, we offer an equivalent replica treatment in 4.A. In Section 4.4 we focus on the case of the random regular graph: we analytically show how the solution for the top eigenpair of the *deflated* adjacency matrix gets modified as the deflation parameter is changed. In Section 4.5, we specialise our results to the case of Markov transition matrices representing random walks on graphs. In Section 4.6, we provide the details of the population dynamics algorithm, focussing on how the extra orthogonality constraint is implemented. We also provide convincing evidence that – at odds with what is commonly believed – the algorithm with finite population size N_P does not actually capture the thermodynamic limit $N \to \infty$, in that there is a non-trivial relation between the size N of the adjacency matrix being diagonalised, and the size N_P of the population one should ideally use to numerically compute its spectral properties. More precisely, the accuracy – measured with different metrics – with which the population dynamics algorithm reproduces numerical diagonalisation of matrices (graphs) of size N has a strongly non-monotonic behaviour as a function of N_P, thus implying that an optimal size $N_P^\star = N_P^\star(N)$ must be chosen to best reproduce the diagonalisation results. Finally, in Section 4.7 we offer a summary of results.

4.2 Formulation of the problem

We consider a real sparse symmetric random matrix $J = (J_{ij})$ and assume that its top eigenpair $(\lambda_1, \boldsymbol{u})$ is known. We define a *deflated* matrix $\tilde{J}(x) = (\tilde{J}_{ij}(x))$ by

$$\tilde{J}_{ij}(x) = J_{ij} - \frac{x}{N} u_i u_j \,, \tag{4.1}$$

where x represents the deflation parameter. The $J_{ij} = c_{ij} K_{ij}$ are the i.i.d. entries of the original matrix J. They are defined in terms of the connectivity matrix $c_{ij} \in \{0,1\}$, i.e. the adjacency matrix of the underlying graph, and the random variables K_{ij} encoding bond weights. The bond weights K_{ij} will be i.i.d. random variables drawn from a parent pdf $p_K(K)$ with bounded support. The top eigenvector $\boldsymbol{u}$ of J, also referred to as the *probe* eigenvector, is normalised such that $|\boldsymbol{u}|^2 = N$.[1] The dense matrix $\boldsymbol{u}\boldsymbol{u}^T/N$ represents the projector onto the top eigenspace of the original matrix J.

As in Chapter 3, we analyse ensembles of *tree-like* matrices characterised by a finite con-

[1] The same normalisation convention applies to all the other eigenvectors of J, $\boldsymbol{v}_\alpha$ with $\alpha = 2, \ldots, N$.

nectivity, i.e. for which the mean node degree $\langle k \rangle = c$ is a finite constant that does not scale with N (entailing $c/N \to 0$ as $N \to \infty$) and also the variance of the degree distribution is finite. Besides, we will consider bounded degree distributions to ensure that the largest eigenvalue λ_1 of J will remain of $\sim \mathcal{O}(1)$ for $N \to \infty$.

The spectral theorem ensures that $\tilde{J}(x)$ can be diagonalised via an orthonormal basis of eigenvectors $\boldsymbol{v}_\alpha(x)$ with corresponding real eigenvalues $\tilde{\lambda}_\alpha(x)$ ($\alpha = 1, \ldots, N$),

$$\tilde{J}\boldsymbol{v}_\alpha = \tilde{\lambda}_\alpha \boldsymbol{v}_\alpha \ , \tag{4.2}$$

for each eigenpair $\alpha = 1, \ldots, N$, where to simplify notation we have omitted the x-dependence. We also assume that there is no eigenvalue degeneracy, and that they are sorted $\tilde{\lambda}_1 > \tilde{\lambda}_2 > \ldots > \tilde{\lambda}_N$, and the same holds for the eigenvalues λ_α ($\alpha = 1, \ldots, N$) of the original matrix J.

For any value of x, the matrices J and $\tilde{J}(x)$ share the same set of eigenvectors (see Section 3.3.2 in [133]). The range of the deflation parameter x is $[0, \lambda_1]$, where the boundaries of this range correspond respectively to no deflation ($x = 0 \Rightarrow J = \tilde{J}$) and full deflation ($x = \lambda_1$).

- When the value of x is smaller than the spectral gap $g = \lambda_1 - \lambda_2$, the top eigenvalue of $\tilde{J}(x)$ is given by $\lambda_1 - x$ with corresponding eigenvector $\boldsymbol{u}$. Indeed:

$$\tilde{J}\boldsymbol{u} = \left(J - \frac{x}{N}\boldsymbol{u}\boldsymbol{u}^T\right)\boldsymbol{u} = (\lambda_1 - x)\boldsymbol{u} \ , \tag{4.3}$$

  with $\lambda_1 - x > \lambda_2$. We recall that $\boldsymbol{u}^T\boldsymbol{u} = N$.
- Conversely, when $x > g$ then the second largest eigenvalue of J, λ_2, and the corresponding eigenvector $\boldsymbol{v}_2$ become the top eigenpair of the matrix $\tilde{J}$. Indeed, following (4.3), the top eigenvector of J, $\boldsymbol{u}$, is still an eigenvector of $\tilde{J}$ related to the eigenvalue $\lambda_1 - x$ but now $\lambda_2 > \lambda_1 - x$. Clearly,

$$\tilde{J}\boldsymbol{v}_2 = \left(J - \frac{x}{N}\boldsymbol{u}\boldsymbol{u}^T\right)\boldsymbol{v}_2 = \lambda_2 \boldsymbol{v}_2 \ , \tag{4.4}$$

  in view of the orthogonality between $\boldsymbol{u} = \boldsymbol{v}_1$ and $\boldsymbol{v}_2$.
- In particular, when $x = \lambda_1$, i.e. the largest eigenvalue of the original matrix J[2], the matrix $\tilde{J}$ is said to be a *fully-deflated* matrix. The top eigenvector of J, $\boldsymbol{u}$, is still an eigenvector

[2] In the thermodynamic limit, the value such that full deflation is achieved is actually the average largest eigenvalue $\langle \lambda_1 \rangle_J$ of the matrix J.

of $\tilde{J}$, but corresponding to a zero eigenvalue. Indeed,

$$\tilde{J}\boldsymbol{u} = \left(J - \frac{\lambda_1}{N}\boldsymbol{u}\boldsymbol{u}^T\right)\boldsymbol{u} = (\lambda_1 - \lambda_1)\boldsymbol{u} = 0\boldsymbol{u}\ . \tag{4.5}$$

- All other eigenpairs are unchanged.

Employing the same statistical mechanics formalism of Chapter 3, we aim to find the average (or typical) value $\langle\lambda_2\rangle_J$ of the second largest eigenvalue λ_2 of J, and the density $\rho_{J,2}(v) = \left\langle \frac{1}{N}\sum_{i=1}^N \delta(v - v_2^{(i)})\right\rangle_J$ of the corresponding *second* eigenvector's components, $\boldsymbol{v}_2 = (v_2^{(1)}, \ldots, v_2^{(N)})$. The second eigenpair statistics of the matrix J is obtained by finding the *top* eigenpair of the *deflated* matrix $\tilde{J}(x)$ when $x > g$ and, in particular, when $x = \lambda_1$. Namely, we study the average largest eigenvalue $\langle\tilde{\lambda}_1\rangle_{\tilde{J}}$ and the density $\rho_{\tilde{J}}(v) = \left\langle \frac{1}{N}\sum_{i=1}^N \delta(v - v_1^{(i)})\right\rangle_{\tilde{J}}$ of the top eigenvector's components, $\boldsymbol{v}_1 = (v_1^{(1)}, \ldots, v_1^{(N)})$ of the deflated matrix $\tilde{J}$, where the average $\langle\cdot\rangle_{\tilde{J}}$ is taken over the distribution of the matrix $\tilde{J}$.

We will follow the same protocol used in Chapter 3 and frame the search for the top eigenpair problem of the matrix $\tilde{J}$ as the optimisation of the quadratic function $\hat{H}(\boldsymbol{v})$, according to which $\boldsymbol{v}_1$ is the vector normalised to N that realises the condition

$$N\tilde{\lambda}_1 = \min_{|\boldsymbol{v}|^2=N}\left[\hat{H}(\boldsymbol{v})\right] = \min_{|\boldsymbol{v}|^2=N}\left[-\frac{1}{2}\left(\boldsymbol{v},\tilde{J}\boldsymbol{v}\right)\right]\ , \tag{4.6}$$

where the round brackets $(\cdot,\cdot)$ indicate the dot product between vectors in $\mathbb{R}^N$. As shown in Section 3.2, the "Hamiltonian $\hat{H}(\boldsymbol{v})$ is bounded and attains its minimum when computed on the top eigenvector. Therefore, for a given instance of $\tilde{J}$, in order to compute the minimum in (4.6) we introduce a fictitious canonical ensemble of N-dimensional vectors $\boldsymbol{v}$ at inverse temperature β, whose Gibbs-Boltzmann distribution reads

$$P_{\beta,\tilde{J}}(\boldsymbol{v}) = \frac{1}{Z}\exp\left[\frac{\beta}{2}(\boldsymbol{v},\tilde{J}\boldsymbol{v})\right]\delta(|\boldsymbol{v}|^2 - N)\ , \tag{4.7}$$

where the delta function enforces normalisation. As before, we expect that in the low temperature limit $\beta \to \infty$, only the ground "state" corresponding to the top eigenvector of $\tilde{J}$, $\boldsymbol{v} = \boldsymbol{v}_1$, remains populated.

4.3 Cavity analysis

In this section we show how to tackle the second largest eigenpair problem using the cavity approach. We first present the general statistical mechanics treatment of the single-instance

case. Then, we describe the application of cavity method in the case of full deflation for a single instance (Section 4.3.2) and in the thermodynamic limit (Sections 4.3.3 and 4.3.4).

4.3.1 Top eigenpair of a single instance: generic deflation case

Using (3.9), given a single instance matrix $\tilde{J}$, its largest eigenvalue $\tilde{\lambda}_1$ can be defined as

$$\tilde{\lambda}_1 = \lim_{\beta\to\infty} \frac{2}{\beta N} \ln Z_N, \qquad Z_N = \int \mathrm{d}\boldsymbol{v} \exp\left[\frac{\beta}{2}\left(\boldsymbol{v}, \tilde{J}\boldsymbol{v}\right)\right] \delta\left(|\boldsymbol{v}|^2 - N\right) . \tag{4.8}$$

The partition function explicitly reads

$$Z_N = \int \mathrm{d}\boldsymbol{v} \exp\left[\frac{\beta}{2}\left(\boldsymbol{v}, J\boldsymbol{v}\right) - \frac{\beta x}{2N}\left(\boldsymbol{u}, \boldsymbol{v}\right)^2\right] \delta\left(|\boldsymbol{v}|^2 - N\right) . \tag{4.9}$$

The square in the exponent can be written as

$$\frac{1}{N}\left(\boldsymbol{u}, \boldsymbol{v}\right)^2 = N\left[\frac{1}{N}\left(\boldsymbol{u}, \boldsymbol{v}\right)\right]^2 = Nq^2 , \tag{4.10}$$

with the identification

$$q = \frac{1}{N}\left(\boldsymbol{u}, \boldsymbol{v}\right) . \tag{4.11}$$

The definition of the order parameter q is enforced via the integral identity

$$1 = \int N\beta \frac{\mathrm{d}q\mathrm{d}\hat{q}}{2\pi} \exp\left(\mathrm{i}N\beta q\hat{q} - \mathrm{i}\beta\hat{q}(\boldsymbol{u}, \boldsymbol{v})\right) . \tag{4.12}$$

By also employing a Fourier representation of the Dirac delta enforcing the normalisation constraint and including all the pre-factors in $\mathscr{C}$, the partition function becomes

$$\begin{aligned} Z_N &= \left(\frac{\beta}{4\pi}\right)\left(\frac{N\beta}{2\pi}\right) \int \mathrm{d}q\mathrm{d}\hat{q}\mathrm{d}\lambda \exp\left[\beta N\left(\mathrm{i}q\hat{q} - \frac{x}{2}q^2 + \mathrm{i}\frac{\lambda}{2}\right)\right] \tilde{Z}_N\left(\hat{q}, \lambda\right) \\ &= \mathscr{C} \int \mathrm{d}q\mathrm{d}\hat{q}\mathrm{d}\lambda \exp\left[\beta N\left(\mathrm{i}q\hat{q} - \frac{x}{2}q^2 + \mathrm{i}\frac{\lambda}{2} + \frac{1}{N\beta}\mathrm{Log}\tilde{Z}_N\left(\hat{q}, \lambda\right)\right)\right] \\ &= \mathscr{C} \int \mathrm{d}q\mathrm{d}\hat{q}\mathrm{d}\lambda \exp\left[\beta N S_N(q, \hat{q}, \lambda)\right] , \end{aligned} \tag{4.13}$$

with

$$\tilde{Z}_N(\hat{q},\lambda) = \int \prod_{i=1}^{N} \mathrm{d}v_i \exp\left[-\frac{\beta}{2}(\boldsymbol{v},A\boldsymbol{v}) - \mathrm{i}\hat{q}\beta(\boldsymbol{u},\boldsymbol{v})\right]$$
$$= \sqrt{\frac{(2\pi)^N}{\beta^N \det(A)}} \exp\left(-\frac{\beta}{2}\hat{q}^2 \boldsymbol{u}^T A^{-1}\boldsymbol{u}\right) . \tag{4.14}$$

The matrix $A^{-1} = (\mathrm{i}\lambda\,\mathbb{1}_N - J)^{-1}$ is akin to the *resolvent* of J. It has the same eigenvectors of J, thus using the spectral theorem it can be expressed as

$$A^{-1} = (\mathrm{i}\lambda\,\mathbb{1}_N - J)^{-1} = \sum_{\alpha=1}^{N} \frac{1}{\mathrm{i}\lambda - \lambda_\alpha} \tilde{\boldsymbol{u}}_\alpha \tilde{\boldsymbol{u}}_\alpha^T , \tag{4.15}$$

where the λ_α are the eigenvalues of J and the $\tilde{\boldsymbol{u}}_\alpha$ are their corresponding eigenvectors. We remark that the $\tilde{\boldsymbol{u}}_\alpha$ are normalised such that $|\tilde{\boldsymbol{u}}_\alpha|^2 = 1$. On the other hand, the vector $\boldsymbol{u}$ appearing in the exponent of $\tilde{Z}_N$ is the top eigenvector of J, $\boldsymbol{u}_1$, normalised such that $|\boldsymbol{u}|^2 = |\boldsymbol{u}_1|^2 = N$. Therefore,

$$\boldsymbol{u} = \boldsymbol{u}_1 = \sqrt{N}\tilde{\boldsymbol{u}}_1 , \tag{4.16}$$

entailing that

$$\tilde{Z}_N(\hat{q},\lambda) \propto \exp\left(-\frac{\beta N}{2}\frac{\hat{q}^2}{\mathrm{i}\lambda - \lambda_1}\right) . \tag{4.17}$$

In turn, the partition function (4.13) becomes

$$Z_N = \mathscr{C} \int \mathrm{d}q\mathrm{d}\hat{q}\mathrm{d}\lambda \exp\left[\beta N\left(\mathrm{i}q\hat{q} - \frac{\lambda_1}{2}q^2 + \mathrm{i}\frac{\lambda}{2} - \frac{\hat{q}^2}{2(\mathrm{i}\lambda - \lambda_1)}\right)\right]$$
$$= \mathscr{C} \int \mathrm{d}q\mathrm{d}\hat{q}\mathrm{d}\lambda \exp\left[\beta N S_N(q,\hat{q},\lambda)\right] . \tag{4.18}$$

Eq. (4.18) can be evaluated with a saddle-point approximation for large β. The stationarity of S_N w.r.t. to λ, $\hat{q}$ and q implies that

$$1 = \frac{(\mathrm{i}\hat{q}^\star)^2}{(\mathrm{i}\lambda^\star - \lambda_1)^2} , \tag{4.19}$$
$$q^\star = \frac{-\mathrm{i}\hat{q}^\star}{\mathrm{i}\lambda^\star - \lambda_1} , \tag{4.20}$$
$$q^\star x = \mathrm{i}\hat{q}^\star . \tag{4.21}$$

Using (4.21) in (4.20), one finds

$$q^\star = \frac{-q^\star x}{\mathrm{i}\lambda^\star - \lambda_1} . \tag{4.22}$$

Two cases can be distinguished, depending on the value of $q^\star$.

1. Assuming $q^\star \neq 0$, Eq. (4.22) yields $\mathrm{i}\lambda^\star = \lambda_1 - x$, while from (4.19) it follows $q^{\star 2} = 1$. Using these results to express the action S_N, one finds

$$S_N = \frac{\mathrm{i}\lambda^\star}{2} + \frac{x}{2} - \frac{x}{2} = \frac{\lambda_1 - x}{2} \,, \tag{4.23}$$

entailing for the largest eigenvalue $\tilde{\lambda}_1$ defined in (4.8)

$$\tilde{\lambda}_1 = \mathrm{i}\lambda^\star = \lambda_1 - x \,. \tag{4.24}$$

As stated in Section 4.2, this is the top eigenvalue of $\tilde{J}$ when $x < g$. Indeed, the value $q^\star = \pm 1$ indicates that the the probe eigenvector $\boldsymbol{u}$ and the top eigenvector of $\tilde{J}$ corresponding to $\lambda_1 - x$ coincide. Thus, when the deflation parameter x is smaller that the spectral gap g, there is no need to use the cavity method to obtain the top eigenpair of the deflated matrix, which is simply given by $(\lambda_1 - x, \boldsymbol{u})$.

2. Assuming $q^\star = 0$, from (4.21) it follows that $\hat{q}^\star = 0$. Thus the action reduces to

$$S_N = \frac{\mathrm{i}\lambda^\star}{2} \Rightarrow \tilde{\lambda}_1 = \mathrm{i}\lambda^\star \,. \tag{4.25}$$

The case $q^\star = 0$ provides the top eigenvalue of the deflated matrix $\tilde{J}$ in the case $x > g$, thereby including the case of full deflation $x = \lambda_1$. Therefore, $q^\star = \hat{q}^\star = 0$ represents the orthogonality condition between the solution $\boldsymbol{v}$ and the probe eigenvector $\boldsymbol{u}$. In this scenario, the top eigenvalue $\tilde{\lambda}_1$ of the matrix $\tilde{J}$ is the *second largest* eigenvalue of the original matrix J, viz.

$$\tilde{\lambda}_1 = \lambda_2 = \mathrm{i}\lambda^\star \,. \tag{4.26}$$

However, the stationarity conditions (4.19), (4.20) and (4.21) do not provide the (real) value $\mathrm{i}\lambda^\star \equiv \lambda$, nor the components of the corresponding eigenvector $\boldsymbol{v}$.

To sum up, the top eigenvalue of the deflated matrix $\tilde{J}$ is always given by the value $\mathrm{i}\lambda^\star \equiv \lambda$, regardless the value of x. However, for $x > g$ this value needs to be determined via the cavity method, as detailed in the next subsection.

4.3.2 Cavity derivation for a single instance in case of full deflation

We focus on the case of full deflation $x = \lambda_1$. This choice is not restrictive, since the solution does not depend on x, for any $x > g$. As shown before, in the range $x > g$ one has $q^\star = 0$. However, for the time being we proceed with a generic $q^\star$. Its actual value will be made explicit in the final result.

One looks at (4.13), without performing explicitly the integration in (4.14). Considering the stationarity of the action $S_N(q, \hat{q}, \lambda)$ w.r.t. q, $\hat{q}$ and λ, the following conditions hold,

$$\mathrm{i}\hat{q}^\star = \lambda_1 q^\star \,, \tag{4.27}$$

$$q^\star = \frac{1}{N}\sum_{i=1}^{N} u_i \langle v_i \rangle \quad , \tag{4.28}$$

$$1 = \frac{1}{N}\sum_{i=1}^{N} \langle v_i^2 \rangle \,, \tag{4.29}$$

where the starred quantities indicate the saddle-point values of the parameters. The angular brackets indicate averaging w.r.t. the distribution

$$P_\beta(\boldsymbol{v}|\hat{q}^\star, \lambda^\star) = \frac{1}{\tilde{Z}_N(\hat{q}^\star, \lambda^\star)} \exp\left(-\mathrm{i}\lambda^\star \frac{\beta}{2}\sum_i v_i^2 - \mathrm{i}\hat{q}^\star \beta\,(\boldsymbol{u}, \boldsymbol{v}) + \frac{\beta}{2}(\boldsymbol{v}, J\boldsymbol{v}) \right) . \tag{4.30}$$

By looking at the saddle point condition (4.27), in what follows we can identify $\mathrm{i}\hat{q}^\star = \lambda_1 q^\star = \lambda_1 q$ (omitting the star for brevity) and define $\mathrm{i}\lambda^\star \equiv \lambda$, such that Eq. (4.30) becomes

$$P_\beta(\boldsymbol{v}|\lambda_1 q, \lambda) = \frac{1}{\tilde{Z}_N(\lambda_1 q, \lambda)} \exp\left(-\lambda \frac{\beta}{2}\sum_i v_i^2 - \lambda_1 q \beta\,(\boldsymbol{u}, \boldsymbol{v}) + \frac{\beta}{2}(\boldsymbol{v}, J\boldsymbol{v}) \right) . \tag{4.31}$$

The components v_i are found in the $\beta \to \infty$ limit by the cavity method applied to the distribution (4.31), which in analogy to Section 3.3 represents the grand-canonical version of the Gibbs-Boltzmann canonical distribution (4.7). To keep this chapter self-contained, we reproduce the key steps of the cavity protocol detailed in Section 3.3.1.

By making a tree-like assumption on the structure of the highly sparse graph encoded in the original matrix J that we deflate, the marginal pdf w.r.t. a certain component i is given by

$$P_i(v_i|\lambda_1 q, \lambda) = \frac{1}{Z_i} \exp\left(-\frac{\beta}{2}\lambda v_i^2 - \beta \lambda_1 q u_i v_i \right) \prod_{j \in \partial i} \int \mathrm{d}v_j \exp\left(\beta v_i J_{ij} v_j\right) P_j^{(i)}(v_j|\lambda_1 q, \lambda) \,, \tag{4.32}$$

where ∂i denotes the immediate neighbourhood of i. The factorisation over the neighbouring

nodes of i is due to the fact that in a tree-like structure the nodes $j \in \partial i$ are connected with each other only through i. The distribution $P_j^{(i)}(v_j|\lambda_1 q, \lambda)$ is called *marginal cavity* distribution: it is the distribution of the components v_j defined on the neighbouring nodes of i, in the network in which i has been removed.

Following Section 3.3.1, for any $j \in \partial i$ the cavity marginal pdf satisfies the self-consistent equation

$$P_j^{(i)}(v_j|\lambda_1 q, \lambda) = \frac{1}{Z_j^{(i)}} \exp\left(-\frac{\beta}{2}\lambda v_j^2 - \beta\lambda_1 q u_j v_j\right) \prod_{\ell \in \partial j \setminus i} \int \mathrm{d}v_\ell \exp\left(\beta v_j J_{j\ell} v_\ell\right) P_\ell^{(j)}(v_\ell|\lambda_1 q, \lambda) \,, \tag{4.33}$$

where $\partial j \setminus i$ indicates the set of neighbours of the node j with the exclusion of i.

A Gaussian ansatz provides the solution to the self consistent equation, viz.

$$P_j^{(i)}(v_j|\lambda_1 q, \lambda) = \sqrt{\frac{\beta\omega_j^{(i)}}{2\pi}} \exp\left(-\frac{\beta h_j^{(i)}}{2\omega_j^{(i)}}\right) \exp\left(-\frac{\beta}{2}\omega_j^{(i)} v_j^2 + \beta h_j^{(i)} v_j\right) \,, \tag{4.34}$$

where the parameters $\omega_j^{(i)}$ and $h_j^{(i)}$ are called *cavity fields*. By inserting the ansatz in (4.33) and performing the Gaussian integrals, the set of self-consistent equations represented by (4.33) translates into a set of recursions for the cavity fields,

$$\omega_j^{(i)} = \lambda - \sum_{\ell \in \partial j \setminus i} \frac{J_{j\ell}^2}{\omega_\ell^{(j)}}, \tag{4.35}$$

$$h_j^{(i)} = -\lambda_1 q u_j + \sum_{\ell \in \partial j \setminus i} \frac{J_{j\ell} h_\ell^{(j)}}{\omega_\ell^{(j)}} \,. \tag{4.36}$$

Likewise, by means of (4.34), the marginal distribution $P_i(v_i|\lambda_1 q, \lambda)$ can be written as

$$P_i(v_i|\lambda_1 q, \lambda) = \frac{1}{Z_i} \exp\left(-\frac{\beta}{2}\omega_i v_i^2 + \beta h_i v_i\right) \,, \tag{4.37}$$

where

$$\omega_i = \lambda - \sum_{j \in \partial i} \frac{J_{ij}^2}{\omega_j^{(i)}} \,, \tag{4.38}$$

$$h_i = -\lambda_1 q u_i + \sum_{j \in \partial i} \frac{J_{ij} h_j^{(i)}}{\omega_j^{(i)}} \,. \tag{4.39}$$

Using the cavity factorisation in (4.37) to express (4.31), we eventually obtain

$$P_\beta(\boldsymbol{v}|\lambda_1 q,\lambda) = \prod_{i=1}^{N} \frac{1}{Z_i} \exp\left(-\frac{\beta}{2}\omega_i v_i^2 + \beta h_i v_i\right) . \tag{4.40}$$

In the $\beta \to \infty$ limit,

$$P_\beta(\boldsymbol{v}|\lambda_1 q,\lambda) \to \prod_{i=1}^{N} \delta\left(v_i - \frac{h_i}{\omega_i}\right) , \tag{4.41}$$

entailing that the components v_i of the top eigenvector of the fully deflated matrix $\tilde{J}$, representing the ground state of the system with Boltzmann distribution (4.7), are given by the ratios h_i/ω_i. The ω_i and the h_i are determined respectively by Eq. (4.38) and (4.39). Because of the full deflation, $\boldsymbol{v}$ also represents the *second* eigenvector of the original matrix J.

In terms of Eq. (4.41), the conditions (4.28) and (4.29) read

$$q = \frac{1}{N}\sum_{i=1}^{N} u_i \frac{h_i}{\omega_i} , \tag{4.42}$$

$$1 = \frac{1}{N}\sum_{i=1}^{N} \left(\frac{h_i}{\omega_i}\right)^2 . \tag{4.43}$$

At this point, we recall that for any $x > g$ (in particular $x = \lambda_1$), we have $q^\star \equiv q = 0$. Therefore $q = 0$ must be considered in Eq. (4.36) and (4.39), and the condition (4.42) becomes

$$0 = \frac{1}{N}\sum_{i=1}^{N} u_i \frac{h_i}{\omega_i} . \tag{4.44}$$

As anticipated in Section 4.3.1, Eq. (4.44) expresses the orthogonality condition between $\boldsymbol{u}$ and $\boldsymbol{v}$. The components u_i and v_i in (4.44) are naturally referring to the same node i with degree k_i of the network represented by J.

To summarise, when considering a fully-deflated single instance matrix $\tilde{J}$, its top eigenpair can be found in terms of the cavity recursions (4.35) and (4.36) along with the normalisation condition (4.43) and the orthogonality constraint (4.44). The value $\lambda = \lambda_2$ represents the second largest eigenvalue of the matrix J (i.e. the top eigenvalue of the deflated matrix $\tilde{J}$), with corresponding eigenvalue $\boldsymbol{v}$ whose components are defined in Eq. (4.41). According to the same mechanism explained in Appendix 3.A, $\lambda = \lambda_2$ is the only value that satisfies the normalisation condition (4.43).

4.3.3 Cavity method: thermodynamic limit

Following the reasoning of Section 3.3.2, in the limit $N \to \infty$ we can consider the *joint probability density* of the cavity fields $\omega_j^{(i)}$ and $h_j^{(i)}$ taking values around respectively ω and h,

$$\pi(\omega,h) = \sum_{k=1}^{k_{\max}} \frac{k}{c} p(k) \int \mathrm{d}u \rho_J(u|k) \int \left[\prod_{\ell=1}^{k-1} \mathrm{d}\pi(\omega_\ell,h_\ell)\right] \times \left\langle \delta\left(\omega - \lambda + \sum_{\ell=1}^{k-1} \frac{K_\ell^2}{\omega_\ell}\right) \delta\left(h - \left(-qu\langle\lambda_1\rangle_J + \sum_{\ell=1}^{k-1} \frac{h_\ell K_\ell}{\omega_\ell}\right)\right)\right\rangle_{\{K\}_{k-1}}, \quad (4.45)$$

where $\mathrm{d}\pi(\omega_\ell,h_\ell) \equiv \mathrm{d}\omega_\ell \mathrm{d}h_\ell \pi(\omega_\ell,h_\ell)$, and the average $\langle\cdot\rangle_{\{K\}_{k-1}}$ is taken over $k-1$ independent realisations of the bond weights K. Here, $\rho_J(u|k)$ is the distribution of the top eigenvector's component of J conditioned on the degree k. The distribution $\frac{k}{c}p(k)$ represents the probability that a randomly chosen link points to a node of degree k and $c = \langle k\rangle$, and appears in (4.45) as cavity fields are related to links. Eq. (4.45) generalises in the thermodynamic limit the recursions (4.35) and (4.36) in the case of full deflation ($x = \lambda_1$).

By using the law of large numbers, in the thermodynamic limit the normalisation condition (4.43) reads

$$1 = \sum_{k=0}^{k_{\max}} p(k) \int \mathrm{d}u \rho_J(u|k) \int \left[\prod_{\ell=1}^{k} \mathrm{d}\pi(\omega_\ell,h_\ell)\right] \left\langle \left(\frac{-qu\langle\lambda_1\rangle_J + \sum_{\ell=1}^k \frac{h_\ell K_\ell}{\omega_\ell}}{\lambda - \sum_{\ell=1}^k \frac{K_\ell^2}{\omega_\ell}}\right)^2 \right\rangle_{\{K\}_k}, \quad (4.46)$$

whereas the orthogonality constraint (4.42) becomes

$$q = \sum_{k=0}^{k_{\max}} p(k) \int \mathrm{d}u \rho_J(u|k) u \int \left[\prod_{\ell=1}^{k} \mathrm{d}\pi(\omega_\ell,h_\ell)\right] \left\langle \frac{-qu\langle\lambda_1\rangle_J + \sum_{\ell=1}^k \frac{h_\ell K_\ell}{\omega_\ell}}{\lambda - \sum_{\ell=1}^k \frac{K_\ell^2}{\omega_\ell}} \right\rangle_{\{K\}_k}. \quad (4.47)$$

Similarly, the distribution of the top eigenvector's components of the fully deflated matrix $\tilde{J}$, i.e. the second largest eigenvector of J, is obtained in terms of averages w.r.t. the distribution $\pi(\omega,h)$ as

$$\rho_{\tilde{J}}(v) = \rho_{J,2}(v) = \sum_{k=0}^{k_{\max}} p(k) \int \mathrm{d}u \rho_J(u|k) \int \left[\prod_{\ell=1}^{k} \mathrm{d}\pi(\omega_\ell,h_\ell)\right] \left\langle \delta\left(v - \frac{-qu\langle\lambda_1\rangle_J + \sum_{\ell=1}^k \frac{h_\ell K_\ell}{\omega_\ell}}{\lambda - \sum_{\ell=1}^k \frac{K_\ell^2}{\omega_\ell}}\right)\right\rangle_{\{K\}_k}. \quad (4.48)$$

We notice that in the equations (4.46), (4.47) and (4.48), the degree distribution $p(k)$ naturally crops up, as they encode properties related to nodes, rather than links. Moreover, Eq. (4.26)

generalises to the thermodynamic limit case, as

$$\langle \tilde{\lambda}_1 \rangle_{\tilde{J}} = \langle \lambda_2 \rangle_J = \lambda \ , \tag{4.49}$$

for any $x > g$. Finally, we remark that Eq. (4.24) generalises at the ensemble level too, entailing the condition

$$\langle \lambda_1 \rangle_{\tilde{J}} = \lambda = \langle \lambda_1 \rangle_J - x \tag{4.50}$$

which is valid when $x < g$.

4.3.4 Cavity method: the orthogonality condition

The condition $q = 0$, valid whenever x exceeds the spectral gap, holds at the ensemble level as well. Indeed, when considering $q = 0$, Eq. (4.47) encodes the orthogonality-on-average condition between the *probe* eigenvector $\boldsymbol{u}$ and the top eigenvector $\boldsymbol{v}$ of the deflated matrix $\tilde{J}$, corresponding to the second largest eigenvector of the original matrix J. The interpretation of Eq. (4.47) for $q = 0$ is made clearer by simply considering the average orthogonality condition between $\boldsymbol{u}$ and $\boldsymbol{v}$, viz.

$$\begin{aligned} 0 &= \int \mathrm{d}u\mathrm{d}v P_J(u,v) uv \\ &= \sum_{k=0}^{k_{\max}} p(k) \int \mathrm{d}u \rho_J(u|k) \mathrm{d}v \rho_{J,2}(v|u,k) uv \\ &= \sum_{k=0}^{k_{\max}} p(k) \int \mathrm{d}u \rho_J(u|k) u \int \left[\prod_{\ell=1}^{k} \mathrm{d}\pi(\omega_\ell, h_\ell) \right] \left\langle \left(\frac{-qu \langle \lambda_1 \rangle_J + \sum_{\ell=1}^{k} \frac{h_\ell K_\ell}{\omega_\ell}}{\lambda - \sum_{\ell=1}^{k} \frac{K_\ell^2}{\omega_\ell}} \right) \right\rangle_{\{K\}_k} , \end{aligned} \tag{4.51}$$

where $P_J(u,v)$ indicates the joint probability density of the first and second largest eigenvector's components of J, and the conditional pdf $\rho_{J,2}(v|u,k)$ is obtained from (4.48) erasing the u-integration and the k-sum. The conditional pdf $\rho_J(u|k)$ is given by omitting the k-sum in the expression for the density of the top eigenvector components $\rho_J(u)$ (4.57). Comparing Eq. (4.51) with (4.47) for $q = 0$, one observes that they are identical.

Taking into account the average orthogonality condition $q = 0$, Eq. (4.45), (4.46), (4.47),

(4.48) and (4.49) simplify to

$$\pi(\omega,h) = \sum_{k=1}^{k_{\max}} p(k) \frac{k}{c} \int \{\mathrm{d}\pi\}_{k-1} \left\langle \delta\left(\omega - \left(\lambda - \sum_{\ell=1}^{k-1} \frac{K_\ell^2}{\omega_\ell}\right)\right) \delta\left(h - \left(\sum_{\ell=1}^{k-1} \frac{h_\ell K_\ell}{\omega_\ell}\right)\right) \right\rangle_{\{K\}_{k-1}} , \tag{4.52}$$

$$1 = \sum_{k=0}^{k_{\max}} p(k) \int \{\mathrm{d}\pi\}_k \left\langle \left(\frac{\sum_{\ell=1}^{k} \frac{h_\ell K_\ell}{\omega_\ell}}{\lambda - \sum_{\ell=1}^{k} \frac{K_\ell^2}{\omega_\ell}} \right)^2 \right\rangle_{\{K\}_k} , \tag{4.53}$$

$$0 = \sum_{k=0}^{k_{\max}} p(k) \int \mathrm{d}u \rho_J(u|k) u \int \{\mathrm{d}\pi\}_k \left\langle \left(\frac{\sum_{\ell=1}^{k} \frac{h_\ell K_\ell}{\omega_\ell}}{\lambda - \sum_{\ell=1}^{k} \frac{K_\ell^2}{\omega_\ell}} \right) \right\rangle_{\{K\}_k} , \tag{4.54}$$

$$\rho_{\tilde{J}}(v) \equiv \rho_{J,2}(v) = \sum_{k=0}^{k_{\max}} p(k) \int \{\mathrm{d}\pi\}_k \left\langle \delta\left(v - \frac{\sum_{\ell=1}^{k} \frac{h_\ell K_\ell}{\omega_\ell}}{\lambda - \sum_{\ell=1}^{k} \frac{K_\ell^2}{\omega_\ell}} \right) \right\rangle_{\{K\}_k} , \tag{4.55}$$

$$\left\langle \tilde{\lambda}_1 \right\rangle_{\tilde{J}} \equiv \langle \lambda_2 \rangle_J = \lambda , \tag{4.56}$$

where we have used the shorthand $\{\mathrm{d}\pi\}_k = \prod_{\ell=1}^{k} \mathrm{d}\omega_\ell \mathrm{d}h_\ell \pi(\omega_\ell, h_\ell)$.

Enforcing the orthogonality condition given by (4.54) is crucial to finding the correct solution. The conditional pdf $\rho_J(u|k)$ appearing in (4.54) is given by omitting the k-sum in the expression for the density of the top eigenvector components $\rho_J(u)$ (see Eq. (3.38) or equivalently (3.145)), reported here

$$\rho_J(u) = \sum_{k=0}^{k_{\max}} p(k) \int \{\mathrm{d}\pi_1\}_k \left\langle \delta\left(u - \frac{\sum_{\ell=1}^{k} \frac{b_\ell K_\ell}{a_\ell}}{\langle \lambda_1 \rangle_J - \sum_{\ell=1}^{k} \frac{K_\ell^2}{a_\ell}} \right) \right\rangle_{\{K\}_k} , \tag{4.57}$$

where $\pi_1(a,b)$ indicates the distribution of cavity fields of type a (inverse cavity variances) and b (cavity biases) for the top eigenpair problem (see Eq. (3.35)). The integration w.r.t. the conditional distribution $\rho_J(u|k)$ in (4.54) generalises to the thermodynamic limit the fact that both the components u_i and $v_i = \frac{h_i}{\omega_i}$ in (4.44) refer to the same node i with degree k_i. Indeed, by comparing (4.57) with (4.55) and (4.54), we notice that the components of $\boldsymbol{u}$ are still coupled to those of $\boldsymbol{v}$ in (4.54) through their structure, as they both refer to the same degree k (see Section 4.6 for more details). The replica derivation in 4.A provides an independent proof of this result.

Therefore, in order to enforce the constraint (4.54) correctly, we need to impose strict orthogonality on-the-fly, i.e. while the components of the top eigenvector $\boldsymbol{u}$ and the components of the second largest eigenvector $\boldsymbol{v}$ are being evaluated at the same time by averaging w.r.t. respectively π_1 and π, as prescribed by (4.57) and (4.52). The way strict orthogonality is imposed

is via a correction to the components of $\boldsymbol{v}$: the details of this procedure and the corresponding algorithm are given in Section 4.6.

To summarise, Eq. (4.52), (4.53), (4.54), (4.55) and (4.56) represent the solution of the second largest eigenpair problem in the thermodynamic limit. This set of equations must be generally solved by a population dynamics algorithm, as detailed in Section 4.6. It is completely equivalent to Eq. (4.A.27), (4.A.28), (4.A.29), (4.A.31) and (4.A.30), respectively, found within the replica framework (See 4.A.2).

The top row and the bottom left plots of Figure 4.1 show numerical results in the case of an Erdős-Rényi (ER) adjacency matrix with $c = 4$ and $k_{\max} = 12$. We find $\langle \lambda_2 \rangle_J = 4.463$, within a 2% error w.r.t. the value $\lambda_{2,\infty} = 4.565$ obtained by extrapolation from the direct diagonalisation data. The bottom right panel of Figure 4.1 refers instead to the case of ER weighted adjacency matrix with $c = 4$ and $k_{\max} = 12$. We consider the case of uniform distribution of bond weights, $p_K(K) = 1$ for $K \in [1,2]$. In this case, we find $\langle \lambda_2 \rangle_J = 7.092$, within a 0.94% error w.r.t. the reference value $\lambda_{2,\infty} = 7.159$ obtained by extrapolation from the direct diagonalisation data. In the plot, we compare the pdf of second largest eigenvector's components obtained via population dynamics with results from the direct diagonalisation of 2000 matrices of size $N = 5000$. The relative error for the two cases studied in Fig. 4.1 is slighlty larger than the error observed in all other cases studied in Chapter 3 and 4. This is mainly due to two factors. One the one hand, when looking for the second largest eigenvalue we approach the value of λ for which the update of the cavity field of type ω, contained in Eq. (4.52), becomes unstable. On the other hand, an extra source of uncertainty comes from the use of an approximation for the population dynamics algorithm in the ER case. (see Section 4.6.3).

Figure 4.2 compares the theoretical results for the pdf of the second largest eigenvector's components with results of direct numerical diagonalisation for adjacency matrices of ER graphs with $c = 10$ and $k_{\max} = 22$. In this case, we find $\langle \lambda_2 \rangle_J = 6.656$, within a 0.04% error w.r.t. the value $\lambda_{2,\infty} = 6.658$ obtained by extrapolation from the direct diagonalisation data. We observe that there are finite size effects in the distribution of eigenvector components that are significantly stronger than those observed in the eigenvalue problem. The bottom panel of figure 4.2 shows the average second largest eigenvalue $\langle \lambda_2 \rangle$ as a function of the matrix size N, obtained via direct diagonalisation of adjacency matrices of ER graphs with $c = 10$ and $k_{\max} = 22$. The data are fitted by a power law curve $\langle \lambda_2 \rangle = aN^{-b} + \lambda_{2,\infty}$, with $b \simeq 0.8115$ for this type of network. The inset shows the plot of $\lambda_{2,\infty} - \langle \lambda_2 \rangle$ against N in log scale, confirming

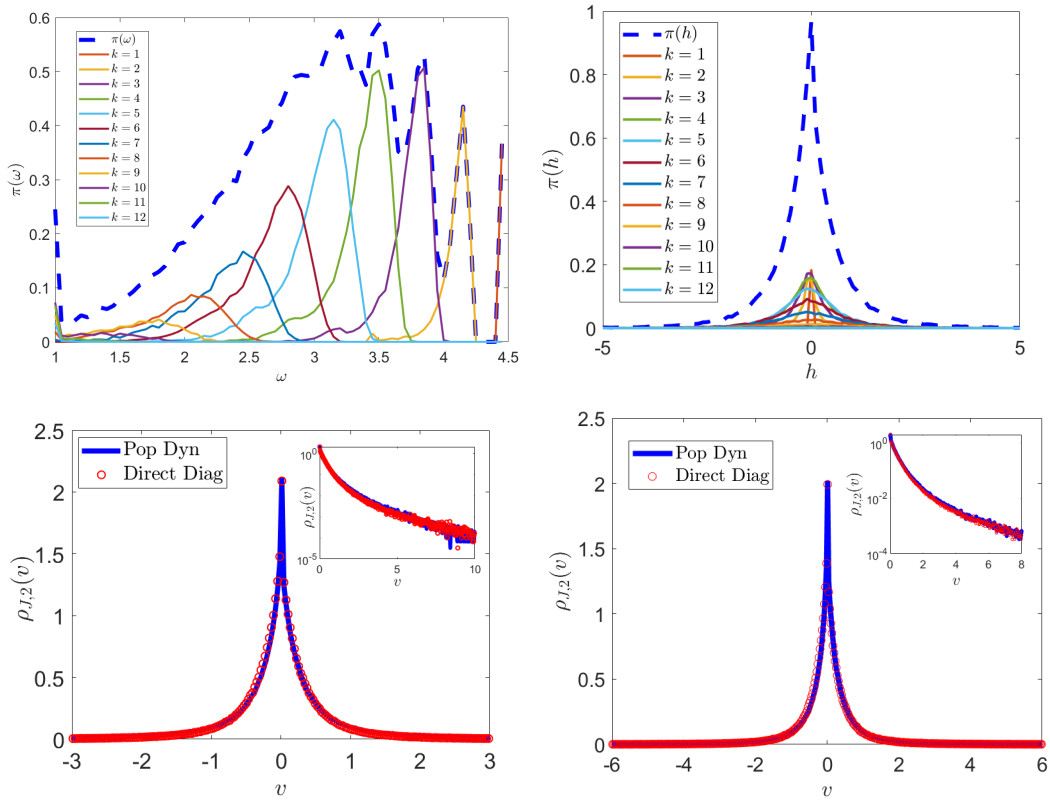

Figure 4.1: Second largest eigenpair of the ER adjacency matrix. **Top left panel**: marginal distribution of the inverse single site variances ω. The thick dashed line represents the full pdf, the thinner curves underneath stand for the single degree contributions, from $k=1$ to $k=12$. The rightmost peak at $\omega=\lambda$ corresponds to $k=1$: the peaks are centred at lower ω as the degree k increases. **Top right panel**: marginal pdf of the single-site bias fields h. Again, the thick dashed line represents the full pdf, the thinner solid curves stand for the degree contributions from $k=1$ to $k=12$. Each curve corresponding to a degree k is symmetric around $h=0$. As k grows, their variance broadens and the curves flatten. **Bottom left panel**: pdf of the second largest eigenvector's components (see (4.55)), obtained by population dynamics (solid blue) and by direct diagonalisation of 2000 matrices of size $N=5000$ (red circles) showing excellent agreement. The population size is $N_P=10^5$. The inset shows the right tail of the pdf in log scale. **Bottom right panel**: pdf of the second largest eigenvector's components in the case of ER weighted adjacency matrices, obtained by population dynamics (solid blue) and by direct diagonalisation of 2000 matrices of size $N=5000$ (red circles) showing excellent agreement. Also in this case, the population size is $N_P=10^5$ and the inset shows the right tail of the pdf in log scale.

that the power law exponent b is positive. The power law convergence is a common behaviour found in all ensembles analysed in this thesis, though the value of the exponent b depends on details of the systems.

4.4 Random regular graphs

For non-weighted adjacency matrices of RRGs, the degree distribution is simply $p(k)=\delta_{k,c}$, and the bond weights distribution is trivially $p_K(K)=\delta(K-1)$, resulting in a constant *probe* top eigenvector $\boldsymbol{u}$, i.e. $\rho_J(u)=\rho_J(u|c)=\delta(u-1)$. The largest eigenvalue λ_1 is non-random and pinned to the value $\lambda_1=c$ (see Section 3.4.1.2 and 3.4.2.2). The spectral density is given

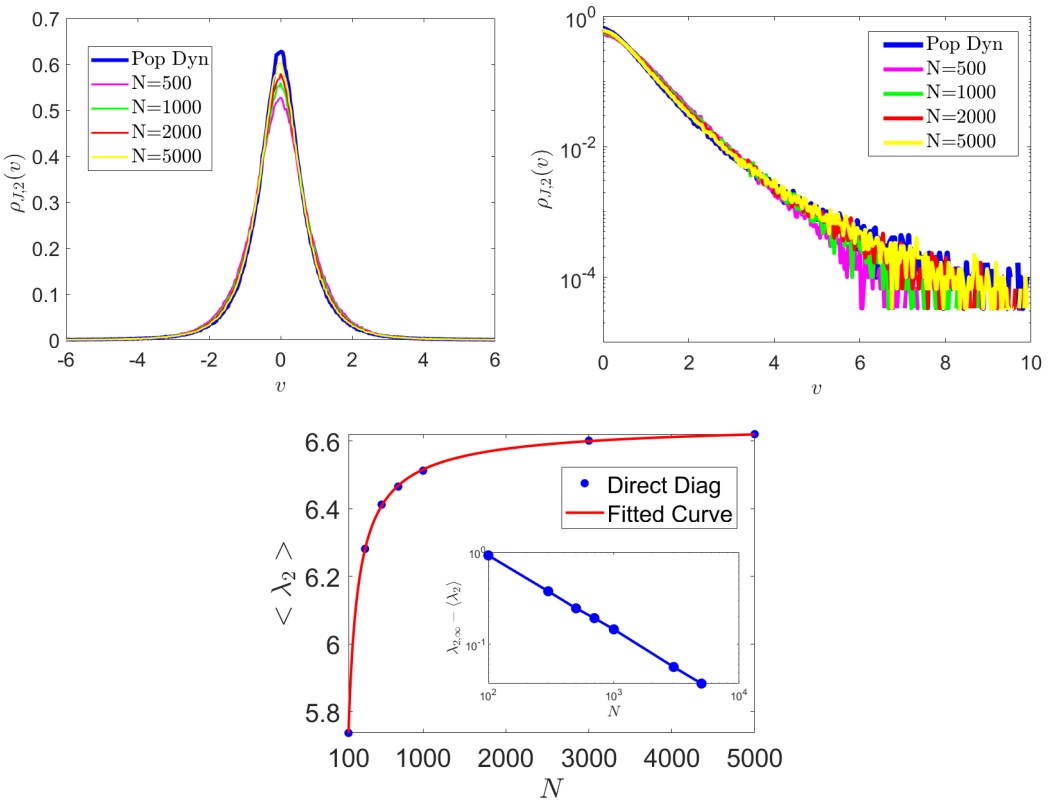

Figure 4.2: Pdf of second largest eigenvector's components in the ER adjacency matrix case, with $c = 10$ and $k_{\max} = 22$. **Top left panel**: Results from population dynamics (blue thick curve) are compared with diagonalisation of matrices of size $N = 500$ (light purple), $N = 1000$ (green), $N = 2000$ (red) and $N = 5000$ (yellow). As N increases, we notice that the direct diagonalisation curves approach the pdf generated by population dynamics with a fairly large population size, $N_P = 10^5$. **Top right panel**: the (right) tails of the distributions shown in the top left panel, shown in log scale. **Bottom panel**: the average second largest eigenvalue $\langle \lambda_2 \rangle$ as a function of N, obtained with direct diagonalisation. The power law fit is superimposed in red. As discussed in the main text, the inset shows the plot of $\lambda_{2,\infty} - \langle \lambda_2 \rangle$ vs N in log scale.

by the Kesten-McKay distribution (see Fig. 4.3 and 2.5 and Appendix 2.F),

$$\rho_{KM}(\lambda) = \frac{c\sqrt{4(c-1)-\lambda^2}}{2\pi(c^2-\lambda^2)}\,, \tag{4.58}$$

for $|\lambda| \leq 2\sqrt{c-1}$, entailing that the spectral gap for this ensemble is $g_{RRG} = c - 2\sqrt{c-1}$. In this section we look at the behaviour of the solution for a generic value of the deflation parameter x in the range $[0, c]$, where the boundaries of this range correspond respectively to no deflation ($x = 0$) and full deflation ($x = c$). Therefore, the value of q is in principle non-zero across the whole range.

For a generic value of the deflation parameter x, the equation (4.45) for $\pi(\omega, h)$, along

with the conditions (4.46) and (4.47) become respectively

$$\pi(\omega,h) = \int \{\mathrm{d}\pi\}_{c-1}\, \delta\left(\omega - \left(\lambda - \sum_{\ell=1}^{c-1} \frac{1}{\omega_\ell}\right)\right) \delta\left(h - \left(-qx + \sum_{\ell=1}^{c-1} \frac{h_\ell}{\omega_\ell}\right)\right) , \tag{4.59}$$

$$1 = \int \{\mathrm{d}\pi\}_c \left(\frac{-qx + \sum_{\ell=1}^{c} \frac{h_\ell}{\omega_\ell}}{\lambda - \sum_{\ell=1}^{c} \frac{1}{\omega_\ell}}\right)^2 , \tag{4.60}$$

$$q = \int \{\mathrm{d}\pi\}_c \left(\frac{-qx + \sum_{\ell=1}^{c} \frac{h_\ell}{\omega_\ell}}{\lambda - \sum_{\ell=1}^{c} \frac{1}{\omega_\ell}}\right) , \tag{4.61}$$

whereas the density of the top eigenvector's components of the deflated matrix $\tilde{J}$ (4.48) is given for general x by

$$\rho_{\tilde{J}}(v) = \int \{\mathrm{d}\pi\}_c\, \delta\left(v - \frac{-qx + \sum_{\ell=1}^{c} \frac{h_\ell}{\omega_\ell}}{\lambda - \sum_{\ell=1}^{c} \frac{1}{\omega_\ell}}\right) . \tag{4.62}$$

We will show that the solution of the self-consistency equation (4.59) along with (4.60), (4.61) and (4.62) crucially depends on the value of the deflation parameter x. Indeed, we can distinguish two different regimes, i.e. the *outer* and *bulk* regimes. Figure 4.3 explains them graphically. We anticipate the following results.

1. In the *outer* regime, i.e. when $x < g_{RRG}$, unsurprisingly we find that the *probe* eigenvector $\boldsymbol{u} = \{1,1,\ldots,1\}$, i.e. the top eigenvector of the original matrix J, is also the top eigenvector of the deflated matrix $\tilde{J}$, with corresponding largest eigenvalue $c-x$ lying outside the bulk of the Kesten-McKay spectrum [39,40]. This confirms the general result discussed in Section 4.3.1.
2. In the *bulk* regime, i.e. when $x > g_{RRG}$, the pdf of the components of the top eigenvector of $\tilde{J}$ is a standard normal distribution, with corresponding largest eigenvalue $2\sqrt{c-1}$. The *probe* all-one eigenvector $\boldsymbol{u}$ is still an eigenvector of $\tilde{J}$ but refers to an eigenvalue $c-x < 2\sqrt{c-1}$. In other words, we show that the second largest eigenpair of the RRG adjacency matrix is given by $\langle\lambda_2\rangle_J = 2\sqrt{c-1}$ and $\rho_{J,2}(v) = \mathscr{N}(0,1)$.

The abrupt change of the solution (from constant $\boldsymbol{u}$ to normally distributed when x hits the value $g_{RRG} = c - 2\sqrt{c-1}$) reflects the fact that the usual peaked ansatz for the RRG case (see Section 3.4.1.2) is not valid in the *bulk* regime $g_{RRG} < x \leq c$. Therefore, in order to solve the

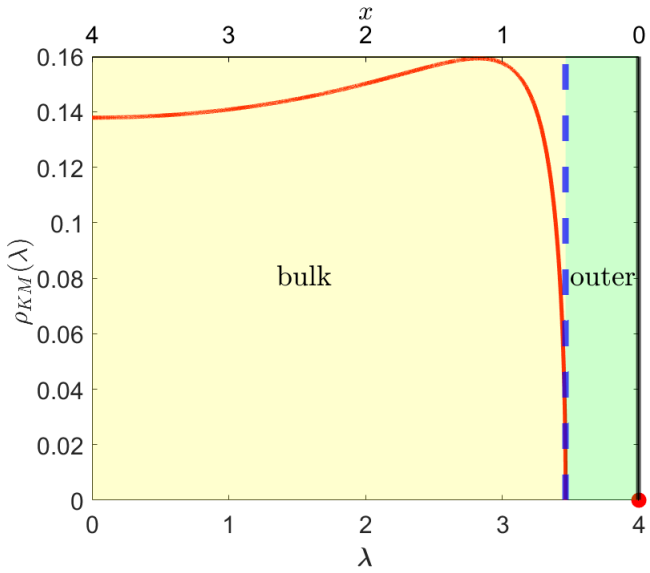

Figure 4.3: The positive branch of the Kesten-McKay distribution (4.58) in solid red for $c = 4$. The red dot at $\lambda = 4$ represents the top eigenvalue $\lambda_1 = c$, which is an outlier. The dashed blue vertical line at $\lambda = 2\sqrt{(c-1)}$ or equivalently $x = g_{RRG} = c - 2\sqrt{(c-1)}$ separates the *outer* regime (light green) from the *bulk* regime (light yellow).

self-consistency equation (4.59), we choose a "mixed" ansatz of the form

$$\pi(\omega,h) = \delta(\omega-\bar{\omega})\sqrt{\frac{1}{2\pi\sigma^2}}\exp\left[-\frac{(h-\bar{h})^2}{2\sigma^2}\right], \tag{4.63}$$

for real $\bar{\omega}$ and $\bar{h}$. We will find that in the range $0 < x < g_{RRG}$, Eq. (4.63) reduces to a peaked ansatz, i.e. $\sigma^2 = 0$ - just like in the case of the largest eigenpair of the original matrix J - whereas in the range $g_{RRG} \leq x < c$, the variance σ^2 must be finite.

Indeed, by inserting Eq. (4.63) into Eq. (4.59) and performing the r.h.s. integrals, we find

$$\pi(\omega,h) = \delta\left(\omega - \left(\lambda - \frac{c-1}{\bar{\omega}}\right)\right)\sqrt{\frac{\bar{\omega}^2}{2\pi\sigma^2(c-1)}}\exp\left[-\frac{\left(h-(-qx+\frac{\bar{h}}{\bar{\omega}}(c-1))\right)^2}{2\sigma^2(c-1)/\bar{\omega}}\right]. \tag{4.64}$$

Comparing (4.64) with the ansatz (4.63), the following relations must be satisfied, viz.

$$\bar{\omega} = \lambda - \frac{c-1}{\bar{\omega}}, \tag{4.65}$$

$$\bar{h} = -qx + \frac{\bar{h}}{\bar{\omega}}(c-1), \tag{4.66}$$

$$\sigma^2 = \sigma^2\frac{c-1}{\bar{\omega}^2}. \tag{4.67}$$

From Eq. (4.67), we can infer that if $\sigma^2 > 0$, then $\bar{\omega} = \sqrt{c-1}$, i.e. a finite variance of the

distribution of components pins $\bar{\omega}$ to a specific value. Only if $\sigma^2 = 0$, then $\bar{\omega}$ can assume values other than $\sqrt{c-1}$, according to Eq. (4.65).

Moreover, inserting the ansatz (4.63) in the normalisation condition (4.60) and in the condition (4.61), we find two extra equations to fix respectively σ^2 and q,

$$\sigma^2 = \frac{\bar{\omega}^2}{c}\left[\left(\lambda - \frac{c}{\bar{\omega}}\right)^2 - \left(c\frac{c}{\bar{\omega}} - qx\right)^2\right] , \tag{4.68}$$

$$q\left(\lambda - \frac{c}{\bar{\omega}}\right) = \left(c\frac{\bar{h}}{\bar{\omega}} - qx\right) . \tag{4.69}$$

By combining (4.65), (4.66) and (4.69), we find an expression for q in terms of $\bar{\omega}$ and $\bar{h}$,

$$q = \frac{\bar{h}}{\bar{\omega} - 1} , \tag{4.70}$$

which in turn can be inserted into Eq. (4.66) to give

$$\bar{h}\left(1 + \frac{x}{\bar{\omega} - 1} - \frac{c-1}{\bar{\omega}}\right) = 0 . \tag{4.71}$$

Comparing eq. (4.65) rewritten as

$$\bar{\omega}^2 - \lambda\bar{\omega} + c - 1 = 0 \tag{4.72}$$

with a slight rewriting of the condition that the expression in the round brackets of (4.71) be zero, viz.

$$\bar{\omega}^2 - (c-x)\bar{\omega} + c - 1 = 0 , \tag{4.73}$$

we notice that (4.72) and (4.73) can be compatible only if the coefficient of $\bar{\omega}$ is the same, entailing $\lambda = c - x$. Moreover, by solving (4.73) for $\bar{\omega}$ we also find the explicit dependence of $\bar{\omega}$ on x. Indeed, we get

$$\bar{\omega}(x)_{1,2} = \frac{c - x \pm \sqrt{(c-x)^2 - 4(c-1)}}{2} . \tag{4.74}$$

By imposing that the radicand be positive in order to get a real solution, we find that Eq. (4.74) yields a x-dependent real solution only for $0 \leq x < c - 2\sqrt{c-1}$. Only in this regime, $\bar{\omega} = \bar{\omega}(x)$ can assume values other than $\sqrt{c-1}$, entailing from (4.67) a peaked solution for

π.[3] Conversely, for any $x > c - 2\sqrt{c-1}$, Eq. (4.74) would produce a x-dependent *complex* solution $\bar{\omega}(x)$, which is not acceptable for this problem (recall that ω and h must be real), thus implying

$$\sigma^2 > 0 \Leftrightarrow \bar{\omega}(x) = \sqrt{c-1} \quad \forall x \in [c - 2\sqrt{c-1}, c] \,. \tag{4.75}$$

4.4.1 RRG-deflated top eigenpair: *outer* regime

From (4.75), it follows that $\sigma^2 = 0$ in the *outer* regime. From (4.68) and (4.69), we thus find

$$\begin{cases} \left(\lambda - \frac{c}{\bar{\omega}}\right)^2 = \left(c\frac{\bar{h}}{\bar{\omega}} - qx\right)^2 \\ q\left(\lambda - \frac{c}{\bar{\omega}}\right) = \left(c\frac{\bar{h}}{\bar{\omega}} - qx\right) \end{cases} \Rightarrow q = \pm 1 \,. \tag{4.76}$$

When solving (4.76), the other possible solution $q = 0$ must be discarded since it would not satisfy the normalisation constraint (4.60). This is in complete agreement with what has been described in Section 4.3.1.

For any $x < g_{RRG}$, the comparison between Eq. (4.72) and (4.73) implies that $\lambda = c - x$. Using Eq. (4.50), the average of the largest eigenvalue of $\tilde{J}$ is given by

$$\left\langle \tilde{\lambda}_1 \right\rangle_{\tilde{J}} = \lambda = c - x \,. \tag{4.77}$$

Therefore, the deflation with a parameter x in the range $0 \leq x < g_{RRG} = c - 2\sqrt{c-1}$ has the effect of decreasing the top eigenvalue c of the original RRG adjacency matrix J by a quantity x, as long as it lies outside the spectral bulk of the Kesten-McKay distribution.

Moreover, since in the outer regime $\sigma^2 = 0$, the ansatz (4.63) for π becomes delta-peaked. Using Eq. (4.63) in Eq. (4.62) and taking into account (4.73) and (4.76), one finds

$$\rho_{\tilde{J}}(v) = \delta\left(v - \frac{c\frac{\bar{h}}{\bar{\omega}} - qx}{\lambda - \frac{c}{\bar{\omega}}}\right) \,, \tag{4.78}$$

but, from (4.76),

$$\left|c\frac{\bar{h}}{\bar{\omega}} - qx\right| = \left|\lambda - \frac{c}{\bar{\omega}}\right| \,, \tag{4.79}$$

implying

$$\rho_{\tilde{J}}(v) = \delta(v-1) \Rightarrow \boldsymbol{v} = \boldsymbol{u} \,, \tag{4.80}$$

[3] We remark that in this regime a finite variance solution for π that pins $\bar{\omega}$ to $\sqrt{c-1}$ is still possible, but yields a higher ground state free energy $\langle F \rangle_{\tilde{J}}$ than the peaked solution. Indeed, $\langle F \rangle_{\tilde{J}} = -\frac{N}{2}\langle \lambda_1 \rangle_{\tilde{J}}$. See Sections 4.4.1 and 4.4.2.

where the choice of the "+" sign solution is not restrictive.

As expected, as long as the largest eigenvalue $c-x$ of the deflated matrix $\tilde{J}$ lies outside the spectral bulk (i.e. for $0 \leq x < g_{RRG} = c - 2\sqrt{c-1}$), the corresponding top eigenvector $\boldsymbol{v}$ is equal to the *probe* eigenvector $\boldsymbol{u} = (1,...,1)^T$, i.e. the top eigenvector of J.

4.4.2 RRG top eigenpair: *bulk* regime

In the regime $x > g_{RRG}$, we have shown in Eq. (4.75) that the variance σ^2 is positive, giving rise to a mixed "delta-Gaussian" ansatz for π. The parameter σ^2 being positive also implies that $\bar{\omega}$ must be pinned to the value $\sqrt{c-1}$.

According to the general analysis in Section 4.3.1, the *bulk* regime entails the condition $q = 0$, encoding the orthogonality between the probe eigenvector $\boldsymbol{u}$ and the top eigenvector $\boldsymbol{v}$ of $\tilde{J}$. As shown in Section 4.3.4, the meaning of the condition $q = 0$ is made clear by comparing the average orthogonality condition between $\boldsymbol{u}$ and $\boldsymbol{v}$, viz.

$$\begin{aligned} 0 &= \int \mathrm{d}u\mathrm{d}v \rho_{\tilde{J}}(u|c)\rho_{\tilde{J}}(v|u,c)uv \\ &= \int \{\mathrm{d}\pi\}_c \frac{\sum_{\ell=1}^{c} \frac{h_\ell}{\omega_\ell} - qx}{\lambda - \sum_{\ell=1}^{c} \frac{1}{\omega_\ell}} , \end{aligned} \tag{4.81}$$

with Eq. (4.61) in which $q = 0$ is considered. In Eq. (4.81), the pdf $\rho_{\tilde{J}}(u|c) = \delta(u-1)$ is the conditional distribution of the probe eigenvector's entries and (4.62) has been used.

Given that $\bar{\omega} = \sqrt{c-1}$ for any $x > g_{RRG}$, from Eq. (4.65), it follows that $\lambda = 2\sqrt{c-1}$. Therefore, using Eq. (4.56) one concludes that the average of the largest eigenvalue of $\tilde{J}$ in the bulk regime is

$$\left\langle \tilde{\lambda}_1 \right\rangle_{\tilde{J}} = \langle \lambda_2 \rangle_J = \lambda = 2\sqrt{c-1} , \tag{4.82}$$

corresponding to the upper edge of the Kesten-McKay distribution and thereby representing the average *second largest* eigenvalue of the matrix J. As expected, the eigenvalue does not depend on the normalisation of the corresponding eigenvector, encoded in σ^2.

The change in the ansatz entails a change in the structure of the largest eigenvector $\boldsymbol{v}$ of $\tilde{J}$. Indeed, using that $\sigma^2 > 0 \Rightarrow \bar{\omega} = \sqrt{c-1}$ and $q = 0$ in Eq. (4.68) and (4.69), one obtains that

$$\sigma^2 = \frac{\bar{\omega}^2}{c}\left(\lambda - \frac{c}{\bar{\omega}}\right)^2 = \frac{(c-2)^2}{c} , \tag{4.83}$$

$$\bar{h} = 0 . \tag{4.84}$$

Then, inserting the ansatz (4.63) in Eq. (4.62) and considering Eq. (4.75), (4.81), (4.83) and (4.84), the density of the components of the top eigenvector of $\tilde{J}$ in the bulk regime $x > g_{RRG} = c - 2\sqrt{c-1}$ is given by

$$\rho_{\tilde{J}}(v) \equiv \rho_{J,2}(v) = \frac{\exp(-v^2/2)}{\sqrt{2\pi}} , \tag{4.85}$$

thus entailing that the eigenvector corresponding to the *second largest* eigenvalue of a RRG adjacency matrix J is normally distributed[4]. We then identify in $x = g_{RRG} = c - 2\sqrt{c-1} \iff \lambda = 2\sqrt{c-1}$ a transition point for the structure of the distribution of the top eigenvector's components of $\tilde{J}(x)$, at which the parameter q changes discontinuously from $q = \pm 1$ to 0.

We remark that this analytical result is in excellent agreement with the statistics of the second largest eigenvector components of the RRG adjacency matrices found by population dynamics, as shown in Figure 4.4. Moreover, it is compatible with previous known results about eigenvectors of random regular graphs [110, 111].

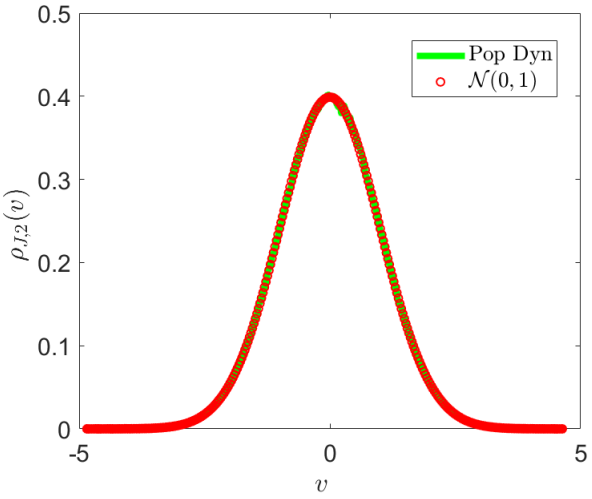

Figure 4.4: In green, the profile of the distribution of the second largest eigenvector's components (4.85) obtained via population dynamics, with population size $N_P = 10^6$. As a reference, we plot the standard normal distribution (red circles), showing perfect matching.

4.5 Sparse random Markov transition matrices

In this section, we apply the deflation formalism to characterise the statistics of the second largest eigenpair of the ensemble of transition matrices W for discrete Markov chains in a N-dimensional state space, already considered in Section 3.5. We recall here that the second

[4] We remark that our method cannot provide the eigenvector statistic for $x = g_{RRG} = c - 2\sqrt{c-1}$. Indeed, for this specific value of x, the *probe* eigenvector $\boldsymbol{u}$ is forced to correspond to the eigenvalue $2\sqrt{c-1}$, which retains its own eigenvector, thus artificially creating a degeneracy. Our method is based on the assumption of non-degeneracy of eigenvalues, so we are not able to give a result about eigenvectors in this marginal case.

largest eigenpair encodes non-equilibrium properties of a Markov process. Indeed, the inverse of the (absolute value) of the second largest eigenvalue represents the slowest relaxation time, whereas the associated *second* eigenvector is the non-equilibrium mode with the largest relaxation time.

We recall that for an irreducible chain, the top right eigenvector of the matrix W corresponding to the Perron-Frobenius eigenvalue $\lambda_1 = 1$ represents the unique equilibrium distribution, i.e. $\boldsymbol{v}^{(1)} = \boldsymbol{p}^{\mathrm{eq}}$. As already noted in Section 3.5, the matrix W is in general not symmetric. However, if the Markov process satisfies a detailed balance condition, i.e. $W_{ij}p_j^{\mathrm{eq}} = W_{ji}p_i^{\mathrm{eq}}\ \forall(i,j)$, it can be symmetrised via a similarity transformation, yielding

$$W_{ij}^S = (p_i^{\mathrm{eq}})^{-1/2} W_{ij} (p_j^{\mathrm{eq}})^{1/2} \,. \tag{4.86}$$

Despite W^S not being itself a Markov matrix, the detailed balance condition W^S implies that W^S has the same real spectrum as W. In Section 3.5 we exploited the fact that the top eigenvector $\boldsymbol{u}$ of W^S is given in terms of the top right eigenvector of W, $\boldsymbol{p}_{\mathrm{eq}}$, namely $u_i = (Np_i^{\mathrm{eq}})^{1/2}$ for any $i = 1,\ldots,N$. Actually, the relation between the eigenvectors of W and those of W^S holds in general and is not limited to the case of the top ones. Indeed, considering a generic eigenvector $\boldsymbol{u}^{(\alpha)}$ of W^S corresponding to the eigenvalue λ_α, one finds

$$v_i^{(\alpha)} = (N^{-1}p_i^{\mathrm{eq}})^{1/2} u_i^{(\alpha)} \quad i = 1,\ldots,N \,, \tag{4.87}$$

where α and i respectively indicate the eigenvector label and the component. For $\alpha = 1$, the known correspondence between top eigenvectors is recovered.

The symmetrised matrix W^S and its deflated version $\tilde{W}^S$ will be the target of our analysis. As in Section 3.5, we consider the case of an unbiased random walk on a graph. The matrix W is then defined as

$$W_{ij} = \begin{cases} \frac{c_{ij}}{k_j}, & i \neq j \\ 1, & i = j \text{ and } k_j = 0 \end{cases} \,, \tag{4.88}$$

where c_{ij} represents the connectivity matrix and $k_j = \sum_i c_{ij}$ is the degree of node j. The top right eigenvector of W is proportional to the vector expressing the degree sequence, i.e. $p_i^{\mathrm{eq}} =$

$k_i/(Nc)$. The corresponding symmetrised matrix W^S is expressed as

$$W_{ij}^S = \begin{cases} \frac{c_{ij}}{\sqrt{k_i k_j}}, & i \neq j \\ 1, & i = j \text{ and } k_j = 0 \end{cases} .$$

As found in Section 3.5, the density of the top eigenvector's components of W^S is given by

$$\rho_{W^S}(u) = \sum_{k \geq k_{\min}} p(k) \delta \left(u - \sqrt{\frac{k}{c}} \right) , \tag{4.89}$$

where $p(k)$ is the degree distribution. Here, we employ the same technical setup of Section 3.5. We consider a generic degree distribution $p(k)$ with $k_{\min} \geq 2$ and finite mean and variance. We will then provide numerical results for the case of a shifted Poissonian degree distribution (see Eq. (3.153)) and the analytical solution for the random regular connectivity case with degree distribution $p(k) = \delta_{k,c}$.

4.5.1 Second largest eigenpair of Markov transition matrices

We focus on the fully deflated symmetrised version of the Markov matrix W by setting $x = \lambda_1(W^S) = 1$, that is

$$\tilde{W}_{ij}^S = W_{ij}^S - \frac{1}{N} u_i u_j , \tag{4.90}$$

where $W_{ij}^S = \frac{c_{ij}}{\sqrt{k_i k_j}}$ and $\boldsymbol{u}$ represents the top eigenvector of W^S, normalised to N, i.e. $u_i = \sqrt{\frac{k_i}{c}}$. Here, c represents the mean degree, $c = \langle k \rangle$. Our aim is to find the typical largest eigenvalue and the pdf of the components of the top eigenvector of $\tilde{W}^S$, respectively equivalent to the typical second largest eigenvalue and the pdf of the components of the *second* eigenvector of W^S.

Here, using the same formalism illustrated in Section 4.3.3, in conjunction with what we observed in Section 3.5, we just report the final equations, corresponding to (4.52) along with

(4.53), (4.54) and (4.56). By taking into account (4.89) and the existence of $k_{\min} = 2$, we find

$$\pi(\omega,h) = \sum_{k=k_{\min}}^{k_{\max}} p(k)\frac{k}{c}\int \{d\pi\}_{k-1}\,\delta\left(\omega - \left(\lambda k - \sum_{\ell=1}^{k-1}\frac{1}{\omega_\ell}\right)\right)\delta\left(h - \left(\sum_{\ell=1}^{k-1}\frac{h_\ell}{\omega_\ell}\right)\right) , \tag{4.91}$$

$$1 = \sum_{k=k_{\min}}^{k_{\max}} p(k)k\int \{d\pi\}_k \left(\frac{\sum_{\ell=1}^{k}\frac{h_\ell}{\omega_\ell}}{\lambda k - \sum_{\ell=1}^{k}\frac{1}{\omega_\ell}}\right)^2 , \tag{4.92}$$

$$0 = \sum_{k=k_{\min}}^{k_{\max}} p(k)\frac{k}{\sqrt{c}}\int \{d\pi\}_k \left(\frac{\sum_{\ell=1}^{k}\frac{h_\ell}{\omega_\ell}}{\lambda k - \sum_{\ell=1}^{k}\frac{1}{\omega_\ell}}\right) , \tag{4.93}$$

$$\left\langle \tilde{\lambda}_1 \right\rangle_{\tilde{J}} \equiv \langle \lambda_2 \rangle_{W^S} = \lambda \ . \tag{4.94}$$

We remark that in the Markov case a bounded largest degree is not strictly necessary as the spectrum is always bounded. However, we will consider a $k_{\max}$ for practical purposes. The self-consistency equation (4.91) along with the normalisation condition (4.92) and the orthogonality constraint (4.93) is solved by a population dynamics algorithm (See Section 4.6). The RRG connectivity case is analytically tractable, as shown in Section 4.5.2.

In analogy to Eq. (4.55), the density of the top eigenvector's component of the matrix $\tilde{W}^S$, corresponding to the second largest eigenvector of W^S, is given by

$$\rho_{\tilde{W}^S}(v) \equiv \rho_{W^S,2}(v) = \sum_{k=k_{\min}}^{k_{\max}} p(k)\int \{d\pi\}_k\,\delta\left(v - \frac{\sum_{j=1}^{k}\frac{h_j}{\omega_j}}{\lambda k - \sum_{j=1}^{k}\frac{1}{\omega_j}}\sqrt{k}\right) , \tag{4.95}$$

where $\pi(\omega,h)$ satisfies the self-consistency equation (4.91), supplemented by the normalisation condition (4.92) and the orthogonality condition (4.93).

Figure 4.5 compares the pdf of the second largest eigenvector's components obtained via population dynamics with results obtained via direct diagonalisation, for the ensemble of unbiased random walk Markov matrices having a shifted Poisson degree distribution (3.153) with $k_{\min} = 2$. We study both a low ($c \simeq 6$, left panel) and a high ($c \simeq 12$, right panel) connectivity case. In the $c \simeq 6$ case with $k_{\max} = 12$, we find $\langle \lambda_2 \rangle_{W^S} = 0.7456$, within a 0.64% error w.r.t. the value $\lambda_{2,\infty} = 0.7504$ obtained by extrapolation from the direct diagonalisation data. In the $c \simeq 12$ case with $k_{\max} = 22$, we find $\langle \lambda_2 \rangle_{W^S} = 0.5530$, within a 0.11% error w.r.t. the value $\lambda_{2,\infty} = 0.5524$ obtained by extrapolation from the direct diagonalisation data. As a reference point, the average value of the second largest eigenvalue in the RRG case with the same c is $\lambda_2(W^S)_{RRG} = 0.5528$. We notice that the agreement near the peak of the distribution is slightly worse for the low connectivity case: this is in agreement with the finding that finite-size effects

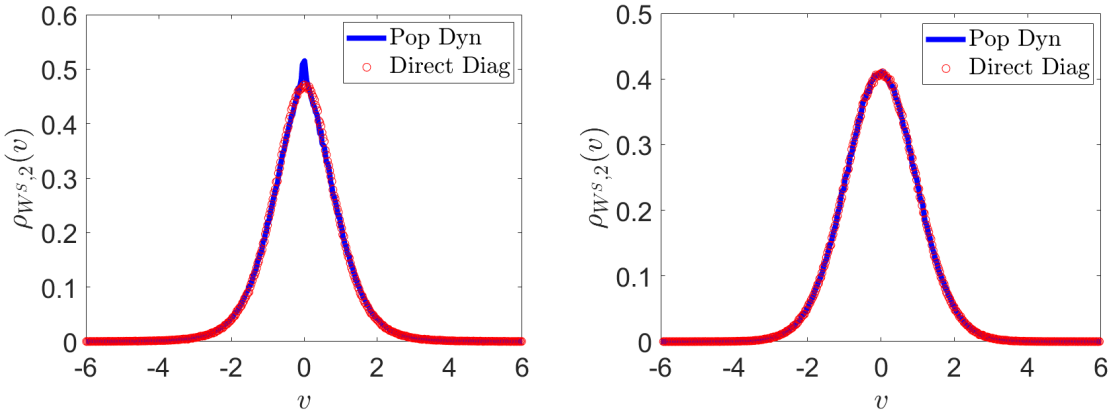

Figure 4.5: Pdf of the components of the second largest eigenvector for the unbiased random walk Markov matrix case (see (4.95)), with shifted Poisson degree distribution ($k_{\min} = 2$). **Left panel**: mean degree $c \simeq 6$ and $k_{\max} = 12$. Results from population dynamics with $N_P = 5000$ (solid blue) compared with the direct diagonalisation of 4000 matrices of size $N = 1000$ (red circles) finding a good agreement. **Right panel**: mean degree $c \simeq 12$ and $k_{\max} = 22$. Results from population dynamics with $N_P = 1500$ (solid blue) compared with the direct diagonalisation of 2000 matrices of size $N = 1000$ (red circles), with excellent agreement. In both cases, the size of the population used is $N_P^\star$, the optimal value corresponding to the finite size N of the matrices being diagonalised (see Section 4.6.4).

are generally more pronounced for lower c (see also discussion in section 4.6.4).

4.5.2 Unbiased random walk on a RRG: second largest eigenpair statistics

For a random regular graph, for which $p(k) = \delta_{k,c}$, we note that the matrix W^S reduces to

$$W_{ij}^S = \frac{c_{ij}}{c} \,, \tag{4.96}$$

implying that all results about the RRG adjacency matrix case stated in Section 4.4.2 carry over to this case too, but with all eigenvalues rescaled by $1/c$. As expected, $\lambda_1(W^S)_{RRG} = 1$, and the second largest eigenvalue corresponding to a $\mathcal{N}(0,1)$-distributed eigenvector is $\lambda_2(W^S)_{RRG} = \frac{2\sqrt{c-1}}{c}$. The spectral gap for this kind of Markov matrices as a function of c is then $g(c) = 1 - \frac{2\sqrt{c-1}}{c}$.

4.6 Population Dynamics

4.6.1 The orthogonality challenge

With the exception of the unweighted adjacency matrix of a RRG, Eq. (4.52) – supplemented with the conditions (4.53) and (4.54) – must be generally solved via a Population Dynamics algorithm, a Monte Carlo technique deeply rooted in the statistical mechanics of spin glasses [121, 122], which we already presented in Section 2.6 and 3.6.

The version of the algorithm that we use for the second largest eigenpair is similar to the one employed in Section 3.6. Here, we will highlight the main differences that stem from the

presence of the orthogonality condition (4.54).

Some observations are in order before sketching the algorithm. As we stated in Section 3.6, within the population dynamics algorithm the definition of the h variables in Eq. (4.52) is effectively converted into a stochastic linear update of h values. Its stability can only be achieved for $\lambda = \langle \lambda_1 \rangle_J$. For any $\lambda > \langle \lambda_1 \rangle_J$, the variables of type h will shrink to zero, whereas for $\lambda < \langle \lambda_1 \rangle_J$ they will explode in norm. In our scenario, where we consider $\lambda < \langle \lambda_1 \rangle_J$, the recursion is thus *a priori* unstable, unless it is otherwise constrained. Therefore, if unconstrained, the population will never spontaneously evolve towards a stable regime, which would at the same time satisfy the conditions (4.53) and (4.54).

As anticipated in Section 4.3.3, this observation entails that the orthogonality condition (4.54) must be strictly enforced on-the-fly – by imposing a correction to the fields h, which once again have no fixed scale given by their update equation. Enforcing the constraint (4.54) is equivalent to looking for a self-consistent solution of (4.52) in a smaller, constrained space. Only once the condition (4.54) has been enforced, a new stable non-trivial fixed point arises, and the behaviour of the h-variables is similar to that in the top eigenvector case: for any value $\lambda > \langle \lambda_2 \rangle_J$, the variables h under iteration of the modified population dynamics algorithm shrink to zero, whereas for $\lambda < \langle \lambda_2 \rangle_J$ they will explode in norm. Hence, Eq. (4.52) – taken together with the condition (4.54) – admits a stable, hence normalisable solution, such that Eq. (4.53) is naturally satisfied only for $\lambda = \langle \lambda_2 \rangle_J$: after the orthogonality correction has been enforced, the procedure we follow is then exactly identical to that used in Section 3.6.

4.6.2 The algorithm

Taking into account the observations made in Section 4.6.1, we briefly sketch the algorithm in the case of full deflation.

Two pairs of (coupled) populations with N_P members each $\{(a_i, b_i)\}_{1 \leq i \leq N_P}$ and $\{(\omega_i, h_i)\}_{1 \leq i \leq N_P}$ are randomly initialised, taking into account that both a_i and ω_i must be larger than ζ, the upper edge of the support of the bond pdf $p_K(K)$. We typically choose $N_P = 10^5$ or larger. In what follows, the parameter λ is the candidate second largest eigenvalue of J, whereas $\langle \lambda_1 \rangle_J$ is the average top largest eigenvalue of J. The first population is employed to solve the top eigenpair problem, and the other to solve the second eigenpair problem; the latter is constrained by results of the former due to the orthogonality constraint.

We therefore first run a short population dynamics simulation following Section 3.6, involving only the population $\{(a_i, b_i)\}_{1 \leq i \leq N_P}$ to find the solution for the first eigenpair problem

and the value $\langle\lambda_1\rangle_J$. This first simulation acts as an equilibration phase for the fields contributing to the largest eigenpair. Then, for any suitable value of $\lambda \in \mathbb{R} < \langle\lambda_1\rangle_J$, the following steps are iterated until stable populations are obtained:

1. Generate a random $k \sim \frac{k}{c}p(k)$, where $c = \langle k\rangle$.

2. Generate $k-1$ i.i.d. random variables K_ℓ from the bond weights pdf $p_K(K)$.

3. Select $k-1$ pairs (a_ℓ, b_ℓ) and (ω_ℓ, h_ℓ) from both populations at random, where the set of $k-1$ population indices for the two randomly selected samples is the same for both samples; compute

$$a^{(new)} = \langle\lambda_1\rangle_J - \sum_{\ell=1}^{k-1} \frac{K_\ell^2}{a_\ell} , \tag{4.97}$$

$$b^{(new)} = \sum_{\ell=1}^{k-1} \frac{b_\ell K_\ell}{a_\ell} , \tag{4.98}$$

$$\omega^{(new)} = \lambda - \sum_{\ell=1}^{k-1} \frac{K_\ell^2}{\omega_\ell} , \tag{4.99}$$

$$h^{(new)} = \sum_{\ell=1}^{k-1} \frac{h_\ell K_\ell}{\omega_\ell} , \tag{4.100}$$

   and replace two randomly selected pairs (a_i, b_i) and (ω_i, h_i) where $i \in \{1,...,N_P\}$ with the pairs $\left(a^{(new)}, b^{(new)}\right)$ and $\left(\omega^{(new)}, h^{(new)}\right)$.

4. Compute the components of the top eigenvector $\boldsymbol{u}$ and the candidate second largest eigenvector $\boldsymbol{v}$. In order to create a sample estimate of the eigenvectors statistics corresponding to the two top eigenvalues, we initialise two empty vectors, respectively $\boldsymbol{u} = \{u_j\}_{1\leq j\leq M}$ and $\boldsymbol{v} = \{v_j\}_{1\leq j\leq M}$ of size M, where $M = [N_P/c]$. The square brackets indicate the integer part. Then for any $j = 1,...,M$:

   (a) Generate $k \sim p(k)$

   (b) Generate k i.i.d. random variables K_ℓ from the weights pdf $p_K(K)$

   (c) Randomly select a subset of k indices from the population indices between 1 and N_P. This subset is denoted by $S_j(k)$. Then, for any $\ell \in S_j(k)$ select k pairs (a_ℓ, b_ℓ)

and (ω_ℓ, h_ℓ) from both populations; compute

$$u_j = \frac{\sum_{\ell \in S_j(k)} \frac{b_\ell K_\ell}{a_\ell}}{\langle \lambda_1 \rangle_J - \sum_{\ell \in S_j(k)} \frac{K_\ell^2}{a_\ell}} \ , \tag{4.101}$$

$$v_j = \frac{\sum_{\ell \in S_j(k)} \frac{h_\ell K_\ell}{\omega_\ell}}{\lambda - \sum_{\ell \in S_j(k)} \frac{K_\ell^2}{\omega_\ell}} \ . \tag{4.102}$$

Each set $S_j(k)$ of k population indices labelled by ℓ contributes uniquely to a single component j of the vectors $\boldsymbol{u}$ and $\boldsymbol{v}$ (see scheme in Figure 4.6). In other words, in view of the rigid matching between each set $S_j(k)$ with each component j, each group of k pairs (a_ℓ, b_ℓ) and (ω_ℓ, h_ℓ) takes part in the definition of just one component j, respectively u_j and v_j. Each set $S_j(k)$ of k population indices corresponding to a specific component j is then saved, along with the set of k weights $\{K_\ell\}$.

5. Compute $q = \frac{(\boldsymbol{u},\boldsymbol{v})}{|\boldsymbol{u}|^2}$, where $(\cdot,\cdot)$ indicates the dot product. In order to enforce the condition $q = 0$, for any component $j = 1, ..., M$ apply the correction

$$v_j \leftarrow v_j - q u_j \ . \tag{4.103}$$

In view of the rigid connection between the population indices labelling the fields and every specific component of $\boldsymbol{u}$ and $\boldsymbol{v}$, the orthogonalisation in (4.103) is practically achieved by correcting each field h_ℓ participating in the definition of every specific component v_j. The values of the indices ℓ here are those saved in each subset $S_j(k)$ in step (4)(c), along with the corresponding weights K_ℓ. For any $j = 1, ..., M$ and for any $\ell \in S_j(k)$ contributing to the single component j of both $\boldsymbol{u}$ and $\boldsymbol{v}$ we have

$$h_\ell \leftarrow h_\ell - q u_j \left(\frac{\lambda \omega_\ell}{K_\ell k} - K_\ell \right) \ , \tag{4.104}$$

where $k = k_j$ is exactly the "degree" drawn from $p(k)$ in step (4)(a) and used to build each component v_j in step (4)(c).

6. Return to (1).

A *sweep* is completed when all the N_P pairs (a_i, b_i) and (ω_i, h_i) have been updated at least once according to the steps above. The update of the pairs (a, b) is stable, thanks to the prior equilibration phase. The convergence is assessed by looking only at the first two

moments of the two vectors formed by the N_P samples of the pairs (ω, h). The parameter λ is varied according to the behaviour illustrated in Section 4.6.1: starting from an initial "large" value $\lambda < \langle\lambda_1\rangle_J$, it is then progressively decreased until a non trivial distribution for the h is achieved, when $\lambda = \langle\lambda_2\rangle_J$. Indeed, we observe that for any $\lambda > \langle\lambda_2\rangle_J$, the h shrink to zero, whereas for any $\lambda < \langle\lambda_2\rangle_J$, they blow up in norm.

Some comments are in order:

- the condition expressed in (4.103) is a Gram-Schmidt orthogonalisation, taking place after every microscopic update of the fields;
- the correction does not take place for components v_j related to $k = 0$, as both v_j and u_j are zero;
- in step (4)(c), we can clearly see that the components u_j and v_j are coupled through their degree and the set of bond weights, as anticipated in Section 4.3.3. Indeed, for any j, the k i.i.d. realisations of the weights $\{K\}_k$ and the "local neighbourhood" $S_j(k)$ that we dynamically create at every step (c) must be exactly the same for both u_j and v_j. In other words, both u_j and v_j must have the same update history.

4.6.3 Potential for simplifications in special cases

The steps (4) and (5) of the algorithm are computationally heavy. We are able in some cases to simplify them.

- For adjacency matrices of RRGs, where the variables a, b and ω are constant, the correction (4.103) translates to forcing the mean of the h to be zero after every update. Both steps (4)-(5) are then replaced by

$$h_i \leftarrow h_i - \bar{h} \qquad \forall i = 1, ..., N_P \,, \tag{4.105}$$

  where $\bar{h}$ indicates the sample mean of the h population.

- In the ER case (both weighted and non-weighted), we take advantage of the fact that in the thermodynamic limit there is no statistical distinction between the cavity fields ω and h (respectively a and b) and the denominator and numerator in (4.102), (respectively in (4.101)), even in presence of the truncation of the Poissonian degree distribution[5].

[5] Provided that the largest degree is reasonably large. The only difference between the distribution $\pi(\omega, h)$ and the distribution of the denominator and numerator of (4.55) can be observed because of the contribution coming from the largest degree, whose probability to occur is negligible.

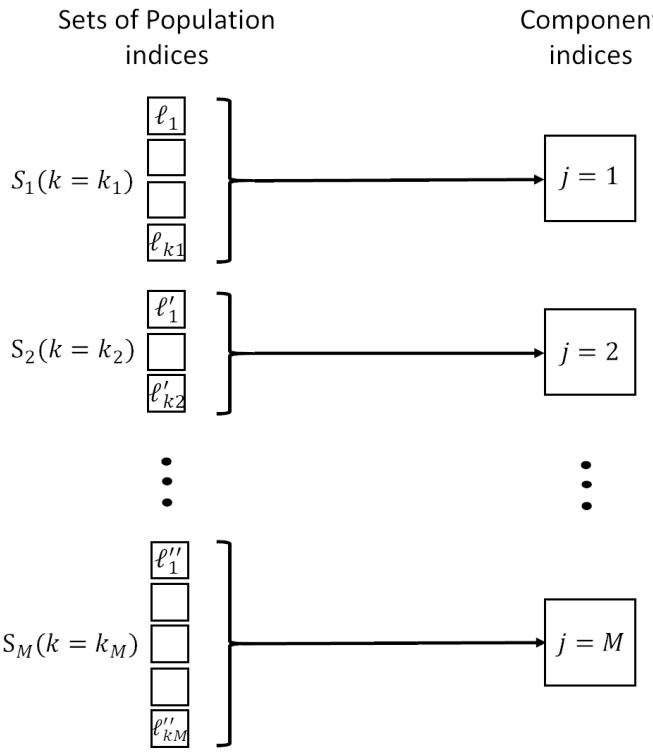

Figure 4.6: A schematic representation of the rigid matching between between each set of k population indices and each component j as illustrated in step (iv)(c) of the Population Dynamics algorithm in Section 4.6.2. The labels k_j with $j=1,...,M$ denote the number of population indices contributing to each component j, i.e. the size of each set $S_j(k=k_j)$.

Hence, we can consider just one couple of fields per species to represent a component, so we identify M=N_P. Steps (4) and (5) are then replaced by

4. Compute eigenvectors $\boldsymbol{u}$ and $\boldsymbol{v}$ as

$$u_i = \frac{b_i}{a_i} \,, \tag{4.106}$$

$$v_i = \frac{h_i}{\omega_i} \quad \forall i = 1,...,N_P \,. \tag{4.107}$$

5. Compute the correction as

$$h_i \leftarrow h_i - u_i \frac{(\boldsymbol{u},\boldsymbol{v})}{|\boldsymbol{u}|^2} \omega_i \quad \forall i = 1,...,N_P \,. \tag{4.108}$$

4.6.4 Population dynamics algorithm describes finite-size systems.

When no simplification can be used, as in the case of Markov matrices, the population dynamics algorithm can be relatively slow, due to the number of nested updates it requires. In these cases, we have therefore been often forced to consider a population size N_P smaller than the values

we would have typically wished ($N_P = \mathcal{O}(10^5)$ or more).

However, what may appear as a limitation at first sight turned out to be a blessing, in that it made us aware of an interesting interplay between the size N_P of the population dynamics, and the size N of the graph whose spectral properties were to be reproduced.

Indeed, we have collected convincing evidence that population dynamics at finite N_P does not really capture the thermodynamic limit $N \to \infty$: for a given graph size $N \gg 1$, there is an optimal size of the population $N_P^\star = N_P^\star(N)$ that best captures the spectral properties of that finite-size graph, and the degree of agreement between "theory" and numerical diagonalisation has a strongly non-monotonic behaviour as a function of N_P. Similarly, a population of given size N_P reproduces well spectral properties of graphs around a certain optimal size $N^\star$, but its accuracy rapidly deteriorates if the graph size N is markedly different from $N^\star$. Of course, the higher N_P (e.g. in cases where it is possible to employ $N_P = \mathcal{O}(10^5)$ or larger), the better the large N limit is captured (see e.g. the case in Fig. 4.2).

This intriguing phenomenon may be related to the existence of cycles, which seem to be more relevant in the eigenvector problem than the spectral problem. Indeed, whatever N_P is, the cavity fields of type ω and h will have common predecessors within their own species after $\sim \ln(N_P)/\ln(c-1)$ updates. This implies the presence of cycles in the population dynamics update history, which lead to correlations between different members of the population. Therefore, the assumption of population elements *independently* drawn from an ensemble, which underlies (4.52) (or equivalently (4.A.27)) is violated. That assumption in turn implements the notion that cycles *in the underlying graph* that is being described will diverge in the thermodynamic limit.

To quantify this effect, we compare the cumulative distribution function (CDF) of the second eigenvector's components of Markov matrices with Poissonian shifted degree distribution, obtained via population dynamics at various N_P, with the result from direct diagonalisation of matrices from the same ensemble at a given size $N = 1000$ – for both low and high mean degree.

In Figure 4.7, we assess the similarity of the two distributions using two figures of merit. The first (left) is the p-value of a 2-sample Kolmogorov-Smirnoff (KS) test: the larger the p-value, the strongest the evidence in favour of the hypothesis that the two distributions are the same. The second (right) is based on the analysis of a so-called *quantile-quantile plot* (Q-Q plot), which is the scatter plot of the quantiles of the two sets of data. Precisely, we focus on the

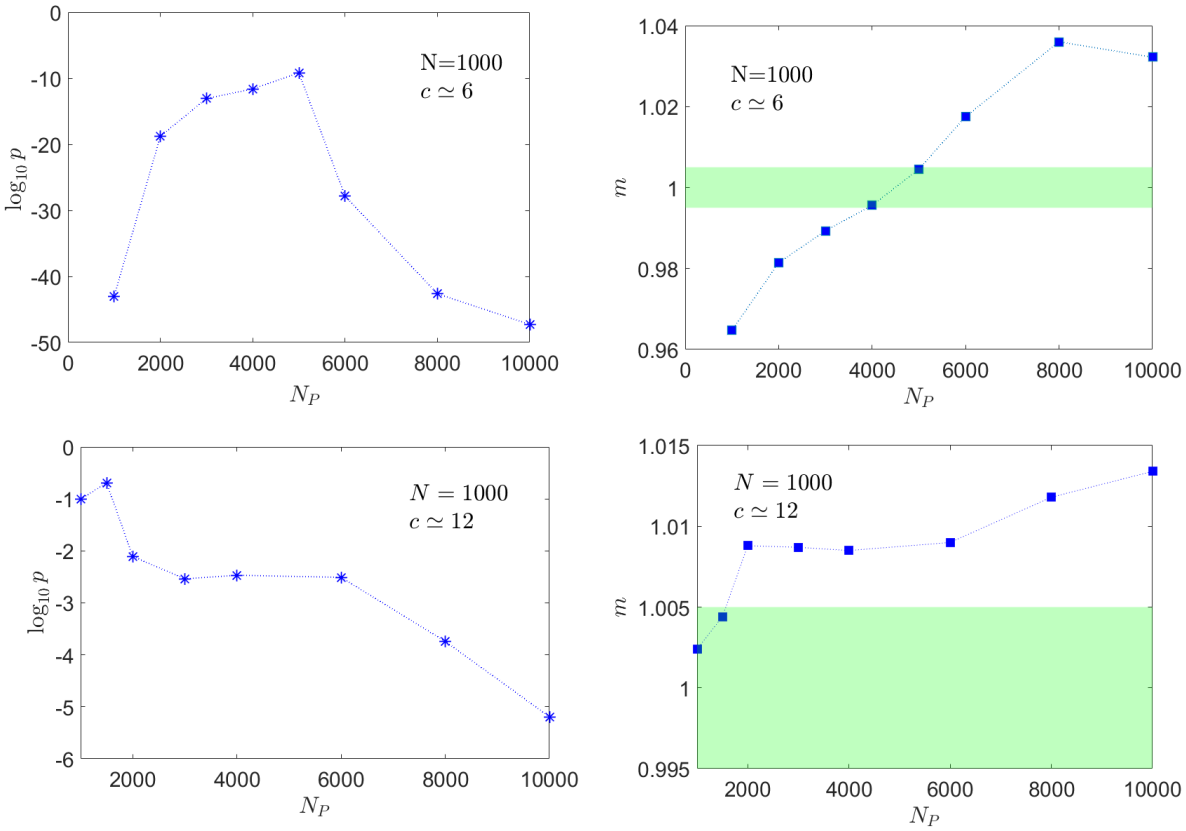

Figure 4.7: Top panels: low mean degree case, $c \simeq 6$, reference matrix size $N = 1000$. The left panel shows the base-10 logarithm of the p-value of the KS two-sample test comparing the two empirical cdfs corresponding to different population sizes. We notice that the p-values are all rather low, yet there is a clear maximum value at $N_P^\star \simeq 5000$, and the non-monotonic behaviour is quite pronounced. The right panel shows the slope m of the best-fit regression line of the Q-Q plot between the 25% and 75% quantiles, for various population sizes. The closer m is to 1, the better the agreement. The plot confirms again that the best agreement with our reference distribution is obtained with $N_P^\star \simeq 5000$. **Bottom panels**: high mean degree case, $c \simeq 12$, reference matrix size $N = 1000$. On the left, we show the p-value of the KS two-sample test against N_P in linear y-scale. The curve is much flatter than the low-c case, and the p-values are all significant, suggesting a high level of similarity between the two distributions throughout the full range of N_P. On the right, we plot the slope m of the best fit regression line of the Q-Q plot between the 25% and 75% quantiles, for various population sizes. For this figure of merit, we again observe a rather flat value of the slope between $N_P \simeq 2000$ and $N_P \simeq 6000$, where $m \simeq 1$ (within a 0.2% error). At high c, we indeed observe negligible finite size effects in the direct diagonalisation samples at different sizes N, and this phenomenon seems to be present also in the population dynamics simulations.

slope m of the best fit regression line $y = mx + b$ of the Q-Q plot, considered between the first and third quartile (respectively, the 0.25 and 0.75 quantiles), to limit spurious effects coming from the under-sampling of the tails. The slope m is directly proportional to the correlation coefficient between the quantiles of the two distributions, and $m = 1$ for identical distributions.

The existence of an optimal population size $N_P^\star$ for a given graph size N – and the non-monotonic behaviour of the accuracy with N_P – is quite evident in the left panels. The optimal value of $N_P^\star(N)$ is consistently identified by both figures of merit. However, the effect is more pronounced in the case of low connectivity (top row of Figure 4.7) – where finite size effects are indeed stronger – than in the case of high connectivity (bottom row of Figure 4.7).

4.7 Summary

We have developed a formalism to compute the statistics of the second largest eigenvalue and of the components of the corresponding eigenvector for some ensembles of sparse symmetric matrices, i.e. weighted adjacency matrices of graphs with finite mean connectivity. By assuming that the top eigenpair is known, we show that for a given matrix, computing the second largest eigenpair is equivalent to computing the top eigenpair of a *deflated* matrix, obtained by subtracting from the original matrix the dense matrix representing a rank-one perturbation proportional to the projector onto its first eigenstate. As in Chapter 3, the search for the top eigenpair of the deflated matrix is then transformed into the optimisation of a quadratic Hamiltonian on a sphere: introducing the associated Gibbs-Boltzmann distribution and a fictitious inverse temperature β, the top eigenvector represents the ground state of the system, reached in the limit $\beta \to \infty$. In order to extract this limit, we have employed two Statistical Mechanics methods, cavity and replicas. We started analysing the case of a single-instance matrix within the cavity framework, showing how our formulation allows for the inclusion of hard constraints.

The single-instance cavity method easily leads to recursion equations, which represent the essential ingredient to obtain the solution of the problem in the thermodynamic limit. We also obtain the exact same equations using replicas as an alternative approach, confirming the equivalence of the two methods in the thermodynamic limit. We employed an improved population dynamics algorithm to solve the stochastic recursion (4.52) complemented by the conditions (4.53) and (4.54), (or equivalently (4.A.27) along with (4.A.28) and (4.A.29)) that enforce normalisation and orthogonality of eigenvectors corresponding to different eigenvalues. We found that the convergence of the algorithm is driven not only by the largest eigenvalue of the deflated matrix (i.e. the second largest eigenvalue of the original matrix) but, most essentially, by the fact that the orthogonality condition (4.54) (or equivalently (4.A.29)) be correctly enforced. Some ensembles permit simplifications of the algorithm used to enforce orthogonality, which we exploited to speed up convergence.

We remark that from the theoretical point of view our method is applicable no matter what the size of the spectral gap is. However, if the gap is very narrow, numerical precision limit may not allow for a sufficiently accurate determination of $\lambda = \langle \lambda_2 \rangle_J$.

The simulations show excellent agreement between the theory and the direct diagonalisation of large matrices, and allow us to unpack the contributions to the average density of the

second eigenvector's components coming from nodes of different degrees.

Our study clearly demonstrates that — in contrast to beliefs commonly held in the community — population dynamics at finite N_P is fundamentally incapable of analysing properties representing the thermodynamic limit behaviour. This discovery is in some sense due to the fact that finite size effects are much stronger for eigenvectors than for eigenvalues (in particular for matrices without random edge weights). That finite population size effects are quantitatively related to finite size effects is, in retrospect, not really surprising, given the clear analogy existing between the emergence of correlations in population values – through cycles of common ancestors of population updates – and common ancestors created through cycles in random graphs of finite size, in which the scaling of cycle lengths with population and graph size follows basically the same logarithmic law.

In the case of the RRG adjacency matrix, we also analytically studied the pdf of the components of the top eigenvector of the deflated matrix as the deflation parameter is continuously changed, showing the abrupt change of the solution as soon as the deflation parameter becomes larger than the spectral gap of the Kesten-McKay distribution.

Lastly, we applied our formalism to sparse Markov matrices representing unbiased random walks on a network, for which the second largest eigenpair plays an important role encoding non-equilibrium properties.

Appendices

4.A Replica derivation in the case of full deflation

In this section, we evaluate the average (or typical) value of the largest eigenvalue and the density of top eigenvectors' components of the matrix $\tilde{J}$ within the replica framework. Our derivation applies to any configuration model graph with degree distribution $p(k)$ having finite mean and variance. We also ask that its support be bounded to ensure that their average largest eigenvalue is finite in the thermodynamic limit. The replica derivation in this appendix matches step by step that in Section 3.4, with the exception of the deflation term that needs to be taken into account. Therefore, to avoid repetitions we will just summarise the main steps.

4.A.1 Typical largest eigenvalue

We consider a $N \times N$ deflated symmetric matrix $\tilde{J}_{ij}(x) = c_{ij}K_{ij} - \frac{x}{N}u_i u_j$. The u_i represents the i-th component of $\boldsymbol{u}$, the top eigenvector of the original matrix J (normalised such that $|\boldsymbol{u}|^2 = N$) which we assume to be known. As in Section 3.4, the joint distribution of the matrix entries J_{ij} reads

$$P\left(\{J_{ij}\}\middle|\{k_i\}\right) = P\left(\{c_{ij}\}\middle|\{k_i\}\right)\prod_{i<j}\delta_{K_{ij},K_{ji}}p\left(K_{ij}\right)\ , \tag{4.A.1}$$

where the distribution $P\left(\{c_{ij}\}\middle|\{k_i\}\right)$ of connectivities $\{c_{ij}\}$ compatible with a given degree sequence $\{k_i\}$ is given by

$$P\left(\{c_{ij}\}\middle|\{k_i\}\right) = \frac{1}{\mathscr{M}}\prod_{i<j}\delta_{c_{ij},c_{ji}}\left(\frac{c}{N}\delta_{c_{ij},1} + \left(1-\frac{c}{N}\right)\delta_{c_{ij},0}\right)\prod_{i=1}^{N}\delta_{\sum_j c_{ij},k_i}\ , \tag{4.A.2}$$

and the pdf $p_K\left(K_{ij}\right)$ of bond weights (over a compact support whose upper edge is denoted by ζ) will be kept unspecified until the very end.

We fix $x = \langle\lambda_1\rangle_J$: in this setting, the second largest eigenvalue of J is represented by the

largest eigenvalue of $\tilde{J}$, which can be computed as the formal limit

$$\langle \lambda_2 \rangle_J = \left\langle \tilde{\lambda}_1 \right\rangle_{\tilde{J}} = \lim_{\beta\to\infty} \frac{2}{\beta N} \langle \ln Z \rangle_{\tilde{J}}, \qquad Z = \int \mathrm{d}\boldsymbol{v} \exp\left[\frac{\beta}{2}(\boldsymbol{v}, \tilde{J}\boldsymbol{v})\right] \delta\left(|\boldsymbol{v}|^2 - N\right) , \tag{4.A.3}$$

in terms of the quenched free energy of the model defined in (4.7). We recall that the round brackets $(\cdot,\cdot)$ indicate the dot product between vectors in $\mathbb{R}^N$. The partition function explicitly reads

$$Z = \int \mathrm{d}\boldsymbol{v} \exp\left[\frac{\beta}{2}(\boldsymbol{v}, J\boldsymbol{v}) - \frac{\beta \langle \lambda_1 \rangle_J}{2N} (\boldsymbol{u}, \boldsymbol{v})^2\right] \delta\left(|\boldsymbol{v}|^2 - N\right) . \tag{4.A.4}$$

By calling $q = \frac{1}{N}(\boldsymbol{u}, \boldsymbol{v})$, we can linearise the square in the exponent of (4.A.4) by means of a Hubbard-Stratonovich identity as follows,

$$\exp\left(-\frac{\beta \langle \lambda_1 \rangle_J N q^2}{2}\right) = \sqrt{\frac{\beta \langle \lambda_1 \rangle_J N}{2\pi}} \int \mathrm{d}z \exp\left(-\frac{\beta \langle \lambda_1 \rangle_J N}{2} z^2 + \beta \mathrm{i} z \langle \lambda_1 \rangle_J N q\right) , \tag{4.A.5}$$

and therefore the partition function reads

$$Z = \sqrt{\frac{\beta \langle \lambda_1 \rangle_J N}{2\pi}} \int \mathrm{d}\boldsymbol{v} \mathrm{d}z \exp\left(-\frac{\beta \langle \lambda_1 \rangle_J N}{2} z^2 + \mathrm{i}\beta \langle \lambda_1 \rangle_J z (\boldsymbol{u}, \boldsymbol{v}) + \frac{\beta}{2}(\boldsymbol{v}, J\boldsymbol{v})\right) \delta\left(|\boldsymbol{v}|^2 - N\right) . \tag{4.A.6}$$

The average over $\tilde{J}$ then reduces to computing the average over J. It is computed using the replica trick as follows

$$\left\langle \tilde{\lambda}_1 \right\rangle_{\tilde{J}} = \lim_{\beta\to\infty} \frac{2}{\beta N} \lim_{n\to 0} \frac{1}{n} \ln \langle Z^n \rangle_J , \tag{4.A.7}$$

Thus, the replicated partition function is

$$\begin{aligned} \langle Z^n \rangle_J = \left(\frac{\beta \langle \lambda_1 \rangle_J N}{2\pi}\right)^{\frac{n}{2}} \int \left(\prod_{a=1}^n \mathrm{d}\boldsymbol{v}_a\right) \left\langle \exp\left(\frac{\beta}{2} \sum_{a=1}^n \sum_{i,j}^N v_{ia} J_{ij} v_{ja}\right) \right\rangle_J \prod_{a=1}^n \delta\left(|\boldsymbol{v}_a|^2 - N\right) \\ \times \int \left(\prod_{a=1}^n \mathrm{d}z_a\right) \exp\left(-\frac{\beta \langle \lambda_1 \rangle_J N}{2} \sum_{a=1}^n z_a^2 + \mathrm{i}\beta \langle \lambda_1 \rangle_J \sum_{a=1}^n \sum_{i=1}^N z_a v_{ia} u_i\right) . \end{aligned} \tag{4.A.8}$$

Since the components of $\boldsymbol{u}$ are assumed to be known and fixed, they are not affected by the ensemble average.

Henceforth, the treatment for the average replicated partition function $\langle Z^n \rangle_J$ will exactly follow the steps in 3.4.1. It can be summarised as follows.

1. Perform the average w.r.t. the joint distribution (4.A.2) of matrix entries in Eq. (4.A.8), as in Eq. (3.54).

2. Use in Eq. (4.A.8) a Fourier representation for the Dirac delta enforcing the normalisation constraint and the Kronecker deltas expressing the degree constraints in (4.A.2).
3. Decouple sites through the integrated version (3.58) of the functional order parameter (3.57).
4. Use the Law of Large Numbers to evaluate the single-site integral

$$
\begin{aligned}
I &= \prod_{i=1}^{N} \int_{-\pi}^{\pi} \frac{\mathrm{d}\phi_i}{2\pi} \int \mathrm{d}\vec{v}_i \exp\left(-\mathrm{i}\phi_i k_i - \mathrm{i}\frac{\beta}{2} \sum_{a=1}^{n} \lambda_a v_{ia}^2 + \mathrm{i}\beta \langle \lambda_1 \rangle_J \sum_{a=1}^{n} z_a v_{ia} u_i + \mathrm{i}\hat{\varphi}(\vec{v}_i) \mathrm{e}^{\mathrm{i}\phi_i} \right) \\
&= \exp\left[\sum_{i=1}^{N} \mathrm{Log} \int \mathrm{d}\vec{v}_i \exp\left(-\mathrm{i}\frac{\beta}{2} \sum_{a=1}^{n} \lambda_a v_{ia}^2 + \mathrm{i}\beta \langle \lambda_1 \rangle_J \sum_{a=1}^{n} z_a v_{ia} u_i \right) \frac{(\mathrm{i}\hat{\varphi}(\vec{v}_i))^{k_i}}{k_i!} \right] \\
&= \exp\left\{ N \sum_{k=k_{\min}}^{k_{\max}} p(k) \left[\int \mathrm{d}u \, \rho_J(u|k) \mathrm{Log} \int \mathrm{d}\vec{v} \exp\left(-\mathrm{i}\frac{\beta}{2} \sum_{a=1}^{n} \lambda_a v_a^2 + \mathrm{i}\beta \langle \lambda_1 \rangle_J u \sum_{a=1}^{n} z_a v_a \right) \right.\right. \\
&\quad \left.\left. \times (\mathrm{i}\hat{\varphi}(\vec{v}))^k - \mathrm{Log}(k!) \right] \right\} , \qquad (4.A.9)
\end{aligned}
$$

where we have used

$$
\frac{1}{N} \sum_{i=1}^{N} \mathrm{Log} f(k_i, u_i) \simeq \sum_{k=k_{\min}}^{k_{\max}} p(k) \int \mathrm{d}u \rho_J(u|k) \mathrm{Log} f(k, u) \, . \qquad (4.A.10)
$$

Here, $p(k)$ is the degree distribution of the graph and $\rho_J(u|k)$ represents the distribution of the top eigenvector's components of the original matrix J conditioned on the degree k. As shown in Chapter 3.4.2, the variables u_i are strongly correlated with the k_i so their dependence on the k_i must be considered.

5. Evaluate the replicated partition function with a saddle-point approximation, viz.

$$
\langle Z^n \rangle_J \propto \int \mathscr{D}\varphi \mathscr{D}\hat{\varphi} \mathrm{d}\vec{\lambda} \mathrm{d}\vec{z} \exp\left(N S_n[\varphi, \hat{\varphi}, \vec{\lambda}, \vec{z}] \right) , \qquad (4.A.11)
$$

6. Obtain the stationarity conditions the action S_n w.r.t. variations of φ, $\hat{\varphi}$, $\vec{\lambda}$ and $\vec{z}$. The sought orthogonality condition will rise from the extra stationarity conditions w.r.t. $\vec{z}$.
7. In view of the similarities between the stationarity conditions for this problem with those for the top eigenpair case (see Eq. (3.72), (3.73), (3.74)), adopt the same replica-symmetric setting given by Eq. (3.75), (3.76) and (3.77), in which the integrated order parameter (3.58) and its conjugate are expressed as uncountably infinite superpositions of Gaussians with a non-zero mean. In (3.76) and (3.77), π and $\hat{\pi}$ are auxiliary normalised joint pdfs of the parameters of the Gaussian distributions. Assume also the condition

$z_{\bar{a}} = z$ for any $\bar{a} = 1, \ldots, n$.

8. As in Section 3.4.1, the ansätze (3.76) and (3.77) allow one to express the action S_n as a functional of π, $\hat{\pi}$, λ and z and perform explicitly the $\vec{v}$-integrals as $n \to 0$. The path integral over φ and $\hat{\varphi}$ in (3.66) is replaced by a path integral over π and $\hat{\pi}$, viz.

$$\langle Z^n \rangle_J \propto \frac{1}{\mathscr{M}} \int \mathscr{D}\pi \mathscr{D}\hat{\pi} \mathrm{d}\lambda \exp\left(N S_n[\pi, \hat{\pi}, \lambda, z]\right) , \tag{4.A.12}$$

9. The $\mathscr{O}(1)$ constant terms surviving in the action S_n as $n \to 0$ are cancelled by the $\mathscr{O}(1)$ terms arising from the evaluation of the normalisation constant $\mathscr{M}$ at the saddle-point (see Eq. (3.89)). The action S_n closely resembles that found in Section 3.4.1. Similarly, for its convergence we require that $\omega > \zeta$, $\omega > \hat{\omega}$ and $\lambda \equiv \mathrm{i}\lambda^\star > \{\hat{\omega}\}_k$.
10. The integral (4.A.12) is finally evaluated with a saddle-point approximation, by considering the stationarity conditions w.r.t. λ, z, π and $\hat{\pi}$ as detailed below.

Following Section 3.4.1, the stationarity condition w.r.t. λ entails

$$\frac{\partial S}{\partial \lambda}\Big|_{\lambda=\lambda^\star} = 0 \Rightarrow 1 = \sum_{k=0}^{k_{\max}} p(k) \int \mathrm{d}u \rho_J(u|k) \int \{\mathrm{d}\hat{\pi}\}_k \langle v^2 \rangle_{\bar{P}} , \tag{4.A.13}$$

where the average $\langle \cdot \rangle_{\bar{P}}$ is taken w.r.t. the Gaussian measure

$$\bar{P}_\beta(v) = \sqrt{\frac{\beta\left(\mathrm{i}\lambda^\star - \{\hat{\omega}\}_k\right)}{2\pi}} \exp\left[-\frac{\beta}{2}\left(\mathrm{i}\lambda^\star - \{\hat{\omega}\}_k\right)\left(v - \frac{\mathrm{i}z^\star \langle \lambda_1 \rangle_J u + \{\hat{h}\}_k}{\mathrm{i}\lambda^\star - \{\hat{\omega}\}_k} \right)^2 \right] . \tag{4.A.14}$$

More explicitly, the condition (4.A.13) reads

$$1 = \sum_{k=0}^{k_{\max}} p(k) \int \mathrm{d}u \rho_J(u|k) \int \{\mathrm{d}\hat{\pi}\}_k \left[\frac{1}{\beta(\mathrm{i}\lambda^\star - \{\hat{\omega}\}_k)} + \left(\frac{\mathrm{i}z^\star \langle \lambda_1 \rangle_J u + \{\hat{h}\}_k}{\mathrm{i}\lambda^\star - \{\hat{\omega}\}_k} \right)^2 \right] , \tag{4.A.15}$$

where the β-dependent term vanishes as $\beta \to \infty$. Similarly, the stationarity condition w.r.t. z entails

$$\frac{\partial S}{\partial z}\Big|_{z=z^\star} = 0 \Rightarrow z^\star = \mathrm{i} \sum_{k=0}^{k_{\max}} p(k) \int \mathrm{d}u \rho_J(u|k) u \int \{\mathrm{d}\hat{\pi}\}_k \langle v \rangle_{\bar{P}} , \tag{4.A.16}$$

where the average $\langle \cdot \rangle_{\bar{P}}$ is taken w.r.t. the Gaussian measure (4.A.14) implying

$$z^\star = \mathrm{i} \sum_{k=0}^{k_{\max}} p(k) \int \mathrm{d}u \rho_J(u|k) u \int \{\mathrm{d}\hat{\pi}\}_k \left(\frac{\mathrm{i}z^\star \langle \lambda_1 \rangle_J u + \{\hat{h}\}_k}{\mathrm{i}\lambda^\star - \{\hat{\omega}\}_k} \right) . \tag{4.A.17}$$

The stationarity condition w.r.t. variations of π, $\frac{\delta S}{\delta \pi} = 0$, is

$$\hat{\pi}(\hat{\omega},\hat{h}) = \int \mathrm{d}\omega \mathrm{d}h \; \pi(\omega,h) \left\langle \delta\left(\hat{\omega} - \frac{K^2}{\omega}\right) \delta\left(\hat{h} - \frac{hK}{\omega}\right) \right\rangle_K , \tag{4.A.18}$$

whereas the stationarity condition w.r.t. variations of $\hat{\pi}$, $\frac{\delta S}{\delta \hat{\pi}} = 0$, produces the condition

$$\pi(\omega,h) = \sum_{k=1}^{k_{\max}} p(k) \frac{k}{c} \int \mathrm{d}u \rho_J(u|k) \int \{\mathrm{d}\hat{\pi}\}_{k-1} \delta\left(\omega - (\mathrm{i}\lambda^\star - \{\hat{\omega}\}_{k-1})\right) \delta\left(h - (\mathrm{i}z^\star \langle \lambda_1 \rangle_J u + \{\hat{h}\}_{k-1})\right) . \tag{4.A.19}$$

Inserting (4.A.18) into (4.A.19) yields

$$\begin{aligned} \pi(\omega,h) = \sum_{k=1}^{k_{\max}} p(k) \frac{k}{c} \int \mathrm{d}u \rho_J(u|k) \int \{\mathrm{d}\pi\}_{k-1} \\ \times \left\langle \delta\left(\omega - (\mathrm{i}\lambda^\star - \sum_{\ell=1}^{k-1} \frac{K_\ell^2}{\omega_\ell})\right) \delta\left(h - \left(\mathrm{i}z^\star \langle \lambda_1 \rangle_J u + \sum_{\ell=1}^{k-1} \frac{h_\ell K_\ell}{\omega_\ell}\right)\right) \right\rangle_{\{K\}_{k-1}} , \end{aligned} \tag{4.A.20}$$

where the brackets $\langle \cdot \rangle_{\{K\}_{k-1}}$ denote averaging with respect to a collection of $k-1$ i.i.d. random variables K, each drawn from the bond weight pdf $p_K(K)$. The symbol $p(k)$ in (4.A.20) denotes the degree distribution of the graph with finite mean c, finite variance and bounded maximal degree. Following Section 3.4.1, we relabel the constant terms $\lambda \equiv \mathrm{i}\lambda^\star$ and $q \equiv -\mathrm{i}z^\star$ since they both turn out to be real-valued. We eventually find

$$\begin{aligned} \pi(\omega,h) = \sum_{k=1}^{k_{\max}} p(k) \frac{k}{c} \int \mathrm{d}u \rho_J(u|k) \int \{\mathrm{d}\pi\}_{k-1} \\ \times \left\langle \delta\left(\omega - \left(\lambda - \sum_{\ell=1}^{k-1} \frac{K_\ell^2}{\omega_\ell}\right)\right) \delta\left(h - \left(-qu \langle \lambda_1 \rangle_J + \sum_{\ell=1}^{k-1} \frac{h_\ell K_\ell}{\omega_\ell}\right)\right) \right\rangle_{\{K\}_{k-1}} . \end{aligned} \tag{4.A.21}$$

The parameter λ must be tuned as to enforce the normalisation condition (4.A.15) as $\beta \to \infty$, which reads

$$1 = \sum_{k=0}^{k_{\max}} p(k) \int \mathrm{d}u \rho_J(u|k) \int \{\mathrm{d}\pi\}_k \left\langle \left(\frac{-qu \langle \lambda_1 \rangle_J + \sum_{\ell=1}^{k} \frac{h_\ell K_\ell}{\omega_\ell}}{\lambda - \sum_{\ell=1}^{k} \frac{K_\ell^2}{\omega_\ell}} \right)^2 \right\rangle_{\{K\}_k} , \tag{4.A.22}$$

whereas Eq. (4.A.17) yields the following condition for q, viz.

$$q = \sum_{k=0}^{k_{\max}} p(k) \int \mathrm{d}u \rho_J(u|k) u \int \{\mathrm{d}\pi\}_k \left\langle \left(\frac{-qu \langle \lambda_1 \rangle_J + \sum_{\ell=1}^{k} \frac{h_\ell K_\ell}{\omega_\ell}}{\lambda - \sum_{\ell=1}^{k} \frac{K_\ell^2}{\omega_\ell}} \right) \right\rangle_{\{K\}_k} . \tag{4.A.23}$$

The structure of the action S_n in (4.A.12) is the same as that found in Section 3.4.1, except for the term $S_4(z) \equiv S_4(q) = n\frac{\beta}{2}\langle\lambda_1\rangle_J q^2$. Therefore, building on the same reasoning, the average largest eigenvalue of $\tilde{J}$, i.e. the average second largest eigenvalue of J is given by

$$\left\langle \tilde{\lambda}_1 \right\rangle_{\tilde{J}} \equiv \langle\lambda_2\rangle_J = \lambda + \langle\lambda_1\rangle_J q^2 \,, \tag{4.A.24}$$

where λ and q are defined by (4.A.22) and (4.A.23). As observed in Section 4.3.4, in case of full deflation we find $q = 0$, hence $\left\langle \tilde{\lambda}_1 \right\rangle_{\tilde{J}} \equiv \langle\lambda_2\rangle_J = \lambda$.

4.A.2 Density of top eigenvector's components using replicas

In this section, we provide the derivation for the density of components of the top eigenvector of the matrix $\tilde{J}$, in the case of full deflation ($x = \langle\lambda_1\rangle_J$). Therefore, the top eigenvector of the deflated matrix $\tilde{J}$ corresponds to the *second* eigenvector of the original matrix J.

The exact same procedure presented in Section 3.4.2 applies to this case. However, here we just take advantage of a convenient shortcut found in that section. Indeed, there we noticed that the density of the top eigenvector components (3.145) was closely related to the distribution (3.99) that had arisen in Section 3.4.1 when evaluating the stationarity condition w.r.t. λ. Moreover, we showed that the joint pdfs π and $\hat{\pi}$ appearing in Section 3.4.2 for the eigenvector calculation satisfied the very same set of coupled saddle-point equations (3.105) and (3.103) that had been found in Section 3.4.1 for the eigenvalue calculation.

In this context, the equivalent of Eq. (3.99) is the β-dependent pdf (4.A.14). Therefore, the density of the components of the top eigenvector of $\tilde{J}$ can be obtained by averaging the pdf (4.A.14) over the factorised joint pdf $\{\hat{\pi}\}_k = \prod_{\ell=1}^{k} \hat{\pi}(\hat{\omega}_\ell, \hat{h}_\ell)$, the conditional pdf $\rho_J(u|k)$ and $p(k)$ and then taking the $\beta \to \infty$ limit, yielding

$$\begin{aligned}
\rho_{\tilde{J}}(v) &= \lim_{\beta\to\infty} \sum_{k=0}^{k_{\max}} p(k) \int \mathrm{d}u \rho_J(u|k) \int \{\mathrm{d}\hat{\pi}\}_k \bar{P}_\beta(v) \\
&= \sum_{k=0}^{k_{\max}} p(k) \int \mathrm{d}u \rho_J(u|k) \int \{\mathrm{d}\hat{\pi}\}_k \delta\left(v - \frac{-qu\langle\lambda_1\rangle_J + \{\hat{h}\}_k}{\lambda - \{\hat{\omega}\}_k} \right) \,,
\end{aligned} \tag{4.A.25}$$

where we have used the identifications $\mathrm{i}\lambda^\star \equiv \lambda$ and $q \equiv -\mathrm{i}z^\star$ and the distribution $\hat{\pi}(\hat{\omega}, \hat{h})$ is

given by Eq. (4.A.18). Expressing Eq. (4.A.25) in terms of π (see Eq. (4.A.21)) gives

$$\rho_{\tilde{J}}(v) \equiv \rho_{J,2}(v) = \sum_{k=0}^{k_{\max}} p(k) \int \mathrm{d}u \rho_J(u|k) \int \{\mathrm{d}\pi\}_k \left\langle \delta\left(v - \frac{-qu\,\langle\lambda_1\rangle_J + \sum_{\ell=1}^{k} \frac{h_\ell K_\ell}{\omega_\ell}}{\lambda - \sum_{\ell=1}^{k} \frac{K_\ell^2}{\omega_\ell}} \right) \right\rangle_{\{K\}_k} , \tag{4.A.26}$$

where we recall that $\langle\cdot\rangle_{\{K\}_k}$ denote averaging w.r.t. a collection of k i.i.d. random variables K, each drawn from the bond weight distribution $p_K(K)$.

Eq. (4.A.26) represents the resulting probability density function of the top eigenvector's component of the deflated matrix $\tilde{J}$ in case of full deflation, which in turn corresponds to the distribution of the second largest eigenvector's components of J. This equation is the large N generalisation of the single-instance result (4.41) found by the cavity method. The set of equations (4.A.21), (4.A.22), (4.A.23), (4.A.24) and (4.A.26) are exactly equivalent to the thermodynamic limit equations (4.45), (4.46), (4.47), (4.48) and (4.49) found within the cavity method in Section 4.3.3.

All the observations made in Section 4.3.4 about the fact that (4.A.23) in case of full deflation encodes the orthogonality condition (hence $q = 0$) hold here as well. Taking into account the average orthogonality condition $q = 0$, we obtain

$$\pi(\omega, h) = \sum_{k=1}^{k_{\max}} p(k) \frac{k}{c} \int \{\mathrm{d}\pi\}_{k-1} \left\langle \delta\left(\omega - \left(\lambda - \sum_{\ell=1}^{k-1} \frac{K_\ell^2}{\omega_\ell} \right) \right) \delta\left(h - \left(\sum_{\ell=1}^{k-1} \frac{h_\ell K_\ell}{\omega_\ell} \right) \right) \right\rangle_{\{K\}_{k-1}} , \tag{4.A.27}$$

$$1 = \sum_{k=0}^{k_{\max}} p(k) \int \{\mathrm{d}\pi\}_k \left\langle \left(\frac{\sum_{\ell=1}^{k} \frac{h_\ell K_\ell}{\omega_\ell}}{\lambda - \sum_{\ell=1}^{k} \frac{K_\ell^2}{\omega_\ell}} \right)^2 \right\rangle_{\{K\}_k} , \tag{4.A.28}$$

$$0 = \sum_{k=0}^{k_{\max}} p(k) \int \mathrm{d}u \rho_J(u|k) u \int \{\mathrm{d}\pi\}_k \left\langle \left(\frac{\sum_{\ell=1}^{k} \frac{h_\ell K_\ell}{\omega_\ell}}{\lambda - \sum_{\ell=1}^{k} \frac{K_\ell^2}{\omega_\ell}} \right) \right\rangle_{\{K\}_k} , \tag{4.A.29}$$

$$\rho_{\tilde{J}}(v) \equiv \rho_{J,2}(v) = \sum_{k=0}^{k_{\max}} p(k) \int \{\mathrm{d}\pi\}_k \left\langle \delta\left(v - \frac{\sum_{\ell=1}^{k} \frac{h_\ell K_\ell}{\omega_\ell}}{\lambda - \sum_{\ell=1}^{k} \frac{K_\ell^2}{\omega_\ell}} \right) \right\rangle_{\{K\}_k} , \tag{4.A.30}$$

$$\left\langle \tilde{\lambda}_1 \right\rangle_{\tilde{J}} \equiv \langle \lambda_2 \rangle_J = \lambda \ . \tag{4.A.31}$$

In summary, Eq. (4.A.27), (4.A.28), (4.A.29), (4.A.30) and (4.A.31) provide the solution of the second largest eigenpair problem in the large N limit. They are identical to eq. (4.52), (4.53),(4.54), (4.55) and (4.56) found with the cavity method.

Chapter 5

Conclusions and Outlook

The overall aim of this thesis was to obtain and study the statistics of the top eigenpairs of ensembles of sparse symmetric random matrices, using methods typically employed in statistical mechanics.

In Chapter 2 we gave an extensive overview of the replica and the cavity method, i.e. the two main techniques that we employed across the whole thesis, taking the calculation of the average spectral density problem for sparse symmetric random matrices as a paradigmatic example.

In Chapter 3 we built a formalism to compute the average largest eigenvalue and the density of the components of the corresponding top eigenvector for some ensembles of sparse symmetric random matrices. This was our first main result. The top eigenpair problem was recast into the search for the ground state of a system of particles interacting on a sparse graph. Indeed, the top eigenpair was obtained by analysing the free energy and the Gibbs-Boltzmann distribution of the system in the zero temperature limit with the cavity and the replica methods, which proved to be equivalent in the thermodynamic limit. Both provided a solution in terms of a functional self-consistency equation, which was efficiently solved by a population dynamics algorithm whose convergence was driven by a parameter that turned out to be the typical largest eigenvalue of the ensemble. We studied different matrix ensembles, providing numerical results for ER matrices and checking the formalism against known cases such as the ensembles of RRG adjacency matrices and sparse Markov transition matrices representing unbiased random walks on a network.

In Chapter 4, combining the formalism of Chapter 3 with a *deflation* mechanism, we were able to compute the statistics of the *second* largest eigenvalue and the pdf of the components of the corresponding eigenvector for the ensembles of sparse symmetric matrices considered

in the previous chapter. This was our second main result. Using the cavity and the replica methods, we noticed that the solution for the second largest eigenpair was given in terms of equations similar to those found in Chapter 3, with the main difference being the presence of the orthogonality condition. The correct enforcement of this new constraint within the population dynamics algorithm proved to be crucial for its convergence. We found evidence that the population dynamics algorithm is incapable to reproduce the thermodynamic limit ($N \to \infty$) properties of eigenvectors when using a finite population of size N_P. Our results suggested that there exists a non-trivial relation between the size N of the matrices of interest and the finite population size N_P used to reproduce the statistics of their eigenvectors. We discussed numerical results for ER graphs and sparse Markov transition matrices representing unbiased random walks on a network. We also discussed the ensemble of RRG adjacency matrices, showing analytically the existence of two separated regimes for the solution.

The validity of our statistical mechanics framework was corroborated by the excellent agreement between our numerical results and direct diagonalisation results. Despite being overall slower and less efficient than any direct diagonalisation routine, our approach has the main advantage of unveiling and explaining quantitatively the heterogeneous structure of the density of the components of the top eigenvectors, which originates from the degree distribution of the underlying graph.

We believe that there are still open pathways for further research in this field. On the one hand, we envisage plenty of possible applications of our formalism. For instance, one of these would be the computation of *eigenvector centrality* for large sparse networks [130]. Centrality is a measure of the importance of each node, in terms of the number and importance of its neighbours. Given a node i, its centrality x_i is defined as $x_i = \frac{1}{\lambda}\sum_{j\in\partial i} A_{ij}x_j$, where A is the $\{0,1\}$-adjacency matrix of the network. Asking that the centralities be positive entails that the vector $\boldsymbol{x}$ is simply the top (Perron-Frobenius) eigenvector of A and λ its corresponding top eigenvalue. Moreover, our framework may be straightforwardly applied to characterise the top eigenpair statistics of the so-called *tilted* Markov transition matrix [134] appearing in the analysis of rare events for random walks on networks [135]. Indeed, the cumulant generating function in this context is dominated by the top eigenvalue of the tilted matrix. Besides, the localisation and the mode-switching dynamical phase transitions occurring for such systems as the deformation parameter is changed are understood in terms of the properties of respectively the top and both the top and the second eigenvector. Another direction would consist in ap-

plying our framework to ensembles of sparse matrices with a power-law degree distribution. Real-world networks are often characterised by such degree distributions too. Thus, comparing the top eigenpair statistics of those ensembles with the results obtained from the analysis of instances of real complex networks may provide useful insights. Moreover, following [36], sparse covariance matrices could also be analysed in our setting. Indeed, it would be interesting to check whether in the dense limit our formalism is able to identify the ensemble average of top eigenvalue as the upper edge of the Marčenko-Pastur distribution.

On the other hand, we also foresee the chance for a number of theoretical developments. A further technical advancement would be studying the top eigenpairs of undirected graphs above the percolation threshold, by isolating the contributions coming solely from nodes on the giant cluster. To this purpose, the cavity equations can be complemented with self-consistency equations for indicator variables, signalling whether a node belongs to the giant cluster or not, as done in [136]. This study would be particularly relevant because it would allow one to separate between trivial localised eigenvectors related to individual finite clusters and non-trivial localised states originating from the giant cluster. With reference to the ground state technique presented in Chapters 3 and 4, we believe that it can be further used for the study of eigenvectors of sparse matrices. Indeed, an immediate application would be obtaining the *smallest* eigenpairs of a sparse matrix A, by applying our formalism to the matrix $-A$. More generally, it could be potentially employed to compute the density of the components of *any* eigenvector of sparse symmetric random matrices. Indeed, the eigenvectors of a $N \times N$ matrix J represent the zero-energy minima of the "Hamiltonian" $H(\boldsymbol{v},\lambda) = \frac{1}{2}\sum_{i=1}^{N}(\lambda \boldsymbol{v} - J\boldsymbol{v})^2$ subject to the constraint $|\boldsymbol{v}|^2 = N$. We conclude by suggesting another intriguing route. The properties of the eigenvectors of sparse random matrices may be also investigated by analysing the statistics of the local resolvent using the cavity method. Indeed, given a $N \times N$ matrix J with eigenpairs $\{(\lambda_\alpha, \boldsymbol{u}_\alpha)\}_{\alpha=1,\dots,N}$, its resolvent being $G(z) = (z\mathbb{1}_N - J)^{-1}$, the following equation holds for $\lambda \in \mathbb{R}$ and for any $i = 1,\dots,N$, viz.

$$\varepsilon \mathrm{Im} G(\lambda - \mathrm{i}\varepsilon)_{ii} = \varepsilon\pi \sum_{\alpha=1}^{N} \delta_\varepsilon(\lambda - \lambda_\alpha) u_{i\alpha}^2 \,, \tag{5.1}$$

where $G_{ii}(z)$ indicates the i-th diagonal entry of the resolvent and $\delta_\varepsilon(x - x_0) = \frac{1}{\pi}\frac{\varepsilon}{(x-x_0)^2+\varepsilon^2}$ approximates the Dirac delta as $\varepsilon \to 0$. When $\lambda = \lambda_\alpha$, then $\varepsilon \mathrm{Im} G(\lambda - \mathrm{i}\varepsilon)_{ii} \simeq u_{i\alpha}^2 + \mathscr{O}(\varepsilon^2)$. On

the other hand, one observes that

$$\mathrm{Re}\left[\frac{1}{\omega_i}\right] = \pi \sum_{\alpha=1}^{N} \delta_\varepsilon(\lambda - \lambda_\alpha) u_{i\alpha}^2 \,, \tag{5.2}$$

where the ω_i are defined in Eq. (2.31). Eq. (5.2) suggests that the distribution of the squares of the eigenvectors can be obtained in terms of that of the ω_i. Some preliminary tests found evidence that Eq. (5.2) may cease to be valid for graphs above the percolation threshold. This could signal that in this specific case the tree-like assumption upon which the cavity method is based actually breaks, due to cycles which are present with probability $\mathscr{O}(1)$ in graphs with a giant component. Moreover, another possible cause may be quasi-degeneracy phenomena for eigenvalues in the continuous part of the spectrum of those graphs. Thus, we foresee that Eq. (5.2) may be aimed specifically at the analysis of localised eigenvectors of trees and sparse matrices below the percolation threshold.

Bibliography

[1] V. A. R. Susca, P. Vivo, and R. Kühn. Top eigenpair statistics for weighted sparse graphs. *Journal of Physics A: Mathematical and Theoretical*, 52(48):485002, 2019.

[2] V. A. R. Susca, P. Vivo, and R. Kühn. Second largest eigenpair statistics for sparse graphs. *Journal of Physics A: Mathematical and Theoretical*, 54(1):015004, 2020.

[3] V. A. R. Susca, P. Vivo, and R. Kühn. Cavity and replica methods for the spectral density of sparse symmetric random matrices. *SciPost Physics Lecture Notes*, 33, 2021.

[4] E. P. Wigner. On the statistical distribution of the widths and spacings of nuclear resonance levels. In *Mathematical Proceedings of the Cambridge Philosophical Society*, volume 47, pages 790–798. Cambridge University Press, 1951.

[5] S. F. Edwards and R. C. Jones. The eigenvalue spectrum of a large symmetric random matrix. *Journal of Physics A: Mathematical and General*, 9(10):1595, 1976.

[6] T. Guhr, A. Müller-Groeling, and H. A. Weidenmüller. Random-matrix theories in quantum physics: common concepts. *Physics Reports*, 299(4-6):189–425, 1998.

[7] D. Cvetković and S. Simić. Graph spectra in computer science. *Linear Algebra and its Applications*, 434(6):1545–1562, 2011.

[8] L. Laloux, P. Cizeau, M. Potters, and J. P. Bouchaud. Random matrix theory and financial correlations. *International Journal of Theoretical and Applied Finance*, 3(03):391–397, 2000.

[9] Z. Burda and J. Jurkiewicz. Signal and noise in financial correlation matrices. *Physica A: Statistical Mechanics and its Applications*, 344(1-2):67–72, 2004.

[10] J. P. Bouchaud and M. Potters. Financial applications of random matrix theory: a short review. *arXiv preprint arXiv:0910.1205*, 2009.

[11] D. Paul and A. Aue. Random matrix theory in statistics: A review. *Journal of Statistical Planning and Inference*, 150:1–29, 2014.

[12] J. Bun, J. P. Bouchaud, and M. Potters. Cleaning large correlation matrices: tools from random matrix theory. *Physics Reports*, 666:1–109, 2017.

[13] E. P. Wigner. On the distribution of the roots of certain symmetric matrices. *Annals of Mathematics*, pages 325–327, 1958.

[14] V. A. Marčenko and L. A. Pastur. Distribution of eigenvalues for some sets of random matrices. *Mathematics of the USSR-Sbornik*, 1(4):457, 1967.

[15] R. Albert and A. L. Barabási. Statistical mechanics of complex networks. *Reviews of Modern Physics*, 74(1):47, 2002.

[16] S. N. Dorogovtsev, A. V. Goltsev, J. F. F. Mendes, and A. N. Samukhin. Spectra of complex networks. *Physical Review E*, 68(4):046109, 2003.

[17] L. Lovász. Random walks on graphs: A survey. *Combinatorics, Paul Erdős is eighty*, 2(1):1–46, 1993.

[18] L. Lovász and J. Pelikán. On the eigenvalues of trees. *Periodica Mathematica Hungarica*, 3(1-2):175–182, 1973.

[19] K. Broderix, T. Aspelmeier, A. K. Hartmann, and A. Zippelius. Stress relaxation of near-critical gels. *Physical Review E*, 64(2):021404, 2001.

[20] F. Zamponi. Mean field theory of spin glasses. *arXiv preprint arXiv:1008.4844*, 2010.

[21] P. Erdős and A. Rényi. On random graphs i. *Publicationes Mathematicae (Debrecen)*, 6(18):290–297, 1959.

[22] P. Erdős and A. Rényi. On the evolution of random graphs. *Publications of the Mathematical Institute of the Hungarian Academy of Sciences*, 5(1):17–60, 1960.

[23] G. J. Rodgers and A. J. Bray. Density of states of a sparse random matrix. *Physical Review B*, 37(7):3557, 1988.

[24] A. J. Bray and G. J. Rodgers. Diffusion in a sparsely connected space: A model for glassy relaxation. *Physical Review B*, 38(16):11461, 1988.

[25] G. J. Rodgers, K. Austin, B. Kahng, and D. Kim. Eigenvalue spectra of complex networks. *Journal of Physics A: Mathematical and General*, 38(43):9431, 2005.

[26] Y. V. Fyodorov and A. D. Mirlin. On the density of states of sparse random matrices. *Journal of Physics A: Mathematical and General*, 24(9):2219, 1991.

[27] O. Khorunzhy, M. Shcherbina, and V. Vengerovsky. Eigenvalue distribution of large weighted random graphs. *Journal of Mathematical Physics*, 45(4):1648–1672, 2004.

[28] G. Biroli and R. Monasson. A single defect approximation for localized states on random lattices. *Journal of Physics A: Mathematical and General*, 32(24):L255, 1999.

[29] G. Semerjian and L. F. Cugliandolo. Sparse random matrices: the eigenvalue spectrum revisited. *Journal of Physics A: Mathematical and General*, 35(23):4837, 2002.

[30] T. Nagao and G. J. Rodgers. Spectral density of complex networks with a finite mean degree. *Journal of Physics A: Mathematical and Theoretical*, 41(26):265002, 2008.

[31] F. Slanina. Localization of eigenvectors in random graphs. *The European Physical Journal B*, 85(11):361, 2012.

[32] S. N. Evangelou. A numerical study of sparse random matrices. *Journal of Statistical Physics*, 69(1-2):361–383, 1992.

[33] R. Kühn. Spectra of sparse random matrices. *Journal of Physics A: Mathematical and Theoretical*, 41(29):295002, 2008.

[34] R. Kühn, J. Van Mourik, M. Weigt, and A. Zippelius. Finitely coordinated models for low-temperature phases of amorphous systems. *Journal of Physics A: Mathematical and Theoretical*, 40(31):9227, 2007.

[35] M. Mézard, G. Parisi, and M. Virasoro. *Spin glass theory and beyond: An Introduction to the Replica Method and Its Applications*, volume 9. World Scientific Publishing Company, 1987.

[36] T. Rogers, I. P. Castillo, R. Kühn, and K. Takeda. Cavity approach to the spectral density of sparse symmetric random matrices. *Physical Review E*, 78(3):031116, 2008.

[37] C. Bordenave and M. Lelarge. Resolvent of large random graphs. *Random Structures & Algorithms*, 37(3):332–352, 2010.

[38] F. Slanina. Equivalence of replica and cavity methods for computing spectra of sparse random matrices. *Physical Review E*, 83(1):011118, 2011.

[39] H. Kesten. Symmetric random walks on groups. *Transactions of the American Mathematical Society*, 92(2):336–354, 1959.

[40] B. D. McKay. The expected eigenvalue distribution of a large regular graph. *Linear Algebra and its Applications*, 40:203–216, 1981.

[41] R. Kühn. Spectra of random stochastic matrices and relaxation in complex systems. *EPL (Europhysics Letters)*, 109(6):60003, 2015.

[42] R. Kühn. Random matrix spectra and relaxation in complex networks. *Acta Physica Polonica B*, 46:1653–1682, 2015.

[43] G. Ergün and R. Kühn. Spectra of modular random graphs. *Journal of Physics A: Mathematical and Theoretical*, 42(39):395001, 2009.

[44] R. Kühn and J. Van Mourik. Spectra of modular and small-world matrices. *Journal of Physics A: Mathematical and Theoretical*, 44(16):165205, 2011.

[45] T. Rogers, C. P. Vicente, K. Takeda, and I. P. Castillo. Spectral density of random graphs with topological constraints. *Journal of Physics A: Mathematical and Theoretical*, 43(19):195002, 2010.

[46] F. L. Metz, I. Neri, and D. Bollé. Localization transition in symmetric random matrices. *Physical Review E*, 82(3):031135, 2010.

[47] Y. Kabashima, H. Takahashi, and O. Watanabe. Cavity approach to the first eigenvalue problem in a family of symmetric random sparse matrices. In *Journal of Physics: Conference Series*, volume 233, page 012001, 2010.

[48] T. Rogers and I. P. Castillo. Cavity approach to the spectral density of non-Hermitian sparse matrices. *Physical Review E*, 79(1):012101, 2009.

[49] I. Neri and F. L. Metz. Spectra of sparse non-Hermitian random matrices: an analytical solution. *Physical Review Letters*, 109(3):030602, 2012.

[50] I. Neri and F. L. Metz. Eigenvalue outliers of non-Hermitian random matrices with a local tree structure. *Physical Review Letters*, 117(22):224101, 2016.

[51] F. L. Metz, I. Neri, and T. Rogers. Spectral theory of sparse non-Hermitian random matrices. *Journal of Physics A: Mathematical and Theoretical*, 52(43):434003, 2019.

[52] A. Saade, F. Krzakala, and L. Zdeborová. Spectral density of the non-backtracking operator on random graphs. *EPL (Europhysics Letters)*, 107(5):50005, 2014.

[53] C. Bordenave, M. Lelarge, and L. Massoulié. Non-backtracking spectrum of random graphs: community detection and non-regular Ramanujan graphs. In *2015 IEEE 56th Annual Symposium on Foundations of Computer Science*, pages 1347–1357. IEEE, 2015.

[54] F. L. Metz and J. D. Silva. Spectral density of dense random networks and the breakdown of the Wigner semicircle law. *Physical Review Research*, 2(4):043116, 2020.

[55] F. A. López and A. C. C. Coolen. Imaginary replica analysis of loopy regular random graphs. *Journal of Physics A: Mathematical and Theoretical*, 53(6):065002, 2020.

[56] F. A. Lopez and A. C. C. Coolen. Transitions in loopy random graphs with fixed degrees and arbitrary degree distributions. *arXiv preprint arXiv:2008.11002*, 2020.

[57] G. T. Cantwell and M. E. J. Newman. Message passing on networks with loops. *Proceedings of the National Academy of Sciences*, 116(47):23398–23403, 2019.

[58] J. G. Restrepo, E. Ott, and B. R. Hunt. Onset of synchronization in large networks of coupled oscillators. *Physical Review E*, 71(3):036151, 2005.

[59] J. G. Restrepo, E. Ott, and B. R. Hunt. Weighted percolation on directed networks. *Physical Review Letters*, 100(5):058701, 2008.

[60] R. M. May. Will a large complex system be stable? *Nature*, 238(5364):413–414, 1972.

[61] J. Moran and J. P. Bouchaud. May's instability in large economies. *Physical Review E*, 100(3):032307, 2019.

[62] C. R. MacCluer. The many proofs and applications of Perron's theorem. *Siam Review*, 42(3):487–498, 2000.

[63] J. J. Sakurai and J. Napolitano. *Modern Quantum Mechanics*. Cambridge University Press, 2017.

[64] J. Ma, R. Dudeja, J. Xu, A. Maleki, and X. Wang. Spectral method for phase retrieval: an expectation propagation perspective. *arXiv preprint arXiv:1903.02505*, 2019.

[65] J. Shlens. A tutorial on principal component analysis. *arXiv preprint arXiv:1404.1100*, 2014.

[66] R. Monasson and D. Villamaina. Estimating the principal components of correlation matrices from all their empirical eigenvectors. *EPL (Europhysics Letters)*, 112(5):50001, 2015.

[67] N. Alon and N. Kahale. A spectral technique for coloring random 3-colorable graphs. *SIAM Journal on Computing*, 26(6):1733–1748, 1997.

[68] A. Coja-Oghlan. A spectral heuristic for bisecting random graphs. *Random Structures & Algorithms*, 29(3):351–398, 2006.

[69] A. Pothen, H. D. Simon, and K. P. Liou. Partitioning sparse matrices with eigenvectors of graphs. *SIAM Journal on Matrix Analysis and Applications*, 11(3):430–452, 1990.

[70] J. Shi and J. Malik. Normalized cuts and image segmentation. *IEEE Transactions on Pattern Analysis and Machine Intelligence*, 22(8):888–905, 2000.

[71] T. Kawamoto and Y. Kabashima. Limitations in the spectral method for graph partitioning: Detectability threshold and localization of eigenvectors. *Physical Review E*, 91(6):062803, 2015.

[72] A. E. Brouwer and W. H. Haemers. *Spectra of graphs*. Springer Science & Business Media, 2011.

[73] S. Brin and L. Page. The anatomy of a large-scale hypertextual web search engine. *Computer Networks and ISDN Systems*, 30(1-7):107–117, 1998.

[74] A. N. Langville and C. D. Meyer. *Google's PageRank and beyond: The science of search engine rankings*. Princeton University Press, 2011.

[75] J. Friedman and J. P. Tillich. Generalized Alon–Boppana theorems and error-correcting codes. *SIAM Journal on Discrete Mathematics*, 19(3):700–718, 2005.

[76] D. Tomić, K. Skala, L. Kranjčevic, B. Pirkić, S. Štifter, and I. Šmit. Evaluation of the efficacy of cancer drugs by using the second largest eigenvalue of metabolic cancer pathways. *Journal of Computer Science & Systems Biology*, 11(3):240–248, 2018.

[77] M. Lucińska and S. T. Wierzchoń. Clustering based on eigenvectors of the adjacency matrix. *International Journal of Applied Mathematics and Computer Science*, 28(4):771–786, 2018.

[78] B. N. Datta. *Numerical linear algebra and applications*, volume 116. Siam, 2010.

[79] I. T. Jolliffe and J. Cadima. Principal component analysis: a review and recent developments. *Philosophical Transactions of the Royal Society A: Mathematical, Physical and Engineering Sciences*, 374(2065):20150202, 2016.

[80] L. Lovász. Eigenvalues of graphs. Lecture notes available at http://www.cs.elte.hu/~lovasz/eigenvals-x.pdf, 2007.

[81] P. Moretti, A. Baronchelli, A. Barrat, and R. Pastor-Satorras. Complex networks and glassy dynamics: walks in the energy landscape. *Journal of Statistical Mechanics: Theory and Experiment*, 2011(03):P03032, 2011.

[82] R. G. Margiotta, R. Kühn, and P. Sollich. Glassy dynamics on networks: local spectra and return probabilities. *Journal of Statistical Mechanics: Theory and Experiment*, 2019(9):093304, 2019.

[83] T. Haveliwala and S. Kamvar. The second eigenvalue of the Google matrix. *Stanford University Technical Report*, available at http://ilpubs.stanford.edu:8090/582/, 2003.

[84] Z. Füredi and J. Komlós. The eigenvalues of random symmetric matrices. *Combinatorica*, 1(3):233–241, 1981.

[85] S. Janson. The first eigenvalue of random graphs. *Combinatorics Probability and Computing*, 14(5/6):815, 2005.

[86] M. Krivelevich and B. Sudakov. The largest eigenvalue of sparse random graphs. *Combinatorics, Probability and Computing*, 12(1):61–72, 2003.

[87] T. Ando, Y. Kabashima, H. Takahashi, O. Watanabe, and M. Yamamoto. Spectral analysis of random sparse matrices. *IEICE Transactions on Fundamentals of Electronics, Communications and Computer Sciences*, 94(6):1247–1256, 2011.

[88] D. Cvetković and S. Simić. The second largest eigenvalue of a graph (a survey). *Filomat*, 9(3):449–472, 1995.

[89] S. K. Simić, M. Andelić, C. M. da Fonseca, and D. Živković. Notes on the second largest eigenvalue of a graph. *Linear Algebra and its Applications*, 465:262–274, 2015.

[90] L. Y. Kolotilina. Upper bounds for the second largest eigenvalue of symmetric nonnegative matrices. *Journal of Mathematical Sciences*, 191(1):75–88, 2013.

[91] N. Alon. Eigenvalues and expanders. *Combinatorica*, 6(2):83–96, 1986.

[92] A. Nilli. On the second eigenvalue of a graph. *Discrete Mathematics*, 91(2):207–210, 1991.

[93] C. E. Porter and R. G. Thomas. Fluctuations of nuclear reaction widths. *Physical Review*, 104(2):483, 1956.

[94] G. Livan, M. Novaes, and P. Vivo. *Introduction to random matrices: theory and practice*, volume 26. Springer, 2018.

[95] J. T. Chalker and B. Mehlig. Eigenvector statistics in non-Hermitian random matrix ensembles. *Physical Review Letters*, 81(16):3367, 1998.

[96] R. A. Janik, W. Nörenberg, M. A. Nowak, G. Papp, and I. Zahed. Correlations of eigenvectors for non-Hermitian random-matrix models. *Physical Review E*, 60(3):2699, 1999.

[97] Y. V. Fyodorov. On statistics of bi-orthogonal eigenvectors in real and complex Ginibre ensembles: combining partial Schur decomposition with supersymmetry. *Communications in Mathematical Physics*, 363(2):579–603, 2018.

[98] Z. Burda, J. Grela, M. A. Nowak, W. Tarnowski, and P. Warchoł. Unveiling the significance of eigenvectors in diffusing non-Hermitian matrices by identifying the underlying Burgers dynamics. *Nuclear Physics B*, 897:421–447, 2015.

[99] M. A. Nowak and W. Tarnowski. Probing non-orthogonality of eigenvectors in non-Hermitian matrix models: diagrammatic approach. *Journal of High Energy Physics*, 2018(6):152, 2018.

[100] E. Gudowska-Nowak, M. A. Nowak, D. R. Chialvo, J. K. Ochab, and W. Tarnowski. From synaptic interactions to collective dynamics in random neuronal networks models: critical role of eigenvectors and transient behavior. *Neural Computation*, 32(2):395–423, 2020.

[101] I. Neri and F. L. Metz. Spectral theory for the stability of dynamical systems on large oriented locally tree-like graphs. *arXiv preprint arXiv:1908.07092*, 2019.

[102] K. Truong and A. Ossipov. Eigenvectors under a generic perturbation: Non-perturbative results from the random matrix approach. *EPL (Europhysics Letters)*, 116(3):37002, 2016.

[103] D. Facoetti, P. Vivo, and G. Biroli. From non-ergodic eigenvectors to local resolvent statistics and back: A random matrix perspective. *EPL (Europhysics Letters)*, 115(4):47003, 2016.

[104] Z. Burda, B. J. Spisak, and P. Vivo. Eigenvector statistics of the product of Ginibre matrices. *Physical Review E*, 95(2):022134, 2017.

[105] R. Allez and J. P. Bouchaud. Eigenvector dynamics: general theory and some applications. *Physical Review E*, 86(4):046202, 2012.

[106] J. Bun, J. P. Bouchaud, and M. Potters. Overlaps between eigenvectors of correlated random matrices. *Physical Review E*, 98(5):052145, 2018.

[107] L. V. Tran, V. H. Vu, and K. Wang. Sparse random graphs: Eigenvalues and eigenvectors. *Random Structures & Algorithms*, 42(1):110–134, 2013.

[108] P. Bourgade, J. Huang, and H. T. Yau. Eigenvector statistics of sparse random matrices. *Electronic Journal of Probability*, 22, 2017.

[109] I. Dumitriu and S. Pal. Sparse regular random graphs: spectral density and eigenvectors. *The Annals of Probability*, 40(5):2197–2235, 2012.

[110] Y. Elon. Eigenvectors of the discrete Laplacian on regular graphs—a statistical approach. *Journal of Physics A: Mathematical and Theoretical*, 41(43):435203, 2008.

[111] Á. Backhausz and B. Szegedy. On the almost eigenvectors of random regular graphs. *Annals of Probability*, 47(3):1677–1725, 2019.

[112] F. L. Metz and I. Neri. Localization and universality of eigenvectors in directed random graphs. *Physical Review Letters*, 126(4):040604, 2021.

[113] Y. Kabashima and H. Takahashi. First eigenvalue/eigenvector in sparse random symmetric matrices: influences of degree fluctuation. *Journal of Physics A: Mathematical and Theoretical*, 45(32):325001, 2012.

[114] H. Takahashi. Fat-tailed distribution derived from the first eigenvector of a symmetric random sparse matrix. *Journal of Physics A: Mathematical and Theoretical*, 47(6):065003, 2014.

[115] P. Vivo. Index of a matrix, complex logarithms, and multidimensional Fresnel integrals. *Journal of Physics A: Mathematical and Theoretical*, 54(2):025002, 2020.

[116] I. S. Gradshteyn and I. M. Ryzhik. *Table of integrals, series, and products*. Academic Press, 2014.

[117] A. Cavagna, I. Giardina, and G. Parisi. Analytic computation of the instantaneous normal modes spectrum in low-density liquids. *Physical Review Letters*, 83(1):108, 1999.

[118] P. M. Goldbart, H. E. Castillo, and A. Zippelius. Randomly crosslinked macromolecular systems: vulcanization transition to and properties of the amorphous solid state. *Advances in Physics*, 45(5):393–468, 1996.

[119] M. Bauer and O. Golinelli. Random incidence matrices: moments of the spectral density. *Journal of Statistical Physics*, 103(1-2):301–337, 2001.

[120] O. Golinelli. Statistics of delta peaks in the spectral density of large random trees. *arXiv preprint cond-mat/0301437*, 2003.

[121] M. Mézard and G. Parisi. The Bethe lattice spin glass revisited. *The European Physical Journal B-Condensed Matter and Complex Systems*, 20(2):217–233, 2001.

[122] F. Krzakala, F. Ricci-Tersenghi, L. Zdeborová, R. Zecchina, E. W. Tramel, and L. F. Cugliandolo. *Statistical physics, optimization, inference, and message-passing algorithms*. Oxford University Press, 2016.

[123] B. Bollobás. The evolution of random graphs. *Transactions of the American Mathematical Society*, 286(1):257–274, 1984.

[124] B. Bollobás. *Random graphs*. Number 73. Cambridge University Press, 2001.

[125] S. N. Dorogovtsev and J. F. F. Mendes. Evolution of networks. *Advances in Physics*, 51(4):1079–1187, 2002.

[126] A. C. C. Coolen, A. Annibale, and E. Roberts. *Generating random networks and graphs*. Oxford University Press, 2017.

[127] J. A. Bondy and U. S. R. Murty. *Graph theory with applications*, volume 290. Macmillan London, 1976.

[128] C. Castellano and R. Pastor-Satorras. Thresholds for epidemic spreading in networks. *Physical Review Letters*, 105(21):218701, 2010.

[129] A. V. Goltsev, S. N. Dorogovtsev, J. G. Oliveira, and J. F. F. Mendes. Localization and spreading of diseases in complex networks. *Physical Review Letters*, 109(12):128702, 2012.

[130] T. Martin, X. Zhang, and M. E. J. Newman. Localization and centrality in networks. *Physical Review E*, 90(5):052808, 2014.

[131] R. Pastor-Satorras and C. Castellano. Eigenvector localization in real networks and its implications for epidemic spreading. *Journal of Statistical Physics*, 173(3):1110–1123, 2018.

[132] K. Hashimoto. Zeta functions of finite graphs and representations of p-adic groups. In *Automorphic forms and geometry of arithmetic varieties*, pages 211–280. Elsevier, 1989.

[133] Å. Björck. *Numerical methods in matrix computations*, volume 59. Springer, 2015.

[134] H. Touchette. The large deviation approach to statistical mechanics. *Physics Reports*, 478(1-3):1–69, 2009.

[135] C. De Bacco, A. Guggiola, R. Kühn, and P. Paga. Rare events statistics of random walks on networks: localisation and other dynamical phase transitions. *Journal of Physics A: Mathematical and Theoretical*, 49(18):184003, 2016.

[136] R. Kühn. Disentangling giant component and finite cluster contributions in sparse random matrix spectra. *Physical Review E*, 93(4):042110, 2016.